UNDERSTANDING THE ROLE OF LIGAND OXIDATION STATE: DESIGN, SYNTHESIS, AND REACTIVITY OF ELECTRONICALLY ASYMMETRIC MOLYBDENUM DITHIOLENE COMPLEXES

by

Sara A. Dille

A Dissertation

Submitted to the Faculty of Purdue University

In Partial Fulfillment of the Requirements for the degree of

Doctor of Philosophy

Department of Chemistry and Chemical Biology

Indianapolis, Indiana

August 2019

THE PURDUE UNIVERSITY GRADUATE SCHOOL
STATEMENT OF COMMITTEE APPROVAL

Dr. Partha Basu, Chair

Department of Chemistry and Chemical Biology

Dr. Lei Li

Department of Chemistry and Chemical Biology

Dr. Robert Minto

Department of Chemistry and Chemical Biology

Dr. Jingzhi Pu

Department of Chemistry and Chemical Biology

Approved by:

Dr. Eric Long

Head of the Graduate Program

To my parents

Allen and Sue Dille

This would not have been possible without your unwavering love and support.

ACKNOWLEDGMENTS

First and foremost I must thank my Ph.D. advisor and mentor, Dr. Partha Basu. Thank you for your support, encouragement, and guidance over the course of my studies. Thank you for pushing me and inspiring me to do my best. I cannot thank you enough for all you have done for me over the last six years.

Thank you to the past Basu Research Group members I have had the pleasure of working with, Dr Benjamin Mogesa, Dr. Igor Pimkov, and Ann Caputo. A special thank you to Dr. John Thomas, and Stephen Ratvasky; graduate school would not have been the same without you guys. John, thank you for bringing humor and laughter to the lab making the stressful times easier and for encouraging me to keep pushing me to reach my goal of completing my Ph.D. My friend Stephen, we started working in the laboratory at the same time and over the years you have gone from undergraduate to friend and collaborator. Thank you for all you have done for me throughout the years, I am extremely grateful.

To the current Basu Research Group members, Dr. Jennifer McGarry, Breeanna Mintmier, Kyle Colston, and Joe Cassell. Breeanna I am so glad you joined our laboratory; you've become a wonderful friend over the years and made the move to IUPUI so much easier. Kyle, I have to first thank you for your collaboration on theoretical calculations, those would not have been possible without you. I know the laboratory is in good hands now that I am leaving.

I would like to thank my friend and undergraduate mentor, Dr. James Coffield. You pushed and inspired me to be the best scientist I could be during my undergraduate studies. I am forever grateful to you and I know I would not have been successful in graduate school without your friendship and support over the years.

To Sarah Sisley, I am so glad we started the program together. I don't think I would have made it through any of the defenses without you! Thank you for always being there whenever I was stressed about school, and for the constant encouragement that I could reach this goal and complete my Ph.D.

To Kim and Joe Rosmus, the two of you are some of the best friends anybody could ask for. You opened your home to me when I needed it and I am forever grateful to the two of you for your kindness and support.

To Dr. Meghan McLeod and Dr. Alicen Teitgen, thank you so much for making the transition to a new university and department much easier. Your friendship and support (and of course the coffee breaks) made the final semesters of graduate school much less stressful.

Finally, to all my friends and family who have had my back since day one of college through my masters and finally completing my Ph.D. Your love and encouragement have meant the world to me.

TABLE OF CONTENTS

LIST OF TABLES

LIST OF FIGURES

ABSTRACT

Author: Dille, Sara, A. Doctor of Philosophy
Institution: Purdue University
Degree Received: June 2019
Title: Understanding the Role of Ligand Oxidation State: Design, Synthesis, and Reactivity of Electronically Asymmetric Molybdenum Dithiolene Complexes
Committee Chair: Partha, Basu

Mononuclear molybdopterin enzymes are a large class of enzymes that are present in all phyla of life. All pterin containing enzymes posses a molybdopterin cofactor made up of a molybdenum metal center coordinated directly by a dithiolene ligand, which is appended to a pyranopterin cofactor. The majority of these enzymes catalyze oxygen atom transfer reactions that are concomitant with a transfer of two-electrons. We are hypothesizing that by altering the oxidation states of the dithiolene, the reactivity of the cofactor can be tuned for different substrates. This investigation focuses on the synthesis and characterization of oxo-Mo^{IV}(dithiolene) complexes that possess a fully reduced dithiolene ligand (dithiolene) and a fully oxidized dithiolene ligand (dithione). These complexes are designed to represent the asymmetry of the dithiolene ligand that is observed in the crystal structures of the DMSO reductase family. Asymmetric oxo-Mo^{IV}(dithiolene) complexes exhibit a unique structural property, a large fold angle along the S•••S vector of the dithione ligand. These complexes also show a positive solvatochromic effect in a range of polar to nonpolar solvents. The rich electrochemical properties of these redox active complexes and other characterization details such as IR, and NMR studies will be presented. Effects on the reactivity of these complexes using biologically relevant substrates will be discussed. The oxygen atom transfer reactivity has been probed by mass spectrometry and NMR spectroscopy. The presented complexes aide in highlighting the effect redox state of the dithiolene ligand has in modulating reactivity.

CHAPTER 1. BASIC DONOR-ACCEPTOR SYSTEMS USING DITHIONE LIGANDS

1.1 Donor Acceptor Systems

Molecular donor-acceptor systems are of great interest in the chemical and materials science field. Such systems are generally composed of a "donor" and an "acceptor", where an electron can be transferred from one unit to another of a molecule. Typically such systems have been organic-based, and exhibit intramolecular charge transfer (ICT), where the charge transfer moves from a donor to the acceptor along a π conjugated system such as benzene or stilbene.[1-4] Such systems have uses in classical molecular engineering designs and can be useful in the development of light-emitting diodes and sensors.[5, 6] Inorganic-based systems incorporating organic ligands have gained interest in recent years due to the charge transfer capabilities of such complexes. Donor-acceptor systems that generate a charge transfer are of interest due to their potential applications, such as artificial photosynthesis and non-linear optics (NLO).[7-16] Charge-transfer transitions such as metal-ligand (MLCT) and ligand-metal (LMCT) charge transfers are common examples of charge transfers in coordination complexes.[17] When the ligand environment surrounding the metal center is one that the ligands are in different oxidation states, it is possible to observe a intraligand charge transfer (ILCT).[18, 19] Such systems can be achieved through the use of non-innocent redox-active ligands, such as dithiolene.

1.2 Dithiolene Ligands

Dithiolene is a classic redox active, non-innocent ligand that can cycle between a fully reduced state (dithiolene) and a fully oxidized state (dithione) through two single-electron transfers (Figure 1.1). Jorgensen has defined a ligand 'innocent' when it allows the oxidation state of the metal in a

complex to be defined e.g. in $Cp_2W(CO)_2$ (where Cp is cyclopentadienyl ligand), W is in the +2 oxidation state.[20] Non-innocent behavior is dependent not just on the ligand but also on the metal center. 1,2-ene dithiolate (dithiolene)

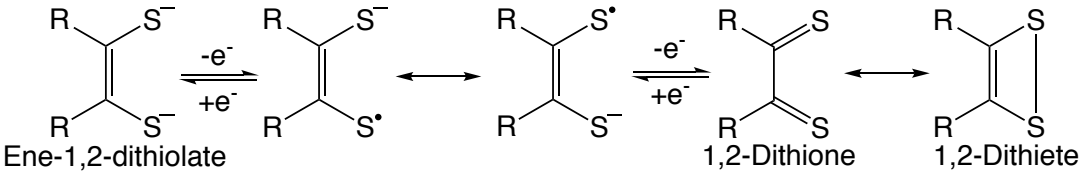

Figure 1.1. Oxidation states of dithiolene

ligands exhibit non-innocent behavior especially towards "soft" transition metal centers.[21, 22] They are involved in a high degree of covalent bonding with extensive delocalization of electron density.[23-31] Dithiolene ligands of varying oxidation state, from fully reduced dithiolate to fully oxidized dithioketone (dithione) form, can coordinate a metal ion. There is a multitude of metal-dithiolene complexes possessing either a single, two, or three dithiolene ligands.

1.3 Dithiolene Ligands in Donor-Acceptor Systems

In terms of donor-acceptor systems, a fully reduced dithiolene, which is electron rich, can act as an electron donor to a metal center; metallo-dithiolene complexes have been heavily studied due to their potential donor-acceptor applications such as; NLO, light-driven information devices, laser dyes, sensors and molecular superconductors.[32-38]

Nickel dithiolene complexes sparked interest in the sixties and their properties are still being explored in present day.[24, 25, 27, 29, 31, 39-41] These complexes have been shown to be very strong chromophores with intense charge transfers observed in the visible and NIR regions.[32] These complexes have sparked interest for commercial development (www.epolin.com) such as Q-switch dyes; these applications are reliant on the low energy charge transfer properties of nickel dithiolene complexes.[42-45]

While bis(dithiolene)-nickel complexes have been heavily studied, trigonal prismatic structures of neutral tris(dithiolene) V, Mo, W, Re complexes have also been heavily reported on in the sixties and seventies. [46-48] These diamagnetic complexes of general formula $[M(bdt)_3]$ (where, bdt^{2-} is benzene 1,2-dithiolate; M= Mo W, and V) were thought to contain formally, Mo(VI), W(VI) or "V(VI)" with a d^0 electronic configuration and three closed-shell dianionic dithiolato (2-) ligands. Recent studies on these classical complexes indicate that the proper description should include an oxidized ligand spin coupled with the metal e.g., for Mo in +5 oxidation state, underscoring the non-innocent nature of the dithiolene ligands.[49] Careful crystallographic analyses can highlight the subtle differences in the metric parameters. The redox states of the ligands can also be probed spectroscopically e.g., by vibrational spectroscopy (infrared, resonance Raman), ^{13}C NMR spectroscopy, and X-ray absorption spectroscopy.[27, 50-52] Similar analyses will be used to explore the complexes presented in the following chapters that are of general structure: $Mo^{IV}O(Dt^{2-})(Dt^0)$ (where Dt^{2-} = fully reduced dithiolene and Dt^0 = fully oxidized dithione) to explore their molecular, electronic, and redox properties.

1.4 Dithione Ligand Basics

As shown in Figure 1.1, the fully oxidized dithiolene ligand can exist in two forms; dithione or dithiete. The exact nature of the oxidized forms of the dithiolene moiety is dependent upon the redox orbital of the dithiolene from which the electrons are removed (Figure 1.2). Both dithione and dithiete can react with metal ions, but dithiete complexes behave similar to those of dithiolene. In contrast, the dithione complexes often remain as dithione and exhibit different reactivity and spectroscopic properties.

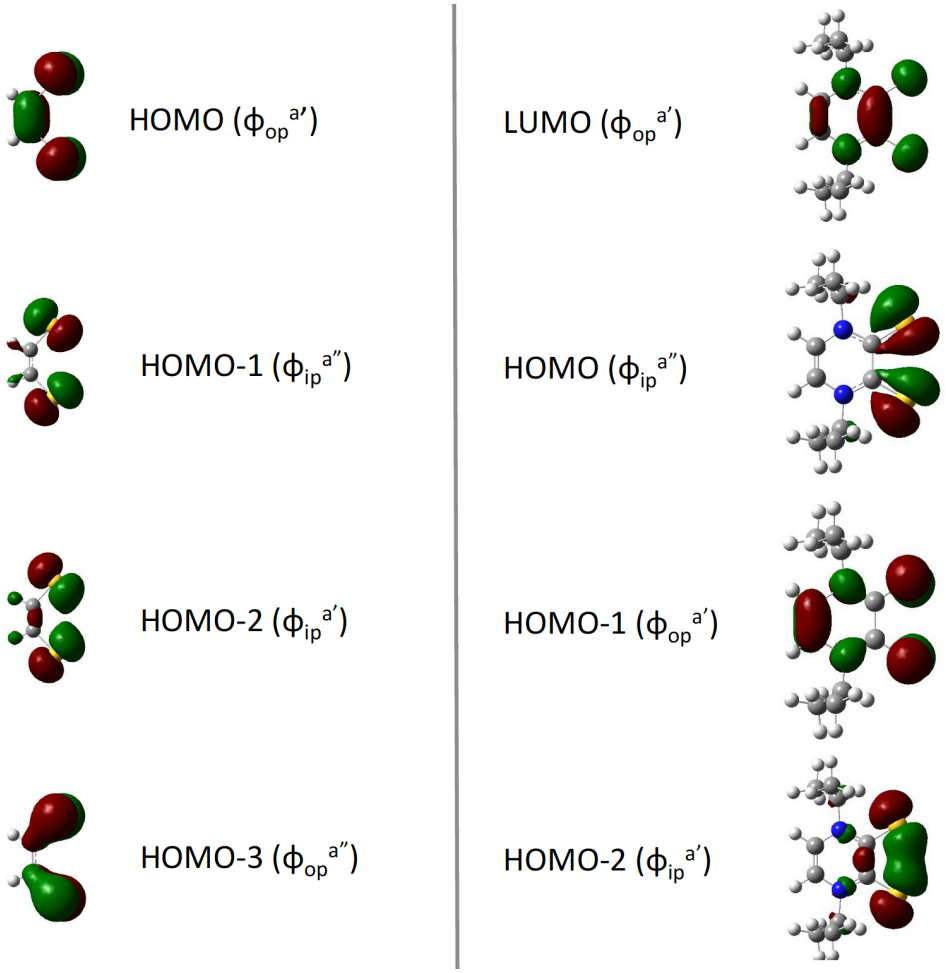

Figure 1.2. (Left) Frontier orbital of dithiolene compared to the frontier orbitals of $^{i}Pr_2Dt^0$ (Right). "Reprinted with permission from Yang, J.; Mogesa, B.; Basu, P.; Kirk, M. L., Large Ligand Folding Distortion in an Oxomolybdenum Donor-Acceptor Complex. *Inorg. Chem* **2016,** *55* (2), 785-793. Copyright 2016b American Chemical Society.

Despite the interest and the non-innocent nature of the dithiolene ligands, well-characterized metal complexes of fully oxidized dithione ligands are rare, and a majority of the research with fully oxidized ligands is focused on lower valent metal complexes. A Cambridge Crystallographic database search conducted on April, 17th, 2019 produced only 63 hits where at least one of the ligands is in two-electron oxidized dithione form, compared to ~2000 hits for the metal-dithiolene complexes, searched at the same time.[53] Therefore, the structure, spectroscopic features and reactivity of metal-dithione complexes are more explored. More importantly, the metal complexes

of the oxidized ligand afford interesting fundamental chemistry that may be important in niche applications and generating new knowledge. In the subsequent section, we will highlight some of the novel chemistry.

The synthesis of a dithione molecule was reported in early seventies.[54, 55] α-Dithiones are known to exist in equilibrium with its valence tautomer 1,2-dithiete and electro-withdrawing substituents on the sp^2 carbon favor the dithiete form.[56] Commonly studied dithione complexes that exhibit donor-acceptor properties are d^8 metals possessing two dithione ligands with the expected square planar geometry for the d^8 electronic configuration, similar to that observed for the reduced dithiolene complexes.[45, 57-65] The electronic properties of the square planar d^8 dithiolene complexes depend upon the distribution of the π electrons in the $M(C_2S_2)_2$ units. The nature of the substituents at the C_2S_2 moieties determines the stabilization of the $M(C_2S_2)_2$ complex with an overall charge that varies between +2 and –2. These limits are due to the isolated frontier molecular orbitals, which have π character and can either be empty (in the case of dithione) or populated (in the case of dithiolene). These dithiooxamide systems were mainly used as ion-paired charge-transfer complexes between cationic and anionic complexes. These charge-transfer salts show strong near-IR transitions, [66] similar to those reported for the complexes with fully reduced dithiolene ligands.[67] [68] Commonly studied dithione ligands are thioamide derivatives 2,3-piperazinedithiones.[69] Complexes possessing *N,N'*-dimethylpiperazine-2,3-dithione (Me_2Dt^0) and *N,N'*-diisopropyl-2,3-dithione ($^iPr_2Dt^0$) will be discussed in the following sections.

Our group has reported on a neutral Mo tetracarbonyl complex coordinated by a single dithione ligand, $Mo(CO)_4(Me_2Dt^0)$, exhibits negative solvatochromism. Density functional theory (DFT) calculations demonstrated the energetically isolated lowest unoccupied molecular orbital (LUMO) is practically a pure π* orbital, localized on the C=S fragment of the dithione ligand. This

energetically isolated LUMO accepts electron density from orbitals, comprised of the metal, carbonyl ligands and the S donors of the dithione ligand. This transition gives rise to a solvent sensitive band at ~600 nm.[70] A corresponding W complex, $W(CO)_4(Me_2Dt^0)$ which exhibits an intense charge transition at 669 nm which much like the charge transfer in $Mo(CO)_4(Me_2Dt^0)$ is solvent sensitive and exhibits a negative solvatochromism. DFT and TD-DFT calculations predicted similar transitions as well; MLCT was observed in both complexes. The HOMO was predicted to be metal based while the LUMO was predicted to be dithione ligand.[71] In addition to the remarkable ability of forming complexes with localized π-electrons, that give rise to exciting optical properties, complexes with dithione ligands exhibit remarkable molecular features e.g., formation of a $[Ni(^iPr_2Dt^0)_3][PF_6]_3$ which is the only reported structure of an octahedral nickel complex possessing three fully oxidized dithione ligands.[53] The molecular structure of $[Ni(^iPr_2Dt^0)_3][PF_6]_3$ demonstrated that the dithione ligands remained in the fully oxidized state during synthesis and crystallization. $[Ni(^iPr_2Dt^0)_3][PF_6]_3$ exhibited longer Ni-S bond lengths (~0.2 Å) when compared to the molecular structure of $[Ni(^iPr_2Dt^0)_2][BF_4]_2$, this is attributed to a steric crowding of the nickel center when three dithione ligands are present. The electronic spectra of $[Ni(^iPr_2Dt^0)_3][PF_6]_3$ and $[Ni(^iPr_2Dt^0)_2][BF_4]_2$ exhibit different charge transfer transitions in the UV-Vis region; no NIR transitions were observed for either complex. $[Ni(^iPr_2Dt^0)_2][BF_4]_2$ exhibits two

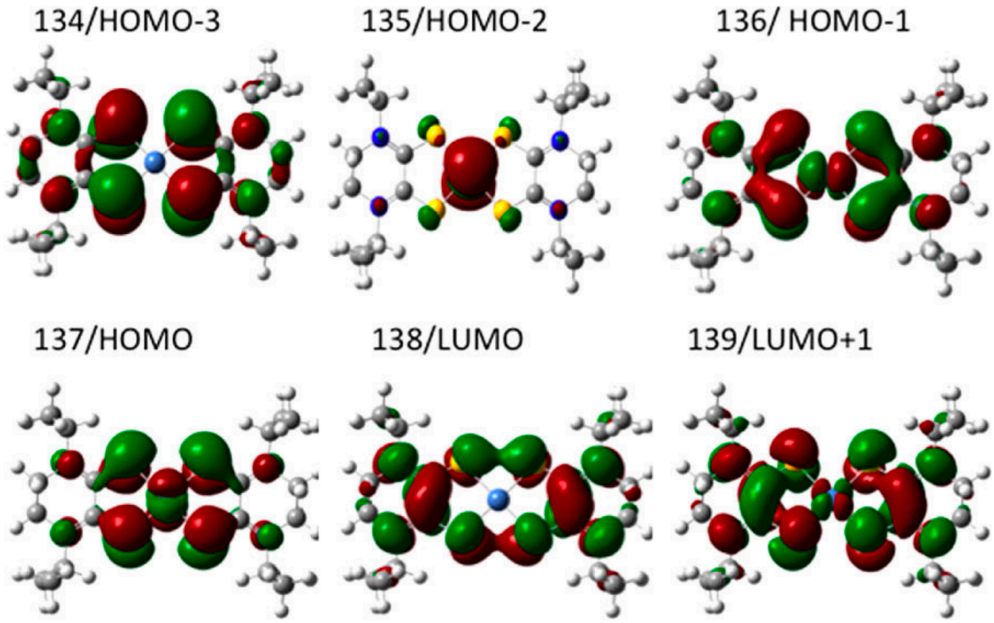

Figure 1.3. Predicted frontier molecular orbitals of $[Ni(^{i}Pr_2Dt^{0})_2]^{2+}$. "Reprinted with permission from Mogesa, B.; Perera, E.; Rhoda, H. M.; Gibson, J. K.; Oomens, J.; Berden, G.; van Stipdonk, M. J.; Nemykin, V. N.; Basu, P., Solution, Solid, and Gas Phase Studies on a Nickel Dithiolene System: Spectator Metal and Reactor Ligand. *Inorg. Chem.* **2015,** *54* (16), 7703-7716. Copyright 2015 American Chemical Society."

intense low energy transitions (604 nm, 5690 $M^{-1}cm^{-1}$ and 540 nm, 4830 $M^{-1}cm^{-1}$). DFT calculations showed that the HOMO, HOMO-1, and HOMO-2 are mainly is nickel d orbital in character whereas the LUMO is primarily dithione ligand based while the LUMO +1 and LUMO +2 exhibit more nickel $d_{x^2-y^2}$ character (Figure 1.3). This would result in a MLCT band in the UV-Vis spectrum of $[Ni(^{i}Pr_2Dt^{0})_2][BF_4]_2$ in the low energy region and intraligand and nickel d-d transitions at higher energies which was further supported by TD-DFT calculations. As mentioned earlier, d^8 metal complexes possessing fully oxidized dithione ligands exhibit similar electronic properties to those of complexes possessing fully reduced dithiolene ligands. $[Ni(^{i}Pr_2Dt^{0})_3][PF_6]_3$ on the other hand exhibited an intense transition at 413 nm (4674 $M^{-1}cm^{-1}$) and a weak band at 750 nm (337 $M^{-1}cm^{-1}$). DFT calculations supported a Ni^{2+} electronic state (paramagnetic) and a nickel

composed SOMO and SOMO-1of the α state and SOMO-4 and SOMO-5 of the β state and the LUMO and unoccupied MOs were dithione ligand based resulting in low energy d-d transitions and a higher energy MLCT transition.[72] Bigoli et. al have presented a similar nickel dithione complex: $[Ni(Me_2Dt^0)_2][BF_4]_2$ which exhibits similar UV-Vis transitions to that of $[Ni(^iPr_2Dt^0)_2][BF_4]_2$, two strong transitions at 540 nm (4000 $M^{-1}cm^{-1}$) and 605 nm (4000 $M^{-1}cm^{-1}$). DFT calculations showed, that much like the $^iPr_2Dt^0$ nickel complex the HOMO and HOMO-1 molecular orbitals are composed of metal frontier orbitals and the LUMO is virtually purely dithione ligand based resulting in MLCT transtions.[73]

It has also been demonstrated that fully oxidized dithione ligands can stabilize an unique low coordinate Mo-cluster; $[(^iPr_2Dt^0)Mo]_4[BF_4]$. The cluster is formed from $[MoO(BF_4)(^iPr_2Dt^0)_2][BF_4]$ and $[MoOCl(^iPr_2Dt^0)_2][MoOCl_4]$ which were the first examples of oxo-Mo(IV) complexes possessing two dithione ligands. $[MoOCl(^iPr_2Dt^0)_2][MoOCl_4]$ was reacted with silver tetrafluoroborate forming $[MoO(BF_4)(^iPr_2Dt^0)_2][BF_4]$ which when in a solution of pyridine formed the cluster $[^iPr_2Dt^0)Mo]_4[BF_4]$. $[MoOCl(^iPr_2Dt^0)_2][MoOCl_4]$ and $[MoO(BF_4)(^iPr_2Dt^0)_2][BF_4]$ exhibit a low energy transition between 718 nm - 741 nm that was proposed to be d-d transitions. Typically, such a transition is not observed in monooxo-Mo(IV) complexes possessing two fully reduced dithiolene ligands. DFT calculations of $[MoOCl(^iPr_2Dt^0)_2]^+$ showed that the LUMO and LUMO+1 are dithione ligand based. TD-DFT demonstrated the low energy transition is MLCT in character. Electron density maps of the transition demonstrated that instead of the metal donating an electron to a single acceptor dithione ligand the electron density is delocalized over both dithione ligands. [74]

1.5 Mixed Ligand Systems

Complexes that possess both a fully oxidized and fully reduced dithiolene ligand have also been presented that result in electronically asymmetric complexes. Electronically asymmetric square planar complexes with a d^8 metal ion possessing dithiolene ligands in different oxidation states result in a ground state that is π delocalized and such a complex can act as a donor-acceptor system much like their electronically symmetric counterparts [M(II)(Et_2dazdt)(mnt)] (where M= Ni, Pd, or Pt; Et_2dazdt = N,N'diethylperhyrodiazepine-2,3-dithione) is an example of such a system. All three complexes exhibit either one or two low energy, strong charge transitions in the UV-Vis region. From DFT and TD-DFT calculations the low energy transitions were attributed to mixed metal-ligand-to-ligand charge transfer (MMLL'CT); such transitions have been indicated in NLO properties such as molecular hyperpolarizability.[8, 11, 75]

In complexes where one dithione and one dithiolene ligand coordinate to the metal ion, the C_2S_2 unit from the dithiolene serves as an electron-donor, while the C_2S_2 unit from fully oxidized ligand accepts electron density, resulting in LL'CT bands. Electron-donating substituents on the dithione raises the energy of the LUMO and to some extent of that of the HOMO.[63] In general, the π-acceptor nature of the dithione ligand favors the formation of low-valent complexes while the reduced form of the ligand stabilizes higher valent complexes. Despite this, it has now been shown that higher valent e.g., Mo(IV) complexes can be stabilized by the fully oxidized ligand.[74, 76] An electronic asymmetry can also be induced with a single fully oxidized dithione ligand and two thiophenol ligands as observed in $Mo^{IV}O(SPh)_2(^iPr_2Dt^0)$ where SPh = thiophenol. This complex was synthesized from $[MoOCl(^iPr_2Dt^0)_2][PF_6]$ through a ligand exchange reaction with SPh. The

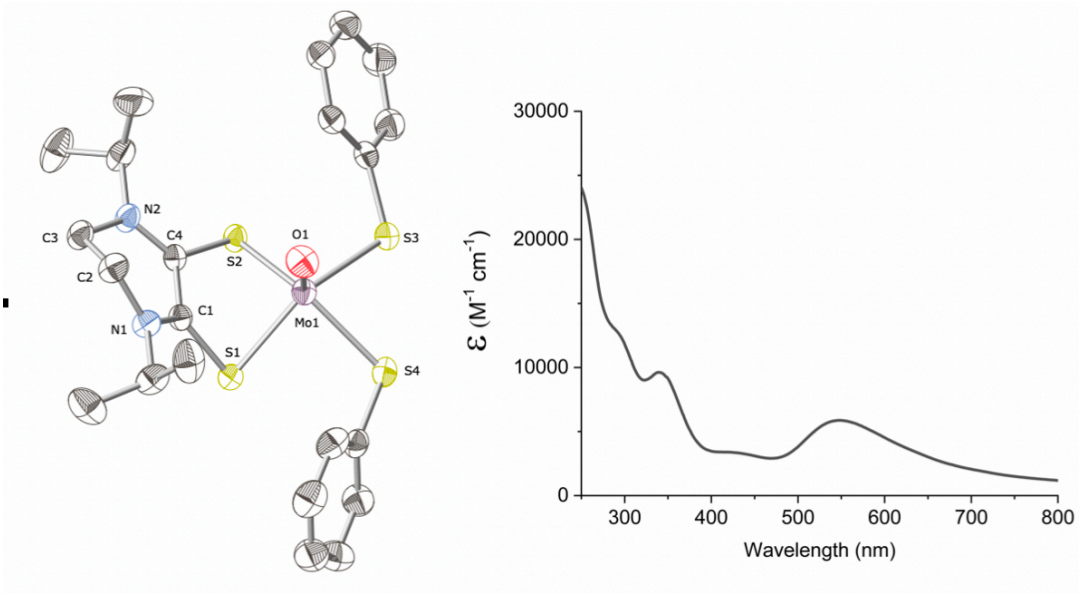

Figure 1.4. (Left) Thermal ellipsoid (40%) plot of $MoO(SPh)_2(^iPr_2Dt^0)$. Hydrogen atoms are omitted for clarity. (Right) Absorbance spectrum of $MoO(SPh)_2(^iPr_2Dt^0)$ in CH_3CN.

UV-Vis spectra of $Mo^{IV}O(SPh)_2(^iPr_2Dt^0)$ exhibited a shift in the low energy band of $[MoOCl(^iPr_2Dt^0)_2][PF_6]$ at ~ 750 nm to ~540 nm, a nearly 200 nm difference in energy. An interesting structural feature was observed when the molecular structure was resolved; a large fold angle along (~70°) the S•••S vector of the dithione ligand was observed (Figure 1.4). Such a large fold angle is not typically in Mo(IV) dithiolene complexes.[77-79] Resonance Raman and DFT calculations indicated that the fold angle and the charge transfer transition were due to a pseudo-Jahn Teller effect and the electron deficient dithione ligand was folding towards the Mo=O moiety which results in an overlap of the out of plane S orbitals of the dithione ligand to overlap with the electron rich S orbital of the thiophenol ligand thus inducing a LL'CT transition observed at ~540 nm. DFT calculations showed a different electronic structure that has been observed in complexes possessing ligands in the same oxidation state. In $Mo^{IV}O(SPh)_2(^iPr_2Dt^0)$ the HOMO is primarily SPh ligand character and the LUMO is dithione ligand in character i.e. the dithione is acting as the "acceptor" and accepting electron density from the "donor" SPh ligand resulting in a LL'CT

transition.[80] We will be examining the electronic structure of Mo(IV)-dithiolene complexes that possess a fully oxidized and fully reduced dithiolene ligands to understand the effects such a system play on the charge transfer properties of such a system.

1.6 Biological systems

1.6.1 Molybdopterin Enzymes

While donor-acceptor systems possessing dithiolene ligands have been popular in materials applications, dithiolene ligands also play a vital role in biological systems due to their inclusion in the molybdenum cofactor (Moco) which is found in molybdopterin enzymes. Molybdenum is the only second row transition metal found in biologically relevant enzymes and molybdopterin enzymes are found in all phyla of life. They catalyze reactions that are vital in life processes, such as cycling of S, As, C, N, and Se; all molybdopterin enzymes possess the fascinating catalytic center Moco. Moco is made up of three redox active groups: a pyranopterin unit, a dithiolene ligand and the molybdenum metal center

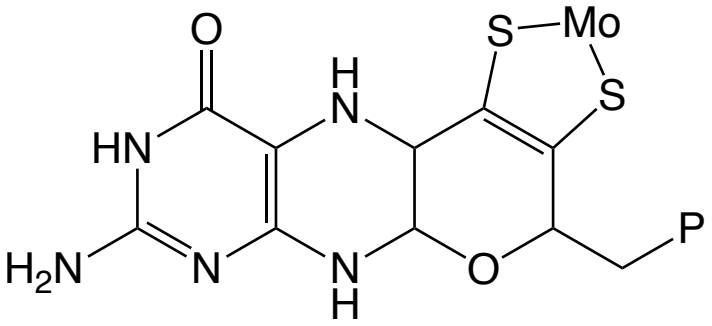

P=Phosphate or dinucleotide

Figure 1.5. General structure of the molybdenum cofactor, present in all molybdopterin enzymes.

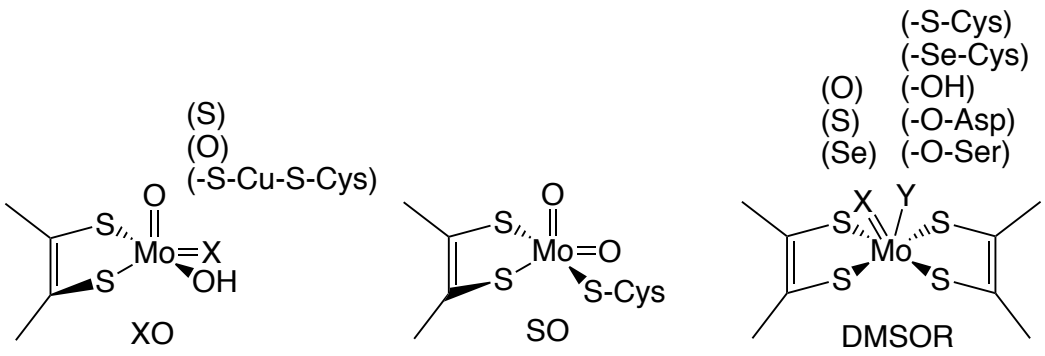

Figure 1.6. Figure 1.6. First coordination sphere of the three molybdopterin enzyme families.

that all must work in concert during the course of catalysis (Figure 1.5). Currently, 50 Moco-containing enzymes have been identified and categorized into three families: xanthine oxidase (XO), sulfite oxidase (SO), and DMSO reductase (DMSOR). The enzyme families are classified by differences in the first coordination sphere, sequence homology, and types of reactions catalyzed (Figure 1.6). Both the XO and SO family enzymes possess a single molybdopterin group whereas the DMSOR family possess two molybdopterin groups.[81] While the general structure of Moco has been ascertained in part, through protein X-ray crystallography, due to the lower resolution of protein crystal structures, details such as the oxidation state of the redox-active ligands coordinated to the molybdenum metal center cannot be determined. [81-84] While there are still uncertainties about the details of the Moco's structure, it has been established that the 1,2-ene dithiolene ligand is at the catalytic center of all pterin containing Mo and W enzymes.[81, 85] While protein crystallography cannot unequivocally differentiate different redox states of the ligand, some of the protein structures have been interpreted to possess oxidized ligands (e.g., dithione), highlighting the potential for ligand-based redox reactions.[84, 86, 87]

The majority of the reactions catalyzed by molybdopterin enzymes are oxygen atom transfer (OAT) reactions, which are concomitant with a two-electron transfer. The three units comprising Moco are all capable of redox activity and existing in various oxidation states (Figure

1.7). The roles that the three redox active units of the cofactor play in the OAT reaction or the transfer of electrons during the regeneration steps remain unclear.[32, 81, 85, 88-90] A fundamental understanding of the chemistry of this cofactor is essential for a comprehensive understanding of vital life processes. Currently the function of these three redox active units in the electron transfer is unclear.

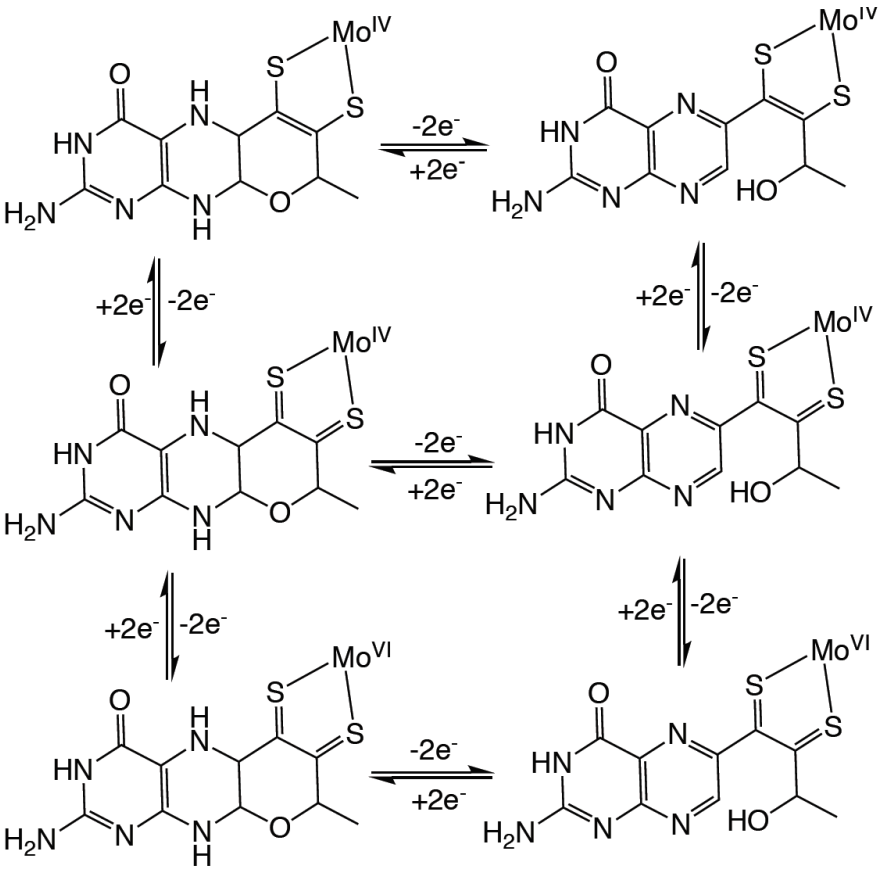

Figure 1.7. Potential oxidation states of the different components that make up the molybdenum cofactor. "Reprinted from reference 119 with permission from The Royal Society of Chemistry.

In order to study how the redox components, work together, it would be ideal to study the cofactor once removed from the protein environment. However, when the cofactor is removed from that environment, it is not stable and can easily be oxidized. Due to the delicate nature of the cofactor, researchers have studied the cofactor in the native protein environment. A commonly

studied molybdopterin enzyme is DMSOR due to the lack of secondary chromophoric cofactors such as iron-sulfur clusters.[83, 91, 92] A crystal structure of DMSOR from *Rhodobacter sphaeroides* (*Rs*) was refined at a resolution of 1.9 Å, and the authors determined that there were differing bond lengths along the S...S vector on the dithiolene ligands. From this crystal structure the authors hypothesized that the two dithiolene ligands coordinated to the molybdenum may be present in differing oxidation states.[84, 87, 93] Another crystal structure of *Rs* DMSOR was refined at a higher resolution, 1.3 Å, which lead to a similar observation of differing bond lengths along the S…S vector on the two dithiolene ligands.[83] However as mentioned, metric parameters of a protein structure must be considered with caution – even when the resolution is high, oxidation states of the ligands cannot be determined. Along with the crystal structure, the resonance Raman (rR) data on DMSOR enzyme suggest that the two dithiolene ligands are not equivalent, and we hypothesize that the inequivalency may be caused by the dithiolene ligands existing in different oxidation states.[81, 82, 94] The rR data indicated one of the dithiolenes appeared to be a discrete ene-dithiolate (fully reduced) and the other dithiolene is more π-delocalized in nature (oxidized by a single electron).[81, 94] The results are reminiscent of observations seen in the SO family and XO family. In the SO family, the dithiolene appears to be π delocalized whereas the XO family dithiolene appears to be a discrete enedithiolate.[81, 94, 95]

1.6.2 Role of Dithiolene in OAT reactions of DMSOR Enzymes

From reaction studies, it is proposed that the discrete ene-dithiolate pyranopterin ligand is involved in the transfer of electrons to or from Mo-center.[81] It has been proposed that the redox active orbitals in Moco are metal based and the non-innocent dithiolene actually behaves innocently and that the ene-dithiolate ligands stabilize the singlet ground state of reduced species which would facilitate two electron chemistry that is required for OAT reactions. The C=C bond

of the dithiolene orients the sulfur p orbitals that are out of plane which leads to π anisotropy in which the Mo d_{xz}/d_{yz} orbitals could interact with the dithiolene ligand orbitals. The anisotropy would lead to a destabilization of the Mo d_{xz}/d_{yz} in relation to the Mo $d_{x^2-y^2}$. This will lead to a stabilized singlet ground state.[3] Resonance Raman of *R. sphaeroides* dimethyl sulfoxide reductase and *E. coli* biotin sulfoxide reductase indicates that the pyranopterins are not equivalent; one of the dithiolene metal unit exhibited higher C=C bond character. This is similar to what is observed in sulfite oxidase; ie one pyranopterin is in the dihydro state (distal) and the other is in the tetrahydro state (proximal). Electron transfer would be probable to or from the Mo/W atom to the proximal pyranopterin not through the distal pterin. The proximal pyranopterin that would support electron transfer would exist in the tetrahydro state. Rothery et al propose that the proximal pyranopterin is inherently resistant to oxidation of the pyranopterin which would have a negative impact on catalysis.[2] In terms of the distal pyranopterin, a mechanism is possible that could modulate the Mo/W reduction potentials by protonation of N-5 an internal redox reaction between the piperazine ring and the dithiolene which would result in a monoanionic thiol-thione ligand. Such a ligand would decrease the net charge on the dithiolene ligand thereby shifting the Mo/W reduction potential to more positive. Stabilization of the thione sulfur that is attached to C3 could play a role in defining the geometry/reactivity through a trans effect/influence.[2, 4]

1.6.3 Proposed Reaction Mechanisms for the DMSOR Family of Enzymes

R. sphaeroides DMSOR has been studied using resonance Raman spectroscopy to understand the potential role the dithiolene ligand may play during catalysis. Resonance Raman was performed on multiple samples of DMSOR: as prepared Mo(VI), dithionite reduced (Mo(IV), DMS reduced Mo(IV), and glycerol-inhibited Mo(V). From this study, a catalytic scheme was proposed in which the oxidation state of the dithiolene ligands coordinated to the metal center did

not change during catalysis ie one is Dt^{1-} and the other is Dt^{2-}. The authors propose that catalytic activity is controlled through the sixth coordination site (oxo group). When the oxo group is lost this would lead to an increase in the Mo-S π bonding in the ene-dithiolate ligand and an increase in the π delocalization of the dithiolene ring. The different oxidation states of the dithiolene ligands would have an effect on the excited state/electronic properties of the enzymes. By examining excitation profiles of the Mo-S and dithiolene modes in DMSOR and human sulfite oxidase (SO possesses a π-delocalized dithiolene), the electronic transitions in DMSOR were assigned as follows:

1. The ene-dithiolate is responsible for the low energy electronic transitions (640 nm in dithionite-reduced Mo(IV), 720 nm Mo(VI) as the prepared enzyme) and can be assigned as thiolate-to-Mo charge-transfer band.
2. The π-delocalized dithiolene is responsible for the higher energy transitions (500 nm<) and have been assigned to and π dithiolene-to-Mo charge-transfer as well.[6]

Biotin sulfoxide reductase (BSO) from *R. sphaeroides* has been studied in a similar manner to that of DMSOR using resonance Raman. Resonance Raman spectroscopy was performed on as prepared and dithionite-reduced samples of BSO. Resonance Raman spectroscopy indicated that the dithiolene ligands exist in two distinct Mo(VI) states of BSO reductase; one is an ene-dithiolate and the second dithiolene has a greater π delocalization. Changes in the π delocalization could drive the Mo(IV) to Mo(VI) step of catalysis. This would mean one of the dithiolene ligands acts as a spectator ligand. One of the dithiolene ligands would need to undergo a change in the extent of the π-delocalization during reduction. A change in the π-delocalization of a single dithiolene ligand is believed to occur due to the fact that dithionite reduced BSO reductase only exhibits a single C=C stretching band but the authors were not able to make an assessment of the extent of

the delocalization.[7] These studies are a positive indication that when designing and synthesizing small molecule mimics of DMSOR Moco an electronically asymmetric dithiolene ligand environment should be considered.

1.6.4 Electronically Symmetric Small Molecule Mimics of Moco

One of the way researchers have been studying Moco is to design and synthesize small molecules. Previously, researchers have utilized molybdenum complexes that possess two dithiolene ligands that are fully reduced; i.e electronically symmetrical complexes. Commonly studied ligands include maleonitrile dithiolate (mnt^{2-}), 1,2-benzene dithiolate (bdt^{2-}), toluene-3,4-dithiolate (tdt^{2-}), 2,3-quinoxaline dithiolate (qdt^{2-}), and 3,6-dichloro-1,2-benzene dithiolate (Cl_2bdt^{2-}).[89, 90, 96-101] Prior to refining the crystal structure of DMSOR, researchers were exploring symmetrical complexes possessing two dithiolene ligands. Electronically speaking these mimics may not be ideal and/or appropriate representations. The absorption spectra for fully oxidized DMSOR (Mo(VI)) features a charge transfer band near 700 nm and the fully reduced DMSOR (Mo(IV)) features a charge transfer (CT) band near 650 nm (Figure 1.8). These charge transfer bands may be ligand to ligand charge transfer bands (LLCT).[102]

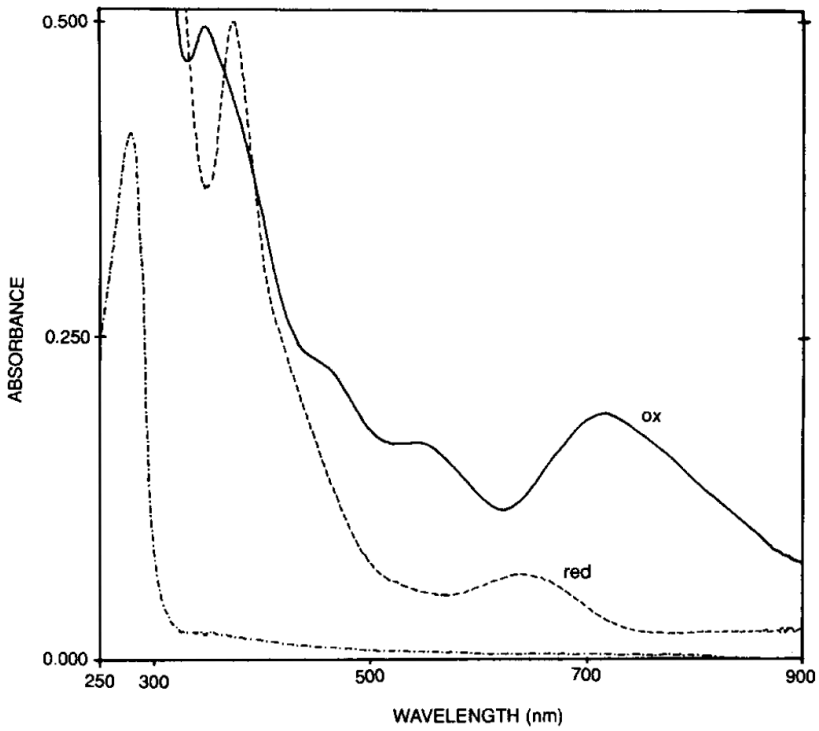

Figure 1.8. Absorption spectra of DMSOR. Top spectrum—fully oxidized enzyme (7.9 mg/mL) Middle spectrum-fully reduced enzyme (7.8 mg/mL) Bottom spectrum-fully oxidized enzyme (0.3mg/mL). "Reprinted with permission from Bastian, N. R. K., C.J; Barber, M.J; Rajagopalan, K.V, Spectroscopic Studies of the Molybdenum Containing Dimethyl Sulfoxide Reductase from *Rhodobacter sphaeroides*. *Journal of Biological Chemistry* **1991,** *266*, 45-51. Copyright 1991 American Society for Biochemistry and Molecular Biology.

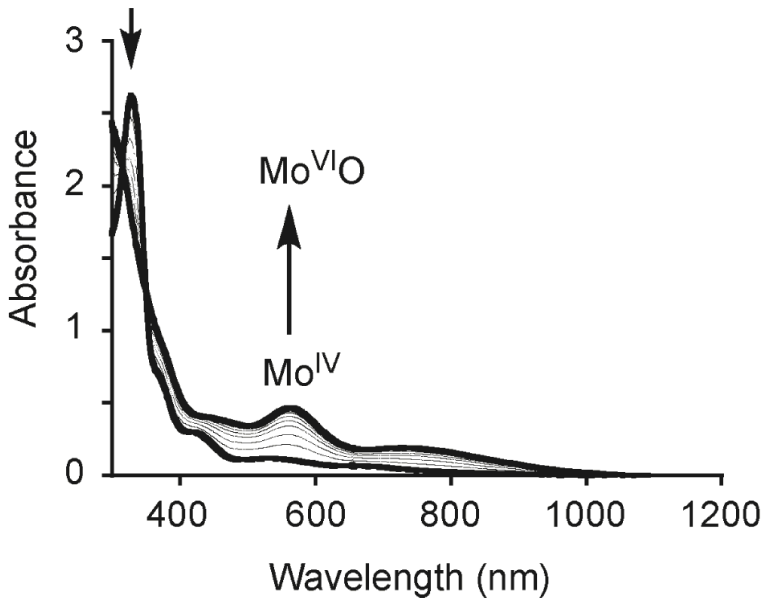

Figure 1.9. Changes in the absorbance spectrum of $[Mo(IV)(OSi^iPr_3)(S_2C_2\text{-}COOMe_2)_2]^{2-}$ during oxygen atom transfer to generate $[Mo(VI)O(OSi^iPr_3)(S_2C_2\text{-}COOMe_2)_2]^-$. "Reprinted with permission from Sugimoto, H. T., S; Suyama, K; Maiyake, H; Mtei, R.P; Itoh, S; Kirk, M.L;, Monooxomolybdenum (VI) Complexes Possessing Olefinic Dithiolene Ligands: Probing Mo-S Covalency Contributions to Electron Transfer in Dimethyl Sulfoxide Reductase Family Molybdoenzymes. *Inorg. Chem.* **2010**, 5368-5370. Copyright 2010 American Chemical Society.

In the case of $[Et_4N]_2[MoO_2(mnt)_2]$, which is a symmetrical dithiolene complex where the Mo-center is coordinated by two equivalent dithiolene ligands, only one absorption band at 525 nm is present in the fully oxidized Mo(VI) state. When the complex is reduced to $[Et_4N]_2[MoO(mnt)_2]$, this absorbance band disappears; there is no CT band observed for $[Et_4N]_2[MoO(mnt)_2]$.[100] More recently, Sugimoto et al. have reported Mo-dithiolene complexes of general formula; $[Mo(VI)O(OSiR_3)(Dt^{2-})_2]^-$. These complexes were generated from the corresponding desoxo Mo(IV) complex and were characterized by UV-Vis (Figure 1.9) and rR spectroscopy. The electronic spectra of the monooxo Mo(VI) complex is very similar to that of the fully oxidized DMSOR with two low energy bands near 563 nm and 800 nm. The rR data indicated a geometric inequivalence in the two dithiolene ligands. There were no low energy bands observed or geometric inequivalency in the dithiolene ligands for the desoxo Mo (IV) complex. The

similarities in absorbance spectra between $[Mo(VI)O(OSiR_3)(Dt^{2-})_2]^-$ and the fully oxidized DMSOR is a positive indication that an asymmetry in the dithiolene ligands is an important component for a successful model for DMSOR. Due to the lack of observed charge transfer band in the desoxo Mo(IV) complex the asymmetry of the dithiolene ligands may not be geometric in the native protein.[96, 103, 104]

1.6.5 OAT Reactivity of Small Molecule Mimics of Moco Possessing Fully Reduced Dithiolene Ligands

The OAT reactivity of electronically symmetric complexes of Moco has been heavily studied using biologically relevant substrate, trimethylamine-N-oxide (TMAO). In general, all complexes that possess two fully reduced dithiolene ligands react with TMAO and the reactions are tabulated in Table 1.1. It is not clear from previous reports whether or not these complexes react with other substrates such as dimethyl sulfoxide (DMSO) or nitrate (NO_3^-).[105-118] To our knowledge, only two electronically symmetric complexes, $[Mo^{IV}O(vdt)_2]^{2-}$ and $[Mo^{IV}O(ntdt)_2]^{2-}$ (where vdt is 4,5-dimethoxy-benzene-1,2-dithol and ntdt is 2-naphthyl-1,4-dithiolate) have exhibited OAT reactivity towards DMSO.[108, 109]

Sarkar et. al developed several asymmetric complexes to mimic the potential asymmetry that has been observed in the native enzymes: [Mo(IV)O(mnt)(DMED)] (where DMED= dimethylethylenedicarboxylate), [Mo(IV)O(mnt)(bdt)], and [Mo(IV)O(mnt)(tdt)] (define DMED).[111] These complexes react with TMAO producing trimethylamine (TMA). The HOMOs for all three complexes, calculated by density functional theory (DFT), were shown to be metal based. Computational studies demonstrated that the two dithiolene ligands controlled the Mo=O bond, which elongated during the reaction; similar results have been observed in native enzymes.[5] While these complexes are electronically asymmetric in the fact that two different dithiolene ligands have been utilized, the oxidation states of the ligands are still fully reduced. The OAT

reactivity and electronic properties of small molecule mimics of Moco possessing fully oxidized dithione ligands has not been studied in detail. We hypothesize that, through modulation of the oxidation state of the redox active components that comprise the cofactor, the electronic structure and charge state of the Mo center can be tuned for substrate catalysis.[119]

Table 1.1. Previously reported OAT reactions of $[Mo(IV)O(Dt^{2-})_2]^{2-}$

OAT Reactions with TMAO	**Reference**
$[Mo^{IV}O(DMED)_2]^{2-} + TMAO \rightarrow [Mo^{VI}O_2(DMED)_2]^{2-} + TMA$	106, 107, 110
$[Mo^{IV}O(mnt)_2]^{2-} + TMAO \rightarrow [Mo^{VI}O_2(mnt)_2]^{2-} + TMA$	106, 107
$[Mo^{IV}O(mnt)(DMED)]^{2-} + TMAO \rightarrow [Mo^{VI}O_2(mnt)(DMED)]^{2-} + TMA$ $[Mo^{IV}O(mnt)(bdt)]^{2-} + TMAO \rightarrow [Mo^{VI}O_2(mnt)(bdt)]^{2-} + TMA$ $[Mo^{IV}O(mnt)(tdt)]^{2-} + TMAO \rightarrow [Mo^{VI}O_2(mnt)(tdt)]^{2-} + TMA$	111
$[Mo^{IV}O(bdt)_2]^{2-} + TMAO \rightarrow [Mo^{VI}O_2(bdt)_2]^{2-} + TMA$	105, 106
$[Mo^{IV}O(Ph_3Si\text{-}bdt)_2]^{2-} + TMAO \rightarrow [Mo^{VI}O_2(Ph_3Si\text{-}bdt)_2]^{2-} + TMA$	120
$[Mo^{IV}O(DMED)(bdt)]^{2-} + TMAO \rightarrow [Mo^{VI}O_2(DMED)(bdt)]^{2-} + TMA$ $[Mo^{IV}O(DMED)(bdtCl_2)]^{2-} + TMAO \rightarrow [Mo^{VI}O(DMED)(bdtCl_2)]^{2-} + TMA$	112
$[Mo^{IV}O(tdt)_2]^{2-} + TMAO \rightarrow [Mo^{VI}O_2(tdt)_2]^{2-} + TMA$ $[Mo^{IV}O(Ph_3Si\text{-}tdt)_2]^{2-} + TMAO \rightarrow [Mo^{VI}O_2(Ph_3Si\text{-}tdt)_2]^{2-} + TMA$	120
$[Mo^{IV}O(S_2C_2(CONH_2)_2)_2]\bullet 0.5(i\text{-}PrOH)\ \bullet DMF]^{2-} + TMAO \rightarrow [Mo^{VI}O_2(S_2C_2(CONH_2)_2)_2]\bullet 0.5(i\text{-}PrOH)\ \bullet DMF]^{2-} + TMA$	110
$[Mo^{IV}O(1,2\text{-}S_2\text{-}3,6\text{-}(Ph_3CCONH)_2C_6H_2)_2]^{2-} + TMAO \rightarrow [Mo^{VI}O_2(1,2\text{-}S_2\text{-}3,6\text{-}(Ph_3CCONH)_2C_6H_2)_2]^{2-} + TMA$	113
$[Mo^{IV}O(1,2\text{-}S_2\text{-}3,6\text{-}(CH_3CONH)_2C_6H_2)_2]^{2-} + TMAO \rightarrow [Mo^{VI}O_2(1,2\text{-}S_2\text{-}3,6\text{-}(CH_3CONH)_2C_6H_2)_2]^{2-} + TMA$ $[Mo^{IV}O(1,2\text{-}S_2\text{-}3,6\text{-}(CF_3CONH)_2C_6H)_2]^{2-} + TMAO \rightarrow [Mo^{Vi}O_2(1,2\text{-}S_2\text{-}3,6\text{-}(CF_3CONH)_2C_6H)_2]^{2-} + TMA$ $[Mo^{IV}O(1,2\text{-}S_2\text{-}3,6\text{-}(^tBuCONH)_2C_6H_2)_2]^{2-} + TMAO \rightarrow [Mo^{VI}O_2(1,2\text{-}S_2\text{-}3,6\text{-}(^tBuCONH)_2C_6H_2)_2]^{2-} + TMA$ $[Mo^{IV}O(1,2\text{-}S_2\text{-}3,6\text{-}(Ph_3CCONH)_2C_6H_2)_2]^{2-} + TMAO \rightarrow [Mo^{VI}O_2(1,2\text{-}S_2\text{-}3,6\text{-}(Ph_3CCONH)_2C_6H_2)_2]^{2-} + TMA$	114
$[Mo^{IV}O(1,2\text{-}S_2\text{-}3,6\text{-}(^tBuCONH)_2C_6H_2)_2]^{2-} + TMAO \rightarrow [Mo^{VI}O_2(1,2\text{-}S_2\text{-}3,6\text{-}(^tBuCONH)_2C_6H_2)_2]^{2-} + TMA$ $[Mo^{IV}O(1,2\text{-}S_2\text{-}3,6\text{-}(Ph_3CCONH)_2C_6H_2)_2]^{2-} + TMAO \rightarrow [Mo^{VI}O_2(1,2\text{-}S_2\text{-}3,6\text{-}(Ph_3CCONH)_2C_6H_2)_2]^{2-} + TMA$	
$[Mo^{IV}O(1,2\text{-}S_2\text{-}3\text{-}^tBuNHCOC_6H_3)_2]^{2-} + TMAO \rightarrow [Mo^{VI}O_2(1,2\text{-}S_2\text{-}3\text{-}^tBuNHCOC_6H_3)_2]^{-2} + TMA$	115

Table 1.1 (cont.)

$[Mo^{IV}O(1,2\text{-}S_2\text{-}3,6\text{-}((4\text{-}^tBuC_6H_4)_3CCONH]_2C_6H_2)_2]^{2-}$ + TMAO → $[Mo^{VI}O_2(1,2\text{-}S_2\text{-}3,6\text{-}((4\text{-}^tBuC_6H_4)_3CCONH]_2C_6H_2)_2]^{2-}$ + TMA $[Mo^{IV}O(1,2\text{-}S_2\text{-}3\text{-}^tBuCONHC_6H_3)_2]^{2-}$ + TMAO → $[Mo^{VI}O_2(1,2\text{-}S_2\text{-}3\text{-}^tBuCONHC_6H_3)_2]^{2-}$ + TMA $[Mo^{IV}O(1,2\text{-}S_2\text{-}3\text{-}CH3CONHC6H3)_2]^{2-}$ + TMAO → $[Mo^{VI}O_2(1,2\text{-}S_2\text{-}3\text{-}CH3CONHC6H3)_2]^{2-}$ + TMA $[Mo^{IV}O(1,2\text{-}S_2\text{-}3\text{-}CF3CONHC6H3)_2]^{2-}$ + TMAO → $[Mo^{VI}O_2(1,2\text{-}S_2\text{-}3\text{-}CF3CONHC6H3)_2]^{2-}$ + TMA $[Mo^{IV}O(1,2\text{-}S_2\text{-}3\text{-}Ph3CCONHC6H3)_2]^{2-}$ + TMAO → $[Mo^{VI}O_2(1,2\text{-}S_2\text{-}3\text{-}Ph3CCONHC6H3)_2]^{2-}$ + TMA $[Mo^{IV}O\{1,2\text{-}S_2\text{-}3\text{-}(4\text{-}^tBuC_6H_4)_3CCONHC_6H_3)_2]^{2-}$ + TMAO → $[Mo^{VI}O_2(1,2\text{-}S_2\text{-}3\text{-}(4\text{-}^tBuC_6H_4)_3CCONHC_6H_3)_2]^{2-}$ + TMA	116
$[Mo^{IV}O(qpdt)_2]^{-2}$ + TMAO → $[Mo^{VI}O_2(qpdt)_2]^{2-}$ + TMA	117
$[Mo^{IV}O(1,2\text{-}S_2\text{-}3\text{-}PhNHCOC_6H_3)_2]^{2-}$ + TMAO → $[Mo^{VI}O(1,2\text{-}S_2\text{-}3\text{-}PhNHCOC_6H_3)_2]^{2-}$ + TMA	118
OAT Reactions with DMSO	
$[Mo^{IV}O(vdt)_2]^{2-}$ + DMSO→ $[Mo^{VI}O_2(vdt)_2]^{2-}$ + DMS	108
$[Mo^{IV}O(ntdt)_2]^{2-}$ + DMSO → $[Mo^{VI}O(ntdt)_2]^{2-}$ + DMS	109
OAT Reactions with HSO_3^-	
$[Mo^{IV}O(mnt)_2]^{2-}$ + HSO_3^- → $[Mo^{VI}O_2(S_2C_2(CN)_2)_2]^{2-}$ + HSO_4^-	100
DMED= 1,2-dicarbomethoxyethylene-1,2-dithiolate mnt= maleonitirledithiolate bdt= 1,2-benzenedithiolate Ph_3Si-bdt=3-(triphenylsilyl)-1,2-benzenedithiolato tdt= toluene-3,4-dithiol Ph_3Si-tdt= 5-(triphenylsilyl)-3,4-benzenedithiolato $S_2C_2(CONH_2)_2$= 1,2-dicarbamoylethylene-1,2-dithiolate vdt= 4,5-dimethoxy-benzene-1,2-dithol qpdt = pyranoquinoxalinedithiolene ntdt= 2-naphthyl-1,4-dithiolate	

Asymmetric monooxo Mo complexes possessing dithiolene ligands have been designed that possess a fully oxidized dithione ligand and a fully reduced dithiolene ligand to generate an asymmetry in the dithiolene ligands. These novel mixed ligand complexes will further the understanding of how Moco functions in the molybdopterin enzymes. Studying small molecule mimics of Moco will enhance fundamental science foundations and increase our knowledge of these vitally important enzymes.

CHAPTER 2. SYNTHETIC METHODS

2.1 Introduction

Monooxo-Mo(IV) dithiolene complexes were first synthesized in the 1960's by McCleverty et al., where they reported the synthesis of $[Mo^{IV}O(S_4C_4(CN)_4]^{2-}$. The synthesis was accomplished following Scheme 2.1 from the starting material $[Mo_7O_{24}]^{6-}$.[121] These complexes possess two fully reduced dithiolene ligands and are of general structure: $[Mo^{IV}O(Dt^{2-})_2]^{2-}$, where Dt^{2-} is a fully reduced dithiolene ligand. As shown in Scheme 2.1, $[Mo^{IV}O(Dt^{2-})_2]^{2-}$ complexes are typically synthesized through oxo-molybdenum starting materials such as $MoOCl_3$, $[MoOCl(MeNC)_4]^+$, and MoO_2Cl_2.[89, 100, 101, 113, 115, 122-127]

Scheme 2.1

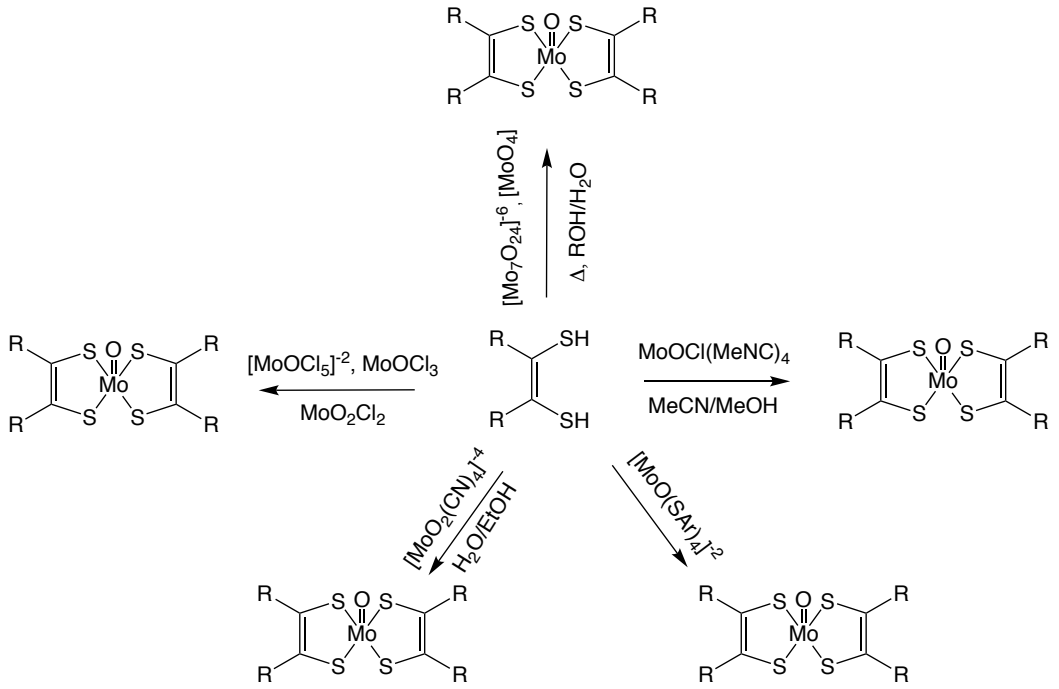

Another commonly used monooxo molybdenum starting material is $[MoO(S_8)]^{2-}$ which can be reacted with an acetylene-containing ligand or benzene-1,2-dithiol; (Scheme 2.2).[97, 128-131]

Scheme 2.2

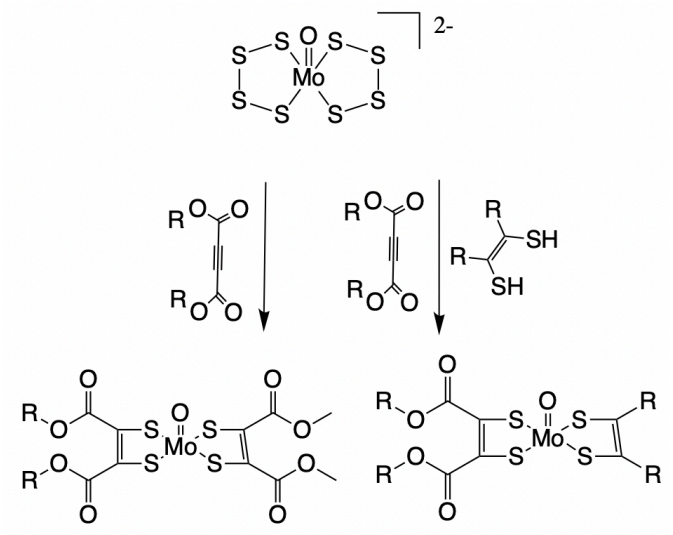

Scheme 2.3

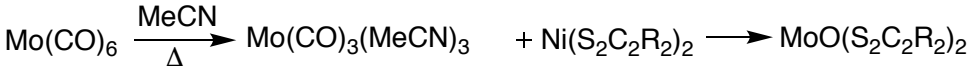

Finally, researchers have shown that non-oxo starting materials can be utilized to synthesize $[Mo^{IV}O(Dt^{2-})_2]^{2-}$ by using a carbonyl based starting material, $Mo(CO)_6$ and a nickel dithiolene complex as shown in Scheme 2.3.[90, 132, 133] Several of these starting materials were utilized in attempts to synthesize complexes of the following general structure: $MoO(Dt^{2-})(Dt^{0})$ where Dt^{0}= a fully oxidized dithione ligand (Scheme 2.4).

Scheme 2.4

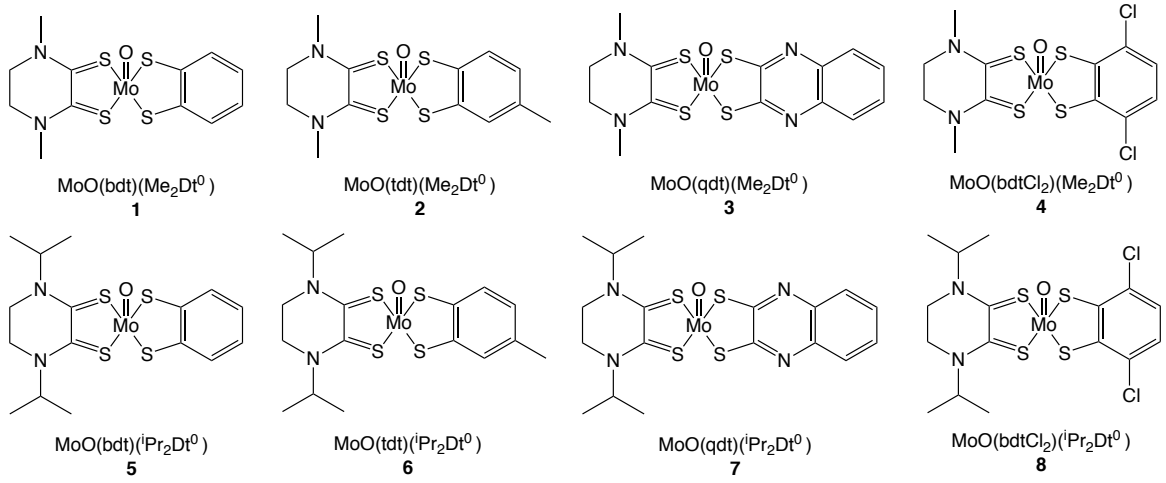

2.2 Materials and Methods

2.2.1 Materials

All reagents and solvents were purchased from either Sigma Aldrich or Thermo Fisher Scientific and used as received without further purification. All work was carried out under an inert atmosphere either in a dry box or using Schlenk line techniques under argon. $[MoOCl(^{i}Pr_2Dt^0)_2][PF_6]$, $[MoOCl(Me_2Dt^0)_2][PF_6]$[76], *N,N'*-diisopropylpiperazine-2,3-dithione ($^{i}Pr_2Dt^0$), and *N,N'*-dimethylpiperazine-2,3-dithione (Me_2Dt^0)[69] were synthesized following literature procedures.

2.2.2 Physical Methods

^{1}H NMR spectra were recorded on either a Bruker 500 MHz Avance spectrometer or a Bruker 400 MHz Avance spectrometer in air-tight NMR tubes. Infrared spectroscopy (FTIR) was recorded using a Thermofisher Nicolet iS10 spectrometer at room temperature using a KBr pellet. Electronic absorbance spectra were collected on a Shimadzu UV-3600 Plus in a quartz cuvette.

2.2.3 Syntheses of Complexes

MoO(bdt)(Me_2Dt^0) (1)

[MoOCl(Me_2Dt^0)$_2$][PF_6] (0.20 g, 0.000312 moles) was dissolved in 9 mL of acetonitrile generating a dark blue solution. A solution of benzenedithiol (0.063 g, 0.00034 moles) and triethylamine (0.069 g, 0.00068 moles) in 1.5 mL of acetonitrile was added dropwise to the dark blue solution initiating an instantaneous color change to dark purple and the release of white vapor (HCl). The reaction mixture was stirred for one hour. The solution was filtered, and dark purple solid was collected. The crude product was washed with cold chloroform to obtain analytically pure product. Yield 56% (0.075 g, 0.000175 moles). Calcd (Expt) for $C_{12}H_{14}MoN_2OS_4$: C, 33.80 (33.95): H, 3.31 (3.34); N, 6.33 (6.57). ^{1}H NMR (CD_3CN): δ 3.77 (s, CH_3, 6H), 3.89 (m, CH_2, 2H), 4.18 (m, CH_2, 2H), 7.10 (dd, *J*= 5.8 Hz, 3.2 Hz, aromatic, 2H), 7.65 (dd, *J*= 5.8 Hz, 3.2 Hz, aromatic, 2H). FTIR(KBr, cm^{-1}): 1531 (vs, C(-N)S), 1354 (vs, C=S), 940 (s, Mo=O). UV-Vis (MeCN): λ_{max} (ε, $M^{-1}cm^{-1}$) 532 nm (4400).

MoO(tdt)(Me_2Dt^0) (2)

[MoOCl(Me_2Dt^0)$_2$][PF_6] (0.20 g, 0.000312 moles) was dissolved in 9 mL of acetonitrile generating a dark blue solution. A solution of toluene-3,4-dithiol (0.053 g, 0.00034 moles) and triethylamine (0.069 g, 0.00068 moles) in 1.5 mL of acetonitrile was added dropwise to the dark blue solution initiating an instantaneous color change to dark purple and the release of white vapor (HCl). The reaction mixture was stirred for one hour. The solution was filtered and dark purple solid was collected. The crude product was washed with cold chloroform to obtain analytically pure product. (0.079 g, 0.000164 mol). 52% Calcd (Expt) for $C_{13}H_{16}MoN_2OS_4$: C, 35.45 (35.44): H, 3.66 (3.74); N, 6.36 (6.24). ^{1}H NMR (CD_3CN): δ 2.34 (s, CH_3, 3H), 3.76 (s, CH_3, 6H), 3.86 (m, CH_2, 2H), 4.14 (m, CH_2, 2H), 6.92 (d, *J*= 7.87 Hz, aromatic 1H), 7.47 (s, aromatic, 1H), 7.51 (d,

J= 7.9 Hz, aromatic, 1H). FTIR(KBr, cm^{-1}): 1534 (vs, C(-N)S), 1355 (vs, C=S), 929 (s, Mo=O). UV-Vis (MeCN): λ_{max} (ε, $M^{-1}cm^{-1}$) 531 nm (6050)

MoO(qdt)(Me_2Dt^0) (3)

[$MoOCl(Me_2Dt^0)_2$][PF_6] (0.20 g, 0.000312 moles) was dissolved in 9 mL of acetonitrile generating a dark blue solution. A solution of qunioxalinedithiol (0.066 g, 0.00034 moles) and triethylamine (0.069 g, 0.00068 moles) in 1.5 mL of acetonitrile was added dropwise to the dark blue solution initiating an instantaneous color change to dark purple and the release of white vapor (HCl). The reaction mixture was stirred for one hour. The solution was filtered and dark purple solid was collected. The crude product was washed with cold chloroform to obtain analytically pure product. (0.020 g, 0.0000401 mol). 11% Calcd (Expt) for $C_{14}H_{14}MoN_4OS_4$ +H_2O: C, 33.87(34.21): H, 3.25(2.82); N, 11.28 11.84). ^{1}H NMR (CD_3CN): δ 3.84 (s, CH_3, 6H), 4.00 (q, *J*= 8.2 Hz, 7.0 Hz, CH_2, 2H), 4.21(q, *J*= 7.0 Hz, 6.4 Hz, CH_2, 2H), 7.63 (dd, *J*= 6.4 Hz, 3.4 Hz, aromatic, 2H), 7.93 (dd, *J*= 6.4 Hz, 3.4 Hz, aromatic, 2H). FTIR(KBr, cm^{-1}): 1524 (vs, C(-N)S), 1350 (vs, C=S), 955 (s, Mo=O). UV-Vis (MeCN): λ_{max} (ε, $M^{-1}cm^{-1}$) 548 nm (7450)

MoO($bdtCl_2$)(Me_2Dt^0) (4)

[$MoOCl(Me_2Dt^0)_2$][PF_6] (0.20 g, 0.000312 moles) was dissolved in 9 mL of acetonitrile generating a dark blue solution. A solution of 3,6-dichloro-1,2-benzenedithiol (0.072 g, 0.00034 moles) and triethylamine (0.069 g, 0.00068 moles) in 1.5 mL of acetonitrile was added dropwise to the dark blue solution initiating an instantaneous color change to dark purple. The reaction mixture was stirred for thirty minutes. The solution was filtered and dark purple solid was collected. The crude product was washed with cold chloroform to obtain analytically pure product. Yield 42% (0.065 g, 0.000132 moles). Calcd (Expt) for $C_{12}H_{12}Cl_2MoN_2OS_4$: C, 29.10 (29.35): H, 2.44 (2.50); N, 5.66 (5.69). ^{1}H NMR (CD_3CN): δ 3.81 (s, CH_3, 6H), 4.10 (m, CH_2, 2H), 4.20 (m,

CH_2, 2H), 7.12 (s, aromatic 2H). FTIR (KBr, cm^{-1}): 1527 (vs, C(-N)S), 1353 (vs, C=S), 926 (s, Mo=O). Electronic spectrum, UV-Vis (MeCN): λ_{max} (ε, $M^{-1}cm^{-1}$) 531 nm (4460)

MoO(bdt)(^{i}Pr$_2$Dt^0) (5)

[MoOCl(^{i}Pr$_2$Dt^0)$_2$][PF_6] (0.20 g, 0.00026 moles) was dissolved in 10.5 mL of acetonitrile generating a dark blue solution. A solution of benzenedithiol (0.49 g, 0.00034 moles) and triethylamine (0.059 g, 0.00058 moles) in 1.5 mL of acetonitrile was added dropwise to the dark blue solution initiating an instantaneous color change to dark purple. The reaction mixture was stirred for one hour. The solution was filtered, and dark purple solid was collected. Free ^{i}Pr$_2$Dt^0 ligand was present in the crude product. To remove the free ligand, the crude product (0.080g moles) was dissolved in 7.5 mL of CH_3Cl. $MoCl_5$ (0.010 g, 0.000037 moles) was dissolved in 3 mL of MeOH generating HCl gas. The $MoCl_5$ was stirred until the cessation of the HCl gas was observed resulting in a green solution. The methanolic solution was added dropwise to the chloroform solution of the crude MoO(bdt)(^{i}Pr$_2$Dt^0). The mixture was stirred for 1.5 hours and filtered. A dark purple filtrate of analytically pure complex was collected. Yield 41% (0.052 g, 0.000107 moles) Calcd (Expt) for $C_{16}H_{22}MoN_2OS_4$: C, 39.82 (40.24): H, 4.60 (4.51); N, 5.81 (5.54). ^{1}H NMR (CD_3CN): δ 1.28 (d, *J*= 6.7 Hz, CH_3, 6H), 1.43 (d, *J*= 6.7 Hz, CH_3, 6H), 3.74 (m, CH_2, 2H), 4.02 (m, CH_2, 2H), 5.23 (h, *J*= 6.7 Hz, CH, 2H), 7.10 (dd, *J*= 5.8 Hz, 3.2 Hz, aromatic, 2H), 7.65 (dd, *J*= 5.8 Hz, 3.3 Hz, aromatic, 2H) FTIR(KBr, cm^{-1}): 1501 (vs, C(-N)S), 1350 (vs, C=S), 931 (s, Mo=O). Electronic spectrum, UV-Vis (MeCN): λ_{max} (ε, $M^{-1}cm^{-1}$) 529 nm (6900)

MoO(tdt)(^{i}Pr$_2$Dt^0) (6)

[MoOCl(^{i}Pr$_2$Dt^0)$_2$][PF_6] (0.20 g, 0.00026 moles) was dissolved in 9 mL of acetonitrile generating a dark blue solution. A solution of toluene-3,4-dithiol (0.45 g, 0.00029 moles) and triethylamine (0.059 g, 0.00058 moles) in 1.5 mL of acetonitrile was added dropwise to the dark

blue solution initiating an instantaneous color change to dark purple. The reaction mixture was stirred for one hour. The solution was filtered and dark purple solid was collected. The crude product was washed with cold chloroform resulting in analytically pure product. Yield 58% (0.077 g, 0.000155 mol). Calcd (Expt) for $C_{17}H_{24}MoN_2OS_4$: C, 41.12 (41.04): H, 4.87 (4.76); N, 5.64 (5.52). ^{1}H NMR (CD_2Cl_2): δ 1.24 (d, CH_3, *J*= 6.9 Hz ,6H), 1.43 (d, *J*= 6.8 Hz, CH_3, 6H), 2.34 (s, CH_3, 3H), 3.62 (m, CH_2, 2H), 3.88 (m, CH_2, 2H), 5.22(h, *J*= 6.7 Hz, CH, 2H), 6.93 (d, *J*=8.1 Hz, aromatic H), 7.47 (s, aromatic, H), 7.51 (d, *J*= 7.9 Hz, aromatic, H). FTIR(KBr, cm^{-1}): 1501 (vs, C(-N)S), 1350 (vs, C=S), 931 (s, Mo=O). UV-Vis (MeCN): λ_{max} (ε, M^{-1}cm^{-1}) 533 nm (7500)

MoO(qdt)(^{i}Pr$_2$Dt^0) (7)

[MoOCl(^{i}Pr$_2$Dt^0)$_2$][PF_6] (0.20 g, 0.00026 moles) was dissolved in 13.5 mL of acetonitrile generating a dark blue solution. A solution of quinoxalinedithiol (0.056 g, 0.00029 moles) and triethylamine (0.059 g, 0.00058 moles) in 4.5 mL of methanol was added dropwise to the dark blue solution initiating an instantaneous color change to dark purple. The reaction mixture was stirred for one hour. The solution was filtered and green solid was collected. The green solid was washed with CH_3Cl to collect a dark purple filtrate. The solvent was dried en vacuo to obtain analytically pure complex. Yield 34% (0.049 g, 0.000091 moles). Calcd (Expt) for $C_{18}H_{22}MoN_4OS_4$ + CH_3Cl: C, 40.27 (39.77): H, 4.63 (4.52); N, 9.89 (9.16). ^{1}H NMR (CD_3CN): δ 1.27(d, *J*= 6.7 Hz, CH_3, 6H), 1.41 (d, *J*= 6.7 Hz, CH_3, 6H), 3.63 (m, CH_2, 2H), 3.87 (m, CH_2, 2H), 5.25 (h, *J*= 6.7 Hz, CH, 2H), 7.54 (dd, *J*= 6.4 Hz, 3.4 Hz, aromatic, 2H), 7.98 (dd, *J*= 6.3 Hz, 3.4 Hz, aromatic, 2H). FTIR(KBr, cm^{-1}): 1491 (vs, C(-N)S), 1351 (vs, C=S), 950 (s, Mo=O). UV-Vis (MeCN): λ_{max} (ε, M^{-1}cm^{-1}) 543 nm (7070).

MoO(bdtCl$_2$)(^{i}Pr$_2$Dt^0) (8)

[MoOCl(^{i}Pr$_2$Dt^0)$_2$][PF$_6$] (0.20 g, 0.00026 moles) was dissolved in 13.5 mL of acetonitrile generating a dark blue solution. A solution of 3,6-dichloro-1,2-benzenedithiol (0.061 g, 0.00029 moles) and triethylamine (0.059 g, 0.00058 moles) in 1.5 mL of acetonitrile was added dropwise to the dark blue solution initiating an instantaneous color change to dark purple. The reaction mixture was stirred for 15 minutes. The solution was filtered and dark purple solid was collected. The crude product was washed with cold chloroform to obtain analytically pure complex. Yield: 68% (0.100 g, 0.000181 moles). Calcd (Expt) for $C_{16}H_{20}Cl_2MoN_2OS_4$: C, 34.85 (34.65): H, 3.66 (3.67); N, 5.08 (5.08). ^{1}H NMR (CD_3CN): δ 1.31 (d, *J*= 6.7 Hz, CH_3, 6H), 1.45 (d, *J*= 6.7 Hz, CH_3, 6H), 3.71 (m, CH_2, 2H), 4.01 (m, CH_2, 2H), 5.28 (h, *J*= 6.7 Hz, CH, 2H), 7.23 (s, aromatic 2H). FTIR(KBr, cm^{-1}): 1507 (vs, C(-N)S), 1356 (vs, C=S), 939 (s, Mo=O). UV-Vis (MeCN): λ_{max} (ε, M^{-1}cm^{-1}) 530 nm (9400).

2.3 Results and Discussion

2.3.1 MoCl$_5$ as a Starting Material

Our group has previously reported the synthesis of [MoOCl(Dt^0)$_2$][PF$_6$] (where Dt^0= Me$_2$Dt^0 or ^{i}Pr$_2$Dt^0).[74, 76] [MoOCl(Dt^0)$_2$][PF$_6$] was synthesized through a reaction with MoCl$_5$ in methanol forming [MoOCl$_3$(MeOH)$_2$]. Dithione ligand is added, neat to a methanolic solution of [MoOCl$_3$(MeOH)$_2$]. Upon addition of counter anion, [MoOCl(Dt^0)$_2$][PF$_6$] precipitated from

Scheme 2.5

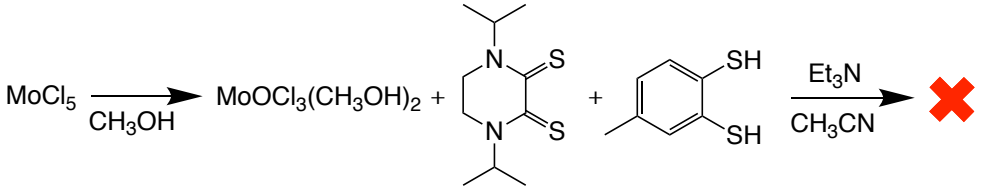

solution. Given the success of forming a monooxo-Mo(IV) complexes possessing two fully oxidized ligands from $MoCl_5$; a similar synthesis was used in attempts to generate complex **6**

(Scheme 2.5). $MoCl_5$ was dissolved in methanol and an acetonitrile solution was added dropwise. Toluene-3,4-dithiol (tdt) was dissolved in acetonitrile and deprotonated by adding dropwise of triethylamine (Et_3N) into the reaction mixture. The reaction mixture was filtered and a green residue and purple filtrate were collected and dried in vacuo. The filtrate proved too unstable and during characterization, the filtrate was not stable in solution to obtain an NMR of the purple material. An IR spectrum of the green residue did not exhibit a characteristic Mo=O vibrational frequency (Figure 2.1); leading to the conclusion that the reaction was unsuccessful.

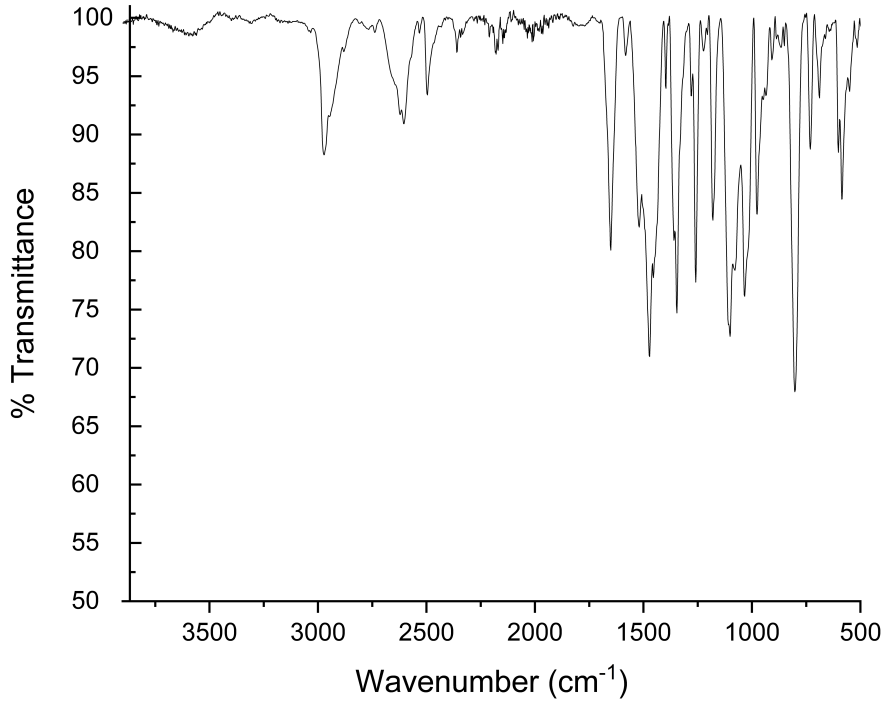

Figure 2.1. IR spectrum (neat) of the crude product from the reaction between $MoCl_5$, $^{i}Pr_2Dt^0$, and deprotonated tdt. No Mo=O vibrational frequency was observed.

2.3.2 MoO_2Cl_2 as a Starting Material

A commonly used starting material as shown in Section 2.1 is MoO_2Cl_2. MoO_2Cl_2 was used as the starting material to synthesize **6** and MoO(mnt)($^iPr_2Dt^0$) where mnt^{2-} sodium maleonitriledithiolate (Scheme 2.6). MoO_2Cl_2 was dissolved in THF and was cooled to -78^{0}C. Sodium maleonitriledithiolate was added neat to the THF solution of MoO_2Cl_2. Once the ligand dissolved completely, solid $^iPr_2Dt^0$ was added to the reaction mixture and the temperature was slowly raised to the room temperature to dissolve the dithione ligand. The reaction mixture was filtered to collect $MoO_2(mnt)_2$. To abstract the oxygen atom to generate the monooxo complex, triphenylphosphine (PPh_3) was added to a THF solution of the crude filtrate. The solvent was

Scheme 2.6

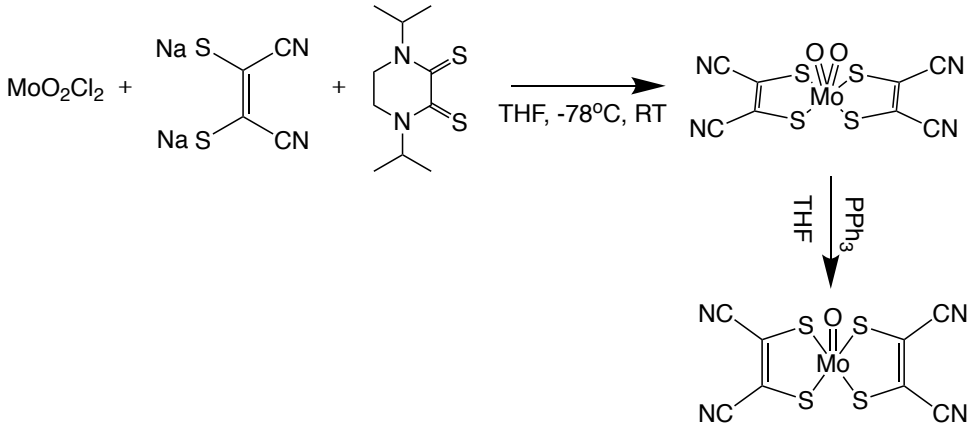

removed en vacuo resulting in a dark purple filtrate. The IR spectrum indicated successful synthesis; vibrational frequencies for the C-(=S)-N, C=S, and Mo=O were observed (Figure 2.2). The crude product yield however, was very low ~9% indicating this is not an efficient means to synthesize MoO(mnt)($^iPr_2Dt^0$). The synthesis of MoO(mnt)($^iPr_2Dt^0$) proved unsuccessful using any other strategy and will not be discussed further. While using MoO_2Cl_2 was a successful starting material for the synthesis of MoO(mnt)($^iPr_2Dt^0$), the same synthetic procedure was not successful for the synthesis of **6**. The target complex was never observed during synthesis (Figure 2.3)

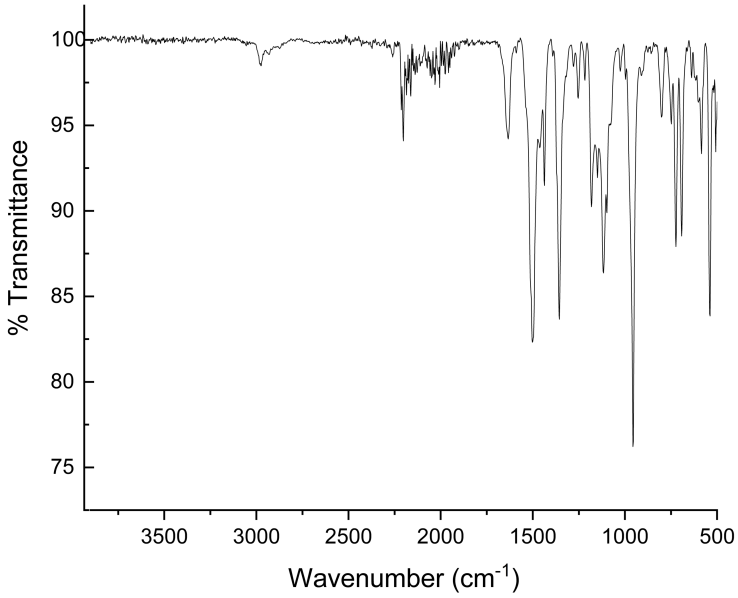

Figure 2.2 IR spectrum (neat) of MoO(mnt)($^{i}Pr_2Dt^0$) synthesized from MoO_2Cl_2; a strong Mo=O vibrational frequency is observed at ~950 cm^{-1}.

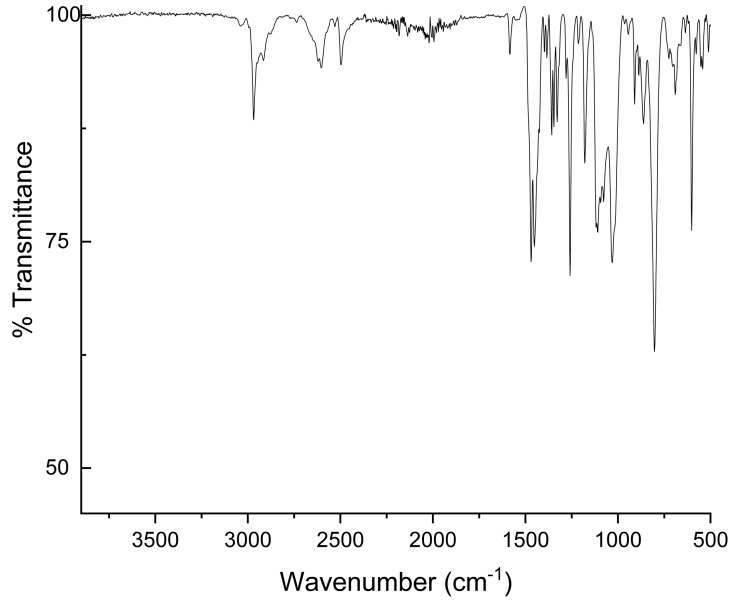

Figure 2.3. IR spectrum (neat) of **6** synthesized from MoO_2Cl_2; no Mo=O vibrational frequency is observed.

2.3.3 Ligand Exchange

Our group has previously utilized $[MoOCl(Dt^0)_2][PF_6]$ as the starting material for the synthesis of $MoO(SPh)_2(Dt^0)$ (where SPh= thiophenol) complexes. $[MoOCl(Dt^0)_2][PF_6]$ was reacted with thiophenol resulting in a ligand exchange reaction. A similar procedure was employed to synthesize complexes **1**-**8** (Scheme 2.7), starting with the synthesis of a fully oxidized dithione ligand. Once the fully oxidized dithione ligand has been synthesized, the synthesis is moved to an inert atmosphere inside a dry box due to the air/water instability of the materials. The starting material is synthesized through a reaction between the fully oxidized dithione ligand and $MoCl_5$. The complex was synthesized in methanol and precipitated out of solution upon addition of sodium hexafluorophosphate. It is imperative that no less than 8 to 10 times excess (compared to $MoCl_5$) was used to form the target complex. After filtration the complex was washed with methanol to remove the excess $NaPF_6$ and chloroform to remove the excess dithione ligand. It should be noted that the dithione ligand is not completely soluble in methanol, multiple washings with chloroform were required to remove the excess free ligand. If all of the free ligand is not removed, purification of the target complexes will be difficult if not impossible. Once all of the free dithione ligand has been removed from the starting material, the target complexes can be synthesized. Even with the removal of the free dithione ligand, isolation of analytically pure complexes has been problematic. The system is very sensitive to solvent environments which is discussed in the following sections.

Scheme 2.7

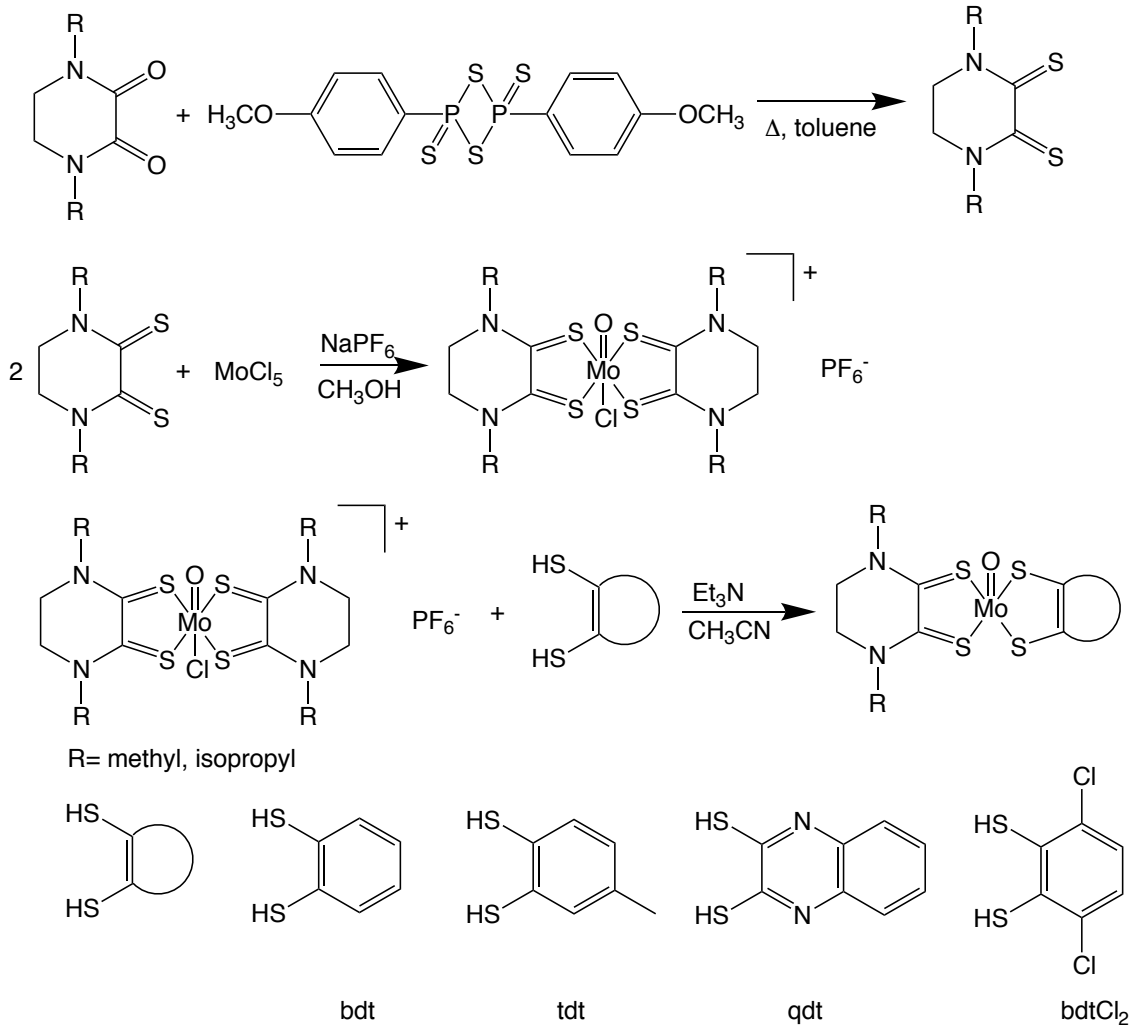

Dichloromethane and Chloroform

$[MoOCl(^{i}Pr_2Dt^{0})_2]^{+}$ was reacted with deprotonated tdt in dry/degassed dichloromethane following the same general procedure that is outlined in Scheme 2.6. During the reaction to synthesize **6**, the reaction was monitored with UV-Vis spectroscopy and while the reaction mixture turned purple, a positive indication that the reaction was successful, the UV-Vis spectrum exhibited a low energy band that is indicative of the starting material and the reaction did not go

to completion. After filtration of the reaction mixture and removal of the solvent from the filtrate, the IR spectrum of the crude product indicated product degradation; no Mo=O vibrational frequency was observed (Figure 2.4). The same reaction was attempted in dry/degassed chloroform and no reaction occurred.

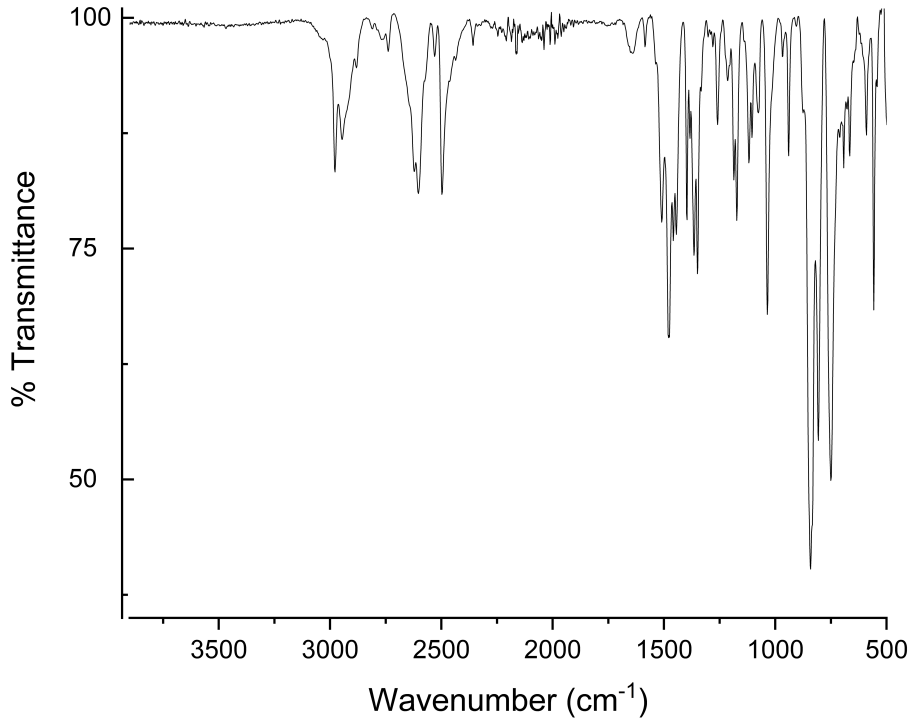

Figure 2.4. IR spectrum (neat) of the crude reaction product from a ligand exchange reaction between $[MoOCl(^{i}Pr_2Dt^0)_2][PF_6]$ and deprotonated tdt in dichloromethane. No strong Mo=O vibrational frequency is observed indicating the reaction was unsuccessful.

Acetonitrile

Previously reported complexes of general structure $MoO(SPh)_2(Dt^0)$ were initially synthesized in large amounts of dry/degassed acetonitrile, ~100 mg of starting material $[MoOCl(Dt^0)_2][PF_6]$ was dissolved in ~25 to 50 mL of acetonitrile. This resulted in a mixture of $MoO(SPh)_2(Dt^0)$ and free dithione ligand. The free dithione ligand impurity could be removed

through recrystallization in acetonitrile/diethyl ether; however analytically pure complexes were not always the outcome of the synthesis and free ligand would persist. The same synthesis strategy was used to synthesize complexes **1**-**8**. Similar results were observed; ^{1}H NMR spectrum of the crude reaction mixture of **6** exhibited resonances of the target complex and free $^{i}Pr_2Dt^0$ ligand. During recrystallization, the amount of free ligand would be reduced but not removed completely and upon second recrystallization the complex would degrade.

From previous experiments, it was determined that the best environment to perform the ligand exchange reaction was dry/degassed acetonitrile. The amount of dithiol ligand used in the reaction is also vitally important. In order to drive the reaction to completion and ensure that the main product should be the target complex, a small excess of dithiol should be used, but no more than a 1:1.1, complex:dithiol. For instance, the reaction between $[MoOCl(^{i}Pr_2Dt^0)_2][PF_6]$ and benzenedithiol forms the target complex when a 1:1.1 ratio is used but anything above 1:1.1, the target complex does not form instead an orange, highly unstable complex is generated (uncharacterized) but when toluenedithiol is used in higher ratios (up to 1:1.5) the target complex is formed successfully however the yields of crude product are poor (~15%). There is always the potential for both of the dithione ligands to be removed from the complex and two dithiol ligands to replace them due to the higher affinity of the negatively charged dithiol ligands.

When ~200 mg of $[MoOCl(Dt^0)_2][PF_6]$ was dissolved in ~9 mL to 13 mL of acetonitrile as opposed to ~25 mL to 50 mL, the target complex precipitated out of solution after the addition of dithiol to the reaction mixture. As mentioned during previous reactions in acetonitrile, the main product was free dithione ligand. During this synthesis, the main product was the target complex with a minor impurity of free dithione ligand. All complexes **1**-**8** were synthesized using this method.

2.3.4 Purification

As discussed, the main impurity of these reactions, irrespective of the ligand used, is free dithione ligand. The free dithione ligand has a very similar solubility compared to the target complexes. Complex stability was a persistent problem due to the neutral charge on the dithione ligand. Recrystallization is a common means for purification but was not successful with $MoO(Dt^{2-})(Dt^{0})$ complexes. Recrystallization in acetonitrile/diethyl ether was successful for previously studied $MoO(SPhX)_2(^{i}Pr_2Dt^{0})$ complexes to generate analytically pure product; recrystallization for similar complexes possessing Me_2Dt^{0} was not successful. Recrystallization was attempted to purify $MoO(Dt^{2-})(Dt^{0})$ complexes. Prior to the methods reported, crude product was recrystallized using acetonitrile/diethyl ether. This would decrease the amount of free ligand but not remove it and a second round of recrystallization would result in complex degradation. Recrystallization using dichloromethane/hexane also resulted in degradation of the complex. Chloroform/pentane was used for a crude sample of **6** that had precipitated out of the concentrated acetonitrile reaction mixture. The crude product had minor free ligand impurity and the recrystallization was successful, however the yield was only ~15%. This did indicate that the amount of free ligand present in the crude sample was crucial to purification by recrystallization. This sample was the first sample generated using saturated reaction conditions which allowed for the precipitation of the target complex from the reaction mixture and this procedure either produced complexes with minimal amounts of free ligand but no more than a 1:1 mixture in other syntheses. Complexes **1**-**4** were not soluble in chloroform and complexes **5**-**8** were partially soluble in chloroform. Due to the instability of these complexes during recrystallization other means of purification were explored. The purification technique, which proved successful, was to wash the crude product with minimal amounts of cold chloroform. This resulted in reaction yields between ~34% to 58%. This technique

has also proven successful in the synthesis of analytically pure samples of $MoO(SPhX)_2(Me_2Dt^0)$ complexes as well.

2.4 Initial Characterization of Analytically Pure Electronically Asymmetric Monooxo-Mo(IV) Dithiolene Complexes

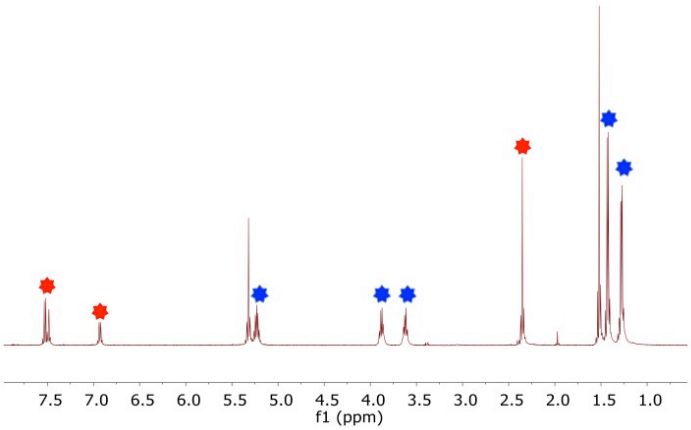

Figure 2.5. ^{1}H NMR spectrum of **6** in CD_2Cl_2; dithione ligand resonances labeled blue and tdt ligand resonances labeled orange.

Complexes **1**-**8** was characterized using ^{1}H NMR and IR spectroscopies. The ^{1}H NMR spectra exhibit resonances due to coordinated dithione ligand and dithiolene ligand which have been tabulated in Table 2.1. An example spectrum of **6** is shown in Figure 2.5; all other spectra can be found in Appendix A1. The solid-state IR spectra exhibits a strong band due to the C=S stretching and a band due to the Mo=O vibration which have been tabulated in Table 2.2. An example spectrum of **6** is shown in Figure 2.6; all other spectra can be found in Appendix A2. These vibrational frequencies are consistent with those reported previously for Mo-dithione complexes.[74, 76, 80]

Table 2.1. ^{1}H NMR Chemical Shifts (ppm) for **1**-**8**.

Complex	Chemical Shifts (ppm)			
	CH_3	CH_2		Aromatic
MoO(bdt)(Me_2Dt^0) (**1**)	3.77 (s)	4.18 (m) 3.89 (m)		7.10 (dd, *J*=5.8, 3.2 Hz) 7.65 (dd, *J*=5.8, 3.2 Hz)
MoO(tdt)(Me_2Dt^0) (**2**)	3.76 (s)	4.14 (m) 3.86 (m)		2.34 (s) 6.93 (d, *J*= 7.8 Hz) 7.46 (s) 7.51(d, *J*= 7.9 Hz)
MoO(qdt)(Me_2Dt^0) (**3**)	3.84 (s)	4.00 (m) 4.21 (m)		7.63 (dd, *J*= 6.4, 3.4 Hz) 7.93 (dd, *J*= 6.3, 3.4 Hz)
MoO($bdtCl_2$)(Me_2Dt^0) (**4**)	3.92 (s)	4.10 (m) 4.40 (m)		7.12 (s)
	CH_3	CH_2	CH	Aromatic
MoO(bdt)($^{i}Pr_2Dt^0$) (**5**)	1.28 (d, *J*= 6.7 Hz) 1.43 (d, *J*= 6.7 Hz)	3.74 (m) 4.02 (m)	5.23 (h, J= 6.7 Hz)	7.09 (m) 7.46 (m)
MoO(tdt)($^{i}Pr_2Dt^0$) (**6**)	1.24 (d, *J*= 6.9 Hz) 1.43 (d, *J*= 6.8 Hz)	3.62 (m) 3.88 (m)	5.22 (h, J= 6.7 Hz)	2.32 (s) 6.93 (d) 7.46 (s) 7.50 (d)
MoO(qdt)($^{i}Pr_2Dt^0$) (**7**)	1.27 (d, *J*= 6.7 Hz) 1.41 (d, *J*= 6.7 Hz)	3.63 (m) 3.87 (m)	5.22 (h, J= 6.7 Hz)	7.54 (m) 7.98 (m)
MoO($bdtCl_2$)($^{i}Pr_2Dt^0$) (**8**)	1.31 (d, *J*= 6.6 Hz) 1.45 (d, *J*= 6.7 Hz)	3.71 (m) 4.01 (m)	5.28 (h, J= 6.7 Hz)	

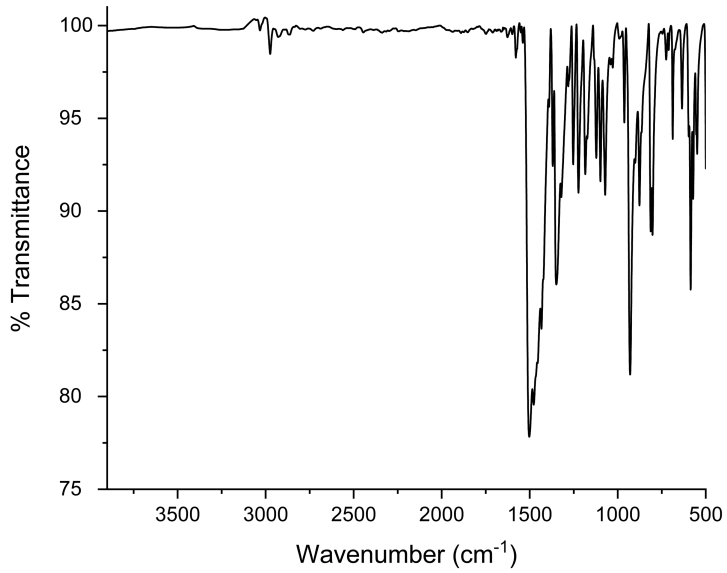

Figure 2.6. IR spectrum (KBr) of **6**. Key vibrational frequencies observed: C=S (1348 cm^{-1}), C(=S)-N (1502 cm^{-1}), and Mo=O (929 cm^{-1}).

Table 2.2. Key Vibrational Frequencies for **1**-**8**

Complex	Vibrational Frequencies (cm^{-1})		
	C=S	C(=S)-N	Mo=O
$MoO(bdt)(Me_2Dt^0)$ (**1**)	1354	1531	940
$MoO(tdt)(Me_2Dt^0)$ (**2**)	1355	1534	929
$MoO(qdt)(Me_2Dt^0)$ (**3**)	1350	1524	955
$MoO(bdtCl_2)(Me_2Dt^0)$ (**4**)	1353	1527	926
$MoO(bdt)(^iPr_2Dt^0)$ (**5**)	1350	1501	930
$MoO(tdt)(^iPr_2Dt^0)$ (**6**)	1348	1502	929
$MoO(qdt)(^iPr_2Dt^0)$ (**7**)	1351	1491	950
$MoO(bdtCl_2)(^iPr_2Dt^0)$ (**8**)	1356	1507	939

2.5 Ligand "Scrambling" Studies of Electronically Asymmetric Monooxo-Mo(IV) Dithiolene Complexes

During reactivity studies (discussed in Chapter 4) it was discovered that complexes **1**-**8** are unstable at low temperature i.e., the dithione ligand can dissociate from the complex. When the complex is brought back to room temperature or slightly higher (40 ^{o}C), the free dithione ligand coordinates to the metal center. This gave rise to the idea of studying the stability of the complexes in a coordinating solvent acetonitrile which allowed for the observation of "ligand scrambling" of the complexes i.e., $^{i}Pr_2Dt^0$ could be replaced with a Me_2Dt^0 ligand added to the solution at low temperatures.

Complex **5** was dissolved in CD_3CN (Figure 2.7) and under argon, Me_2Dt^o was added to the solution at room temperature. No color change occurred however, resonances corresponding to **1** were observed alongside resonances for the original complex **5.** The solution was cooled in an acetone/dry ice bath for 10 minutes and allowed to reach room temperature. After cooling, the amount of **1** increased from the initial room temperature reaction and there was observed degradation of the initial complex **5**. The same procedure was used to examine the ligand scrambling affinity of **1** with $^{i}Pr_2Dt^0$ and the same results were not observed (Figure 2.8). At room temperature, and after an initial cooling period, **5** was not observed. After 24 hours, however, **5** was observed along-side the original complex indicating that **1** is more stable at lower temperatures than the corresponding $^{i}Pr_2Dt^0$ complexes. The same experiments using **5** were run in acetone, a non-coordinating solvent, and no ligand scrambling occurred (Figure 2.9).

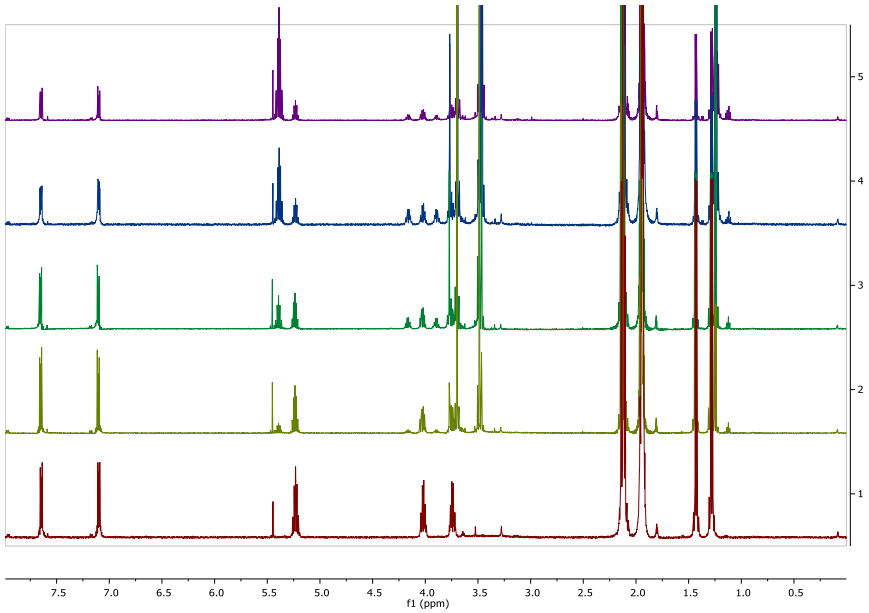

Figure 2.7. ^{1}H NMR spectra of **5** in CD_3CN (1) undergoing ligand scrambling with Me_2Dt^0 (2-5). Spectrum 2 is the addition of Me_2Dt^0 at room temperature. Spectrum 3 shows the increase of **1**. Spectra 4 and 5 are after 24 and 48 hours respectively, after 48 hours both of the complexes have begun to degrade.

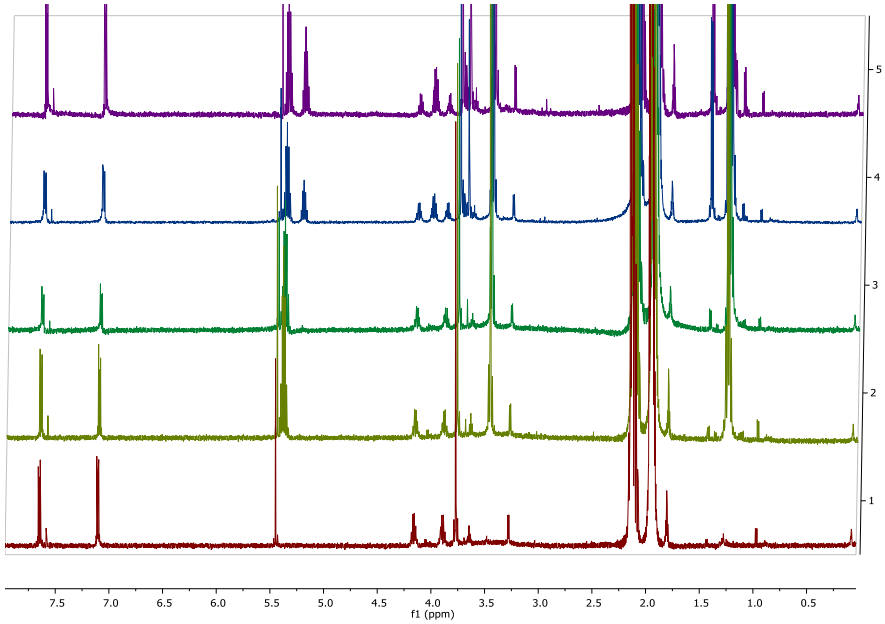

Figure 2.8. ^{1}H NMR spectra of **1** in CD_3CN (1) undergoing ligand scrambling with $^{i}Pr_2Dt^0$ (2-5). Spectrum 2 is the addition of $^{i}Pr_2Dt^0$ at room temperature. Spectrum 3 shows the increase of **5**. Spectra 4 and 5 are after 24 and 48 hours respectively, after 48 hours both of the complexes have begun to degrade.

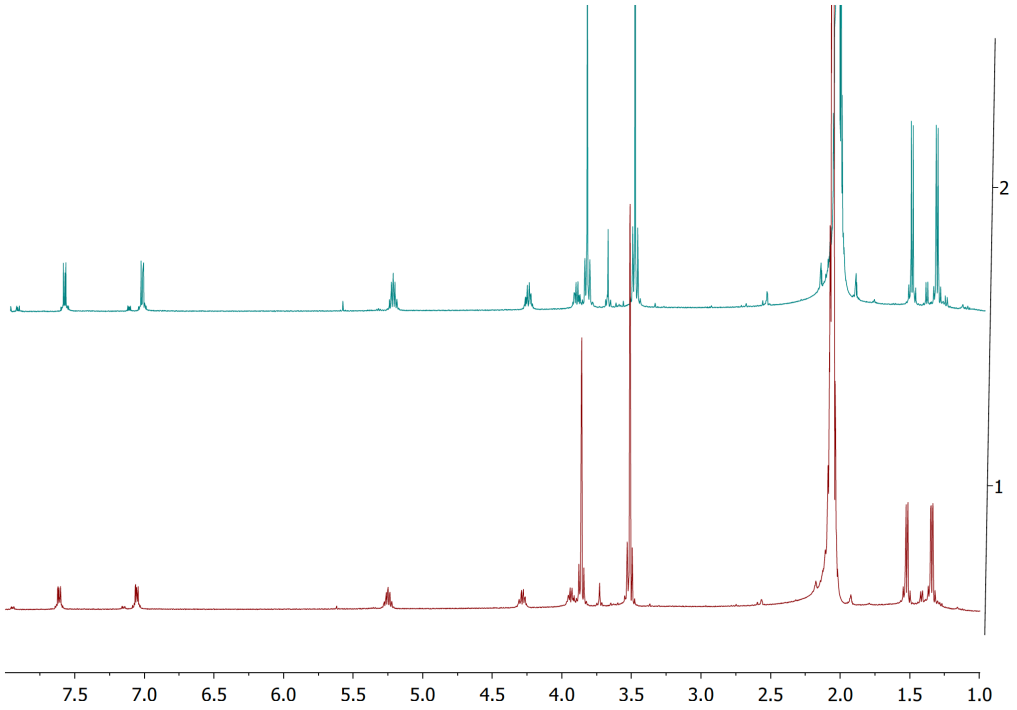

Figure 2.9. ^{1}H NMR spectra of **5** in deuterated acetone with Me_2Dt^0 (1) at room temperature. Spectrum 2 is after cooling the solution. There is no formation of **1**.

These studies are a good example of the target complexes instability in the solution phase. The complexes are not highly stable in acetonitrile solutions; isolation of analytically pure complex would and did prove difficult. When the reaction mixture is more concentrated and the complex precipiates out of solution in the solid state, the amount of free dithione ligand is lessened and purification is more straightforward and successful. Due to the lack of ligand dissociation during the experiments in acetone; a ligand exchange reaction to synthesize **6** was run in acetone. During the course of the reaction the target complex was not formed; no reaction occurred. This speaks to the solvent sensitivity discussed earlier; complexes **1**-**8** are only successfully formed in dry and degassed acetonitrile.

CHAPTER 3. MOLECULAR STRUCTURE, REDOX, AND ELECTRONIC CHARACTERIZATION OF ELECTRONICALLY ASYMMETRIC MONOOXO-MO(IV) DITHIOLENE COMPLEXES

3.1 Introduction

Oxo-molybdenum complexes possessing two dithiolene ligands can exist either in the +4, +5 or +6 oxidation state. The oxidation state of the metal can dictate the methods that are used to characterize the complexes. For instance, electron paramagnetic resonance (EPR) spectroscopy has been widely used to understand the coordination environment of the Mo complexes that are in the +5-oxidation state with d^1 electron configuration. In contrast, Mo(IV) and Mo(VI) states are diamagnetic with d^2 and d^0 electron configuration respectively, and normal perpendicular mode EPR spectroscopy is not applicable.[123, 134, 135] Paramagnetic molecules can exhibit resonances outside the diamagnetic envelope in NMR spectroscopy and indeed, NMR spectroscopy has been used in studying paramagnetic molecules of Fe(III), Co(II) etc. In contrast, Mo(V) complexes are not very amenable to NMR spectroscopy because of their long electronic relaxation time which essentially broadens the signals. General methods that can be used in all three oxidation states include electronic and vibrational spectroscopies, electrochemistry, mass spectrometry and crystallography. Density functional theory (DFT) is often used in interpreting the data and in understanding the electronic structure. We have used a combination of techniques to fully characterize the complexes discussed in Chapter 2. The overall goal is to gain an understanding into the molecular structure, the redox properties, and the electronic structure of the electronically asymmetric complexes with a general formula: $MoO(Dt^{2-})(Dt^0)$ where Dt^{2-}= fully reduced dithiolene and Dt^0= fully oxidized dithione. Three main characterization techniques have been used:

1. X-ray crystallography has been used to determine the molecular structure of MoO(tdt)(^{i}Pr$_2$Dt^0) (**6**) (where tdt is toluene-3,4-ditholate).
2. Cyclic voltammetry has been used to understand the redox properties of all complexes.
3. A description of the electronic structure has been put forward using UV-Vis spectroscopy and theoretical calculations (density functional theory and time dependent-density functional theory).

3.2 Materials and Methods

Syntheses of the complexes are presented in Section 2.1.

3.2.1 Physical Methods

^{1}H NMR spectra were recorded on either a Bruker 500 MHz Avance spectrometer or a Bruker 400 MHz Avance spectrometer in air-tight NMR tubes. Infrared spectroscopy (FTIR) was recorded using a Thermo-Fisher Nicolet iS10 spectrometer at room temperature using a KBr pellet. Electronic absorbance spectra were collected on a Shimadzu UV-3600 Plus in a quartz cuvette. Cyclic voltammetry was recorded on a Metorhm PGSTAT204 galvanostat/potentiostat. A Pt disk working electrode, Ag^+/Ag reference electrode and Pt wire auxillary electrode and tetrabutylammonium hexafluorophosphate supporting electrolyte were used.

3.2.2 Computational Methods

All computational work was performed using *Gaussian 09* software package running on UNIX OS and visualized utilizing *GaussView 5.0.9*. Calculations were done using the Lee-Yang-Parr nonlocal correlation functional[136] (B3LYP) and a combination of the LANL2DZ[137] effective core potential basis set for molybdenum and the 6-31G** basis set for all other atoms. The crystal structure geometry was optimized using DFT to afford the geometry used for subsequent

calculations. Atomic composition for molecular orbitals was determined using C-squared population analysis from single-point calculations with the program *QM-Forge*. The lowest 60 transition energies were generated using non-equilibrium TDDFT calculations with the polarizable continuum model (PCM) algorithm. PCM-TDDFT calculations were performed using acetonitrile as the solvent to match experimental conditions. Electron density difference maps (EDDMs) were generated using the *cubman* package in *Gaussian09*.

3.2.3 X-Ray Crystallography

Single crystals were mounted using glass fiber and data collected using a Bruker SMART Apex II diffractometer with a graphite monochromator for Mo Kα radiation (0.71073 Å). The absorption correction was performed using SADABS routine.[138] The structure solution and the refinement were done using SHELXS-97[139] and SHEXLX-2018 programs.[140] The X-ray data were collected at room temperature (296 K). Hydrogen atoms were placed at calculated positions and refined as riding atoms with isotropic displacement parameters. The methyl group on the toluene-2,3-dithiolene moiety of MoO(tdt)(ipr) was refined as disordered over two moieties with different rotational orientations. The disorder extends to the other carbon and sulfur atoms of the toluene-2,3-dithiolene moiety, and they were included in the disorder modeling. The two moieties were restrained to have similar geometries (SAME command of Shelxl) and U_{ij} components of ADPs for disordered atoms closer to each other than 2.0 Angstrom were restrained to be similar. Subject to these conditions, the occupancy ratio refined to 0.517(5) to 0.483(5). Details of the structure determination are listed in Table 3.1.

Table 3.1. Crystallographic Data for MoO(tdt)($^{i}Pr_2Dt^0$)

Formula	$C_{17}H_{24}MoN_2OS_4$
Formula weight	496.56
Temperature	296 K
Crystal system	Orthorhombic
Space group	Pbca
Unit cell dimensions	a=12.6981 (1) Å b= 15.8799 (2) Å c= 21.2754 (2) Å
Volume	4290.07(8)Å^3
Z, Formula unit/unit cell	8
density (calculated)	1.534 Mg m^{-3}
crystal color, morphology	Purple, block
u	1.01 mm^{-1}
F(000)	2024
Diffractometer	Bruker Smart Apex II
Radiation, graphite monochrome	Mo Kα (λ=0.71073 Å)
Crystal size	0.20 x 0.11 x 0.08 mm
Crystal color, morphology	Purple, block
Reflections collected/unique	70727/6665
R_{int}	0.054
Refinement method	Full-matrix least-squares on F^2
Goodness-of-fit on F^2	
Final R indices [I>2σ(I)]	R=0.041 wR2=0.100
R indices (all data)	
Maximum residue peaks (e·Å^{-3})	0.53 and -0.44

3.3 Results and Discussion

3.3.1 Molecular Structure

The molecular structure of **6** was determined by X-ray crystallography (Figure 3.1). Single crystals of **6** were grown via vapor diffusion using acetonitrile/diethyl ether. During structure refinement, it was observed that the methyl group on the tdt ligand was disordered due to different rotational orientations and this disorder extended to the other carbon and sulfur atoms of the ligand all, of which were included in disorder modeling. Selected bond lengths and angles are listed in Table 3.2.

The five-coordinate Mo center in **6** exhibits a distorted square-pyramidal geometry as measured by the distortion parameter $\tau = (\beta - \alpha/60)$ (where β= the largest basal angle and α= the second largest angle) (Figure 3.2). For **6**, the τ was calculated to be 0.18, whereas the τ for ideal square pyramidal geometry should be 0.00.[141-143] Similar distortion has been observed in other $[Mo^{IV}O(Dt^{2-}{}_2)]^{2-}$ with τ values between 0.002-0.213.[144] The Mo-center is coordinated by a terminal oxo group coordinated axially, and the four sulfur donors defining the equatorial plane with the

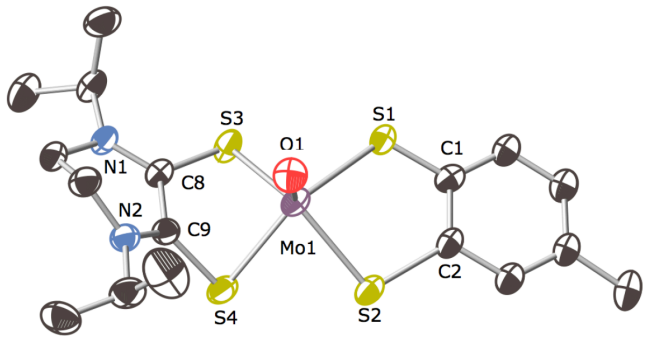

Figure 3.1. Thermal ellipsoid plot (30%) of MoO(tdt)($^{i}Pr_2Dt^0$). Space group, Pbca; R_1, 0.054; wR_2, 0.100.

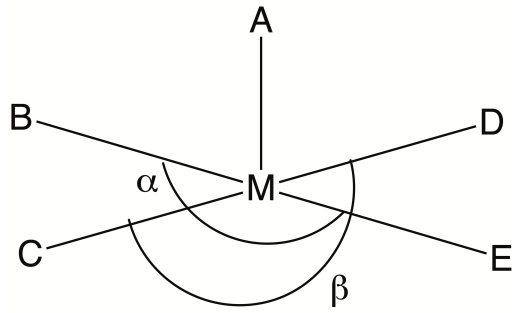

Figure 3.2. Angles used in calculating τ.

Mo atom raised 0.84 Å above this equatorial plane. This geometric arrangement is similar to oxo-Mo dithiolene complexes where the Mo- center is located, on average, 0.74 Å above the equatorial plane.[145]

In **6**, the Mo=O bond distance is 1.681(2) Å. In the coordinated $^{i}Pr_2Dt^0$ fragment, the C=S distances are 1.724(3) Å and 1.717(3) Å and the C-C distance is 1.475(4) Å. In the coordinated tdt ligand, the average C–S bond distances are 1.776(17) Å and 1.765(16) Å, and the average C=C bond length is 1.382(9) Å. All four Mo-S bonds are of a similar length with an average bond length of 2.376(16) Å.

Table 3.2. Key bond lengths (Å) and bond angles (°) in the molecular structure of **6**.

O1—Mo1	1.681 (2)	C4—C5*	1.356 (9)
Mo1-S3	2.3971 (8)	S3-Mo1-S4	84.87(3)
Mo1-S4	2.3714 (9)	O1-Mo1-S1*	110.7
S3-C8	1.724 (3)	O1-Mo1-S2*	106.5
S4-C9	1.717 (3)	S2-Mo1-S3*	110.5
C8—C9	1.475 (4)	S1-Mo1-S3*	105.4
C10—C11	1.493 (4)	S2-Mo1-S4*	115.8
Mo1—S1*	2.374 (16)	S1-Mo1-S4*	110.4
Mo1—S2*	2.356 (12)	S1-Mo1-S2*	83.7
S1—C1*	1.765(16)	O1-Mo1-S3	115.23(8)
S2—C2*	1.776 (17)	O1-Mo1-S4	109.14(8)
C1—C2*	1.382 (9)		

* Average bond lengths are reported due to the disorder on the tdt ring

The molecular structure of **6** can provide insight into the oxidation state of the dithione ligand thus aiding in assignment of the oxidation state of the metal. Given the non-innocent nature of the dithiolene ligands the difficulty in ascertaining the oxidation state of the metal in such complexes, structural descriptions of the putative oxidation states in known $[MoO(Dt)_2]^{2-}$ (where Dt is reduced dithiolene ligand) complexes were used in understanding the redox states of the ligand and metal center in **6**.[146-149] The C-S bond distances (S3-C8, S4-C9) in the dithione ligand was 1.724(3) Å and 1.717(3) Å, whereas the average C-S bond lengths (S1-C1, S2-C2) of the dithiolene ligand was 1.765(16) Å and 1.776(17) Å. $[Et_4N]_2[MoO(bdt)_2]$ (where bdt = 1,2-benzenedithiol) exhibits an average C-S bond length of 1.764(6) Å and $[Et_4N]_2[MoO(tdt)_2]$ exhibits an average C-S bond length of 1.758(1) Å; these bond lengths are similar to the C-S bond lengths of the tdt ligand in **6**.[120, 125, 150] The longer C-S bond lengths of the dithiolene ligand compared to the shorter C-S bond lengths of the dithione ligand indicate that the C-S bond in the dithione ligand has double bond character compared to the single C-S bond character of the dithiolene ligand.

The C-C (C8-C9) bond length of the $^{i}Pr_2Dt^0$ ligand was 1.475(4) Å and the C-C (C10-C11) bond in the methylene backbone was 1.493(4) Å. The methylene backbone can was utilized as an "internal standard" due to the fact that both bonds should be C-C single bonds. The C-C (C1-C2) average bond length of the tdt ligand was 1.382(9) Å which is shorter than the C-C bond lengths of the $^{i}Pr_2Dt^0$ ligand by 0.093 Å (C8-C9) and 0.111 Å (C10-C11). The C-C (C1-C2) bond length in the dithiolene moiety was consistent with the average C=C bond length in the benzene ring (1.384 Å) indicating a similar bond character. The average C-C bond length of the dithiolene moiety of $[Et_4N]_2[MoO(bdt)_2]$ and $[Et_4N]_2[MoO(tdt)_2]$ are 1.400(9) Å and 1.387(1) Å respectively;

similar to the C-C bond length in **6**.[120, 125, 150] These bond distances indicate the $^{i}Pr_2Dt^0$ remained fully oxidized in **6**, at least in the solid state.

The Mo=O bond length provided an insight into the oxidation state of the molybdenum metal center. From a CCDC search, the typical distance of the Mo^{IV}=O bond length (excluding dithiolene complexes) was found to be 1.686 Å, and the bond length of the Mo=O bond in **6** was 1.681 Å. These results are consistent with 4+ oxidation state of the Mo-center in **6**. When the structure search was narrowed to look only at molybdenum-dithiolene complexes, there was a marked difference in the average Mo=O bond length for Mo(IV) complexes. The average Mo^{IV}=O bond length is 1.696 Å and the average Mo^{V}=O bond length is 1.680 Å .[145] The Mo=O bond length in **6** can be interpreted to suggest a Mo(V) state. However, we propose that the Mo=O in **6** is slightly shorter than the average Mo(IV)=O of dithiolene complexes due to increased electron density toward the electron-deficient dithione ligand from the molybdenum atom thus resulting in some Mo(V) character. Finally, the Mo-S bond lengths were consistent in both ligand fragments; 2.3714 (9) Å and 2.3971(8) Å in $^{i}Pr_2Dt^0$ and 2.356(12) Å and 2.374(16) Å in the tdt ligand. There was a difference of 0.032 Å in the shortest and longest Mo-S bond in **6** indicating that the oxidation state of the dithiolene fragment does not have a significant effect on the Mo–S bond length, which is further corroborated by a comparison to known dithiolene complexes possessing two fully reduced dithiolene ligands. The Mo-S bond lengths in $[Et_4N]_2[MoO(bdt)_2]$ varies between 2.384 Å and 2.391 Å and $[Et_4N]_2[MoO(tdt)_2]$ exhibits Mo-S bond lengths between 2.356 Å - 2.424 Å. [120, 125, 150] The average Mo-S bond lengths of 35 known $[Mo^{IV}O(Dt)_2]^{2-}$ complexes is 2.386 Å. By examining the bond lengths of **6** and through comparison to known molecular structures of $[Mo^{IV}O(Dt)_2]^{2-}$ complexes we suggest the dithione ligand has remained fully oxidized and the metal center is Mo(IV).

In **6**, the angle between the plane containing S3, C8, C9, and S4 and the plane containing Mo, S3 and S4 was 62.6º, such that the ligand is bent towards the terminal oxo group along the S•••S vector of $^{i}Pr_2Dt^0$. The angle between the plane containing S1, C1, C2 and S2 and the plane containing Mo, S1, and S2 of the tdt ligand was 12.3º, folded towards the oxo group.

Structures of reduced electron-rich dithiolene complexes and 'electron-deficient' metal ions often exhibit a large folding of the dithiolene ligand along the S•••S vector. Early work by Hoffman, and later by Enemark have provided a "bending" scheme for the bent-metallocene (Cp) dithiolene.[77-79] Complex **6** is fundamentally different because the Mo-center is coordinated by two dithiolene ligands and one of the dithiolene ligands is 'electron-deficient'. Both ligands are folded towards the terminal oxo-group and the difference in folding between the two ligands is 49º. A similar complex, $MoO(SPh)_2(^{i}Pr_2Dt^0)$ (where the Mo center is coordinated by one dithione and two thiolate ligands) exhibited a fold of 70º along the S•••S vector of $^{i}Pr_2Dt^{0,}$ which we attributed to a strong pseudo Jahn-Teller effect generating a double well potential in the electronic ground state.[80] We surmise that a similar situation is operative in **6**, and a detailed spectroscopic investigation is underway to further elaborate this aspect.

We have previously studied the dithiolene fold angle of $[MoO(mnt)_2]^{2-}$ in the gas phase using infrared multiple-photon dissociation spectroscopy (IRMPD) coupled with density functional theory (DFT) of the complex anion to optimize the geometry of $[MoO(mnt)_2]^{2-}$ and to predict the IR frequencies. IRMPD allows for the coupling of mass spectrometry and infrared spectroscopy; desired ions can be selected and the ions are irradiated at mid-IR wavelengths in the gas phase using a free electron laser. Observed frequencies in the IRMPD spectrum were assigned to the Mo=O stretch, C-C≡N, and C=C (of the dithiolene ligands); the experimental gas phase spectrum, matched well with the theoretically derived frequencies. The studies offer support that

the fold along the S•••S vector is inherent to molybdenum-dithiolene unit. Further examination of the molecular structure of **6** indicated that there are no bonding interactions. The unit cell density is 1.538 g/cm^3 compared to the unit cell density of $[Et_4N]_2[MoO(mnt)_2]$ which equals 1.333 g/cm^3; a higher density and no interaction is a positive indication that the fold angle of **6** is similar to that of $[Et_4N]_2[MoO(mnt)_2]$ and intrinsic to the molecule.[89] Further gas phase studies are underway using electronically asymmetric complexes **1**-**8**.[151]

3.3.2 Redox Properties

3.3.2.a Reduction of electronically asymmetric monooxo Mo(IV)- dithiolene complexes

The redox reactivity of complexes **1**-**8** was investigated by cyclic voltammetry in acetonitrile solutions. Cyclic voltammograms exhibit two, one-electron reversible reduction couples due to the reduction of the oxidized dithione ligand. A representative cyclic voltammogram for complex **6** is shown in Figure 3.3 and all redox potentials are listed in Table 3.3. Cyclic voltammograms were collected for multiple scan rates (100 mV to 900 mV). The data was fit to the Randles-Sevcik equation (eqn 1), the linear fit of the peak current versus square root of the scan rate is shown in Figure 3.3.

$$i_p = 2.69 \times 10^5 n^{3/2} A D^{1/2} C^b \nu^{1/2.} \quad (1)$$

where: n= number of electrons

A= area of electrode, cm^2

D= diffusion coefficient, cm^2 s^{-1}

C^b= concentration, mol cm^{-3}

ν= scan rate V/s^{-1}

All couples are diffusion-controlled processes due to the linearity of the peak current with the square root of the scan rate as shown in Figure 3.4 for complex **6**. As shown in Table 3.3, ΔEp for both couples across multiple scan rates are larger than 59 mV indicating quasi-reversible nature of the couples.

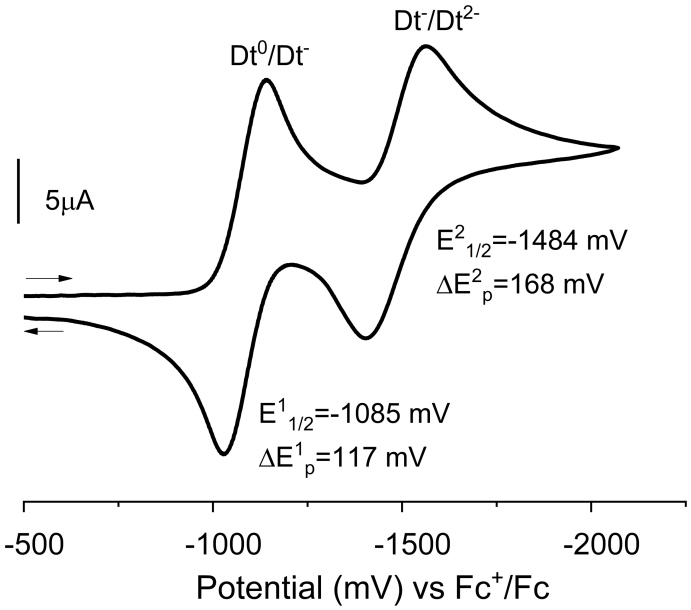

Figure 3.3. Cyclic voltammogram of MoO(tdt)($^{i}Pr_2Dt^0$). Scan rate, 100 mV s^{-1}; solvent, acetonitrile; temperature, 25 °C; Pt-disk working electrode, Ag/Ag^+ reference electrode, and a Pt-wire auxiliary electrode; supporting electrolyte, Bu_4NPF_6. Potentials referenced internally to Fc^+/Fc couple.

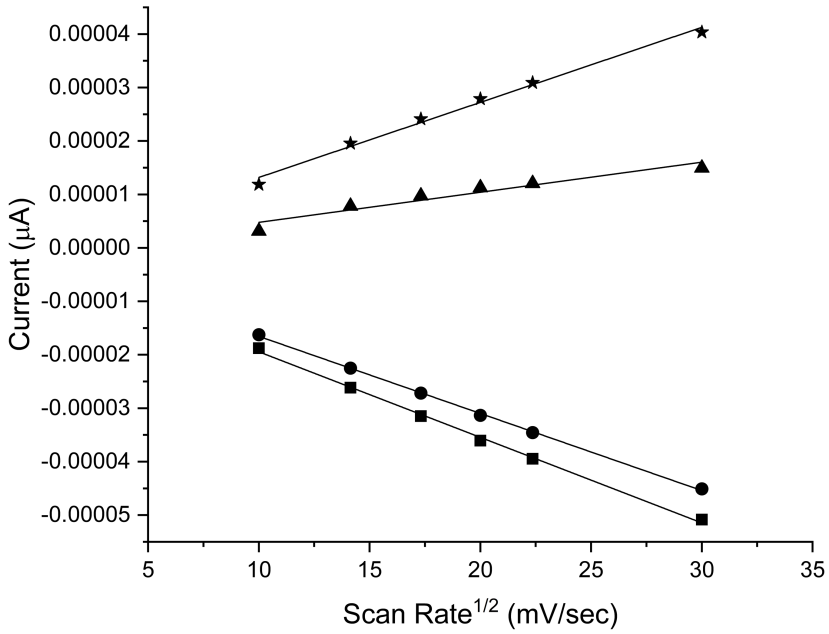

Figure 3.4. A plot showing the linearity of the peak current (i_p) versus the square root of the scan rate(v) for complex **6** suggesting diffusion-controlled processes. Fit of the equations are given below.

Oxidation

★ i_p= 1.40E-6(+/-6.36E-8)$n^{3/2}AD^{1/2}C^b$ -8.71E-7(+/-1.27E-6); r^2=0.99

▲ i_p= 5.63E-7 (+/-7.84E-8) $n^{3/2}AD^{1/2}C^b$ -8.56E-7 (+/- 1.57E-6); r^2=0.93

Reduction

● i_p= -1.44E-6 (+/- 1.91 E-8) $n^{3/2}AD^{1/2}C^b$ – 2.12E-6 (+/- 3.82E-7); r^2= 0.99

■ i_p= -1.60E-6 (+/- 3.78E-8) $n^{3/2}AD^{1/2}C^b$ – 3.44E-6 (+/- 7.56E-7); r^2= 0.99

Table 3.3. Redox potentials for the reduction of complexes **1**-**8** in acetonitrile at 100 mV/sec scan rate.

Complex	$E^1_{1/2}(\Delta E^1_p)$ (mV)	$E^2_{1/2}(\Delta E^2_p)$ (mV)
MoO(bdt)(Me_2Dt^0) (**1**)	-1058(86)	-1368(95)
MoO(tdt)(Me_2Dt^0) (**2**)	-1071(73)	-1375(73)
MoO(qdt)(Me_2Dt^0) (**3**)	-945(93)	-1289(96)
MoO($bdtCl_2$)(Me_2Dt^0) (**4**)	-1001(90)	-1346(93)
MoO(bdt)($^iPr_2Dt^0$) (**5**)	-1061(95)	-1455(107)
MoO(tdt)($^iPr_2Dt^0$) (**6**)	-1085(117)	-1484(168)
MoO(qdt)($^iPr_2Dt^0$) (**7**)	-938(58)	-1399(115)
MoO($bdtCl_2$)($^iPr_2Dt^0$) (**8**)	-1010(105)	-1431(127)

We propose that the redox couples are dithione ligand based. Previous reports of nickel dithione complexes show that when two fully oxidized dithione ligands are present, the reduction of the complexes exhibits four reversible reduction couples.[72] If only one dithione ligand is present as is the case in **6** only two reduction couples should be observed. Interestingly, reduction potentials of free $^iPrDt^0$ exhibits two redox couples at -1887 mV and -2088 mV (Figure 3.5), indicating that the reduction of the dithione ligand becomes easier upon metal coordination.

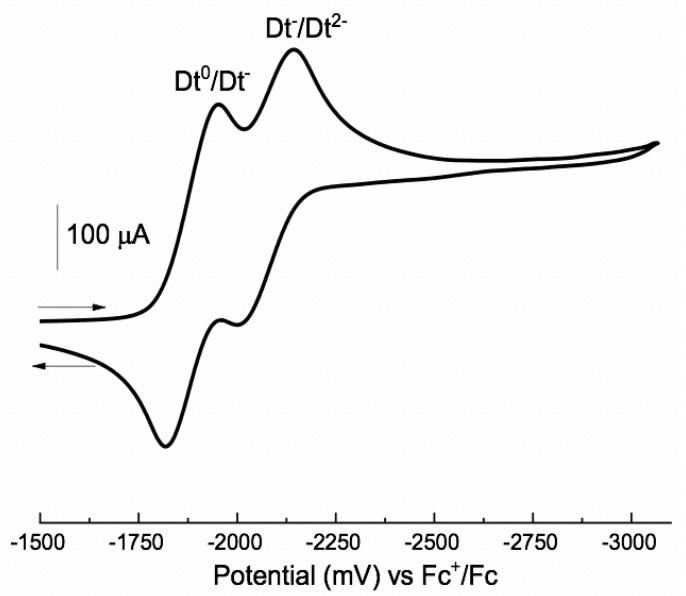

Figure 3.5. Cyclic voltammogram of $^{i}Pr_2Dt^0$ ligand. Scan rate, 100mV s^{-1}; solvent, acetonitrile; temperature, 25 ^{o}C; Glassy carbon working electrode, Ag/Ag+ reference electrode, and a Pt-wire auxiliary electrode; supporting electrolyte, Bu_4NPF_6. Potentials referenced internally to Fc^+/Fc couple.

We have previously reported on bis(dithione)-Ni(II) complexes; $[Ni(^{i}Pr_2Dt^0)_2][BF_4]_2$ and $[Ni(Me_2Dt^0)_2][BF_4]_2$ (where Me_2Dt^0= *N,N'*-dimethylpiperazine-2,3-dithione), whose reduction, we attributed to the reduction of the two dithione ligands. To further examine the nature of the reduction couples observed in **6**, the electrochemistry of Zn(mnt)($^{i}Pr_2Dt^0$) (where mnt= maleonitriledithiolate) was studied (Figure 3.6).[152] The redox properties are presented to demonstrate that the reduction of complex **6** is solely based on the $^{i}Pr_2Dt^0$. The reduction of Zn(mnt)($^{i}Pr_2Dt^0$) exhibited two quasi-reversible couples at -939 mV (ΔE_p= 115 mV) and -1365 mV (ΔE_p= 125 mV). Given that the metal center is a d^{10} metal, no reduction of the metal center is possible; we attribute the two couples in Zn(mnt)($^{i}Pr_2Dt^0$) to the reduction of the dithione ligand. The reduction couples of **6** and Zn(mnt)($^{i}Pr_2Dt^0$) are observed at similar potentials. In Zn(mnt)($^{i}Pr_2Dt^0$), two additional couples, although less defined, were observed ($E_{1/2}$ = -1556 mV, ΔEp= 90 mV and $E_{1/2}$ = -1862 mV, ΔEp= 122 mV), which are less negative than the couples

observed for free $^{i}Pr_2Dt^0$ ligand. We believe these two couples are due to dissociation of $^{i}Pr_2Dt^0$ ligand. The reduction of Zn(mnt)($^{i}Pr_2Dt^0$) was performed at multiple scan rates (Figure 3.6). As scan rate increases, the couple at $E_{1/2}$ = -1556 mV (ΔEp= 90 mV) is no longer observed. The peak height of the two reversible couples attributed to the coordinated ligand increase with increasing scan rate whereas the peak heights of the couple at $E_{1/2}$ = -1556 mV (ΔEp= 90 mV) does not increase. At a scan rate of 100 mV/sec the peak heights -1923 mV is ~50% and at a scan rate of 900 mV/sec the peak height at -1923 mV is ~8% of the peak height at -1601 mV. Dissociation of the ligand is a slow process and the concentration of free ligand can be decreased by increasing the scan rate. While the dithione ligand is able to easily dissociate from complexes **1-8** as shown in Chapter 2 Section 2.4 and the dissociation is observed in an electronically asymmetric zinc complex during the cyclic voltammetry time scale, such a phenomenon was not observed in the reduction of complexes **1-8**. The electron-withdrawing/donating capabilities of both the dithione and dithiolene ligand effect the ease at which the complexes were reduced. When comparing complexes with the same dithiolene ligand, complexes with the more electron-donating $^{i}Pr_2Dt^0$ resulted in more negative redox potentials. A similar trend was also observed when examining the electron-withdrawing/donating properties of the dithiolene ligand, which is interesting as the dithione ligands are able to effect small electronic perturbation at the dithiolene ligand indicating communication between the two ligands. Redox potentials are less negative when there is an

electron-withdrawing dithiolene like qdt and $bdtCl_2$ compared to the more negative redox potentials of the complexes possessing an electron-donating group like tdt.

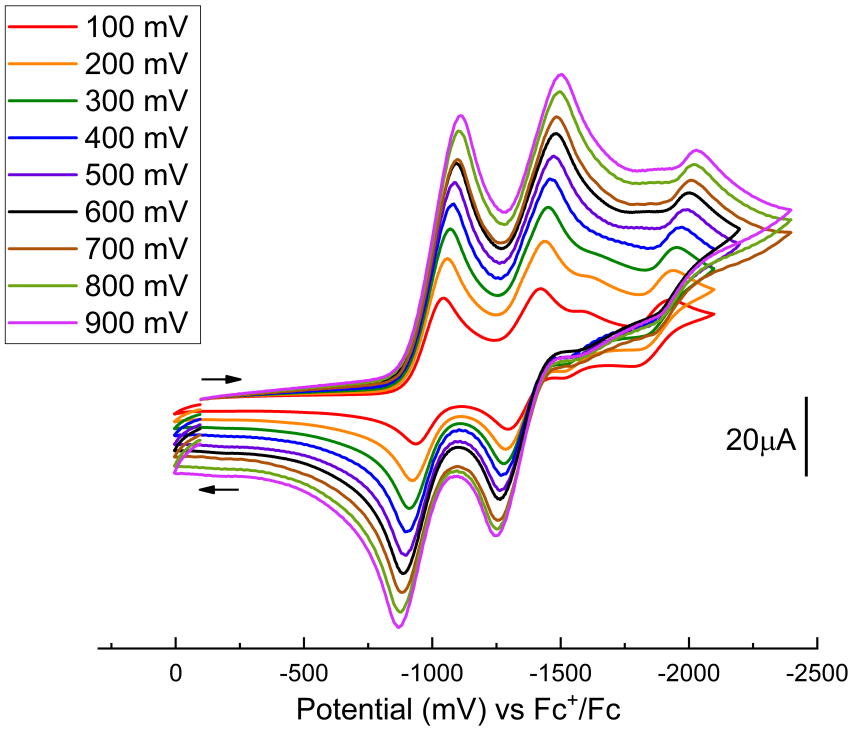

Figure 3.6. Cyclic voltammogram of Zn(mnt)($^{i}Pr_2Dt^0$) at varying scan rates ; solvent, acetonitrile; temperature, 25 °C; Pt-disk working electrode, Ag/Ag^+ reference electrode, and a Pt-wire auxiliary electrode; supporting electrolyte, Bu_4NPF_6. Potentials referenced internally to Fc^+/Fc couple.

3.3.2.b Oxidation of electronically asymmetric monooxo Mo(IV)- dithiolene complexes

Oxidation of the metal center in complexes **1-8** was shown to be irreversible with a representative cyclic voltammogram shown in Figure 3.7 (see Appendix A3 for further details). Two irreversible signals were observed at 262 mV and -277 mV for complex **6.** Typically, complexes of the general formula: $[Mo(IV)O(S_2C_2R_2)_2]^{2-}$ exhibit a reversible oxidation of the given Mo(IV) species to corresponding Mo(V) species. For instance $[MoO(bdt)_2]^{2-}$ exhibits a

redox potential of -39 mV for the oxidation to the Mo(V) species.[89] $[MoO(tdt)_2]^{2-}$ and $[MoO(mnt)_2]^{2-}$ exhibit redox potentials of -46 mV and 48 mV

respectively for the oxidation to Mo(V) (Table 3.4).[89, 120]

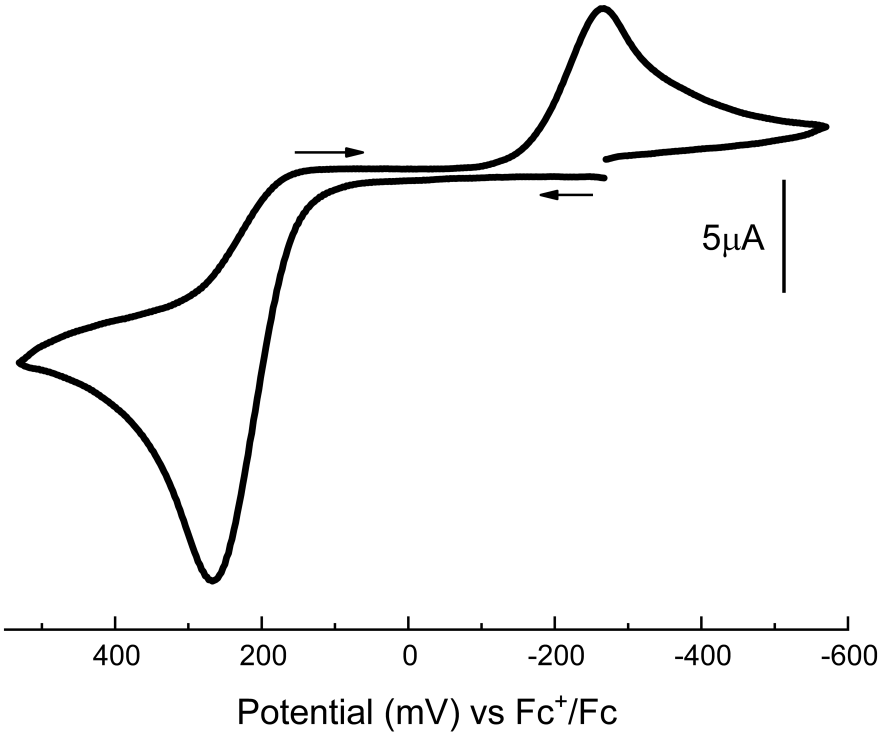

Figure 3.7. Cyclic voltammogram of complex **6**. Scan rate, 100 mV s^{-1}; solvent, acetonitrile; temperature, 25 °C; Pt-disk working electrode, Ag/Ag^+ reference electrode, and a Pt-wire auxiliary electrode; supporting electrolyte, Bu_4NPF_6. Potentials referenced internally to Fc^+/Fc couple.

Table 3.4. Redox potentials of $[MoO(Dt^{2-})_2]^{2-}$ complexes.

Complex	Mo^V/Mo^{IV}	Mo^{VI}/Mo^V	References
$[Mo^{IV}O(tdt)_2]^{2-}$	-0.46	Irr.	89
$[Mo^{IV}O(mnt)_2]^{2-}$	0.48	Irr	89
$[Mo^{IV}O(bdt)_2]^{2-}$	-0.39		89
$[Mo(bdtCl_2)_2]^{2-}$	-0.1		101

We hypothesize a structural change occurs in **6** during oxidation in terms of the fold angle that is observed in the crystal structure along the dithione ligand. Oxidation of the metal center from Mo(IV) to Mo(V) would facilitate electron donation from the electron-rich dithiolene ligand. This would decrease the electron density available for donation to the dithione ligand resulting in a decrease of the fold angle along the S•••S vector of the dithione ligand. Further investigation is ongoing into the irreversibility of the oxidation of **6**.

3.3.4 Generation of a π delocalized system: [MoO(Dt^{2-})(Dt^{1-})]$^{+}$

One of the main goals of this project was to develop a system that may exist in the molybdopterin enzyme cofactor in which one of the dithiolene ligands is a fully reduced ene-dithiolate and the other dithiolene ligand is π-delocalized. Initially from the cyclic voltammetry that was presented in Section 3.3.2.a, a comproportionation constant (K_c) can be calculated using the redox potentials following equation 2, where ΔE is the difference between the two redox couples.

$$\Delta G^{o} = -RT(\ln K_c) = -nF(\Delta E) \qquad (2)$$

The comproportionation constant gives insight into the stability of the local mixed valent species. All comproportionation constants (K_c) are tabulated in Table 3.5. The magnitude of K_c for complexes **1**-**8** are large, which indicates that the mixed valence species can be stabilized, and the electrons would not be redistributed to the redox-active dithiolene ligands at least in voltammetric time scale. The K_c values for complexes **5**-**8** possessing an $^{i}Pr_2Dt^{0}$ are an order of magnitude larger than complexes **1**-**4**. A similar trend was observed in previously reported $[Ni(Dt^{0})_2]^{2+}$ complexes.[72]

Table 3.5. Comproportionation constants for all electronically asymmetric complexes.

Complex	K_c
MoO(bdt)(Me_2Dt^0) (**1**)	$1.98x10^5$
MoO(tdt)(Me_2Dt^0) (**2**)	$1.63x10^5$
MoO(qdt)(Me_2Dt^0) (**3**)	$1.12x10^6$
MoO($bdtCl_2$)(Me_2Dt^0) (**4**)	$7.86x10^5$
MoO(bdt)($^iPr_2Dt^0$) (**5**)	$5.38x10^6$
MoO(tdt)($^iPr_2Dt^0$) (**6**)	$6.55x10^6$
MoO(qdt)($^iPr_2Dt^0$) (**7**)	$4.18x10^7$
MoO($bdtCl_2$)($^iPr_2Dt^0$) (**8**)	$1.56x10^7$

In order to study such a system, initially bulk coulometry followed with electron paramagnetic resonance (EPR) of **1** was performed. Mo(V) is typically characterized in EPR by the presence of an intense peak (I= 0) and six smaller satellite peaks. The smaller satellite peaks are due to the two naturally abundant isotopes, Mo^{95} (I= 5/2) and Mo^{97} (I=5/2).[153] If there is also a free sulfur radical signal, an intense peak at $g > 2.000$ present in the EPR.[71, 154-156] A sulfur radical signal was not observed. The EPR spectrum collected exhibited a weak peak at g=1.99528. Due to the low intensity of the central peak, the resulting satellite peaks are difficult to define. Prior to additional EPR studies, spectroelectrochemistry was used in attempts to generate a reduced species of **6**, $[MoO(tdt)(^iPr_2Dt^{\bullet})]^-$. During the course of the experiments, it was shown that the dithione ligand dissociated from the complex resulting in complex degradation. For further details, see Appendix A6.

3.4 Electronic Structure

3.4.1 UV-Vis Spectroscopy

The electronic spectra for complexes **1**-**4** and **5**-**8** in acetonitrile are presented in Figures 3.8 and 3.9. Complexes **1**, **2**, **4**, **5**, **6**, and **8** exhibit a similar absorption profile with a strong charge transfer (CT) transition at ~530 nm and a higher energy shoulder at ~380 nm and are tabulated for complexes **1**-**8** in Table 3.6. There is no observed change in the position of the CT bands based on the nature of the ligands present; complexes possessing either an $^{i}Pr_2Dt^0$ or Me_2Dt^0 dithione ligand exhibit a CT band at the same energy. The inclusion of electron-withdrawing/donating substituents on the dithiolene ligand does not cause a shift in the CT band energy. Previous reports on monodithiolene molybdenum complexes have demonstrated that dithiolene ligand substituents do not have an effect on the charge transfer energy.[157]

Table 3.6. Absorbance maxima for electronically asymmetric Mo(IV) complexes in acetonitrile.

Complex	Wavelength (nm)	ε ($M^{-1}cm^{-1}$)
MoO(bdt)(Me_2Dt^0) (**1**)	532	4400
MoO(tdt)(Me_2Dt^0) (**2**)	531	6050
MoO(qdt)(Me_2Dt^0) (**3**)	548	7450
MoO($bdtCl_2$)(Me_2Dt^0) (**4**)	531	4460
MoO(bdt)($^{i}Pr_2Dt^0$) (**5**)	529	6900
MoO(tdt)($^{i}Pr_2Dt^0$) (**6**)	533	7500
MoO(qdt)($^{i}Pr_2Dt^0$) (**7**)	543	7070
MoO($bdtCl_2$)($^{i}Pr_2Dt^0$) (**8**)	530	9400

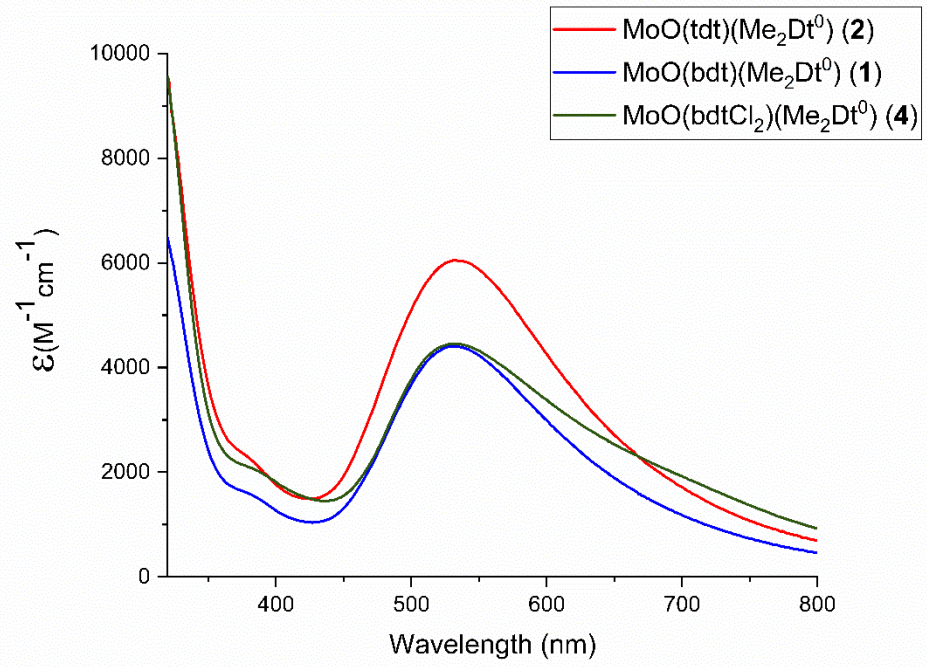

Figure 3.8 Absorbance spectra for complexes possessing the Me_2Dt^0 dithione ligand in acetonitrile.

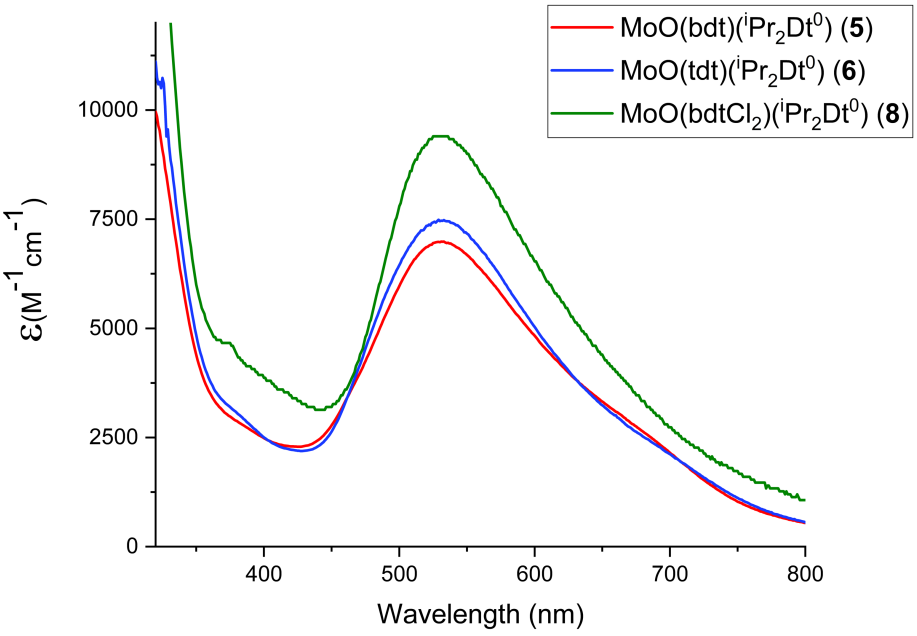

Figure 3.9. Absorbance spectra for complexes possessing the $^{i}Pr_2Dt^0$ dithione ligand in acetonitrile.

While the position of the CT band did not shift for complexes possessing bdt, tdt, and $bdtCl_2$ dithiolene ligands, there is a shift in energy of the CT band in complexes possessing qdt dithiolene ligand by ~10 nm (Figure 3.10). Even though there is no shift in the CT energy for all complexes except **3** and **7,** there is a change in the molar absorptivity that appears to be dependent upon the nature of the ligands coordinated to the molybdenum metal center. Complexes possessing the $^{i}Pr_2Dt^0$ dithione ligand exhibit a larger molar absorptivity than corresponding complexes possessing the Me_2Dt^0 dithione ligand. For example, there is a 2500 $M^{-1}cm^{-1}$ difference between complexes **5** and **1** and a 4940 M^{-1} cm^{-1} between complexes **4** and **8**. Complexes possessing $^{i}Pr_2Dt^0$ exhibit lower molar absorptivity when an electron-donating group is present (tdt) then when an electron- withdrawing group is present ($bdtCl_2$), the molar absorptivity of **8** is ~1900 $M^{-1}cm^{-1}$ higher than the molar absorptivity of **6**.

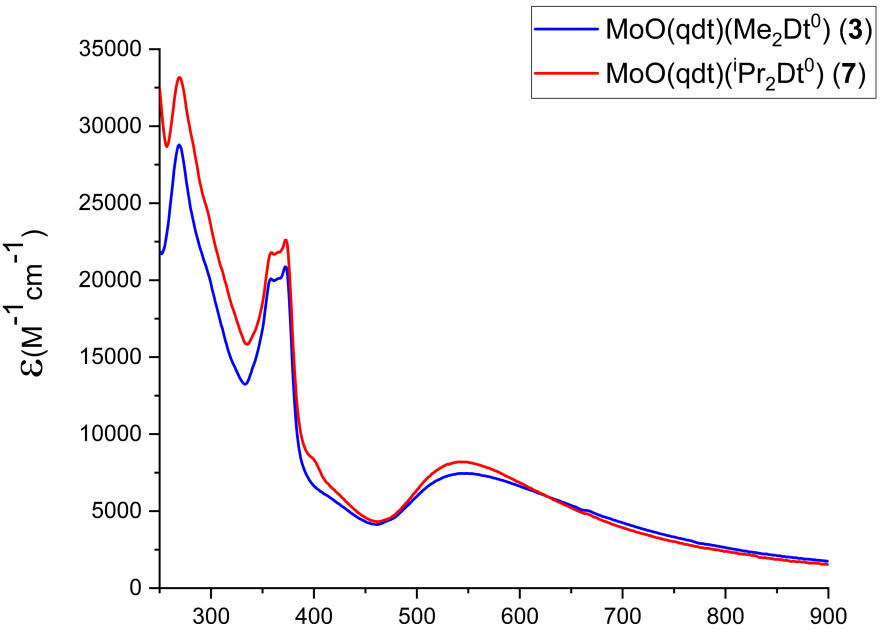

Figure 3.10. Absorbance spectra of **3** and **7** possessing the qdt ligand in acetonitrile.

The electronic spectra of electronically asymmetric complexes $[Mo^{IV}O(Dt^{2-})(Dt^{0})]$ exhibit significantly shifted charge transfer bands when compared to the electronically symmetrical complexes $[Mo^{IV}O(Dt^{2-})_2]^{2-}$. The absorbance maxima are tabulated in Table 3.6 for complexes of general structure $[Mo^{IV}O(Dt^{2-})_2]^{2-}$. While complexes **1**-**8** exhibit charge transfer bands at ~530 nm, $[Mo^{IV}O(Dt^{2-})_2]^{2-}$ complex exhibit charge transfer bands between ~301 nm - 363 nm; these charge transfers will be discussed in the next section.

3.4.2 Computational Investigation of the Electronic Structure of Electronically Asymmetric Complexes

3.4.2.a Density functional theory (DFT) of MoO(tdt)($^{i}Pr_2Dt^{0}$)

The electronic structure of **6** was explored computationally using density functional level of theory (DFT). The orbital energy diagram and the corresponding molecular orbitals are presented in Figure 3.11; C-squared population analysis is presented in Table 3.7. The energy difference between the HOMO and LUMO of **6** is 2.11 eV. HOMO-2/-3 and LUMO/+1 have the next largest energy differences at 1.21 eV and 1.40 eV, respectively. The HOMO and HOMO-1 orbitals exhibit similar electron distributions, both are ~85% tdt ligand in character. The largest contributors from the tdt ligand are the sulfur atoms that contributes ~44% to the total molecular orbital character. The HOMO-2 differs from the rest of the occupied orbitals by a large (44%) contribution from the Mo d_{xy} orbital. Virtual orbitals are distinguished by the increased participation of Mo and $^{i}Pr_2Dt^{0}$ ligand. The LUMO is composed of 69% $^{i}Pr_2Dt^{0}$ ligand, roughly a third of which is contributed by the sulfur atoms of $^{i}Pr_2Dt^{0}$. The Mo d_{xy} orbital also plays a significant role with a 25% orbital contribution to the LUMO. Subsequent virtual orbitals show a

~15% increase in Mo d orbital contribution and a ~35% decrease in $^{i}Pr_2Dt^0$ ligand orbital contribution.

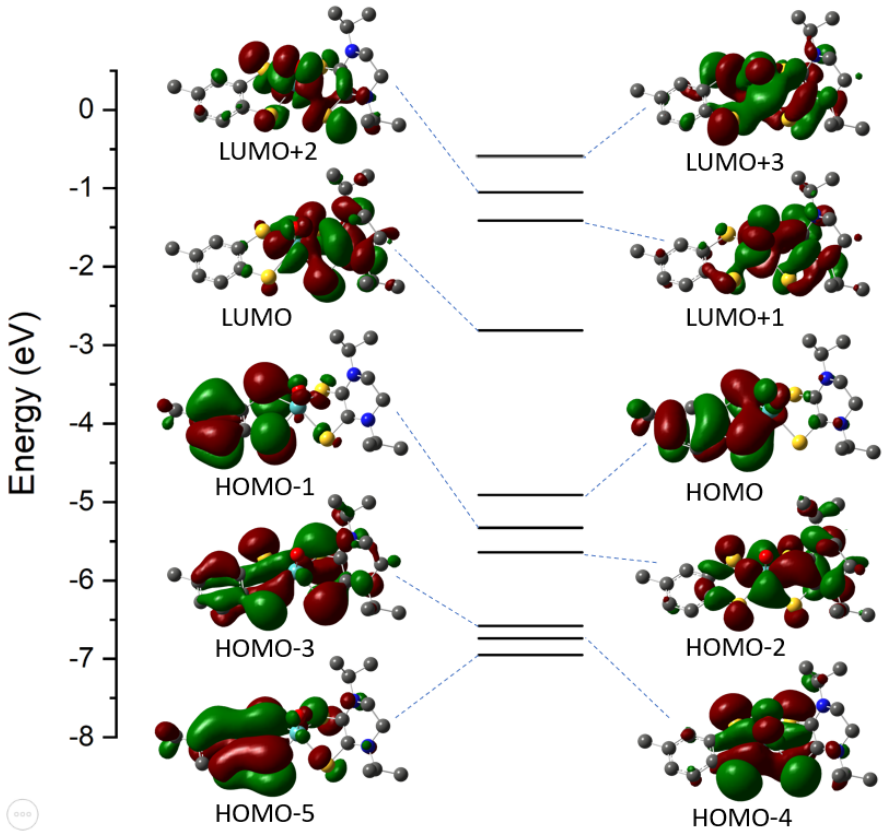

Figure 3.11. Orbital energy diagram and corresponding molecular orbitals for **6.**

Table 3.7. Atomic orbital composition for **6**. HOMO and LUMO orbitals are bolded.

Orbital	E, eV	Mo	Mo(d)	O	tdt	tdt (S)	$^{i}Pr_2Dt^0$	$^{i}Pr^2Dt^0$ (S)
LUMO+3	-0.69	39.60	31.74	6.57	27.26	23.50	26.57	5.76
LUMO+2	-1.05	48.47	39.81	10.24	17.89	16.34	23.40	17.21
LUMO+1	-1.41	42.55	35.40	9.71	9.32	7.67	38.42	14.78
LUMO	**-2.81**	**25.82**	**25.37**	**1.70**	**3.08**	**1.56**	**69.40**	**22.97**
HOMO	**-4.91**	**7.46**	**4.16**	**5.63**	**82.26**	**39.79**	**4.66**	**1.60**
HOMO-1	-5.33	1.36	1.05	1.99	87.81	49.26	8.84	6.62
HOMO-2	-5.64	46.93	44.00	0.11	13.71	8.27	39.25	6.25
HOMO-3	-6.58	4.30	3.58	0.03	34.40	25.13	61.27	47.93
HOMO-4	-6.74	9.25	4.94	9.11	38.01	33.47	43.63	36.03
HOMO-5	-6.95	1.93	0.99	1.12	82.96	47.75	13.99	10.29

Complex **6** exhibits a markedly different electronic structure when compared to previously studied $[MoO(bdt)_2]^{2-}$, $[MoO(tdt)_2]^{2-}$, $[MoO(bdtCl_2)_2]^{2-}$, $[MoO(qdt)_2]^{2-}$, and $[MoO(mnt)_2]^{2-}$ complexes possessing two fully reduced dithiolene ligands.[120] These electronically symmetric complexes exhibit a ligand-to-metal charge transfer band (LMCT) at 328 nm - 364 nm (30,487 cm^{-1} - 27,472 cm^{-1}) and are tabulated in Table 3.8. Complex **6** exhibits a band at 18,660 cm^{-1} that is shifted from the band observed at 13,510 cm^{-1} (1065 $M^{-1}cm^{-1}$) for precursor complex, $[MoOCl(^{i}Pr_2Dt^0)_2][PF_6]$, and is reminiscent of intense charge transfer transitions observed at ~18,000 cm^{-1} in $MoO(SPh)_2(^{i}Pr_2Dt^0)$.[80] We suggest that in the present case, the tdt ligand is acting as an electron donor while the dithione is serving as an electron acceptor; forming a donor-acceptor system. This electronic interaction is also consistent with the large fold angle observed in the solid state which facilitates increased orbital overlap, allowing more facile intramolecular electron transfer.

Table 3.8. Electronic properties of $[MoO(Dt^{2-})_2]^{2-}$ complexes.

Complex	λ_{max} (nm), (ε $M^{-1}cm^{-1}$)	Reference
$[Mo^{IV}O(bdt)_2]^{2-}$	328 (12000) 385 (980) 452 (470)	89, 120
$[Mo^{IV}O(tdt)_2]^{2-}$	331 (11000) 380 (700) 454 (370)	120
$[Mo(bdtCl_2)_2]^{2-}$	330 (9500) 394 (950)	101
$[Mo^{IV}O(Ph_3Si\text{-}bdt)_2]^{2-}$	359 (13000) 456 (300)	120
$[Mo^{IV}O(Ph_3Si\text{-}tdt)_2]^{2-}$	363 (15000) 447 (1600)	120
$[Mo^{IV}O(qdt)_2]^{2-}$	337 474 498	123

3.4.2.b Time-dependent density functional theory (TD-DFT) of MoO(tdt)($^{i}Pr_2Dt^{0}$)

Using the PCM-TDDFT approach, we further probed the electronic origin of these bands. The calculational data matched well with experimental data (Figure 3.12) and allow for the assignment of experimentally observed bands. It should be noted that the DFT-predicted HOMO-1 and HOMO-2 molecular orbitals are very close in energy (~ 0.31 eV). PCM-TDDFT calculations involving these orbitals also predict excited state transitions that are only ~880 cm^{-1} apart. Due to the similarity in energy, TDDFT calculations predict a transition from HOMO-2 to LUMO that is lower in energy than a transition from HOMO-1 to LUMO. The low energy 18660 cm^{-1} band observed in the UV-Vis spectrum of **6** corresponds to primarily an inter-ligand charge transfer (LL'CT) from the tdt ligand to the $^{i}Pr_2Dt^{0}$ ligand (excited states 1-3). Participation in the low energy LL'CT is limited to the HOMO/-1/-2 and LUMO orbitals. HOMO/-1/-2 to LUMO transitions can be visualized with electron density distribution maps (EDDMs) shown in Figure 3.12. EDDMs show HOMO/-1 to LUMO transitions to be a charge transfer from the electron-rich tdt ligand to the electron deficient $^{i}Pr_2Dt^{0}$ ligand. The HOMO-2 to LUMO transition shows the Mo

d_{xy} orbital donating electron density to the $^{i}Pr_2Dt^0$ ligand in a metal-to-ligand charge transfer (MLCT). The change in electron distribution can be followed with the population analysis of participating orbitals. Calculations support that the band includes participation of both the tdt ligand and the solely occupied Mo d_{xy} orbital. EDDMs and orbital diagrams of the virtual orbitals show the $^{i}Pr_2Dt^0$ ligand becomes reduced as the conjugated dithiolene system accepts electron density from the tdt ligand and Mo d_{xy} orbitals. Any transitions involving orbitals below HOMO-2 or above the LUMO corresponds to higher energy transitions due to the large energy difference to reach the HOMO-3 and LUMO+1 orbitals. The higher energy shoulder observed at 26000 cm^{-1} corresponds to a transition outside of the HOMO-2/LUMO domain (Figure 3.12). The most prominent transition as determined by CI expansion coefficients is from HOMO-1 to LUMO+2. The differential map clearly shows the transition to be a ligand-to-metal charge transfer (LMCT) as the tdt ligand transfers an electron to the Mo d_{yz} orbital.

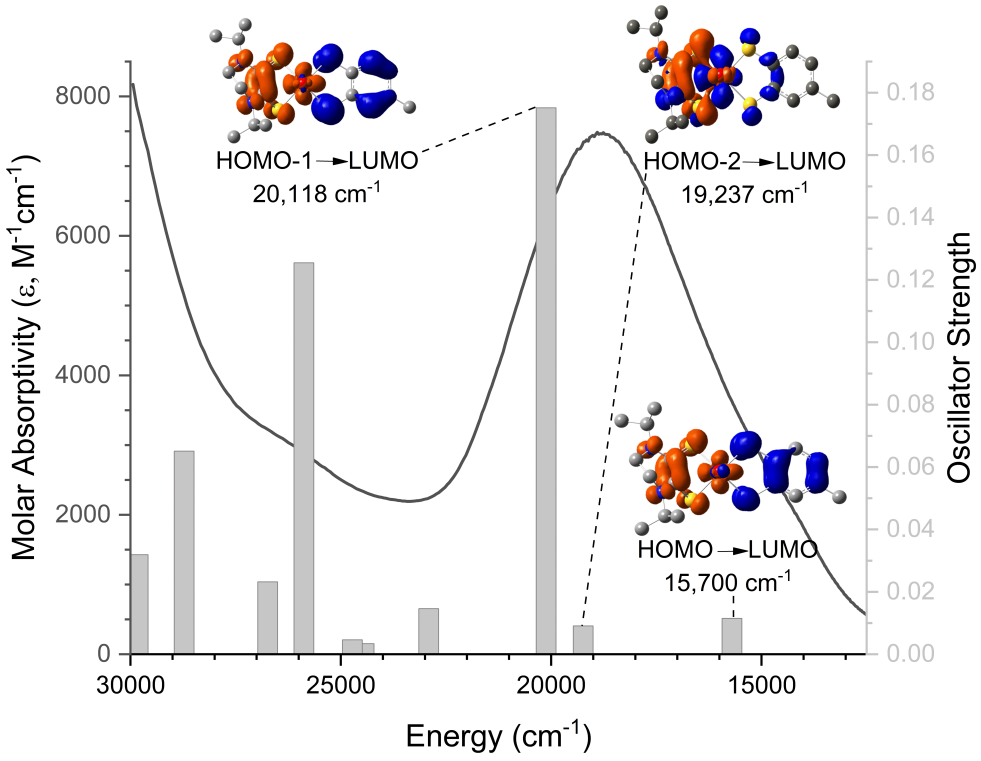

Figure 3.12. Calculated transitions (bars) imposed on experimental UV-Vis data of **6**. PCM-TDDFT calculations were done using acetonitrile as the solvent to match experimental conditions. Transitions for the low energy band are paired with their corresponding electron density differential map (EDDM). Electron-donating orbitals are blue and electron-accepting orbitals are orange. Energies are relative to the maximal value for each set of data in the given range.

3.5.2.c Effects Ligand Substituents Effects on the Electronic Structure of Electronically Asymmetric Complexes MoO(Dt^{2-})(Dt^{0})

DFT and TD-DFT analysis of complexes **1**-**5**,**7**, and **8** are performed identically to that of **6** in order to probe the effect that different ligand substituents have on the electronic structure. Molecular orbital diagrams and population analysis for **2** are shown in Figure 3.13 and Table 3.9, respectively. Molecular orbital diagrams for complexes **1**,**3**,**4**, and **5** are tabulated in the Appendix. The HOMO-2 and LUMO for **1**-**5** are energetically separated from subsequent orbitals by ~0.8 eV and ~1.6 eV, respectively, which was also observed in **6**. The HOMO and HOMO-1 orbitals

exhibit similar electron distribution as **6**; all have ~80% dithiolene ligand (Dt^{2-}) character with the sulfur atoms being the largest contributors. The HOMO-2 differs in that it is primarily occupied by a large contribution from the Mo d_{xy} (~45%) orbital. The LUMO is composed of ~70% dithione (Dt^{0}) ligand in composition with ~25% contribution from the Mo d_{xy} orbital which is facilitating the charge transfer from the dithiolene ligand. The atomic composition of the orbitals for complexes **1-8** within the HOMO-2 thru LUMO vary by less than 2%, although lower energy occupied molecular orbitals (<HOMO-3) do fluctuate in the atomic contributions of the ligands. These calculations suggest that changing substituents on the dithione and/or dithiolene ligands does not have a profound impact on the electronic structures of the complexes.

Table 3.9. Atomic orbital composition for **2**. HOMO and LUMO orbitals are bolded.

Orbital	eV	Mo	Mo(d)	O	tdt	Me_2Dt^0
LUMO+3	-0.709	35.64	32	3.9	32.1	28.36
LUMO+2	-1.093	49.02	39.9	10.6	18.59	21.79
LUMO+1	-1.357	45.72	37.2	9.8	7.27	37.2
LUMO	**-3.039**	**26.15**	**25.73**	**0.82**	**4.93**	**68.1**
HOMO	**-4.961**	**7.17**	**4.18**	**6.02**	**80.32**	**6.49**
HOMO-1	-5.389	1.45	1.05	1.85	87.43	9.28
HOMO-2	-5.726	47.78	45.08	0.07	14.97	37.18
HOMO-3	-6.705	9.85	7.31	1.78	63.7	24.67
HOMO-4	-6.848	4.59	1.97	6.54	18.54	70.33
HOMO-5	-7.013	1.41	0.43	3.54	75.34	19.7

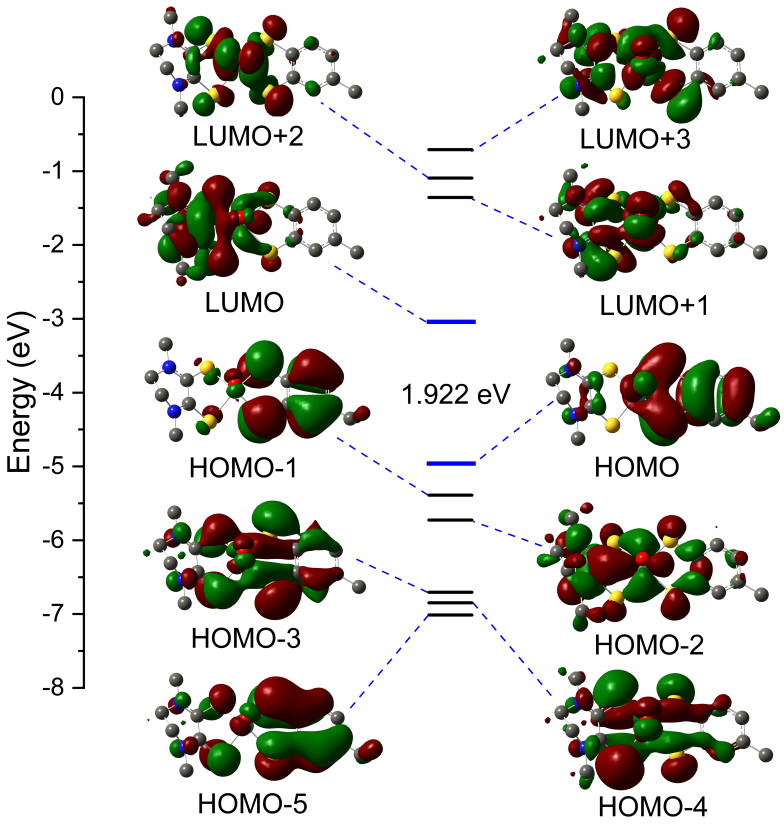

Figure 3.13. Molecular orbital diagrams for **2.** The energy gap between frontier orbitals (blue) is listed for each complex. Energies presented are relative.

TD-DFT calculations of complexes **1**-**8** match well with experimental spectra, as shown for **2** in Figure 3.14 (see Appendix for further details). The low energy charge transfer bands of complexes **1**-**8** are all LL'CT from the electron rich Dt^{2-} to the electron poor Dt^{0} ligand. All complexes besides **3** and **7** (which possess a qdt ligand) show the LL'CT bands are dominated by a HOMO-1 to LUMO charge transfers. The LL'CT bands for **3** and **7** are HOMO to LUMO charge transfers. The calculated energies of these transfers change less than 10 nm when comparing between methyl and isopropyl substituents on the Dt^{o} ligand. The calculated excited state transition energy for **3** and **7** are 40 nm and 25 nm greater than the other asymmetric complexes presented. EDDMs of the low energy charge transfer process for **1**-**4** is shown Figure 3.15. EDDMs of these complexes further support that the donor and acceptor orbitals remain similar despite changing the

substituents on the dithiolene and dithione ligands. While the energy of the LL'CT does not shift upon change of the coordinating ligands, there is a noticeable change in the molar absorptivity; complexes possessing $^{i}Pr_2Dt^0$ dithione ligand exhibited higher molar absorptivity as did complexes possessing dithiolene ligands with electron-donating substituents, such as tdt and qdt. There is change in lower energy molecular orbitals (<HOMO-3) which could have some effect the donor-acceptor relationship of higher energy LL'CT. Calculations cannot model difference in molar absorptivity observed between complexes as TD-DFT calculations are not reliable for accurately quantifying excited state oscillator strengths.

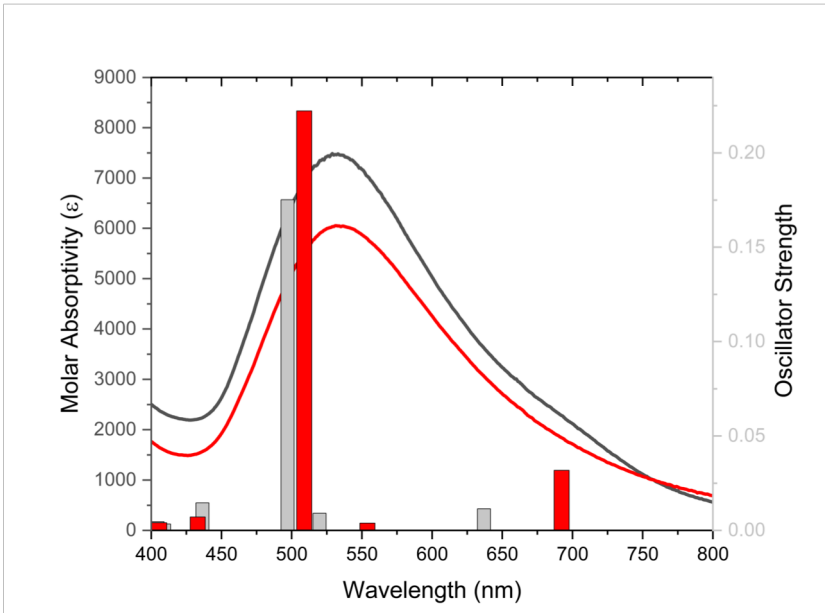

Figure 3.14. Electronic spectra (lines) with calculated excited state transitions superimposed (bars) for **2** (red line and bar) and **6** (black line/gray bar).

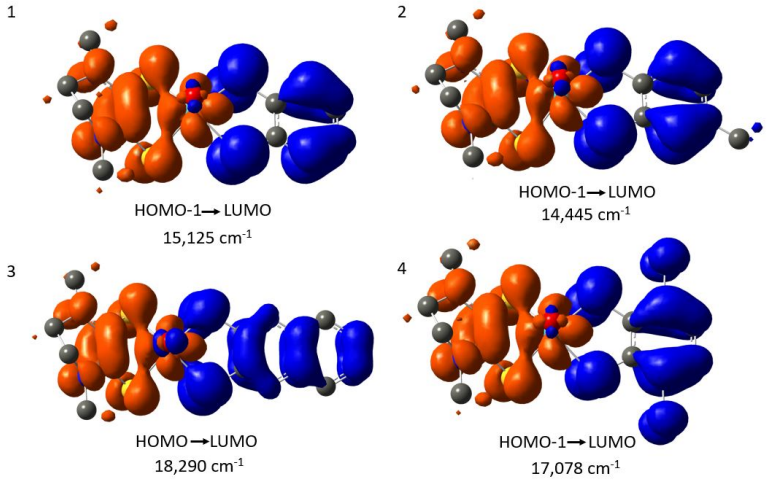

Figure 3.15. EDDMs of **1**,**2**,**3** and **4** corresponding to low energy LL'CT. Orange orbitals are electron-accepting while blue orbitals are electron-donating.

3.4.3 Positive Solvatochromic Effect Observed in Electronically Asymmetric Complexes

While the energy of the CT band does not shift upon changing the ligand coordinated to the molybdenum center, there is a shift in energy of the CT band upon change of the solvent environment. The energy of the CT band for all complexes in all solvents examined is tabulated in Table 3.10. Previously reported electronically asymmetric complexes, $M(Dt^{2-})(Dt^{0})$ where M= Ni, Pd, Pt, and Mo, have been shown to exhibit a negative solvatochromic effect. [10, 11, 70, 75, 158-160]

Table 3.10. Observed peak maxima of **1**,**2**,**4**,**5**,**6**, and **8** in different solvents.

Complex	Solvent	Maxima in nm and cm^{-1}
$MoO(bdt)(Me_2Dt^0)$ (**1**)	Tetrahydrofuran	512, 19531
	Dichloromethane	503, 19880
	Acetone	530, 18867
	Dimethylformamide	540, 18518
	Acetonitrile	533, 18769
	Dimethyl Sulfoxide	549, 18214
$MoO(tdt)(Me_2Dt^0)$ (**2**)	Tetrahydrofuran	494, 20242
	Dichloromethane	497, 20120
	Acetone	531, 18832
	Dimethylformamide	544, 18382
	Acetonitrile	535, 18691
	Dimethyl Sulfoxide	554, 18050
$MoO(bdtCl_2)(Me_2Dt^0)$ (**4**)	Tetrahydrofuran	517, 19342
	Dichloromethane	511, 19569
	Acetone	527, 18975
	Dimethylformamide	543, 18416
	Acetonitrile	533, 18762
	Dimethyl Sulfoxide	554, 18282
$MoO(bdt)(^iPr_2Dt^0)$ (**5**)	Tetrahydrofuran	510, 19607
	Dichloromethane	512, 19531
	Acetone	529, 18903
	Dimethylformamide	536, 18652
	Acetonitrile	531, 18832
	Dimethyl Sulfoxide	545, 18348
$MoO(tdt)(^iPr_2Dt^0)$ (**6**)	Tetrahydrofuran	495, 20202
	Dichloromethane	501, 19960
	Acetone	525, 19047
	Dimethylformamide	535, 18691
	Acetonitrile	532, 18796
	Dimethyl Sulfoxide	548, 18248
	Table 3.10 continued	
$MoO(bdtCl_2)(^iPr_2Dt^0)$ (**8**)	Tetrahydrofuran	519, 19268
	Dichloromethane	516, 19380
	Acetone	528, 18939
	Dimethylformamide	539, 18553
	Acetonitrile	531, 18832
	Dimethyl Sulfoxide	547, 18282

As shown in Table 3.10, as the polarity of the solvent increases, there is an increase in the energy of the CT band indicating a positive solvatochromic effect. A positive solvatochromic

effect is observed when the excited state of a complex is stabilized in more polar solvents. As discussed in Section 3.5.2, the nature of the CT band is that of a LL'CT transition indicating that the excited state would be a system in which the fully oxidized dithione has accepted an electron from the fully reduced dithiolene ligand generating a dithione ligand that is π delocalized in nature. The data for all complexes except **3** and **7** was fit to solvent dipole moment using a linear regression. The fit of the energy data for complex **6** is shown in Figure 3.16 and all of the correlation coefficients are shown in Table 3.11. The Kamlet-Taft Model was also employed to explore the positive solvatochromism (using multivariate analysis) using the following equation.[70, 161]

$E(cm^{-1}) = E^0 + s(\pi^*) + a\alpha + b\beta$

where s, a, and b are coefficients determined by the regression

π^*= parameter that describes the polarity and polarizability of the solvent
α= hydrogen bond donation ability of the solvent
β= hydrogen bond acceptance ability of the solvent

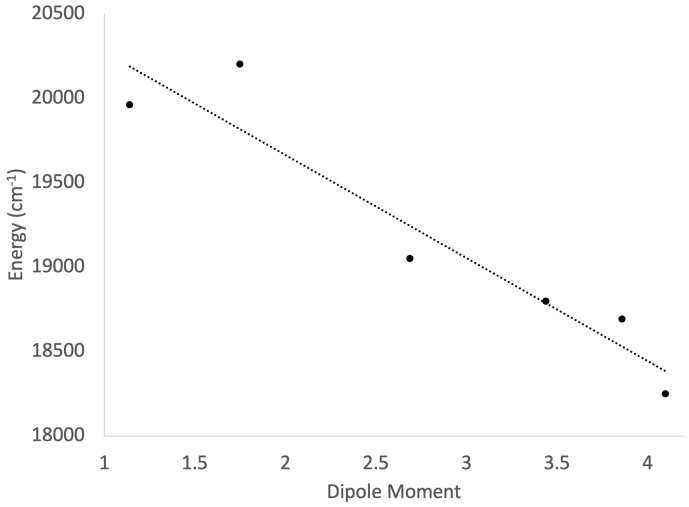

Figure 3.16. Linear correlation between dipole moment (μ) and the energy of the LL'CT of MoO(tdt)($^{i}Pr_2Dt^0$) (Equation of fit: E = -610.17μ + 20884)

The correlation coefficients for solvent dipole moment and the Kamlet Taft regression are tabulated in Table 3.11. Complexes **3** and **7** were highly unstable in the solution phase which did not allow for enough data points to be collected to fit to the Kamlet-Taft Model. Due to the limited number of solvents these results should be used with caution.

Table 3.11. Correlation coefficients of peak maxima fit to the Kamlet-Taft model.

Complex	**Dipole Moment**	**Kamlet-Taft**
	r^2	**r^2**
MoO(bdt)(Me_2Dt^0) (**1**)	0.97	0.98
MoO(tdt)(Me_2Dt^0) (**2**)	0.93	0.94
MoO($bdtCl_2$)(Me_2Dt^0) (**4**)	0.98	0.98
MoO(bdt)($^iPr_2Dt_0$) (**5**)	0.92	0.96
MoO(tdt)($^iPr_2Dt_0$) (**6**)	0.90	0.97
MoO($bdtCl_2$)($^iPr_2Dt^0$) (**8**)	0.93	0.99

3.5 Conclusion

In conclusion, we have presented the first series of a monooxo-Mo(IV) dithiolene complexes possessing two dithiolene ligands in different oxidation states. The molecular structure of **6** confirms the presence of both discrete oxidized and reduced dithiolene ligands bound to an oxo Mo^{IV}- center. Cyclic voltammetry studies demonstrate dithione ligand-based oxidation of **1**-**8**. Theoretical calculations and experimental results show an intense charge transfer band at 529 nm can be assigned to LL'CT from the dithiolene ligand to the dithione ligand.

CHAPTER 4. OXYGEN ATOM TRANSFER REACTIVITY OF THREE CLASSES OF MO(IV) MONOOXO DITHIOLENE COMPLEXES

4.1 Introduction

As discussed in Chapter 1, molybdopterin enzymes primarily function by transferring an oxygen atom (OAT) to or from the substrate. For example, DMSO reductase (DMSOR) transfers an oxygen atom from the substrate, dimethylsulfoxide (DMSO), producing water via electron and proton transfer process (Figure 4.1).[81] It has been proposed through resonance Raman studies of molybdopterin enzymes that the redox-active dithiolene ligands of the molybdenum cofactor (Moco) may exist in differing oxidation states during catalysis.[162] As opposed to two fully reduced dithiolene ligands, it has been shown that one dithiolene ligand is ene-1,2-dithiolate character and the second dithiolene is π delocalized in nature.[81] Previously studied small molecule mimics of Moco were designed to possess two fully reduced dithiolene ligands (Dt^{2-}) and a terminal oxo group $[Mo(IV)O(Dt^{2-})_2]^{2+}$ (Figure 4.2). We hypothesize that through modulation of the oxidation

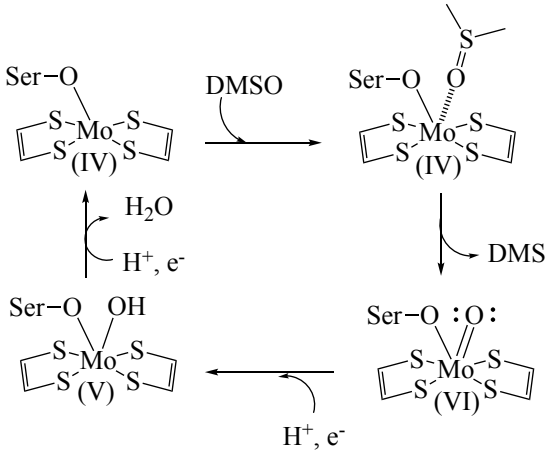

Figure 4.1. The proposed reaction scheme for the reduction of DMSO to DMS by Moco in dimethylsulfoxide reductase.

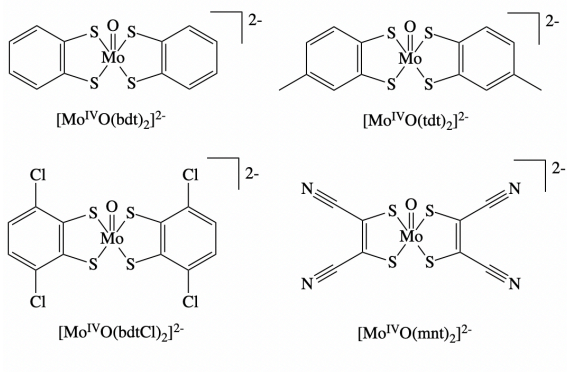

Figure 4.2. Examples of previously studied electronically symmetric small molecule mimics of the molybdenum- dithiolene moiety of Moco.

state of the redox active components that comprise the cofactor, the electronic structure and charge state of the Mo center is tuned for substrate catalysis.[119] To this end, we have designed three sets of complexes possessing fully oxidized dithiolene ligands and have studied their reactivity towards TMAO, DMSO, and NO_3^-.Two pathways can be studied to understand the OAT reactivity of molybdenum-dithiolene complexes:

1. A substrate donates an oxygen atom to the Mo metal center; one of the most heavily studied substrates for such reactions is trimethylamine-*N*-oxide (Scheme 4.1).[104, 105, 110-115, 118, 120, 163]

Scheme 4.1

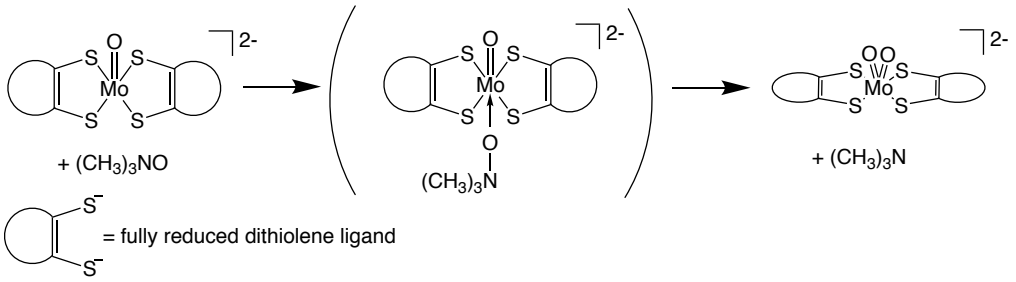

2. The Mo metal center donates an oxygen atom to the substrate; common substrates utilized are tertiary phosphines (Scheme 4.2).[89, 98, 101, 103, 164-168]

Scheme 4.2

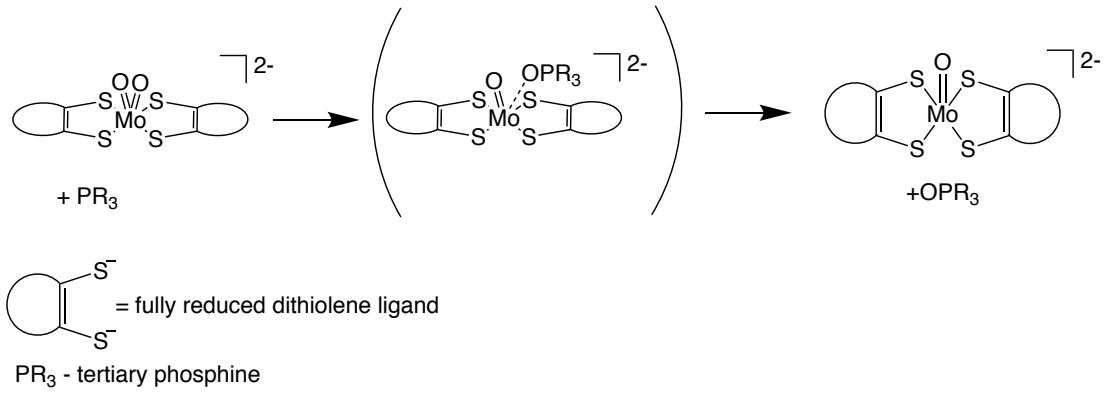

OAT reactivity of molybdenum-dithiolene complexes has commonly been explored using ^{1}H NMR, ^{31}P NMR, and mass spectrometry.[89, 105, 110, 115, 165-171] Both reactions are going to be explored in the following sections.

4.2 Materials and Methods

$MoO(tdt)(^{i}Pr_2Dt^{0})$ (**6**) was synthesized according to the methods in Chapter 2. $MoO(SPh)_2(^{i}Pr_2Dt^{0})$ (**10**) and $[MoOCl(^{i}Pr_2Dt^{0})_2][PF_6]$ (**12**) were synthesized according to literature procedures.[76, 80]

4.2.1. Physical Methods

^{1}H and ^{31}P NMR spectral data were collected using a Bruker 400 MHz spectrometer. Mass spectra were collected using either an Agilent Technologies 6520 Accurate Mass-QTOF LC/MS or an Agilent Technologies 6130 Quadrupole LC/MS.

4.2.2 Syntheses of Complexes

$MoO(SPh)_2(Me_2Dt^{0})$ (**9**): $[MoOCl(Me_2Dt)_2][PF_6]$ (150 mg, 0.154 mmol, based on **2a**.$2NaPF_6$) was dissolved in 50 mL of acetonitrile. Benzenethiol (146 mg, 1.33 mmol) and triethylamine (134 mg, 1.33 mmol) in acetonitrile was added, resulting in a purple solution. After 20 mins of stirring, the purple solution was dried in vacuum and the crude product dissolved in a minimum amount of acetonitrile, layered with ether and kept at 4 °C overnight. Purple crystals were collected via filtration. Yield: 83% (65 mg, 0.128 mmol) Anal. Calcd. (Experimental) for $C_{18}H_{20}N_2S_4MoO$: C, 42.85(42.68); H, 4.00(3.91), N, 5.55(5.51). ^{1}H NMR (CD_3CN): δ = 7.65 (d, Ph, 2H, *J*= 10 Hz); 7.24 (t, 4H, Ph, *J*= 10 Hz); 7.13 (t, 4H, Ph, *J*=10 Hz), 3.97 (m, 2H, CH_2); 3.72 (m, 2H, CH_2); 3.42 (s, 6H, CH_3). ^{13}C NMR (CD_3CN): δ = 181.5 (C=S), 134.32, 127.54, 125.71 (Ph), 49.03 (CH_3), 44.34 (CH_2). IR (neat, cm^{-1}): 1511 (vs, C-N), 1348 (vs, C=S), 947 (vs, Mo=O) 824(PF_6). λ_{max},

nm (ε, $M^{-1}cm^{-1}$) in CH_3CN: 554 (2880) 415 (sh, 1790) 339 (sh, 6400) 290 (sh, 8810) 237 (sh, 17750).

$[MoOCl(Me_2Dt^0)_2][PF_6]$ (**11**): Into a dry Schlenk flask, $MoCl_5$ (150 mg, 0.549 mmol) was dissolved in 5 mL of methanol resulting in the production of HCl (g). The solution was stirred until the cessation of HCl(g). Me_2Dt^0 (190 mg, 1.09 mmol) was added neat, and the reaction mixture was stirred for 30 minutes before adding 460 mg (2.74 mmol) of $NaPF_6$ in methanol (5 mL). After stirring for an additional 30 mins, the solution was filtered and the precipitate was washed with methanol and CH_2Cl_2 several times to obtain final product. Yield: 51% (0.270 mg, 0.276 mmol based on **1a**.2$NaPF_6$). Anal. Calcd (Experimental) for $C_{12}H_{20}ClF_{18}MoN_4Na_2OP_3S_4$ (**1a** + 2$NaPF_6$): C, 14.75 (14.27); H, 2.06 (2.11); N, 5.74 (5.42). FTIR (neat, cm^{-1}): 1551 (vs, C-N), 1366 (vs, C=S), 1261, 1099, 980 (vs, Mo=O), 830 (vs, PF_6). ^1H NMR (CD_3CN): δ = 4.22 (s, 4H, CH_2), 3.91(s, 6H, CH_3); ^{13}C NMR (CD_3CN): δ= 180.75 (C=S), 43.16 (CH_2), 17.69 (CH_3). $\lambda_{max,}$ nm (ε, $M^{-1}cm^{-1}$) in CH_3CN: 746 (3370), 507 (1920), 421 (sh, 2660), 313 (19900), 208 (3980). Molar Λ (MeCN): 220 Ω cm^2mol^{-1}.

4.2.3 Reactivity Studies

4.2.3.a. Probing by ^1H and ^{31}P NMR Spectroscopy

OAT reactivity was explored for five different complexes: $MoO(tdt)(^iPr_2Dt^0)$ (**6**), $MoO(SPh)_2(Me_2Dt^0)$ (**9**), $MoO(SPh)_2(^iPr_2Dt^0)$ (**10**), $[MoOCl(Me_2Dt^0)_2][PF_6]$ (**11**), and $[MoOCl(^iPr_2Dt^0)_2][PF_6]$ (**12**). Sample preparation was similar for all reactions. Stock solutions of complex (0.027 mmol-0.035 mmol) in 2.0 mL of CD_3CN, TMAO (0.053 mmol-0.066 mmol in 0.5 mL CD_3CN, and tertiary phosphine (0.027 mmol-0.035 mmol) in 0.5 mL of CD_3CN were prepared. ^1H NMR and ^{31}P NMR spectroscopy were used to probe the following reactions:

1. Complex + TMAO; 5 μL of TMAO was dissolved in 400 μL of CD_3CN. 100 μL of complex was added to the reaction mixture
2. Complex + Tertiary phosphine; 10 μL of phosphine was dissolved in 400 μL of CD_3CN. 100 μL of complex was added to the reaction mixture
3. Complex + TMAO + Tertiary phosphine; 5 μL of TMAO and 10 μL of phosphine was dissolved in 400 μL of CD_3CN. 100 μL of complex was added to the reaction mixture

Specific stock solutions that were used are listed below:

a. $MoO(tdt)(^{i}Pr_2Dt^0)$ (16 mg, 0.033 mmol), TMAO (5.0 mg, 0.066 mmol), PEt_2Ph (5.9 μL, 0.033 mmol)
b. $MoO(SPh)_2(Me_2Dt^0)$ (13 mg, 0.027 mmol), TMAO (4.0 mg 0.053 mmol), PEt_2Ph (4.6 μL, 0.027 mmol)
c. $MoO(SPh)_2(^{i}Pr_2Dt^0)$ (15 mg, 0.027 mmol), TMAO (4.0 mg 0.053 mmol), PEt_2Ph (4.6 μL, 0.027 mmol)
d. $MoOCl(Me_2Dt^0)_2][PF_6]$ (17 mg, 0.027 mmol), TMAO (4.0 mg 0.053 mmol), PEt_2Ph (4.6 μL, 0.027 mmol)
e. $[MoOCl(^{i}Pr_2Dt^0)_2][PF_6]$ (20 mg, 0.033 mmol), TMAO (4.9 mg 0.066 mmol), PEt_2Ph (5.9μL, 0.033 mmol)
f. $[MoOCl(Me_2Dt^0)_2][PF_6]$ (20 mg, 0.031 mmol), TMAO (4.6 mg 0.062 mmol), PEt_3 (4.5 μL, 0.031 mmol)
g. $[MoOCl(^{i}Pr_2Dt^0)_2][PF_6]$ (20 mg, 0.027 mmol), TMAO (43.8 mg 0.053 mmol), PEt_3 (3.9μL, 0.027 mmol)
h. $[MoOCl(Me_2Dt^0)_2][PF_6]$ (20 mg, 0.031 mmol), TMAO (4.6 mg 0.062 mmol), PPh_2Et (6.3 μL, 0.031 mmol)

i. [MoOCl(^{i}Pr$_2$Dt^0)$_2$][PF$_6$] (20 mg, 0.035 mmol), TMAO (3.9 mg 0.053 mmol), PPh$_2$Et (7.2 μL, 0.035 mmol)

4.2.3.b Probing with Mass Spectrometry

All of the reactions presented in Section 4.2.3.1 were also probed using mass spectrometry. MoO(tdt)(^{i}Pr$_2$Dt^0) was dissolved in a solution of acetonitrile with 0.1 % formic acid and NH$_4$Cl. MoO(SPh)(Me$_2$Dt^0) and MoO(SPh)$_2$(^{i}Pr$_2$Dt^0) were dissolved in a solution of acetonitrile and NH$_4$Cl. [MoOCl(Me$_2$Dt^0)$_2$][PF$_6$] and [MoOCl(^{i}Pr$_2$Dt^0)$_2$][PF$_6$] were dissolved in acetonitrile. TMAO, PEt$_2$Ph, PEt$_3$, and PPh$_2$Et were dissolved in acetonitrile. Complex solution and substrate solutions were simultaneously injected into the mass spectrometer.

OAT reactivity of MoO(tdt)(^{i}Pr$_2$Dt^0) was probed using an Agilent Technologies 6520 Accurate Mass-QTOF LC/MS over a drying gas temperature range of 150 ^{o}C- 350 ^{o}C and fragmentor voltages of 45 V-125 V. OAT reactivity of MoO(SPh)$_2$(Me$_2$Dt^0), MoO(SPh)$_2$(^{i}Pr$_2$Dt^0), [MoOCl(Me$_2$Dt^0)$_2$][PF$_6$], and [MoOCl(^{i}Pr$_2$Dt^0)$_2$][PF$_6$] was probed using an Agilent Technologies 6130 Quadrupole LC/MS over a range of drying gas temperature range 150 ^{o}C- 350 ^{o}C and fragmentor voltages of 45 V- 125 V.

4.3 Results

The chemical reactivity of three series of monooxo-Mo(IV) dithiolene complexes towards biologically relevant substrates has been explored. Three different substrates were used: dimethyl sulfoxide (DMSO), trimethylamine-*N*-oxide (TMAO), and tetrabutylammonium nitrate (Bu$_4$N[NO$_3$]). Complexes were reacted with substrate in acetonitrile solutions. TMAO was the only substrate that reacted with all three classes of complexes and the results of those reactivity studies are presented in the following sections. The reactions were probed using both NMR

spectroscopy and mass spectrometry; full experimental details are presented in Section 4.2. Three reactions were explored:

1. Target complex and TMAO

As will be discussed in the following sections, all complexes studied proved unstable in the presence of TMAO which resulted in degradation of the desired dioxo complexes. Excess complex was used in all NMR reactions in attempts to slow down the OAT processes to allow for observation of the corresponding dioxo complex.

2. Target complex and tertiary phosphines

3. Target complex, TMAO, and tertiary phosphines

Tertiary phosphines, which are well known oxygen-atom abstracting agents, were utilized to indirectly probe the presence of a $Mo^{VI}O_2$ unit.[89, 98, 101, 164, 166-168, 172-181] First, a control reaction between target complex and tertiary phosphine was performed to observe any reactivity that may impact the OAT reaction with TMAO. Second, a mixture of TMAO and tertiary phosphine was reacted with target complex. This was done to observe if free phosphine oxide was generated from abstracting the oxygen atom from the unstable $Mo^{VI}O_2$ complex prior to degradation.

All reactions discussed were monitored with ^{1}H NMR and ^{31}P NMR (when tertiary phosphine was used as a reactant) spectroscopy. Due to the instability of the $Mo^{VI}O_2$ complex, mass spectrometry was used to monitor the reaction to observe potential reaction intermediates or products. Acetonitrile solutions of the target complex and substrate were injected simultaneously into the mass spectrometer. We have successfully used this approach to understand the reactivity of oxo-Mo complexes.[167, 169-171]

4.3.1 Oxygen Atom Reactivity of Electronically Asymmetric Complexes: MoO(Dt^2)(Dt^0)

No reaction between DMSO or $Bu_4N[NO_3]$ and electronically asymmetric complexes (**1**-**8**) was observed; only TMAO reacted with all complexes. The reactivity of complex **6** was explored as a representative example for all electronically asymmetric complexes.

When an excess (> 2 equivalents) of TMAO is added to the solution of **6**, the purple solution changes to brown. The ^1H NMR spectrum of the reaction mixture (Figure 4.3) exhibits resonances for TMAO (δ_H 3.28 ppm (s)), TMA (δ_H 2.8 ppm(s, 9H)), **6** (δ_H 1.27 ppm (d, *J*=7.22 Hz, 6H); 1.43 ppm (d, *J*=6.85, 6H); 2.34 ppm (s, 3H); 3.73 (m, 2H); 4.01(m, 2H); 5.22 (hept, *J*= 6.7 Hz, 2H); 6.93 ppm (d, *J*= 8.15 Hz, 1H); 7.47 ppm (s, 1H); 7.51 ppm (d, *J*=7.93 Hz, 1H)), and the uncoordinated dithione ligand (δ_H 1.24 ppm (d, *J*= 6.87 Hz, 12H); 3.40 ppm (s, 4Hs); 5.39 ppm (p, *J*= 6.9 Hz, 2H)). The observation of TMA is consistent with the formation of a $Mo^{VI}O_2$ complex due to the oxygen atom transfer (OAT) from TMAO to **6** generating TMA. Due to the inherent instability of the corresponding dioxo complex, $MoO_2(tdt)(^iPr_2Dt^0)$, it was not observed in the NMR experiment.

The reaction between TMAO and **6** was further probed by mass spectrometry. In the reaction mixture, a peak cluster consistent with [**6**+ TMAO]$^{+}$ was observed at m/z ~ 574 (Figure 4.4). The isotope distribution pattern of the observed and predicted ion match well with the formulation, further supporting the composition of the species. A peak cluster consistent with the

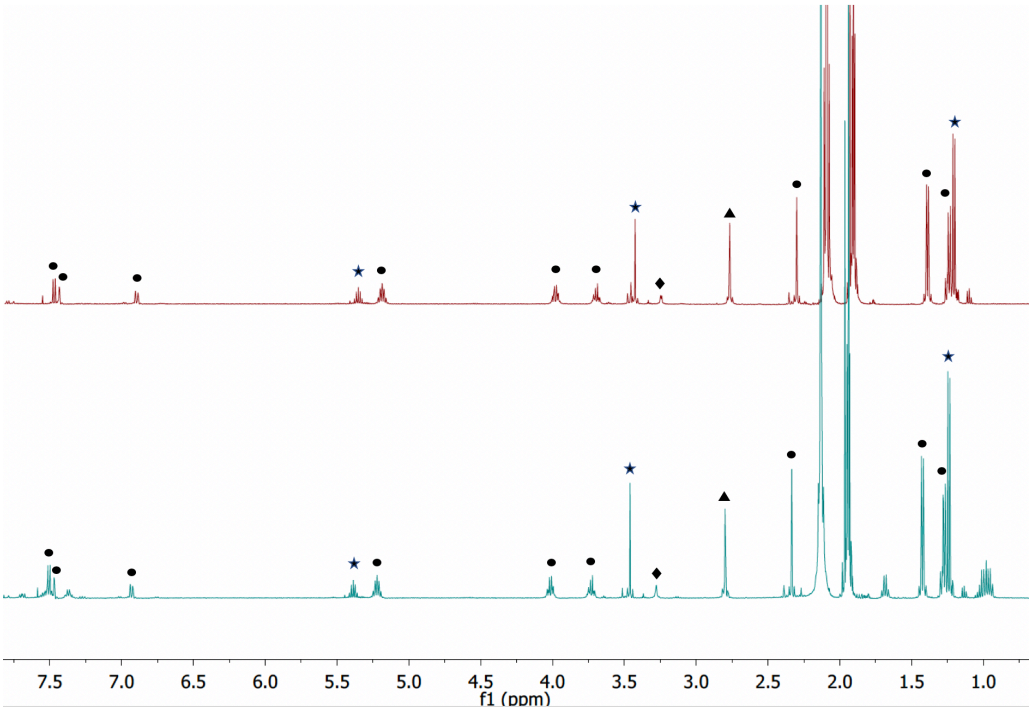

Figure 4.3. ^{1}H NMR (CD_3CN) spectra of the reaction between TMAO, PEt_2Ph and MoO(tdt)($^{i}Pr_2Dt^{0}$) in acetonitrile at room temperature. Top spectrum; Reaction between TMAO and MoO(tdt)($^{i}Pr_2Dt^{0}$) , Bottom spectrum; Reaction between PEt_2Ph and MoO(tdt)($^{i}Pr_2Dt^{0}$). Chemical shifts are denoted symbolically: MoO(tdt)($^{i}Pr_2Dt^{0}$) = ●; free $^{i}Pr_2Dt^{0}$ = ★; TMAO =. ♦;TMA = ▲.

formation of [MoO(tdt)$_2$]$^{-}$ was also observed, which suggests the formation of [MoO(tdt)$_2$]$^{-}$ from the unstable $Mo^{VI}O_2$ complex through loss the oxidized dithione ligand (Figure 4.5).

The formation of a $Mo^{VI}O_2$ complex was probed by reaction with diethylphenylphosphine (PEt_2Ph). In control experiments, **6** was reacted with PEt_2Ph under similar conditions. Three resonances consistent with unreacted PEt_2Ph (δ_P= 15.74 ppm), $OPEt_2Ph$ (δ_P= 41.89 ppm, which is also observed in free PEt_2Ph samples) and a peak at δ_P= 51.95 ppm due to coordinated phosphine

complex, MoO(tdt)(PEt_2Ph)($^iPr_2Dt^0$) were observed (Figure 4.6). Another possibility would be a phosphine oxide complex, Mo($OPEt_2Ph$) (tdt)($^iPr_2Dt^0$), however previously reported molybdenum phosphoryl complexes exhibit chemical shifts between 64.7 ppm - 69.2 ppm for the coordinated $OPEt_2Ph$.[172] Another control experiment shows that TMAO does not react with PEt_2Ph (Figure 4.7). The reaction of **6** and PEt_2Ph was also probed by mass spectrometry. When acetonitrile solutions of **6** and PEt_2Ph were injected simultaneously into the mass spectrometer, a peak cluster consistent with [**6** + PEt_2Ph]$^+$ was observed at m/z ~665 (Figure 4.8).

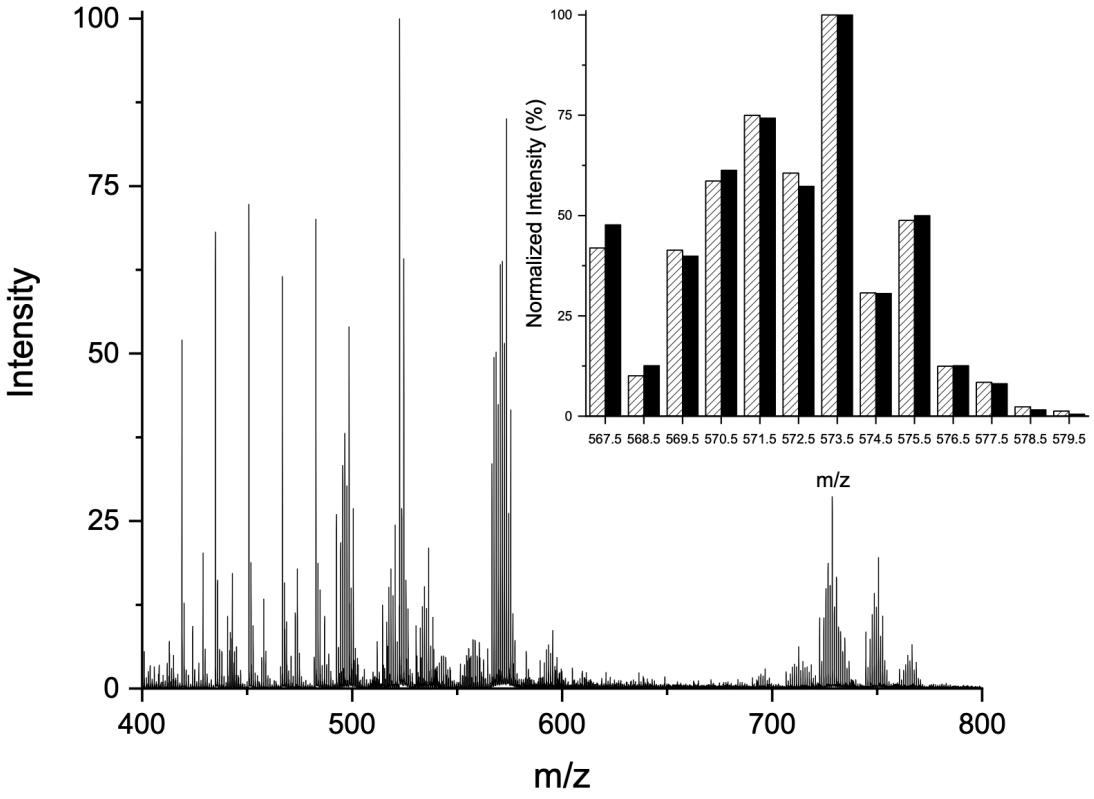

Figure 4.4. ESI-MS of the reaction between **6** and TMAO. Inset: ESI-MS parent ion of MoO(tdt)(Me_3NO)($^iPr_2Dt^0$) intermediate formed during the reaction between MoO(tdt)($^iPr_2Dt^0$) and trimethylamine-*N*-oxide. Plotted are the experimental (hatched) and calculated (solid) spectra for $C_{20}H_{33}MoN_3O_2S_4^+$.

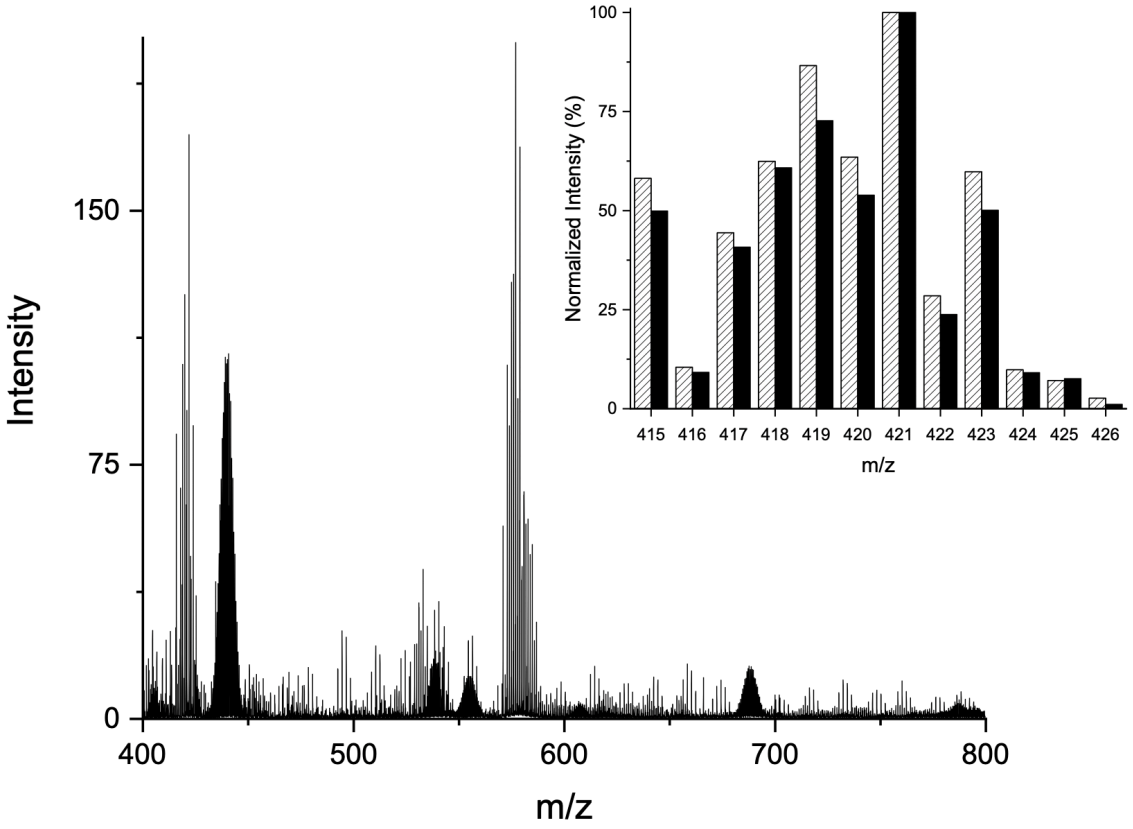

Figure 4.5. ESI-MS of the reaction between **6** and TMAO. Inset: ESI-MS parent ion of $[MoO(tdt)_2]^-$ formed during the reaction between $MoO(tdt)(^iPr_2Dt^0)$ and TMAO. Plotted are the experimental (hatched) and calculated (solid) spectra for $C_{14}H_{12}MoOS_4^+$

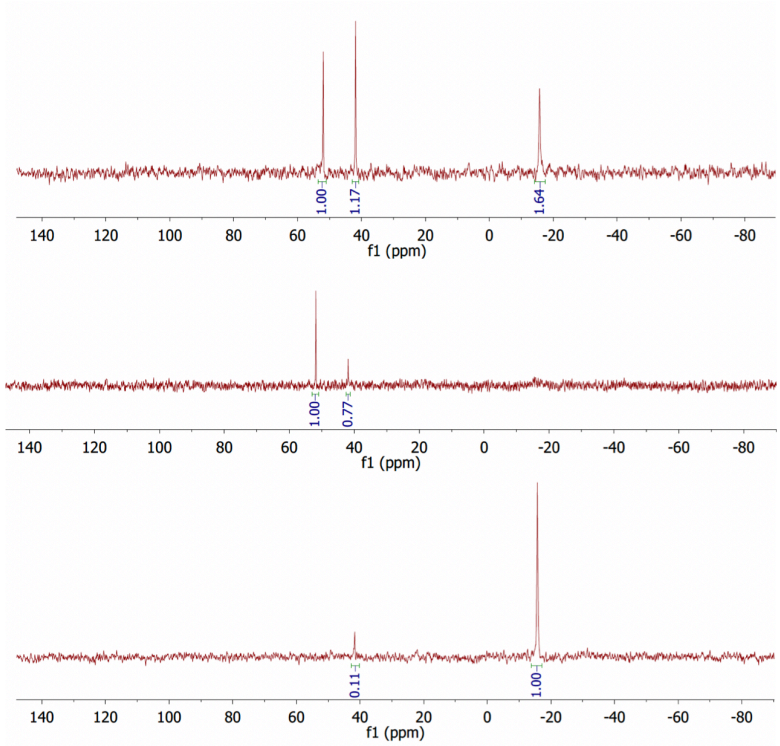

Figure 4.6. ^{31}P NMR (CD_3CN) spectral studies on the reaction between TMAO, PEt_2Ph and MoO(tdt)($^{i}Pr_2Dt^0$) in acetonitrile at room temperature. Top spectrum is the reaction between **6**, TMAO, and PEt_2Ph. Middle spectrum is the reaction between **6** and PEt_2Ph. The bottom spectrum is PEt_2Ph. Integration is shown to determine if the $OPEt_2Ph$ (~41 ppm) originates from the stock of PEt_2Ph or is formed during the reaction between 6 and PEt_2Ph.

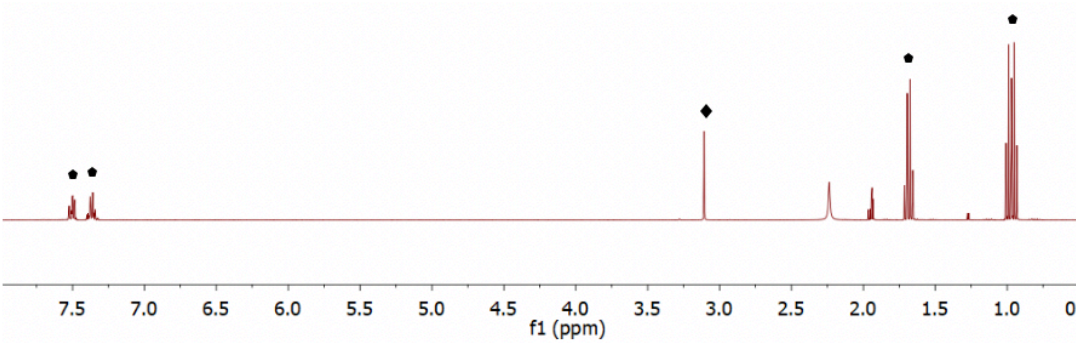

Figure 4.7. 1H NMR (CD_3CN) spectrum testing the reactivity of TMAO and PEt_2Ph. The study indicates that the two substrates do not react with each other; TMAO is represented with a ♦ and PEt_2Ph is represented with a ♠.

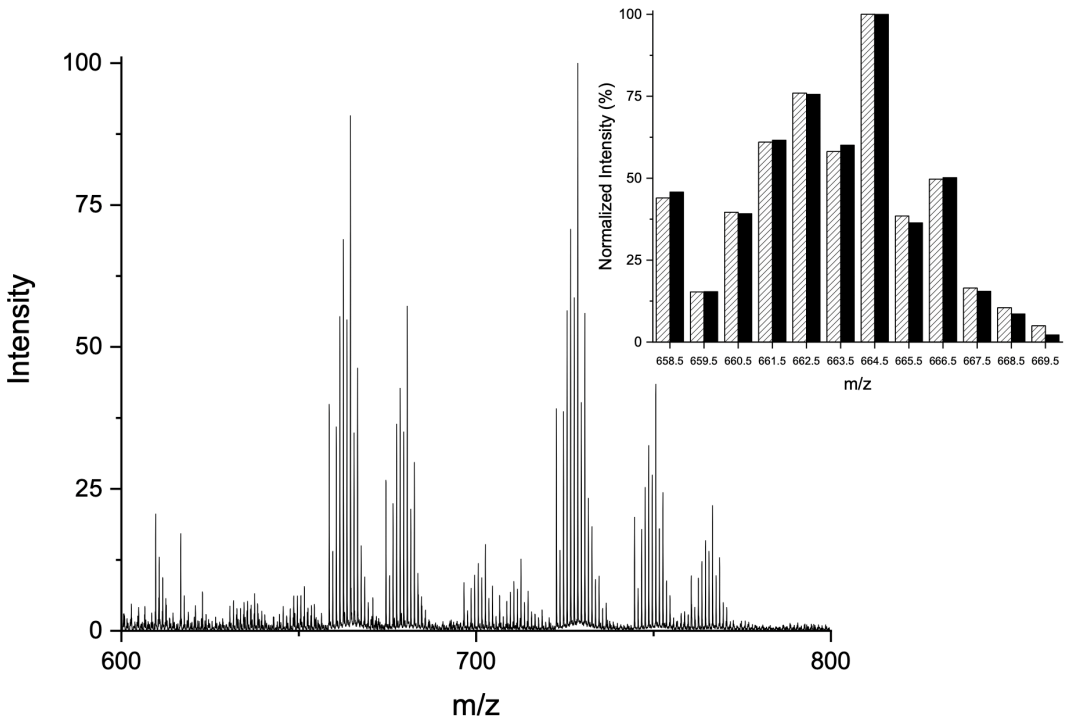

Figure 4.8. ESI-MS parent ion of MoO(PEt$_2$Ph)(tdt)(^{i}Pr$_2$Dt^0) formed during the reaction between MoO(tdt)(^{i}Pr$_2$Dt^0) and PEt2Ph. Plotted are the experimental (hatched) and calculated (solid) spectra for $C_{27}H_{39}MoN_2OPS_4^+$.

Finally, a solution of TMAO and PEt_2Ph was reacted with **6** and the reaction followed with ^1H NMR.^{31}P NMR spectroscopy and mass spectrometry (Figure 4.3/4.6). The ^1H NMR spectrum exhibited a chemical shift for TMA ((δ_H= 2.8 ppm) as well as uncoordinated $^iPr_2Dt^0$ ligand which are similar results that were observed during the reaction between **6** and TMAO. The ^{31}P NMR spectrum (Figure 4.6) exhibited a strong resonance at δ_P= 41.89 ppm due to $OPEt_2Ph$ was observed as well as a less intense resonance at δ_P= 51.95 ppm that we attribute to the phosphine binding to the molybdenum center forming $MoO(tdt)(PEt_2Ph)(^iPr_2Dt^0)$.

4.3.2 Oxygen Atom Reactivity of Complexes with a Single Dithione: $MoO(SPh)_2(Dt^0)$

No reaction between DMSO or $[^tBu]_4[NO_3]$ was observed, only TMAO reacted with complexes possessing a single dithione ligand and two thiophenol ligands: $MoO(SPh)_2(Me_2Dt^0)$ (**9**) (where SPh = thiophenol) and $MoO(SPh)_2(^iPr_2Dt^0)$ (**10**).–Complexes **9** and **10** exhibited identical reactivity compared to the electronically asymmetric complexes (**1**-**8**). The OAT reactivity was explored using the same methods presented in Section 4.2 and the results are summarized in Table 4.1. All pertinent data can be found in the Appendix. The results are similar to those observed in **6**, the corresponding dioxo complexes of **9** and **10** are unstable and were not observed in solution.

Table 4.1. NMR and mass spectrometry results of the OAT reactivity for $MoO(SPh)_2(Dt^0)$ complexes.

$MoO(SPh)_2(Me_2Dt^0)$ **9**	
Substrate	Spectral Signatures
TMAO	TMAO (δ_H 3.28 ppm (s)); Me_2Dt^0 (δ_H 3.48 ppm (s,6H); 3.69 ppm (s, 4H))
PEt_2Ph	$MoO(SPh)_2(Me_2Dt^0)$ (δ_H 3.48 ppm (s, 6H), 3.79 ppm (m, 2H), 4.01 ppm (m, 2H), 7.14 ppm (m, 2H), 7.23 ppm (m, 4H), 7.50 ppm (m. 4H)); PEt_2Ph (δ_P -15.63 ppm)
PEt_2Ph + TMAO	TMAO (δ_H 3.28 ppm (s)); Me_2Dt^0 (δ_H 3.48 ppm (s, 6H); 3.69 ppm (s, 4H)); PEt_2Ph (δ_P -15.63 ppm); 457 m/z= $[Mo(SPh)(TMAO)(Me_2Dt^0)]^+$
$MoO(SPh)_2(^iPr_2Dt^0)$ **10**	
Substrate	Spectral Signatures
TMAO	TMA (δ_H 2.78 ppm (s, 9H)); $MoO(SPh)_2(^iPr_2Dt^0)$ (δ_H 4.70 ppm (hept, J =6.8 Hz, 2H), 3.87 ppm (m, 2H), 3.58 ppm (m, 2H), 1.26 ppm (d, J =6.7 Hz, 6H), 1.12 ppm (d, J =6.72 Hz, 6H)); $^iPr_2Dt^0$ (δ_H 5.39 ppm (pent, J= 6.6 Hz, 2H), 3.46 ppm (m, 4H), 1.24 ppm (d, J= 6.7 Hz, 12H)); 622 m/z= $MoO(TMAO)(SPh)_2(^iPr_2Dt^0)^+$
PEt_2Ph	$MoO(SPh)_2(^iPr_2Dt^0)$ (δ_H 4.70 ppm (hept, J =6.8 Hz, 2H), 3.87 ppm (m, 2H), 3.58 ppm (m, 2H), 1.26 ppm (d, J =6.7 Hz, 6H), 1.12 ppm (d, J =6.72 Hz, 6H)); $^iPr_2Dt^0$ (δ_H 5.39 ppm (p, J= 6.6 Hz, 2H), 3.46 ppm (m, 4H), 1.24 ppm (d, J= 3.14 Hz, 12H)); PEt_2Ph (δ_P -15.63 ppm), 18.36*ppm, $OPEt_2Ph$ (δ_P 41.80 ppm), $MoO(SPh)_2(PEt_2Ph)(^iPr_2Dt^0)$ (δ_P 51.94 ppm); 545 m/z = $[Mo(SPh)_2(^iPr_2Dt^0)]^+$
PEt_2Ph + TMAO	TMA (δ_H 2.78 ppm (s, 9H)); $MoO(SPh)_2(^iPr_2Dt^0)$ (δ_H 4.70 ppm (hept, J =6.8 Hz, 2H), 3.87 ppm (m, 2H), 3.58 ppm (m, 2H), 1.26 ppm (d, J =6.7 Hz, 6H), 1.12 ppm (d, J =6.72 Hz, 6H); $^iPr_2Dt^0$ (δ_H 5.39 ppm (p, J= 6.6 Hz, 2H); 3.46 ppm (m, 4H), 1.24 ppm (d, J= 6.7 Hz, 12H)); PEt_2Ph (δ_P -15.63 ppm); $OPEt_2Ph$ (δ_P 41.80ppm); $MoO(SPh)_2(PEt_2Ph)(^iPr_2Dt^0)$ (δ_P 51.94 ppm); 712 m/z= $[Mo(SPh)_2(PEt_2Ph)(^iPr_2Dt^0)]^+$
*unknown phosphine complex	

4.3.3 Oxygen Atom Reactivity of Electronically Symmetric Complexes: [MoOCl(Dt^0)$_2$]$^+$

Electronically symmetric complexes [MoOCl(Me_2Dt^0)$_2$][PF_6] (**11**) and [MoOCl($^iPr_2Dt^0$)$_2$][PF_6] (**12**) were reactive towards all three substrates (DMSO, TMAO, and [^{t}Bu]$_4$[NO_3]) in acetonitrile. The reaction between **11**/**12** and TMAO is presented as a representative reaction. The OAT reactivity was explored using the same methods presented in Section 4.2 and the results are summarized in Table 4.2. All pertinent data can be found in the Appendix. No dioxo species were observed during the course of the OAT reaction similar to complexes **6**,**9** and **10.** Complexes **11** and **12** were reactive towards tertiary phosphine PEt_2Ph and the complexes underwent a loss of a dithione ligand resulting in a monodithione product: [MoOCl(PEt_2Ph)(Dt^0)]. Reactivity towards two other tertiary phosphines, triethylphosphine (PEt_3) and diphenylethylphosphine (PPh_2Et), was explored.

Table 4.2. NMR and mass spectrometry results of the OAT reactivity for $[MoOCl(Dt^0)_2][PF_6]$ complexes.

$[MoOCl(Me_2Dt^0)_2][PF_6]$ **11**	
Substrate	Spectral Signatures
TMAO[a]	TMAO (δ_H 3.46 (s)); TMAH (δ_H 2.8 ppm (d, *J*= 5.2 Hz)); $[MoOCl(Me_2Dt^0)_2][PF_6]$ (δ_H 3.89 ppm (s, 6H), 4.19 ppm (s, 4H)); Me_2Dt^0 (δ_H 3.46 ppm (s, 6H), 3.69 ppm (s, 4H))
PEt_2Ph[b]	$[MoOCl(PEt_2Ph)(Me_2Dt^0)]^+$ (δ_P 19.62 ppm); $[MoO(PEt_2Ph)(Me_2Dt^0)_2]^+$ (δ_P 51.94 ppm); PF_6^- (δ_P hept, -144.61 ppm); 489 m/z= $[MoOCl(PEt_2Ph)(Me_2Dt^0)]^+$
PEt_2Ph + TMAO[a, b]	TMAH (δ_H 2.8 ppm (d, *J*= 5.2 Hz)); $[MoOCl(Me_2Dt^0)_2][PF_6]$ (δ_H 3.89 ppm (s, 6H), 4.19 ppm (s, 4H)); Me_2Dt^0 (δ_H 3.46 ppm (s, 6H), 3.69 ppm (s, 4H)); $[MoOCl(PEt_2Ph)(Me_2Dt^0)]^+$ (δ_P 19.62 ppm); δ_P 29.01 ppm*; δ_P 26.49 ppm*; $[MoO(PEt_2Ph)(Me_2Dt^0)_2]^+$ (δ_P 51.94 ppm); PF_6^- (δ_P hept, -144.61 ppm); 489 m/z = $[MoOCl(PEt_2Ph)(Me_2Dt^0)]^+$
PEt_3 [b]	$[MoOCl(PEt_3)(Me_2Dt^0)]^+$(δ_P 22.17 ppm); δ_P 25.17 ppm*; $[MoO(PEt_3)(Me_2Dt^0)_2]^+$ (δ_P 55.19 ppm); PF_6^- (δ_P hept, -144.61 ppm); 425 m/z= $[MoOCl(PEt_3)(Me_2Dt^0)]^+$
PEt_3 + TMAO[a, b]	TMAH (δ_H 2.8 ppm (d, *J*= 5.2 Hz)); $[MoOCl(PEt_3)(Me_2Dt^0)]^+$($\delta_P$ 22.17 ppm); δ_P 25.17 ppm*; $[MoO(PEt_3)(Me_2Dt^0)_2]^+$ (δ_P 55.19 ppm); PF_6^- (δ_P hept, -144.61 ppm); 425 m/z= $[MoOCl(PEt_3)(Me_2Dt^0)]^+$
PPh_2Et [b]	$OPPh_2Et$ (δ_P 45.19 ppm); 537 m/z= $[MoOCl(PPh_2Et)(^iPr_2Dt^0)]^+$
PPh_2Et + TMAO[a, b]	TMAO (δ_H 3.27 ppm, (s)); TMAH (δ_H 2.8 ppm (d, *J*= 5.2 Hz)); δ_P 33.60 ppm*; $OPPh_2Et$ (δ_P 45.19 ppm); PF_6^- (δ_P hept, -144.61 ppm); 537 m/z= $[MoOCl(PPh_2Et)(Me_2Dt^0]^+$
$[MoOCl(^iPr_2Dt^0)_2][PF_6]$ **12**	
Substrate	Spectral Signatures
TMAO[a]	TMAH (δ_H 2.8 ppm (d, *J*= 5.2 Hz)); $[MoOCl(^iPr_2Dt^0)_2][PF_6]$ (δ_H 5.53 ppm (pent, *J*= 6.5 Hz, 4H), 3.96 ppm (s br, 8H), 1.44 ppm (s br, 24H)); $^iPr_2Dt^0$ (δ_H 5.42 ppm (pent, *J*= 6.8 Hz 2H), 3.46 ppm (s, 4H), 1.27 ppm (d, *J*= 6.7 Hz, 12H))

Table 4.2 (cont.)

PEt_2Ph [b]	PEt_2Ph (δ_P -15.89 ppm); [MoOCl(PEt_2Ph)($^iPr_2Dt^0$)] (δ_P 18.36 ppm); PF_6^- (δ_P hept, -144.61 ppm); 545 m/z = [MoOCl(PEt_2Ph)($^iPr_2Dt^0$)]$^+$
PEt_2Ph + TMAO[a, b]	TMAH (δ_H 2.8 ppm (d, *J*= 5.2 Hz)); PEt_2Ph (δ_P -15.89 ppm); [MoOCl(PEt_2Ph)($^iPr_2Dt^0$)]$^+$ (δ_P 18.36 ppm); [MoOCl(PEt_2Ph)($^iPr_2Dt^0$)$_2$]$^+$ (δ_P 51.94 ppm); PF_6^- (δ_P hept, -144.61 ppm); 545 m/z= [MoOCl(PEt_2Ph)($^iPr_2Dt^0$)]$^+$
PEt_3 [b]	δ_P 15.92 ppm*; [MoOCl(PEt_3)($^iPr_2Dt^0$)]$^+$ (δ_P 22.12 ppm); [MoOCl(PEt_3)($^iPr_2Dt^0$)$_2$]$^+$ (δ_P 55.16 ppm); PF_6^- (δ_P hept, -144.61 ppm); 497 m/z= [MoOCl(PEt_3)($^iPr_2Dt^0$)]$^+$
PEt_3 + TMAO[a, b]	TMAH (δ_H 2.8 ppm(d, *J*= 5.2 Hz)); δ_P 15.92 ppm*; [MoOCl(PEt_3)($^iPr_2Dt^0$)]$^+$ (δ_P 22.12 ppm); [MoOCl(PEt_3)($^iPr_2Dt^0$)$_2$]$^+$ (δ_P 55.16 ppm); PF_6^- (δ_P hept, -144.61 ppm); 497 m/z =[MoOCl(PEt_3)($^iPr_2Dt^0$)]$^+$
PPh_2Et [b]	$OPPh_2Et$ (δ_P 45.19 ppm); PF_6^- (δ_P hept, -144.61 ppm); 593 m/z =[MoCl($^iPr_2Dt^0$)$_2$]$^+$
PPh_2Et + TMAO[a]	TMAH (δ_H 2.8 ppm (d, *J*= 5.2 Hz)); [MoOCl($^iPr_2Dt^0$)$_2$][PF_6] (δ_H 5.52 ppm (pent, *J*= 6.6 Hz, 4H), 3.97 ppm (s br, 8H), 1.45 ppm (s br, 24H)); $^iPr_2Dt^0$ (δ_H 5.41 ppm (pent, *J*= 6.8 Hz 2H), 3.50 ppm (s, 4H), 1.27 ppm (d, *J*= 6.7 Hz, 12H)); $OPPh_2Et$ (δ_P 45.19 ppm); PF_6^- (δ_P hept, -144.61 ppm); 593 m/z =[MoCl($^iPr_2Dt^0$)$_2$]$^+$

* unknown phosphine species

[a] Leyden, D. E.; Morgan, W. R., Kinetics of proton exchange of trimethylammonium ion by N.M.R. Laboratory experiment. *J. Chem. Educ.* **1969,** *46* (3), 169-71[182]

[b] ^{31}P NMR data is shown for clarity.

4.4 Discussion

Complexes **1**-**10** exhibit selective OAT reactivity with biologically relevant substrates; and only exhibited OAT reactivity towards TMAO. Due to the presence of TMA in the ^{1}H NMR spectrum of the reaction between **6** and TMAO, and the observation of a peak cluster consistent with a TMAO-containing species, $[MoO(TMAO)(tdt)(^{i}Pr_2Dt^{0})]^{+}$ in mass spectrometric studies, we suggest that TMAO coordinates to **6**, thus forming a putative intermediate in the oxygen atom transfer (OAT) reaction (Figure 4.4). Using tertiary phosphine, PEt_2Ph, to indirectly probe the presence of an unstable $Mo^{VI}O_2$ complex has indicated that PEt_2Ph reacts with the $Mo^{VI}O_2$ species forming $OPEt_2Ph$ prior to degradation. The ^{31}P NMR spectrum of a control experiment between **6** and PEt_2Ph exhibited a resonance for the coordinated PEt_2Ph species, $MoO(tdt)(PEt_2Ph)(^{i}Pr_2Dt^{0})$ and free $OPEt_2Ph$. As shown in Figure 4.6, there is a minor $OPEt_2Ph$ impurity in the initial PEt_2Ph. While the integration of the resonance due to $OPEt_2Ph$ shows an increase in $OPEt_2Ph$ present in solution, the major product of the reaction between **6** and PEt_2Ph is $MoO(tdt)(PEt_2Ph)(^{i}Pr_2Dt^{0})$. The relative amount of the $OPEt_2Ph$ is shown to significantly increase during the reaction of **6**, TMAO and PEt_2Ph; more phosphine oxide is generated during this reaction compared to the reaction between **6** and PEt_2Ph, and we hypothesize this is due to the PEt_2Ph abstracting an oxygen atom from the unstable $MoO_2(tdt)(^{i}Pr_2Dt^{0})$.

Reactions between **6** and PEt_2Ph and a mixture of PEt_2Ph and TMAO were also examined using mass spectrometry. A peak cluster at m/z ~ 665 consistent with an isotope distribution pattern for the $MoO(tdt)(PEt_2Ph)(^{i}Pr_2Dt^{0})$ complex (Figure 4.8) was observed during the reaction between **6** and PEt_2Ph. Simultaneously a peak cluster at m/z ~545 consistent with an isotope distribution pattern for $MoO(TMAO)(tdt)(^{i}Pr_2Dt^{0})$ was also observed during the reaction between **6** and TMAO with PEt_2Ph. Scheme 4.3 shows the proposed reaction cycle for the OAT reaction where

coordination of phosphine and decomposition of the dioxo-species prevents the system from being deemed a catalytic cycle; **6** is reacting with TMAO but cannot be regenerated with the addition of phosphine. Acetonitrile is known to coordinate to metal centers and to explore if the solvent environment was affecting the stability of the $Mo^{VI}O_2$ the reaction between **6** and TMAO was run in acetone. The results were the same as those observed in acetonitrile, uncoordinated $^{i}Pr_2Dt^0$ dithione ligand and TMA were observed in the ^1H NMR.

Scheme 4.3

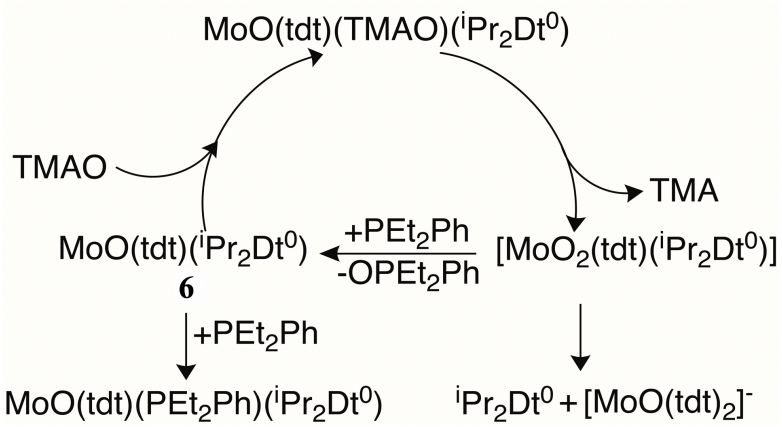

While thiophenol complexes **9** and **10** exhibited similar reactivity towards TMAO as complex **6**, complexes **9** and **10** proved to be more unstable during the OAT reaction with TMAO and exhibited different reactivity towards tertiary phosphines than complex **6**. No TMA was observed during the reaction between **9** and TMAO. This may indicate that if the TMAO coordinated to the metal center in a similar manner observed in **6**, the complex degraded prior to reduction of TMAO. Indirectly probing the presence of a $Mo^{VI}O_2$ complex with PEt_2Ph demonstrated a lack of reactivity between **9** and PEt_2Ph; no phosphine-coordinated species was observed. The reaction between TMAO, PEt_2Ph and **9** did not exhibit a chemical shift for free phosphine oxide $OPEt_2Ph$, or TMA due to the instability of the complex in the presence of TMAO. While no TMA was observed during the reactions probed by NMR, a TMAO species was observed

during mass spectrometry studies. A peak cluster for $[Mo(SPh)(TMAO)(Me_2Dt^0)]^+$ was observed at m/z ~457 (see Appendix) and while losses of a thiophenol ligand and oxo group were observed, we interpret the presence of TMAO in the peak cluster to show that TMAO can potentially coordinate to the metal.

Complex **10** proved more stable in the presence of TMAO, and TMA was observed in the ^1H NMR spectrum of the reaction between **10** and TMAO. A putative TMAO intermediate, $MoO(SPh)_2(TMAO)(^iPr_2Dt^0)$, was observed in mass spectrometry studies, results similar to those observed in the reaction between **6** and TMAO. Complex **10** was reactive towards PEt_2Ph. A chemical shift consistent with free $OPEt_2Ph$ (δ_P= 41.80 ppm) and a resonance at δ_P 51.95 ppm. A similar resonance for phosphine coordinated species, $MoO(tdt)(PEt_2Ph)(^iPr_2Dt^0)$, was observed during the reaction between **6** and PEt_2Ph.

During mass spectrometry experiments a peak cluster consistent with desoxo species, $Mo(SPh)_2(^iPr_2Dt^0)$ was observed. These results indicate that PEt_2Ph can abstract the oxygen atom from complex **10** and is consistent with the observation of free $OPEt_2Ph$ observed in the ^{31}P NMR spectrum**.** A peak cluster consistent with a phosphine coordinated complex, $Mo(SPh)_2(PEt_2Ph)(^iPr_2Dt^0)$ was also observed. While a TMAO-coordinated intermediate and TMA were observed during the reaction between **10** and TMAO, the TMAO-coordinated intermediate and TMA were not observed during the reaction between **10**, TMAO, and PEt_2Ph. We propose this may be due to the complex being unreactive towards TMAO in the presence of PEt_2Ph, perhaps due to the loss of the terminal oxo ligand. Scheme 4.4 and 4.5 show the proposed reaction cycles of **9** and **10,** respectively. Neither system is deemed a catalytic cycle as **9** decomposed in the presence of TMAO and **10** cannot be regenerated after the reduction TMAO to TMA.

Scheme 4.4.

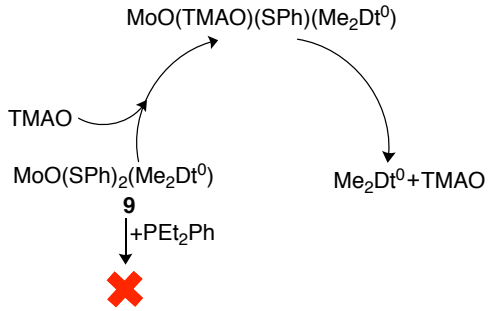

Scheme 4.5

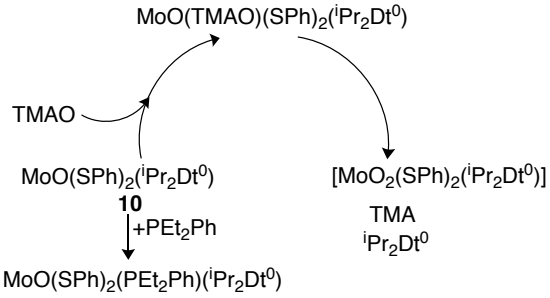

Finally, complexes possessing two fully oxidized dithione ligands (**11** and **12**) were less selective towards substrates examined for this study. These results are comparable to the reactions previously presented in this chapter; corresponding dioxo complexes $[MoO_2(Me_2Dt^0)_2]^{2+}$ or $[MoO_2(^iPr_2Dt^0)_2]^{2+}$ were not observed in solution, but the presence of protonated TMA indicates successful reduction of TMAO.[182] Unlike complexes **6**, **9**, and **10**, no TMAO-coordinated intermediate was observed during the mass spectrometry experiments of complexes **11** and **12**. The absence of any observable reaction intermediates or dioxo species may be due to the inherent instability of complexes possessing two fully oxidized dithione ligands.

As shown during the reaction between **6** and PEt_2Ph, PEt_2Ph does coordinate to the molybdenum metal center of **11** and **12** in a similar manner, but the complex also loses one of the dithione ligands coordinated to the molybdenum metal center. The formation of a monodithione complex was observed during the reaction for both **11** and **12** with PEt_2Ph. The formation of the monodithione, $[MoOCl(PEt_2Ph)(Dt^0)]$ rendered the phosphine unreactive towards the unstable $Mo^{VI}O_2$ complex formed during the OAT. Similar monodithione complexes were formed when PEt_3 was reacted with complex **11** and **12.** No monodithione complex was observed during the reaction between **12** and PPh_2Et, instead, free phosphine oxide, $OPPh_2Et$ and a desoxo species, $[MoCl(^iPr_2Dt^0)_2]^+$ were formed during the reaction. Due to the unfavorable reactivity towards

tertiary phosphines and the inherent instability of complex **11** and **12,** no TMAO-coordinated intermediate was observed and the presence $Mo^{VI}O_2$ species was not indirectly probed using tertiary phosphines. All degradation pathways similar to complexes **6**, **9**, and **10** are presented in Scheme 4.6.

Scheme 4.6

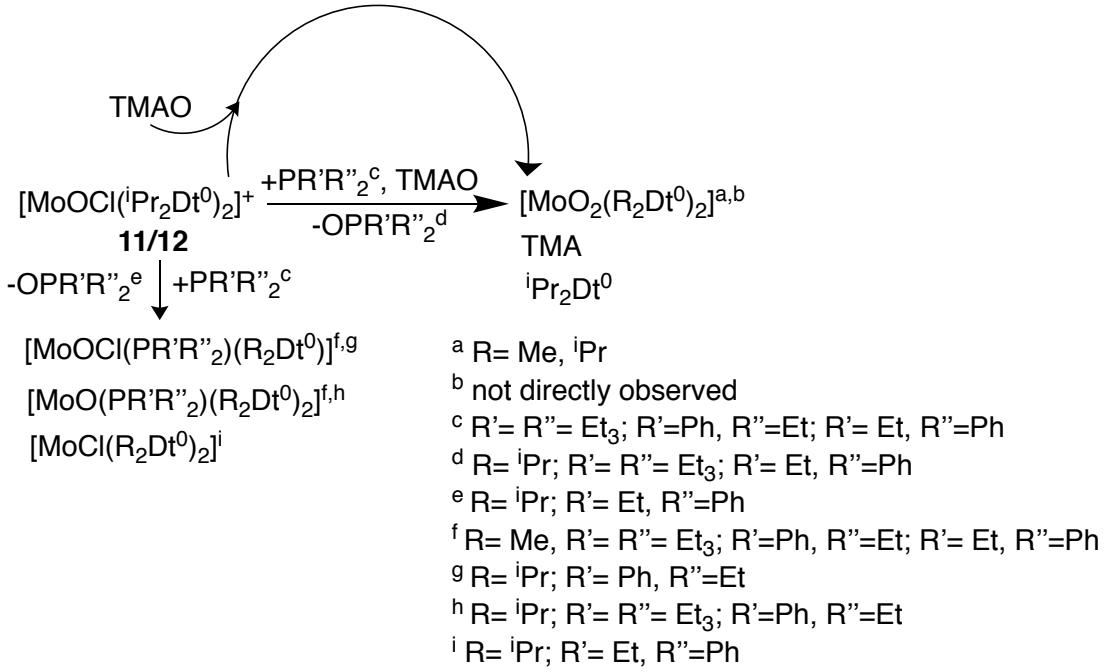

4.5 Implication to the Reactivity of Moco

Overall, these studies indicate that small molecule mimics possess a fully oxidized dithiolene ligand can exhibit OAT reactivity towards biologically relevant substrates. Interestingly, **6**, **9**, and **10** did not exhibit any reactivity towards DMSO or NO_3^-. The only complexes that exhibited reactivity with all three substrates were **11** and **12** that possess two fully oxidized dithiolene ligands. The redox potential of TMAO is +130 mV, making TMAO easier to reduce than the other two substrates.[119] Complex **6** exhibits OAT reactivity similar to previously

studied complexes of general formula, $[MoO(Dt)_2]^{2-}$ (Dt = reduced dithiolene) complexes for example; $[MoO(mnt)_2]^{2-}$ and $[MoO(bdt)_2]^{-2}$. These two complexes serve as representative examples for oxo-Mo complexes of reduced dithiolene ligands. Both of these complexes react with TMAO but not with DMSO or NO_3^-.[105, 107, 120] There have been multiple reports of $[MoO(Dt)_2]^{2-}$ complexes that react with TMAO, but to our knowledge, only $[Mo^{IV}O(vdt)_2]^{2-}$ and $[Mo^{IV}O(ntdt)_2]^{2-}$ (where vdt is 4,5-dimethoxy-benzene-1,2-dithol and ntdt is 2-naphthyl-1,4-dithiolate) have been reported to reduce DMSO.[108, 109] Reduction of NO_3^- has not been reported in these systems.[82, 105, 107-109, 111, 112, 114-118, 120]

Complex **6** is the first example of an oxo-Mo(IV) complex possessing two dithiolene ligands in different oxidation states. It has been proposed that given the non-innocent nature of the pyranopterin and dithiolene ligands of Moco, an electronically asymmetric environment may exist in molybdopterin enzymes. This work shows that an electronically asymmetric complex can undergo an OAT reaction with TMAO; an indication that Moco can function when the dithiolene ligands exist in different oxidation states.

CHAPTER 5. SUMMARY AND FUTURE WORK

5.1 Summary

This work is the first example of monooxo-Mo(IV) dithiolene complexes possessing two dithiolene ligands in different oxidation states. These electronically asymmetric were designed and characterized to generate a mixed ligand system to study what effects that may play on the electronics and reactivity of the molybdenum cofactor found in molybdopterin enzymes. Asymmetric oxo-Mo^{IV}(dithiolene) complexes exhibit a unique structural property, a large fold angle along the S•••S vector of the dithione ligand. Absorbance spectrum of complexes **1-8** exhibit a strong transition at ~530 nm -540 nm. DFT and TD-DFT calculations have predicted this transition to be a LL'CT transition. The composition of the frontier orbitals was shown to be dithiolene based and the LUMO is mainly dithione ligand based; i.e. the electron rich dithiolene ligand can donate electron density to the electron deficient dithione ligand. These complexes also show a positive solvatochromic effect in a range of polar to nonpolar solvents. The complexes have exhibited OAT reactivity towards TMAO a biologically relevant substrate of molybdopterin enzymes, demonstrating a potential means to modulate reactivity of the enzymes.

5.2 Future Work

As mentioned, the complexes presented here are the first electronically asymmetric Mo(IV) dithiolene complexes. There are molybdopterin enzymes that have tungsten at the heart of the active site as opposed to molybdenum. Tungsten dithione complexes chemistry is significantly underdeveloped with only 6 known structures of tungsten dithione complexes reported; none of which are bis-dithione complexes. A potential avenue to explore the fundamental science of tungsten dithione complexes possessing two fully oxidized dithione ligand and similar

electronically asymmetric complexes with a single fully oxidized and fully reduced dithiolene ligand.

Tungsten complexes are also known to be less reactive than their molybdenum counterparts. Slower reactivity may aid in the exploration of the OAT reactivity. These proposed tungsten complexes will still suffer from instability due to the neutral dithione ligand however, if the reactivity of such complexes is slower than the corresponding molybdenum complexes this may allow for the observation of reaction intermediates or even the dioxo W(VI) complexes that result from the OAT reaction.

The reactivity of $MoO(Dt^{2-})(Dt^{0})$ complexes can be further explored. As it stands only three biologically relevant substrates have been explored and this can be expanded to fully explore the reactivity of $MoO(Dt^{2-})(Dt^{0})$ complexes. It was observed that $MoO(Dt^{2-})(Dt^{0})$ complexes react with pyridine. A similar reaction was observed between $[MoO(BF_4)(^{i}Pr_2Dt^{0})_2][BF_4]$ which resulted in a low coordinate Mo cluster. Such reactivity was out of the scope of this project and should be further explored.

REFERENCES

1. Meyers, F.; Marder, S. R.; Pierce, B. M.; Bredas, J. L., Electric Field Modulated Nonlinear Optical Properties of Donor-Acceptor Polyenes: Sum-Over-States Investigation of the Relationship between Molecular Polarizabilities (α, β, and γ) and Bond Length Alternation. *J. Am. Chem. Soc.* **1994,** *116* (23), 10703-14.
2. Albert, I. D. L.; Marks, T. J.; Ratner, M. A., Large Molecular Hyperpolarizabilities. Quantitative Analysis of Aromaticity and Auxiliary Donor-Acceptor Effects. *J. Am. Chem. Soc.* **1997,** *119* (28), 6575-6582.
3. Suguna, S.; Anbuselvi, D.; Jayaraman, D.; Nagaraja, K. S.; Jeyaraj, B., Synthesis, Growth, Structural and Optical Studies of Organic Nonlinear Optical Material - Piperazine-1,4-Diium Bis 2,4,6-Trinitrophenolate. *Spectrochim. Acta, Part A* **2014,** *132*, 330-338.
4. Raja, R.; Seshadri, S.; Gnanasambandan, T.; Saravanan, R. R., Crystal Growth and Properties of NLO Optical Crystal - Butylated Hydroxy Toluene (BHT). *Spectrochim. Acta, Part A* **2015,** *138*, 13-20.
5. Miyasaka, H., Control of Charge Transfer in Donor/Acceptor Metal-Organic Frameworks. *Acc. Chem. Res.* **2013,** *46* (2), 248-257.
6. Gnaim, S.; Shabat, D., Quinone-Methide Species, A Gateway to Functional Molecular Systems: From Self-Immolative Dendrimers to Long-Wavelength Fluorescent Dyes. *Acc. Chem. Res.* **2014,** *47* (10), 2970-2984.
7. Di Bella, S.; Fragala, I.; Ledoux, I.; Marks, T. J., Role of Metal Electronic Properties in Tuning the Second-Order Nonlinear Optical Response of Coordination Complexes. A Combined Experimental and Theoretical Investigation of a Homologous Series of (N,N'-Disalicylidene-1,2-phenylenediaminato)M(II) (M = Co, Ni, Cu) Complexes. *J. Am. Chem. Soc.* **1995,** *117* (37), 9481-5.
8. Cummings, S. D.; Cheng, L.-T.; Eisenberg, R., Metalloorganic Compounds for Nonlinear Optics: Molecular Hyperpolarizabilities of M(diimine)(dithiolate) Complexes (M = Pt, Pd, Ni). *Chem. Mater.* **1997,** *9* (2), 440-450.
9. Base, K.; Tierney, M. T.; Fort, A.; Muller, J.; Grinstaff, M. W., On the Second-Order Nonlinear Optical Structure-Property Relationships of Metal Chromophores. *Inorg. Chem.* **1999,** *38* (2), 287-289.
10. Espa, D.; Pilia, L.; Marchio, L.; Mercuri, M. L.; Serpe, A.; Barsella, A.; Fort, A.; Dalgleish, S. J.; Robertson, N.; Deplano, P., Redox-Switchable Chromophores Based on Metal (Ni, Pd, Pt) Mixed-Ligand Dithiolene Complexes Showing Molecular Second-Order Nonlinear-Optical Activity. *Inorg. Chem.* **2011,** *50* (6), 2058-2060.
11. Pilia, L.; Espa, D.; Barsella, A.; Fort, A.; Makedonas, C.; Marchio, L.; Mercuri, M. L.; Serpe, A.; Mitsopoulou, C. A.; Deplano, P., Combined Experimental and Theoretical Study on Redox-Active d8 Metal Dithione-Dithiolato Complexes Showing Molecular Second-Order Nonlinear Optical Activity. *Inorg. Chem.* **2011,** *50* (20), 10015-10027.
12. Vogler, A.; Adamson, A. W., Photosensitized Decomposition of Some Cobalt Ammines. *J. Amer. Chem. Soc.* **1968,** *90* (21), 5943-5.
13. Adamson, A. W.; Chiang, A.; Zinato, E., Photochemistry of Aqueous Cobalt(III) Cyano Complexes. *J. Amer. Chem. Soc.* **1969,** *91* (20), 5467-75.

14. Demas, J. N.; Adamson, A. W., Tris (2,2'-Bipyridine)Ruthenium(II) Sensitized Reactions of Some Oxalato Complexes. *J. Amer. Chem. Soc.* **1973,** *95* (16), 5159-68.
15. Bock, C. R.; Meyer, T. J.; Whitten, D. G., Electron Transfer Quenching of the Luminescent Excited State of Tris(2,2'-Bipyridine)Ruthenium(II). Flash Photolysis Relaxation Technique for Measuring the Rates of very Rapid Electron Transfer Reactions. *J. Amer. Chem. Soc.* **1974,** *96* (14), 4710-12.
16. Young, R. C.; Meyer, T. J.; Whitten, D. G., Electron Transfer Quenching of Excited States of Metal Complexes. *J. Am. Chem. Soc.* **1976,** *98* (1), 286-7.
17. Kivala, M.; Diederich, F., Acetylene-Derived Strong Organic Acceptors for Planar and Nonplanar Push-Pull Chromophores. *Acc. Chem. Res.* **2009,** *42* (2), 235-248.
18. Vogler, A.; Kunkely, H., Optical Ligand to Ligand Charge Transfer of Metal Complexes Including Ligand-Based Mixed-Valence Systems. *Comments Inorg. Chem.* **1990,** *9* (3-4), 201-20.
19. Vogler, A.; Kunkely, H., Photochemistry of Transition Metal Complexes Induced by Outer-Sphere Charge Transfer Excitation. *Top. Curr. Chem.* **1990,** *158* (Photoinduced Electron Transfer 2), 1-30.
20. Joergensen, C. K., Differences Between the Four Halide Ligands, and Discussion Remarks on Tigonal-Bipyramidal Complexes, on Oxidation States, and on Diagonal Elements of One-Electron Energy. *Coord. Chem. Rev.* **1966,** *1* (1-2), 164-78.
21. Ward, M. D.; McCleverty, J. A., Non-Innocent Behaviour in Mononuclear and Polynuclear Complexes: Consequences for Redox and Electronic Spectroscopicproperties. *Journal of Chemical society, Dalton Transanctions* **2002**, 275-288.
22. McCleverty, J. A.; Ward, M. D., Innocent or Guilty? Redox Activity in and Magnetic and Optical Behaviour of Dinuclear Molybdenum Complexes. *Proceedings - Indian Academy of Sciences, Chemical Sciences* **2002,** *114* (4), 291-309.
23. Davison, A.; Edelstein, N.; Holm, R. H.; Maki, A. H., Concerning the Existence of High-Spin Planar Cobaltous Complexes: Bis(1,2-dicyanomaleonitriledithiolato)cobalt(II) Dianion. *Journal of the American Chemical Society* **1963,** *85* (19), 3049-3050.
24. Davison, A.; Edelstein, N.; Holm, R. H.; Maki, A. H., The Preparation and Characterization of Four-Coordinate Complexes Related by Electron-Transfer Reactions. *Inorg. Chem.* **1963,** *2* (6), 1227-32.
25. Davison, A.; Edelstein, N.; Holm, R. H.; Maki, A. H., Electron Spin Resonance (E.S.R.) Studies of Four-Coordinate Complexes of Nickel, Palladium, and Platinum Related by Electron Transfer Reactions. *J. Am. Chem. Soc.* **1963,** *85* (13), 2029-30.
26. Sproules, S.; Benedito, F. v. L.; Bill, E.; Weyhermüller, T.; DeBeer George, S.; Wieghardt, K., Characterization and Electronic Structures of Five Members of the Electron Transfer Series [Re(benzene-1,2-dithiolato)3]z (z = 1+, 0, 1−, 2−, 3−): A Spectroscopic and Density Functional Theoretical Study. *Inorganic Chemistry* **2009,** *48* (23), 10926-10941.
27. Ghosh, M.; Weyhermueller, T.; Wieghardt, K., Electronic Structure of the Members of the Electron Transfer Series [NiL]z (z = 3+, 2+, 1+, 0) and [NiL(X)]n (X = Cl, CO, $P(OCH_3)_3$) Species Containing a Tetradentate, Redox-Noninnocent, Schiff Base Macrocyclic Ligand L: An Experimental and Density Functional Theoretical Study. *Dalton Trans.* **2010,** *39* (8), 1996-2007.

28. Stiefel, E. I.; Waters, J. H.; Billig, E.; Gray, H. B., The Myth of Nickel(III) and Nickel(IV) in Planar Complexes. *Journal of the American Chemical Society* **1965,** *87* (13), 3016-17.
29. Maki, A. H.; Edelstein, N.; Davison, A.; Holm, R. H., Electron Paramagnetic Resonance Studies of the Electronic Structures of Bis(maleonitriledithiolato)copper(II), -nickel(III), -cobalt(II), and -rhodium(II) Complexes. *Journal of the American Chemical Society* **1964,** *86* (21), 4580-4587.
30. Balch, A. L.; Röhrscheid, F.; Holm, R. H., New Systems of Complexes Related by Electron-Transfer Reactions. *Journal of the American Chemical Society* **1965,** *87* (10), 2301-2302.
31. Schrauzer, G. N.; Mayweg, V., Reaction of Diphenylacetylene with Nickel Sulfides. *J. Am. Chem. Soc.* **1962**, 3221.
32. Stiefel, E. I., *Dithiolene Chemistry: Synthesis, Properties, and Applications*. Wiley and Sons Inc.: 2004; Vol. 52.
33. Robertson, N.; Cronin, L., Metal Bis-1,2-Dithiolene Complexes in Conducting or Magnetic Crystalline Assemblies. *Coord. Chem. Rev.* **2002,** *227* (1), 93-127.
34. Fourmigue, M., Mixed cyclopentadienyl/dithiolene complexes. *Coord. Chem. Rev.* **1998,** *178-180* (Pt. 1), 823-864.
35. Pleniceanu, M., Electrochemical Sensors for Potentiometric Determination of Ni(II). *An. Univ. Craiova, Ser. Chim.* **1994,** *21*, 45-54.
36. Pleniceanu, M.; Popescu, A.; Preda, M.; Baniceru, M., Electrochemical Sensors for Potentiometric Determination of Cu(II) and Ni(II). *Rev. Chim.* **1995,** *46* (10), 929-32.
37. Marbella, L.; Serli-Mitasev, B.; Basu, P., Development of a Fluorescent Pb^{2+} Sensor. *Angew. Chem., Int. Ed.* **2009,** *48* (22), 3996-3998, S3996/1-S3996/4.
38. Kato, R., Conducting Metal Dithiolene Complexes: Structural and Electronic Properties. *Chem. Rev.* **2004,** *104* (11), 5319-5346.
39. Eisenberg, R.; Khare, G. P.; Schultz, A. J., Crystal and Molecular Structure of Bis(Dithiotropolonato)Nickel(II). *J. Amer. Chem. Soc.* **1971,** *93*, 3597-602.
40. Stiefel, E. I.; Waters, J. H.; Billig, E.; Gray, H. B., The Myth of Nickel(III) and Nickel(IV) in Planar Complexes. *J. Am. Chem. Soc.* **1965,** *87* (13), 3016-17.
41. Ghosh, P.; Stobie, K.; Bill, E.; Bothe, E.; Weyhermuller, T.; Ward, M. D.; McCleverty, J. A.; Wieghardt, K., Electronic Structure of Nitric Oxide Adducts of Bis(diaryl-1,2-dithiolene)iron Compounds: Four-Membered Electron-Transfer Series [Fe(NO)(L)2]z (z) 1+, 0, 1-, 2-). *Inorg Chem* **2007,** *46*, 522-532.
42. Fabian, J.; Nakazumi, H.; Matsuoka, M., Near-Infrared Absorbing Dyes. *Chem. Rev.* **1992,** *92* (6), 1197-1226.
43. Chanishvili, A.; Chilaya, G.; Petriashvili, G.; Barberi, R.; Bartolino, R.; Cipparrone, G.; Mazzulla, A.; Gimenez, R.; Oriol, L.; Pinol, M., Widely Tunable Ultraviolet-Visible Lquid Crystal Laser. *Appl. Phys. Lett.* **2005,** *86* (5), 051107/1-051107/3.
44. Marshall, K. L.; Painter, G.; Lotito, K.; Noto, A. G.; Chang, P., Transition Metal Dithiolene Near-IR Dyes and their Applications in Liquid Crystal Devices. *Mol. Cryst. Liq. Cryst.* **2006,** *454*, 449-481.
45. Lehmann, U.; Heizler, D. Dithiolene Metal Complex Colorless IR Absorbers. 2007-EP64102-2008086931, 20071218., 2008.

46. Schrauzer, G. N.; Mayweg, V. P., Coordination Compounds with Delocalized Ground States. Tris(Dithioglyoxal) and Related Prismatic α-Dithiodiketone Complexes of Transition Metals. *Journal of the American Chemical Society* **1966,** *88* (14), 3235-42.
47. Cowie, M.; Bennett, M. J., Trigonal-Prismatic vs. Octahedral Coordination in a Series of Tris(Benzene-1,2-dithiolato) Complexes. 2. Crystal and Molecular Structure of Tetraphenylarsonium Tris(Benzene-1,2-dithiolato)niobate(V), $[(C_6H_5)_4As][Nb(S_2C_6H_4)_3]$. *Inorganic Chemistry* **1976,** *15* (7), 1589-1595.
48. Eisenberg, R.; Pierpont, C. G., Trigonal Prismatic Coordination. Crystal and Molecular Structure of Tris[Cis-1,2-Di(Trifluoromethyl)ethylene-1,2-diselenato]Molybdenum. *J. Chem. Soc. A* **1971**, 2285-9.
49. Kapre, R. R.; Bothe, E.; Weyhermuller, T.; DeBeer George, S.; Wieghardt, K., Electronic Structure of Neutral and Monoanionic Tris(Benzene-1,2-dithiolato)Metal Complexes of Molybdenum and Tungsten. *Inorg Chem* **2007,** *46* (14), 5642-50.
50. Ray, K.; George, S. D.; Solomon, E. I.; Wieghardt, K.; Neese, F., Description of the Ground-State Covalencies of the Bis(dithiolato) Transition-Metal Complexes from X-ray Absorption Spectroscopy and Time-Dependent Density-Functional Calculations. *Chem. Eur. J.* **2007,** *13*, 2783 – 2797.
51. Solomon, E. I.; Hedman, B.; Hodgson, K. O.; Dey, A.; Szilagyi, R. K., Ligand K-Edge X-ray Absorption Spectroscopy: Covalency of Ligand-Metal Bonds. *Coord. Chem. Rev.* **2005,** *249*, 97-129.
52. Ray, K.; Petrenko, T.; Wieghardt, K.; Neese, F., Joint Spectroscopic and Theoretical Investigations of Transition Metal Complexes Involving Non-innocent Ligands. *Dalton Trans.* **2007,** (16), 1552-1566.
53. CCDC, Strucutre Search for all Transition Metal Complexes Possesing either Dithione or Dithiolene Ligands. Cambridge Crystallographic Data Centre: April, 17 2018.
54. Kuesters, W.; De Mayo, P., Photochemical synthesis. 52. Thione photochemistry. II. Preparation of an α -dithione and the α-dithione-1,2-dithiete equilibrium. *Journal of the American Chemical Society* **1973,** *95* (7), 2383-2384.
55. Kusters, W.; De Mayo, P., Photochemical Synthesis. 56. Thione Photochemistry. 15. Preparation and Properties of the α -Dithione System. *Journal of the American Chemical Society* **1974,** *96* (11), 3502-3511.
56. Ono, Y.; Sugihara, Y.; Ishii, A.; Nakayama, J., Synthesis and Characterization of Aliphatic α-Dithiones, Di(1-adamantyl)- and Di-tert-butylethanedithiones. *Journal of the American Chemical Society* **2003,** *125* (40), 12114-12115.
57. Shibahara, S.; Kitagawa, H.; Kubo, T.; Nakasuji, K., A New Hydrogen-Bonded Charge-Transfer Complex $[Ni(Hpydt)_2]$TNAP: Synthesis, Structure and Electrical Conductivity. *Inorganic Chemistry Communications* **2007,** *10* (8), 860-862.
58. Shibahara, S.; Kitagawa, H.; Ozawa, Y.; Toriumi, K.; Kubo, T.; Nakasuji, K., Syntheses and Unusual Segregated-Alternated Hybrid Stacking Structure of Hydrogen-Bonded Charge-Transfer Complexes Composed of Bis[2,3-pyridinedithiolate]metal Complexes. *Inorganic Chemistry* **2007,** *46* (4), 1162-1170.
59. Lanza, S.; Loiseau, F.; Tresoldi, G.; Serroni, S.; Campagna, S., Heteropolymetallic Complexes Containing 1,1'-Diphenylphosphino-Ferrocene. *Inorganica Chimica Acta* **2007,** *360* (6), 1929-1934.

60. Aragoni, M. C.; Arca, M.; Demartin, F.; Devillanova, F. A.; Lelj, F.; Isaia, F.; Lippolis, V.; Mancini, A.; Pala, L.; Verani, G., A Theoretical Investigation of the Donor Ability of [M(R,R'timdt)$_2$] Dithiolene Complexes Towards Molecular Diiodine (M = Ni, Pd, Pt; R,R'timdt = Formally Monoreduced Disubstituted Imidazolidine-2,4,5-Trithione). *European Journal of Inorganic Chemistry* **2004,** (15), 3099-3109.
61. Cui, J.-Z.; Pan, S.-W.; Cheng, P.; Liao, D.-Z.; Jiang, Z.-H.; Yan, S.-P.; Wang, G.-L., Syntheses and Properties of Hetero-Trinuclear Mn(II)-Cu(II)-Mn(II), Ni(II)-Cu(II)-Ni(II) and Trinuclear Ni(II) Complexes Bridged with N,N'-bis(2-pyridylethyl)dithiooxamidate. *Wuji Huaxue Xuebao* **2005,** *21* (11), 1627-1631.
62. Al-Maydama, H.; El-Shekeil, A.; Khalid, M. A.; Al-Karbouly, A., Thermal Degradation Behaviour of some Polydithiooxamide Metal Complexes. *Ecletica Quimica* **2006,** *31* (1), 45-52.
63. Geary, E. A. M.; Yellowlees, L. J.; Parsons, S.; Pilia, L.; Serpe, A.; Mercuri, M. L.; Deplano, P.; Clark, S. J.; Robertson, N., Influence of the R-Substituents on the Properties of [Ni(R$_2$pipdt)(dmit)] Complexes and Crystal Structure where R = $CH_2C_6H_5$. *Dalton Transactions* **2007,** (46), 5453-5459.
64. Marshall, K. L.; Wang, R.; Coan, M.; Noto, A. G.; Leskow, K.; Pauszek, R.; Moore, A., Using Time-Dependent Density Functional Theory (TDDFT) in the Design and Development of Near-IR Dopants for Liquid Crystal Device Applications. *Proceedings of SPIE-The International Society for Optical Engineering* **2007,** *6654* (Liquid Crystals XI), 66540F/1-66540F/13.
65. Deplano, P.; Pilia, L.; Espa, D.; Mercuri, M. L.; Serpe, A., Square-Planar d8 Metal Mixed-Ligand Dithiolene Complexes as Second Order Nonlinear Optical Chromophores: Structure/Property Relationship. *Coordination Chemistry Reviews* **2010,** *254* (13-14), 1434-1447.
66. Bigoli, F.; Cassoux, P.; Deplano, P.; Mercuri, M. L.; Pellinghelli, M. A.; Pintus, G.; Serpe, A.; Trogu, E. F., Synthesis, Structure and Properties of New Unsymmetrical Nickel Dithiolene Complexes Useful as Near-Infrared Dyes. *Dalton Transactions* **2000,** (24), 4639-4644.
67. Mueller-Westerhoff, U. T.; Vance, B.; Yoon, D. I., The Synthesis of Dithiolene Dyes with Strong Near-IR Absorption. *Tetrahedron* **1991,** *47* (6), 909-32.
68. Deplano, P.; Mercuri, M. L.; Marchio, L.; Pilia, L.; Salidu, M.; Serpe, A.; Congiu, F.; Sanna, S., Electro-Conducting Properties of Charge-Transfer Salts Based on Cationic and Anionic Platinum Dithiolenes - Crystal Structure of [Pt(Me2pipdt)2][Pt(dtcr)2]. *Eur. J. Inorg. Chem.* **2005**, 1829-1835.
69. Isaksson, R.; Liljefors, T.; Sandstroem, J., Synthesis of some Five-, Six-, and Seven-Membered Cyclic Oxamides and their Mono- and Dithio Analogs. *J. Chem. Res., Synop.* **1981,** (2), 43.
70. Nemykin, V. N.; Olsen, J. G.; Perera, E.; Basu, P., Synthesis, Molecular and Electronic Structure, and TDDFT and TDDFT-PCM Study of the Solvatochromic Properties of (Me_2Pipdt)Mo(CO)$_4$ Complex (Me_2Pipdt = *N,N′*-Dimethylpiperazine-2,3-dithione). *Inorg. Chem.* **2006,** *45* (9), 3557-3568.
71. Yan, Y.; Chandrasekaran, P.; Mague, J. T.; DeBeer, S.; Sproules, S.; Donahue, J. P., Redox-Controlled Interconversion between Trigonal Prismatic and Octahedral Geometries in a Monodithiolene Tetracarbonyl Complex of Tungsten. *Inorg. Chem.* **2012,** *51* (1), 346-361.

72. Mogesa, B.; Perera, E.; Rhoda, H. M.; Gibson, J. K.; Oomens, J.; Berden, G.; van Stipdonk, M. J.; Nemykin, V. N.; Basu, P., Solution, Solid, and Gas Phase Studies on a Nickel Dithiolene System: Spectator Metal and Reactor Ligand. *Inorg. Chem.* **2015,** *54* (16), 7703-7716.
73. Bigoli, F.; Deplano, P.; Mercuri, M. L.; Pellinghelli, M. A.; Pilia, L.; Pintus, G.; Serpe, A.; Trogu, E. F., Ion Pair Charge-Transfer Complexes between Anionic and Cationic Metal-Dithiolenes [M(II) = Pd, Pt]. *Inorg. Chem.* **2002,** *41* (20), 5241-5248.
74. Perera, E.; Basu, P., Synthesis, Characterization and Structure of a Low Coordinate Desoxomolybdenum Cluster Stabilized by a Dithione Ligand. *Dalton Trans.* **2009,** (25), 5023-5028.
75. Espa, D.; Pilia, L.; Makedonas, C.; Marchio, L.; Mercuri, M. L.; Serpe, A.; Barsella, A.; Fort, A.; Mitsopoulou, C. A.; Deplano, P., Role of the Acceptor in Tuning the Properties of Metal [M(II) = Ni, Pd, Pt] Dithiolato/Dithione (Donor/Acceptor) Second-Order Nonlinear Chromophores: Combined Experimental and Theoretical Studies. *Inorg. Chem.* **2014,** *53* (2), 1170-1183.
76. Mtei, R. P.; Perera, E.; Mogesa, B.; Stein, B.; Basu, P.; Kirk, M. L., A Valence Bond Description of Dizwitterionic Dithiolene Character in an Oxomolybdenum-Bis(dithione) Complex. *Eur. J. Inorg. Chem.* **2011,** *2011*, 5467-5470.
77. Lauher, J. W.; Hoffmann, R., Structure and Chemistry of Bis(cyclopentadienyl)-MLn Complexes. *J. Am. Chem. Soc.* **1976,** *98* (7), 1729-42.
78. Joshi, H. K.; Cooney, J. J. A.; Inscore, F. E.; Gruhn, N. E.; Lichtenberger, D. L.; Enemark, J. H., Investigation of Metal-Dithiolate Fold Angle Effects: Implications for Molybdenum and Tungsten Enzymes. *Proc. Natl. Acad. Sci. U. S. A.* **2003,** *100*, 3719-3724.
79. Wiebelhaus, N. J.; Cranswick, M. A.; Klein, E. L.; Lockett, L. T.; Lichtenberger, D. L.; Enemark, J. H., Metal-Sulfur Valence Orbital Interaction Energies in Metal-Dithiolene Complexes: Determination of Charge and Overlap Interaction Energies by Comparison of Core and Valence Ionization Energy Shifts. *Inorg. Chem.* **2011,** *50* (21), 11021-11031.
80. Yang, J.; Mogesa, B.; Basu, P.; Kirk, M. L., Large Ligand Folding Distortion in an Oxomolybdenum Donor-Acceptor Complex. *Inorg. Chem.* **2016,** *55* (2), 785-793.
81. Hille, R.; Hall, J.; Basu, P., The Mononuclear Molybdenum Enzymes. *Chem. Rev.* **2014,** *114* (7), 3963-4038.
82. Garton, S. D.; Hilton, J.; Oku, H.; Crouse, B. R.; Rajagopalan, K. V.; Johnson, M. K., Active Site Structures and Catalytic Mechanism of Rhodobacter sphaeroides Dimethyl Sulfoxide Reductase as Revealed by Resonance Raman Spectroscopy. *J. Am. Chem. Soc.* **1997,** *119*, 12906-12916.
83. Li, H.-K.; Temple, C.; Rajagopalan, K. V.; Schindelin, H., The 1.3 Å Crystal Structure of Rhodobacter sphaeroides Dimethyl Sulfoxide Reductase Reveals Two Distinct Molybdenum Coordination Environments. *J. Am. Chem. Soc.* **2000,** *122* (32), 7673-7680.
84. McAlpine, A. S.; McEwan, A. G.; Bailey, S., The High Resolution Crystal Structure of DMSO reductase in Complex with DMSO. *J. Mol. Biol.* **1998,** *275*, 613-623.
85. Basu, P.; Burgmayer, S. J. N., Pterin Chemistry and its Relationship to the Molybdenum Cofactor. *Coord. Chem. Rev.* **2011,** *255* (9-10), 1016-1038.
86. Romao, M. J., Molybdenum and Tungsten Enzymes: A Crystallographic and Mechanistic Overview. *Dalton Trans.* **2009,** (21), 4053-4068.

87. McAlpine, A. S.; McEwan, A. G.; Shaw, A. L.; Bailey, S., Molybdenum Active Center of DMSO reductase from Rhodobacter capsulatus: Crystal Structure of the Oxidized Enzyme at 1.82-Å Resolution and the Dithionite-Reduced Enzyme at 2.8-Å Resolution. *JBIC, J. Biol. Inorg. Chem.* **1997,** *2* (6), 690-701.
88. Romao, M. J.; Knablein, J.; Huber, R.; Moura, J. J., Structure and Function of Molybdopterin Containing Enzymes. *Prog Biophys Mol Biol* **1997,** *68*, 121-44.
89. Donahue, J. P.; Goldsmith, C. R.; Nadiminti, U.; Holm, R. H., Synthesis, Structures, and Reactivity of Bis(dithiolene)molybdenum(IV,VI) Complexes Related to the Active Sites of Molybdoenzymes. *J. Am. Chem. Soc.* **1998,** *120* (49), 12869-12881.
90. Lim, B. S.; Donahue, J. P.; Holm, R. H., Synthesis and Structures of Bis(dithiolene)molybdenum Complexes Related to the Active Sites of the DMSO Reductase Enzyme Family. *Inorg. Chem.* **2000,** *39* (2), 263-273.
91. George, G. N.; Hilton, J.; Rajagopalan, K. V., X-ray Absorption Spectroscopy of Dimethyl Sulfoxide Reductase from Rhodobacter sphaeroides. *J. Am. Chem. Soc.* **1996,** *118* (5), 1113-17.
92. George, G. N.; Hilton, J.; Temple, C.; Prince, R. C.; Rajagopalan, K. V., Structure of the Molybdenum Site of Dimethyl Sulfoxide Reductase. *J. Am. Chem. Soc.* **1999,** *121* (6), 1256-1266.
93. Schindelin, H.; Kisker, C.; Hilton, J.; Rajagopalan, K. V.; Rees, D. C., Crystal Structure of DMSO reductase: Redox-Linked Changes in Molybdopterin Coordination. *Science* **1996,** *272* (5268), 1615-21.
94. Garton, S. D.; Garrett, R. M.; Rajagopalan, K. V.; Johnson, M. K., Resonance Raman Characterization of the Molybdenum Center in Sulfite Oxidase: Identification of Mo:O Stretching Modes. *J. Am. Chem. Soc.* **1997,** *119* (10), 2590-2591.
95. Rothery, R. A.; Stein, B.; Solomonson, M.; Kirk, M. L.; Weiner, J. H., Pyranopterin Conformation Defines the Function of Molybdenum and Tungsten Enzymes. *Proc. Natl. Acad. Sci. U. S. A.* **2012,** *109* (37), 14773-14778.
96. Sugimoto, H.; Tano, H.; Miyake, H.; Itoh, S., Generation of Bis(dithiolene)dioxomolybdenum(VI) Complexes from Bis(dithiolene)monooxomolybdenum(IV) Complexes by Proton-Coupled Electron Transfer in Aqueous Media. *Dalton Trans.* **2011,** *40* (10), 2358-2365.
97. Sugimoto, H.; Suyama, K.; Sugimoto, K.; Miyake, H.; Takahashi, I.; Hirota, S.; Itoh, S., A New Class of Sulfido/Oxo(dithiolene)-Molybdenum(IV) Complexes Derived from Sulfido/Oxo-Bis(tetrasulfido)molybdenum(IV) Anions. *Inorg. Chem.* **2008,** *47* (21), 10150-10157.
98. Sugimoto, H.; Tarumizu, M.; Miyake, H.; Tsukube, H., Bis(dithiolene) Molybdenum Complex that Promotes Combined Coupled Electron-Proton Transfer and Oxygen Atom Transfer Reactions: a Water-Active Model of the Arsenite oxidase Molybdenum Center. *Eur. J. Inorg. Chem.* **2006,** (22), 4494-4497.
99. Enemark, J. H.; Cooney, J. J. A.; Wang, J.-J.; Holm, R. H., Synthetic Analogues and Reaction Systems Relevant to the Molybdenum and Tungsten Oxotransferases. *Chem. Rev.* **2004,** *104* (2), 1175-1200.
100. Das, S. K.; Chaudhury, P. K.; Biswas, D.; Sarkar, S., Modeling for the Active Site of Sulfite Oxidase: Synthesis, Characterization, and Reactivity of $[MoVIO_2(mnt)_2]^{2-}$ (mnt2- = 1,2-Dicyanoethylenedithiolate). *J. Am. Chem. Soc.* **1994,** *116* (20), 9061-70.

101. Sugimoto, H.; Tarumizu, M.; Tanaka, K.; Miyake, H.; Tsukube, H., A New Series of Molybdenum-(IV), -(V), and -(VI) Dithiolate Compounds as Active Site Models of Molybdoenzymes: Preparation, Crystal Structures, Spectroscopic/Electrochemical Properties and Reactivity in Oxygen Atom Transfer. *Dalton Trans.* **2005,** (21), 3558-3565.
102. Bastian, N. R. K., C.J; Barber, M.J; Rajagopalan, K.V, Spectroscopic Studies of the Molybdenum Containing Dimethyl Sulfoxide Reductase from Rhodobacter sphaeroides. *Journal of Biological Chemistry* **1991,** *266*, 45-51.
103. Sugimoto, H.; Tatemoto, S.; Toyota, K.; Ashikari, K.; Kubo, M.; Ogura, T.; Itoh, S., Oxo-Sulfido- and Oxo-Selenido-=Molybdenum(VI) Complexes Possessing a Dithiolene Ligand Related to the Active Sites of Hydroxylases of Molybdoenzymes: Low Temperature Preparation and Characterisation. *Chem. Commun.* **2013,** *49* (39), 4358-4360.
104. Sugimoto, H. T., S; Suyama, K; Maiyake, H; Mtei, R.P; Itoh, S; Kirk, M.L;, Monooxomolybdenum (VI) Complexes Possessing Olefinic Dithiolene Ligands: Probing Mo-S Covalency Contributions to Electron Transfer in Dimethyl Sulfoxide Reductase Family Molybdoenzymes. *Inorg. Chem.* **2010**, 5368-5370.
105. Ueyama, N.; Oku, H.; Nakamura, A., cis-Dioxobis(benzenedithiolato)Tungsten(VI) and the Related Monooxotungsten(V) and -(IV) Complexes. Models of Tungsten oxidoreductases. *J. Am. Chem. Soc.* **1992,** *114* (18), 7310-11.
106. Oku, H.; Ueyama, N.; Nakamura, A.; Kai, Y.; Kanehisa, N., The Stabilization of Dioxomolybdenum(VI) Dithiolene Complex by the Electron-withdrawing Substituent on the Dithiolene Ligand: Comparison of Reactivities of Monooxomolybdenum(IV) Complex with $R_2S_2C_2$ (R = -CN and -COOMe) Ligands as Models of Molybdenum oxidoreductases. *Chem. Lett.* **1994,** (3), 607-10.
107. Oku, H.; Ueyama, N.; Nakamura, k., Thiolato-Activated Oxo-Metal Bond Features in Molybdenum and Tungsten Oxidoreductase Models As Revealed by Raman Spectroscopy. *Inorg. Chem.* **1995,** *34* (14), 3667-76.
108. Doering, A.; Fischer, C.; Schulzke, C., Mono-Oxo-Bis-Dithioveratrol-Molybdate - In Solution a Model for Arsenite Oxidase and in the Solid State a Coordination Polymer with Unprecedented Binding Motifs. *Z. Anorg. Allg. Chem.* **2013,** *639* (8-9), 1552-1558.
109. Ghosh, A. C.; Samuel, P. P.; Schulzke, C., Synthesis, Characterization and Oxygen Atom Transfer Reactivity of a pair of Mo(IV)O- and Mo(VI)O_2-enedithiolate Complexes - A Look at Both Ends of the Catalytic Transformation. *Dalton Trans.* **2017,** *46* (23), 7523-7533.
110. Oku, H.; Ueyama, N.; Nakamura, A., Association of Oxo-Molybdenum Dithiolene Complexes with a Multiamide Additive and Its Influence on the Ease of O-Atom Transfer. *Inorg. Chem.* **1997,** *36* (7), 1504-1516.
111. Moula, G.; Bose, M.; Sarkar, S., Replica of a Fishy Enzyme: Structure-Function Analogue of Trimethylamine-*N*-oxide Reductase. *Inorg. Chem.* **2013,** *52* (9), 5316-5327.
112. Sugimoto, H.; Tatemoto, S.; Suyama, K.; Miyake, H.; Itoh, S.; Dong, C.; Yang, J.; Kirk, M. L., Dioxomolybdenum(VI) Complexes with Ene-1,2-dithiolate Ligands: Synthesis, Spectroscopy, and Oxygen Atom Transfer Reactivity. *Inorg. Chem.* **2009,** *48* (22), 10581-10590.

113. Baba, K.; Okamura, T.-A.; Yamamoto, H.; Yamamoto, T.; Ohama, M.; Ueyama, N., Monooxomolybdenum(IV) Complex with Extremely Bulky Dithiolate Ligands - Acceleration of O-Atom Transfer by Distorted Square Pyramidal Conformation. *Chem. Lett.* **2005,** *34* (1), 44-45.
114. Baba, K.; Okamura, T.; Suzuki, C.; Yamamoto, H.; Yamamoto, T.; Ohama, M.; Ueyama, N., O-Atom-Transfer Oxidation of [Molybdenum(IV) Oxo{3,6-(acylamino)$_2$-1,2-benzenedithiolato}$_2$]$^{2-}$ Promoted by Intramolecular NH···S Hydrogen Bonds. *Inorg. Chem.* **2006,** *45* (2), 894-901.
115. Okamura, T.-A.; Tatsumi, M.; Omi, Y.; Yamamoto, H.; Onitsuka, K., Selective and Effective Stabilization of MoVI=O Bonds by NH···S Hydrogen Bonds via Trans Influence. *Inorg. Chem.* **2012,** *51* (21), 11688-11697.
116. Okamura, T.-A.; Omi, Y.; Hirano, Y.; Onitsuka, K., Comparative Studies on the Contribution of NH···S Hydrogen Bonds in Tungsten and Molybdenum Benzenedithiolate Complexes. *Dalton Trans.* **2016,** *45* (39), 15651-15659.
117. Porcher, J.-P.; Fogeron, T.; Gomez-Mingot, M.; Chamoreau, L.-M.; Li, Y.; Fontecave, M., Synthesis and Reactivity of a Bio-inspired Dithiolene Ligand and its Mo Oxo Complex. *Chem. - Eur. J.* **2016,** *22* (13), 4447-4453.
118. Okamura, T.-A.; Kunisue, K.; Omi, Y.; Onitsuka, K., Strong NH···S Hydrogen Bonds in Molybdoenzyme Models Containing Anilide Moieties. *Dalton Trans.* **2013,** *42* (21), 7569-7578.
119. Sparacino-Watkins, C.; Stolz, J. F.; Basu, P., Nitrate and Periplasmic Nitrate Reductases. *Chem. Soc. Rev.* **2014,** *43* (2), 676-706.
120. Oku, H.; Ueyama, N.; Kondo, M.; Nakamura, A., Oxygen Atom Transfer Systems in which the μ-Oxodimolybdenum(V) Complex Formation does not occur: Syntheses, Structures, and Reactivities of Monooxomolybdenum(IV) Benzenedithiolato Complexes as Models of Molybdenum Oxidoreductases. *Inorg. Chem.* **1994,** *33* (2), 209-16.
121. McCleverty, J. A.; Locke, J.; Ratcliff, B.; Wharton, E. J., Transition Metal Dithiolene Complexes. X. Oxy-Metal Bis-1,2-dithiolenes. *Inorg. Chim. Acta* **1969,** *3* (2), 283-6.
122. Fischer, B.; Schmalle, H.; Dubler, E.; Schaefer, A.; Viscontini, M., Functional and Structural Model for the Molybdenum-Pterin Binding Site in Dimethyl Sulfoxide Reductase. Synthesis, Crystal Structure, and Spectroscopic Investigations of Trichloro(quinoid-N(8)H-6,7-dihydropterin)oxomolybdenum(IV). *Inorg. Chem.* **1995,** *34* (23), 5726-34.
123. Davies, E. S.; Beddoes, R. L.; Collison, D.; Dinsmore, A.; Docrat, A.; Joule, J. A.; Wilson, C. R.; Garner, C. D., Synthesis of Oxomolybdenum Bis(dithiolene) Complexes Related to the Cofactor of the Oxomolybdoenzymes. *J. Chem. Soc., Dalton Trans.* **1997**, 3985-3996.
124. Mitchell, P. C. H.; Pygall, C. F., Oxomolybdenum(IV) Bis(dithiolato) Complexes. *Inorg. Chim. Acta* **1979,** *33* (1), L109-L111.
125. Boyde, S.; Ellis, S. R.; Garner, C. D.; Clegg, W., Structural Comparison of Oxobis(benzene-1,2-dithiolato)Molybdenum(V) and -(IV) Complexes. *J. Chem. Soc., Chem. Commun.* **1986,** (20), 1541-3.
126. Matsubayashi, G.-E.; Nojo, T.; Tanaka, T., X-ray Molecular Structure of Bis(tetrabutylammonium) Bis(4,5-dimercapto-1,3-dithiole-2-thionate)oxomolybdate and its Oxidation. *Inorg. Chim. Acta* **1988,** *154* (2), 133-5.

127. Sarkar, S.; Das, S. K., Synthesis of the Active Sites of Molybdoenzymes: MoO_2(VI) and MoO(IV)-dithiolene Complexes Mimicking Enzymatic Reactions of Sulfite Oxidase with Saturation Kinetics. *Proceedings - Indian Academy of Sciences, Chemical Sciences* **1992,** *104* (3), 437-41.
128. Coucouvanis, D.; Hadjikyriacou, A.; Draganjac, M.; Kanatzidis, M. G.; Ileperuma, O., Unique Reactivity Characteristics of Molybdenum-Coordinated Disulfido($^{2-}$) and Tetrasulfido($^{2-}$) Ligands. *Polyhedron* **1986,** *5* (1-2), 349-56.
129. Ansari, M. A.; Chandrasekaran, J.; Sarkar, S., Synthesis and Characterization of a Mononuclear Molybdenum(IV) Oxo Complex $(Et_4N)_2[MoO(S_2C_2(COPh)_2)_2]$. *Inorg. Chim. Acta* **1987,** *133* (1), 133-6.
130. Subramanian, P.; Burgmayer, S.; Richards, S.; Szalai, V.; Spiro, T. G., Resonance Raman Signatures of Oxomolybdenum Thiolate and Dithiolene Models of Molybdenum Proteins. *Inorg. Chem.* **1990,** *29* (19), 3849-53.
131. Coucouvanis, D.; Hadjikyriacou, A.; Toupadakis, A.; Koo, S. M.; Ileperuma, O.; Draganjac, M.; Salifoglou, A., Studies of the Reactivity of Binary Thio- and Tertiary Oxothiomolybdates Toward Electrophiles. Reactions with Dicarbomethoxyacetylene and the Synthesis and Structures of the $[Et_4N_2[MoO(L)_2]$, anti-$[Et_4N]_2[Mo_2O_2S_2(L)_2]]$, syn-$[Ph_4P]_2[Mo_2O_2S_2(L)_2]\cdot 2DMF$, $Ph_4P]_2[Mo(L)_3]DMF\cdot C_6H_6$, and $[Ph_4P]_2[Mo_2S_2(L)_4]_2CH_2Cl_2$ Complexes (L = 1,2-dicarbomethoxy-1,2-ethylenedithiolate). *Inorg. Chem.* **1991,** *30* (4), 754-67.
132. Sugimoto, H.; Harihara, M.; Shiro, M.; Sugimoto, K.; Tanaka, K.; Miyake, H.; Tsukube, H., Dioxo-Molybdenum(VI) and Mono-oxo-Molybdenum(IV) Complexes Supported by New Aliphatic Dithiolene Ligands: New Models with Weakened Mo:O Bond Characters for the Arsenite Oxidase Active Site. *Inorg. Chem.* **2005,** *44* (18), 6386-6392.
133. Lim, B. S.; Sung, K.-M.; Holm, R. H., Structural and Functional Bis(dithiolene)-Molybdenum/Tungsten Active Site Analogues of the Dimethylsulfoxide Reductase Enzyme Family. *J. Am. Chem. Soc.* **2000,** *122* (30), 7410-7411.
134. Sproules, S.; Banerjee, P.; Weyhermuller, T.; Yan, Y.; Donahue, J. P.; Wieghardt, K., Monoanionic Molybdenum and Tungsten Tris(dithiolene) Complexes: A Multifrequency EPR Study. *Inorg. Chem.* **2011,** *50* (15), 7106-7122.
135. Mitra, J.; Sarkar, S., Oxo-Mo(IV)(dithiolene)thiolato Complexes: Analogue of Reduced Sulfite Oxidase. *Inorg. Chem.* **2013,** *52* (6), 3032-3042.
136. Lee, C. Y., Weitao; Parr, Robert G., Developoment of the Colle-Salvetti Correlation-Energy Formula into a Functional of the Electron Density. *Physical Review B.* **1988,** *37* (0163-1829), 785-759.
137. Hay, P. J. W., Willard R., Ab Initio Effective Core Potentials for Molecular Calucations. Potentials for Potassium to Gold including the Outermost Core Orbitals. *Journal of Chemical Physics* **1985,** *82* (1), 299-310.
138. Sheldrick, G. M., SADABS Version 2.03. *University of Göttingen,Germany* **2002**.
139. Sheldrick, G. M., *Acta Cryst.* **2008,** *A64*, 112-122.
140. Sheldrick, G. M., Crystal Structure Refinement with SHELXL. *Acta Cryst.* **2015,** *C71*, 3-8.

141. Marlin, D. S.; Olmstead, M. M.; Mascharak, P. K., Structure-Spectroscopy Correlation in Distorted Five-Coordinate Cu(II) Complexes: A Case Study with a Set of Closely Related Copper Complexes of Pyridine-2,6-dicarboxamide Ligands. *Inorg. Chem.* **2001,** *40* (27), 7003-7008.
142. Marchivie, M.; Guionneau, P.; Letard, J. F.; Chasseau, D., Photo-Induced Spin-Transition: the Role of the Iron(II) Environment Distortion. *Acta Crystallogr., Sect. B: Struct. Sci.* **2005,** *B61* (1), 25-28.
143. Addison, A. W.; Rao, T. N.; Reedijk, J.; Van Rijn, J.; Verschoor, G. C., Synthesis, Structure, and Spectroscopic Properties of Copper(II) Compounds Containing Nitrogen-Sulfur Donor Ligands: The Crystal and Molecular Structure of Aqua[1,7-bis(N-methylbenzimidazol-2'-yl)-2,6-dithiaheptane]copper(II) Perchlorate. *J. Chem. Soc., Dalton Trans.* **1984,** (7), 1349-56.
144. CCDC, Structure Search of all Monooxo-Molybdenum Bis Dithiolene Complexes Measuring the Basal and Axial Angle to Calculate the Distortion Parameter Tau. Cambridge Crystallographic Data Centre: May, 15 2019.
145. CCDC, Structure Search of: 1. All Molybdenum-Bis Dithiolene Complexes Measuring Mo=O, C-S and C-C Bond Lenghs of the Ditholene Ligands. 2. Strucutre Search for Monooxo-Molybdenum Complexes, Examining Mo=O Bond Lengths. 3. Structure Search of all Monooxo-Molybdenum Bis Dithiolene Complexes Measuring the Distance between the Molybdenum Metal Center and the Plane of the Four Sulfur Atoms of the Ditholene Ligands. Cambridge Crystallographic Data Centre: November, 25, 2018.
146. Kaim, W.; Schwederski, B., Non-Innocent Ligands in Bioinorganic Chemistry: An Overview. *Coord. Chem. Rev.* **2010,** *254* (13-14), 1580-1588.
147. Chirik, P. J., Preface: Forum on Redox-Active Ligands. *Inorg. Chem.* **2011,** *50* (20), 9737-9740.
148. Skara, G.; Pinter, B.; Geerlings, P.; De Proft, F., Revealing the Thermodynamic Driving Force for Ligand-Based Reductions in Quinoids; Conceptual Rules for Designing Redox Active and Non-Innocent Ligands. *Chem. Sci.* **2015,** *6* (7), 4109-4117.
149. Eisenberg, R.; Gray, H. B., Noninnocence in Metal Complexes: A Dithiolene Dawn. *Inorg. Chem.* **2011,** *50* (20), 9741-9751.
150. Samuel, P. P.; Horn, S.; Doering, A.; Havelius, K. G. V.; Reschke, S.; Leimkuehler, S.; Haumann, M.; Schulzke, C., A Crystallographic and Mo K-Edge XAS Study of Molybdenum Oxo Bis-, Mono-, and Non-Dithiolene Complexes - First-Sphere Coordination Geometry and Noninnocence of Ligands. *Eur. J. Inorg. Chem.* **2011,** *2011* (28), 4387-4399.
151. van Stipdonk, M. J.; Basu, P.; Dille, S. A.; Gibson, J. K.; Berden, G.; Oomens, J., Infrared Multiple Photon Dissociation Spectroscopy of a Gas-Phase Oxo-Molybdenum Complex with 1,2-Dithiolene Ligands. *J. Phys. Chem. A* **2014,** *118* (29), 5407-5418.
152. Ratvasky, S. C.; Mogesa, B.; van Stipdonk, M. J.; Basu, P., A Mixed Valence Zinc Dithiolene System with Spectator Metal and Reactor Ligands. *Polyhedron* **2016,** *114*, 370-377.
153. Basu, P., Use of EPR Spectroscopy in Elucidating Electronic Structures of Paramagnetic Transition Metal Complexes. *J. Chem. Educ.* **2001,** *78* (5), 666-669.

154. Geary, E. A. M.; Yellowlees, L. J.; Parsons, S.; Pilia, L.; Serpe, A.; Mercuri, M. L.; Deplano, P.; Clark, S. J.; Robertson, N., Influence of the R-substituents on the properties of [Ni(R_2pipdt)(dmit)] complexes and crystal structure where R = $CH_2C_6H_5$. *Dalton Trans.* **2007,** (46), 5453-5459.
155. Bolman, P. S. H.; Safarik, I.; Stiles, D. A.; Tyerman, W. J. R.; Strausz, O. P., Electron Paramagnetic Resonance Spectra of some Sulfur-Containing Radicals. *Can. J. Chem.* **1970,** *48* (24), 3872-6.
156. Preston, K. F.; Sutcliffe, L. H., Electron Spin Resonance Spectroscopy of Free Radicals Containing Sulfur Linked to Nitrogen. *Magn. Reson. Chem.* **1990,** *28* (3), 189-204.
157. Inscore, F. E.; Joshi, H. K.; McElhaney, A. E.; Enemark, J. H., Remote Ligand Substituent Effects on the Properties of Oxo-Mo(V) Centers with a Single Ene-1,2-Dithiolate Ligand. *Inorg. Chim. Acta* **2002,** *331*, 246-256.
158. Attar, S. S.; Artizzu, F.; Marchio, L.; Espa, D.; Pilia, L.; Casula, M. F.; Serpe, A.; Pizzotti, M.; Orbelli-Biroli, A.; Deplano, P., Uncommon Optical Properties and Silver-Responsive Turn-Off/On Luminescence in a PtII Heteroleptic Dithiolene Complex. *Chem. - Eur. J.* **2018,** *24* (41), 10503-10512.
159. Chen, C. T.; Liao, S. Y.; Lin, K. J.; Lai, L. L., Syntheses, Charge Distribution, and Molecular Second-Order Nonlinear Optical Properties of Push-Pull Bis-dithiolene Nickel Complexes. *Adv. Mater. (Weinheim, Ger.)* **1998,** *10* (4), 334-338.
160. Bigoli, F.; Chen, C.-T.; Wu, W.-C.; Deplano, P.; Mercuri, M. L.; Pellinghelli, M. A.; Pilia, L.; Pintus, G.; Serpe, A.; Trogu, E. F., [Ni(R_2pipdt)$_2$](BF4)$_2$ (R_2pipdt = 1,4-disubstituted-piperazine-3,2-dithione) as useful precursors of mixed-ligand dithiolenes of interest for non-linear optics. *Chem. Commun. (Cambridge, U. K.)* **2001,** (21), 2246-2247.
161. Kamlet, M. J.; Abboud, J. L.; Taft, R. W., The Solvatochromic Comparison Method. 6. The π* Scale of Solvent Polarities. *J. Am. Chem. Soc.* **1977,** *99* (18), 6027-38.
162. Dong, C.; Yang, J.; Leimkuehler, S.; Kirk, M. L., Pyranopterin Dithiolene Distortions Relevant to Electron Transfer in Xanthine Oxidase/Dehydrogenase. *Inorg. Chem.* **2014,** *53* (14), 7077-7079.
163. Okamura, T.-A.; Yamada, T.; Hasenaka, Y.; Yamashita, S.; Onitsuka, K., Unexpected Reaction Promoted by NH+···O=Mo Hydrogen Bonds in Nonpolar Solvents. *Eur. J. Inorg. Chem.* **2016,** *2016* (18), 2952-2961.
164. Lorber, C.; Plutino, M. R.; Elding, L. I.; Nordlander, E., Kinetics of Oxygen-Atom Transfer Reactions Involving Molybdenum Dithiolene Complexes. *J. Chem. Soc., Dalton Trans.* **1997,** (21), 3997-4004.
165. Nemykin, V. N.; Laskin, J.; Basu, P., Isolation, Characterization of an Intermediate in an Oxygen Atom-Transfer Reaction, and the Determination of the Bond Dissociation Energy. *J Am Chem Soc* **2004,** *126* (28), 8604-5.
166. Millar, A. J.; Doonan, C. J.; Smith, P. D.; Nemykin, V. N.; Basu, P.; Young, C. G., Oxygen Atom Transfer in Models for Molybdenum Enzymes: Isolation and Structural, Spectroscopic, and Computational Studies of Intermediates in Oxygen Atom Transfer from Molybdenum(VI) to Phosphorus(III). *Chem. - Eur. J.* **2005,** *11* (11), 3255-3267.
167. Nemykin, V. N.; Basu, P., Oxygen Atom Transfer Reactivity from a Dioxo-Mo(VI) Complex to Tertiary Phosphines: Synthesis, Characterization, and Structure of Phosphoryl Intermediate Complexes. *Inorg. Chem.* **2005,** *44* (21), 7494-7502.

168. Sengar, R. S.; Nemykin, V. N.; Basu, P., Synthesis, Electrochemistry, Geometric and Electronic Structure of Oxo-Molybdenum Compounds Involved in an Oxygen Atom Transferring System. *J. Inorg. Biochem.* **2008,** *102* (4), 748-756.
169. Smith, P. D.; Millar, A. J.; Young, C. G.; Ghosh, A.; Basu, P., Detection, Isolation, and Characterization of Intermediates in Oxygen Atom Transfer Reactions in Molybdoenzyme Model Systems. *J. Am. Chem. Soc.* **2000,** *122* (38), 9298-9299.
170. Nemykin, V. N.; Davie, S. R.; Mondal, S.; Rubie, N.; Kirk, M. L.; Somogyi, A.; Basu, P., An Analogue System Displaying All the Important Processes of the Catalytic Cycles Involving Monooxomolybdenum(VI) and Desoxomolybdenum(IV) Centers. *J. Am. Chem. Soc.* **2002,** *124* (5), 756-757.
171. Nemykin, V. N.; Basu, P., A Bifurcated Pathway of Oxygen Atom Transfer Teactions from a Monooxo Molybdenum(VI) Complex Under Electrospray Ionization Mass Spectrometric Conditions. *Dalton Trans.* **2004,** (13), 1928-1933.
172. Basu, P.; Kail, B. W.; Adams, A. K.; Nemykin, V. N., Quantitation of the Ligand Effect in Oxo-Transfer Reactions of Dioxo-Mo(VI) Tris(pyrazolyl)borate Complexes. *Dalton Trans.* **2013,** *42* (9), 3071-3081.
173. Basu, P.; Kail, B. W.; Young, C. G., Influence of the Oxygen Atom Acceptor on the Reaction Coordinate and Mechanism of Oxygen Atom Transfer From the Dioxo-Mo(VI) Complex, $Tp^{i}PrMoO_2(OPh)$, to Tertiary Phosphines. *Inorg. Chem.* **2010,** *49* (11), 4895-4900.
174. Basu, P.; Nemykin, V. N.; Sengar, R. S., Substituent Effect on Oxygen Atom Transfer Reactivity from Oxomolybdenum Centers: Synthesis, Structure, Electrochemistry, and Mechanism. *Inorg. Chem.* **2009,** *48* (13), 6303-6313.
175. Ueyama, N.; Oku, H.; Kondo, M.; Okamura, T.-A.; Yoshinaga, N.; Nakamura, A., Trans Influence of Oxo and Dithiolene Coordination in Oxidized Models of Molybdenum Oxidoreductase: Synthesis, Structures, and Properties of $Q_2[MoVIO_2(1,2\text{-benzenedithiolato})_2]$ (Q = NEt_4, PPh_4) and Related Complexes. *Inorg. Chem.* **1996,** *35* (3), 643-50.
176. Nagarajan, K.; Chaudhury, P. K.; Srinivasan, B. R.; Sarkar, S., Oxoanionic or Sulfur Lone Pair Attack? The Difference in Reactivity of Hydrogensulfite Anion and Neutral Dimethylsulfite towards $[Bu_4N]_2[MoO_2\{S_2C_2(CN)_2\}_2]$ in the Model Reductive Half Reaction of Sulfite Oxidase. *Chem. Commun.* **2001,** (18), 1786-1787.
177. Hoffman, J. M.; Oliver, A. G.; Brown, S. N., The Metal or the Ligand? The Preferred Locus for Redox Changes in Oxygen Atom Transfer Reactions of Rhenium Amidodiphenoxides. *J. Am. Chem. Soc.* **2017,** *139* (12), 4521-4531.
178. Fortner, K. C.; Laitar, D. S.; Muldoon, J.; Pu, L.; Braun-Sand, S. B.; Wiest, O.; Brown, S. N., Ultrafast and Ultraslow Oxygen Atom Transfer Reactions between Late Metal Centers. *J. Am. Chem. Soc.* **2007,** *129* (3), 588-600.
179. Moesch-Zanetti, N. C.; Sachse, A.; Pfoh, R.; Vidovic, D.; Magull, J., Rhenium Oxo Compounds Containing η2-Pyrazolate Ligands. *Dalton Trans.* **2005,** (12), 2124-2129.
180. Jacobi, B. G.; Laitar, D. S.; Pu, L.; Wargocki, M. F.; DiPasquale, A. G.; Fortner, K. C.; Schuck, S. M.; Brown, S. N., Stoichiometric and Catalytic Oxygen Activation by Trimesityliridium(III). *Inorg Chem* **2002,** *41* (18), 4815-23.
181. Seymore, S. B.; Brown, S. N., Charge Effects on Oxygen Atom Transfer. *Inorg Chem* **2000,** *39* (2), 325-32.

182. Leyden, D. E.; Morgan, W. R., Kinetics of Proton Exchange of Trimethylammonium Ion by N.M.R. Laboratory Experiment. *J. Chem. Educ.* **1969,** *46* (3), 169-71.

APPENDIX

A1. ^{1}H NMR Spectra

^{1}H NMR spectra were recorded on either a Bruker 500 MHz Avance spectrometer or a Bruker 400 MHz Avance spectrometer in air-tight NMR tubes. All spectra were collected at room temperature (X K) in deuterated acetonitrile (CD_3CN).

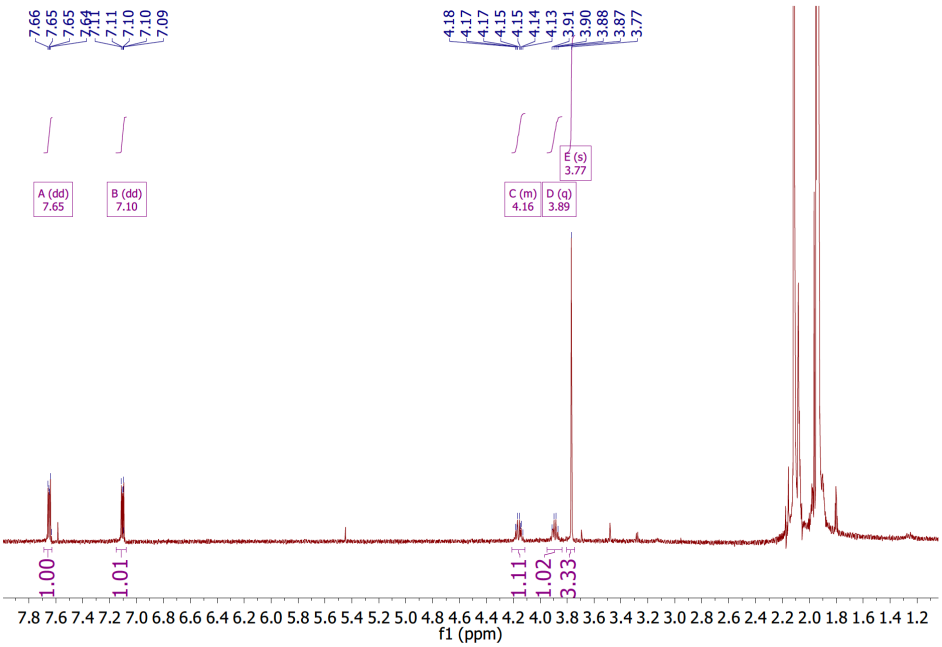

Figure A1.1. ^{1}H NMR spectrum (CD_3CN) of $MoO(bdt)(Me_2Dt^0)$

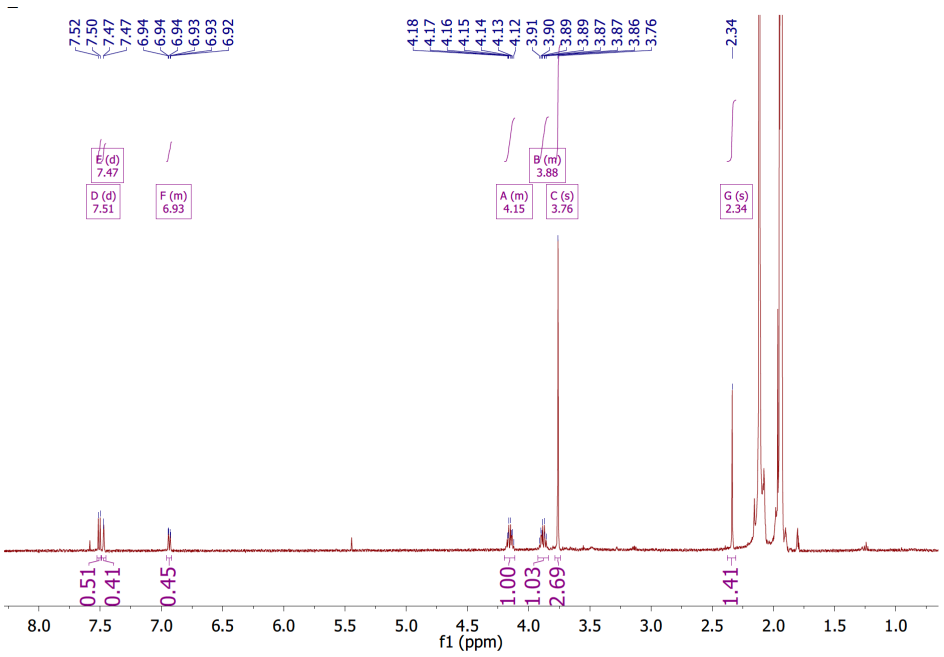

Figure A1.2. ^{1}H NMR spectrum (CD_3CN) of $MoO(tdt)(Me_2Dt^0)$

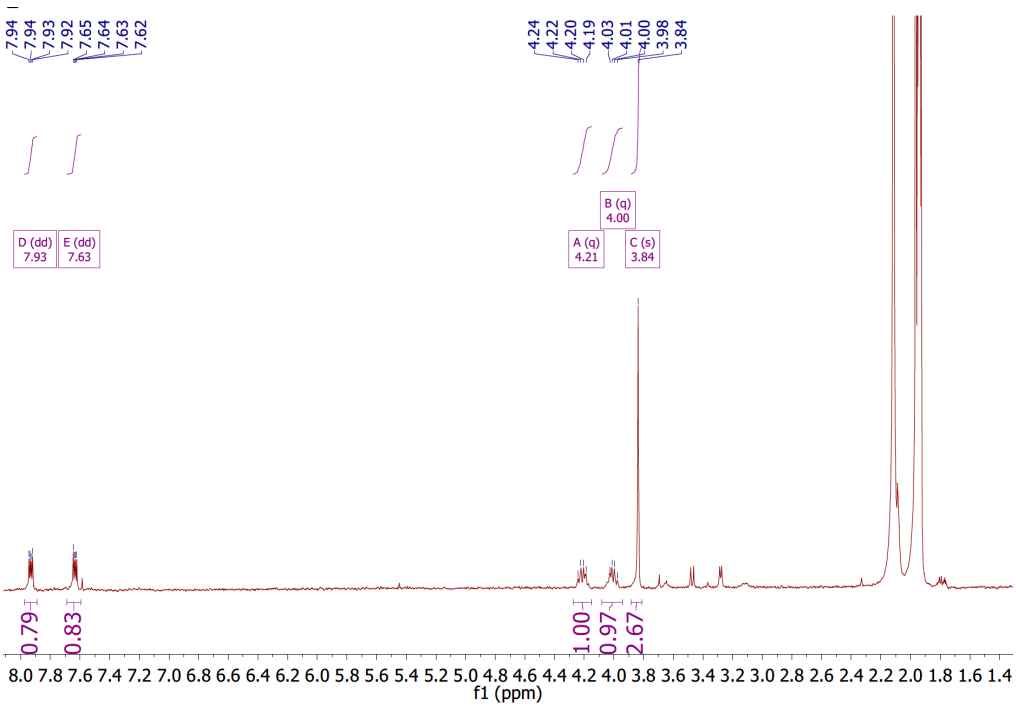

Figure A1.3 ^{1}H NMR spectrum (CD_3CN) of $MoO(qdt)(Me_2Dt^0)$

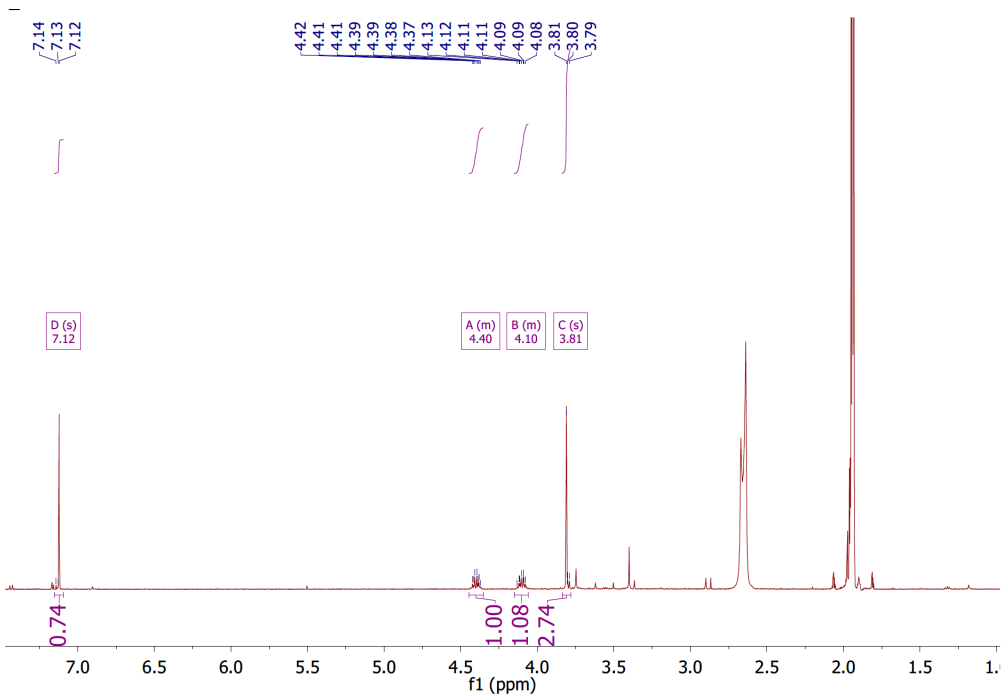

Figure A1.4 ^{1}H NMR spectrum (CD_3CN) of $MoO(bdtCl_2)(Me_2Dt^0)$

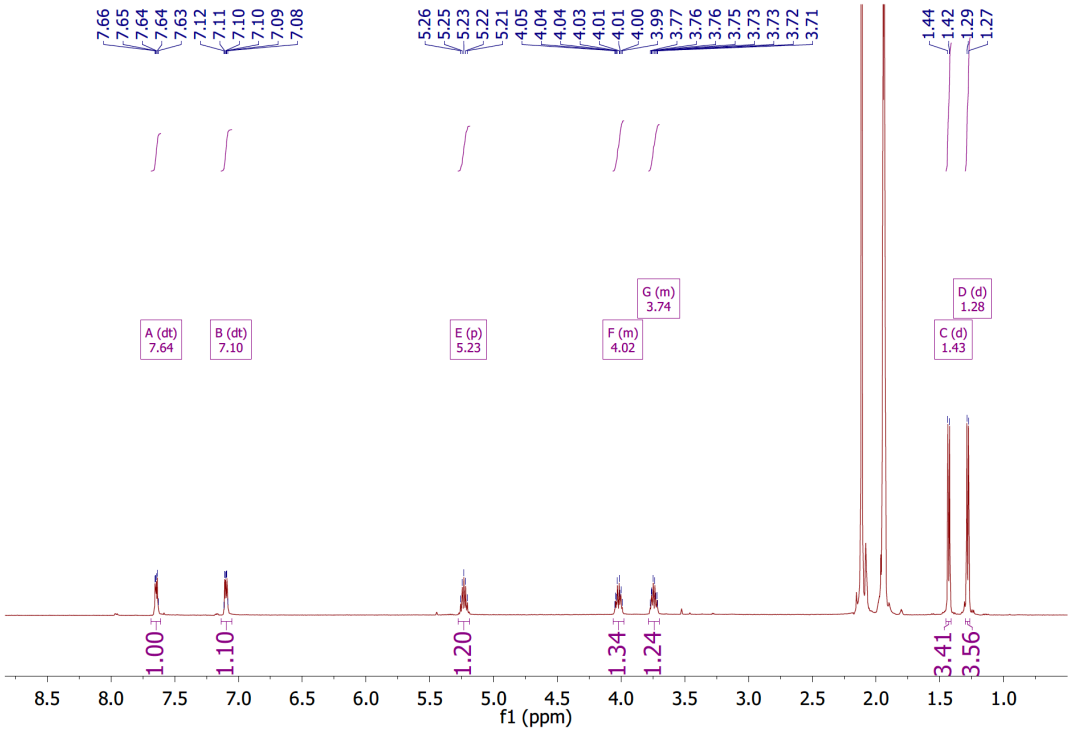

Figure A1.5 ^{1}H NMR spectrum (CD_3CN) of $MoO(bdt)(^{i}Pr_2Dt^0)$

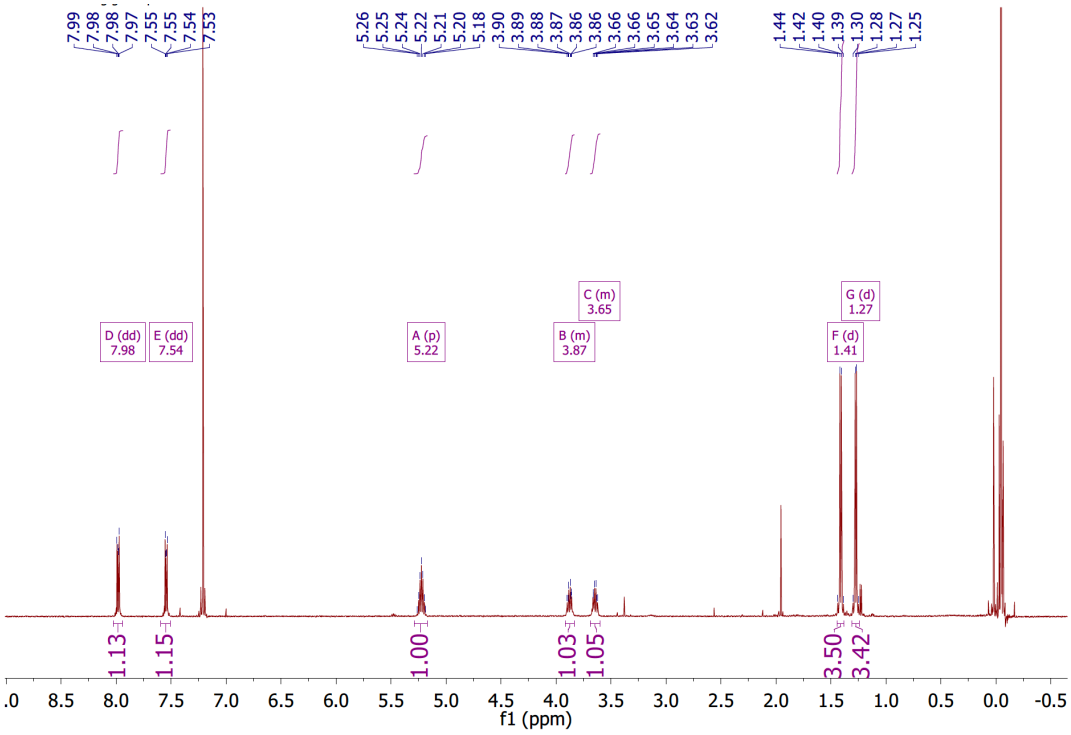

Figure A1.6 1H NMR spectrum ($CDCl_3$) of MoO(qdt)($^{i}Pr_2Dt^0$)

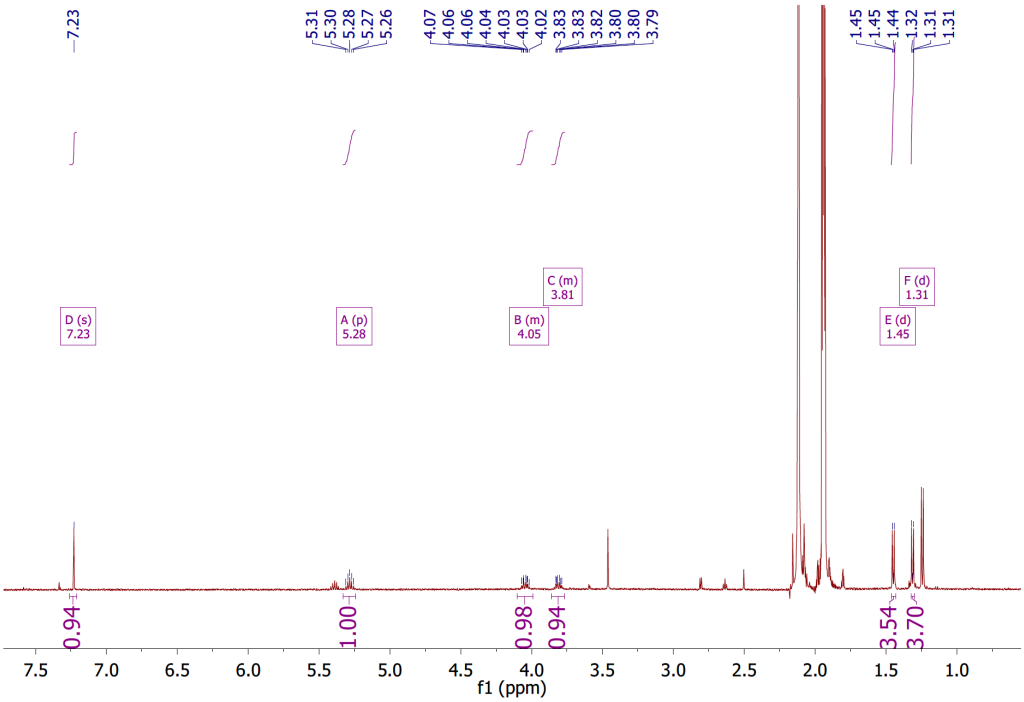

Figure A1.7 ^{1}H NMR spectrum (CD_3CN) of MoO($bdtCl_2$)($^{i}Pr_2Dt^0$)

A2. IR Spectra

Infrared spectroscopy (FTIR) was recorded using a Thermo-Fisher Nicolet iS10 spectrometer at room temperature using a KBr pellet.

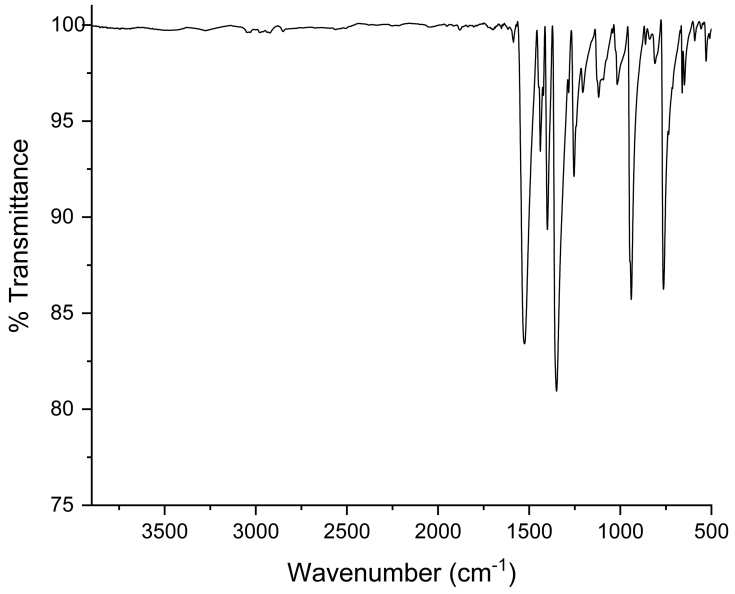

Figure A2.1 IR spectrum (KBr) of MoO(bdt)(Me_2Dt^0)

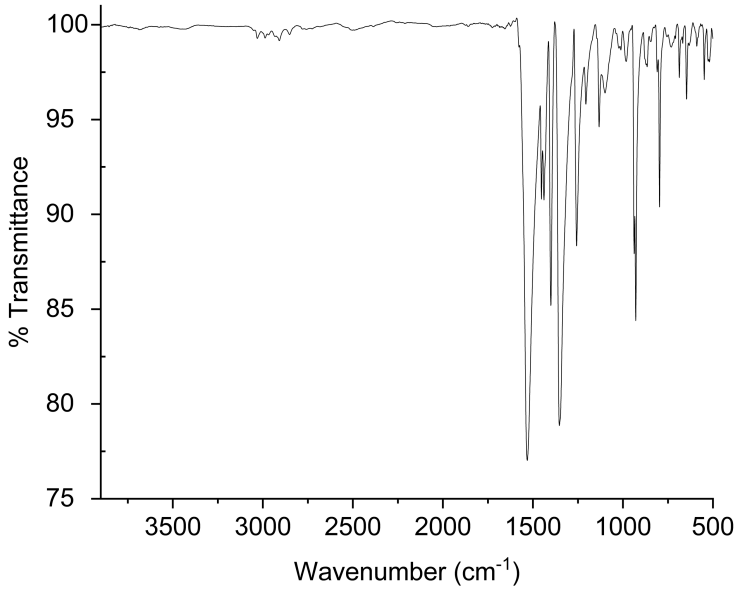

Figure A2.2 IR spectrum (KBr) of MoO(tdt)(Me_2Dt^0)

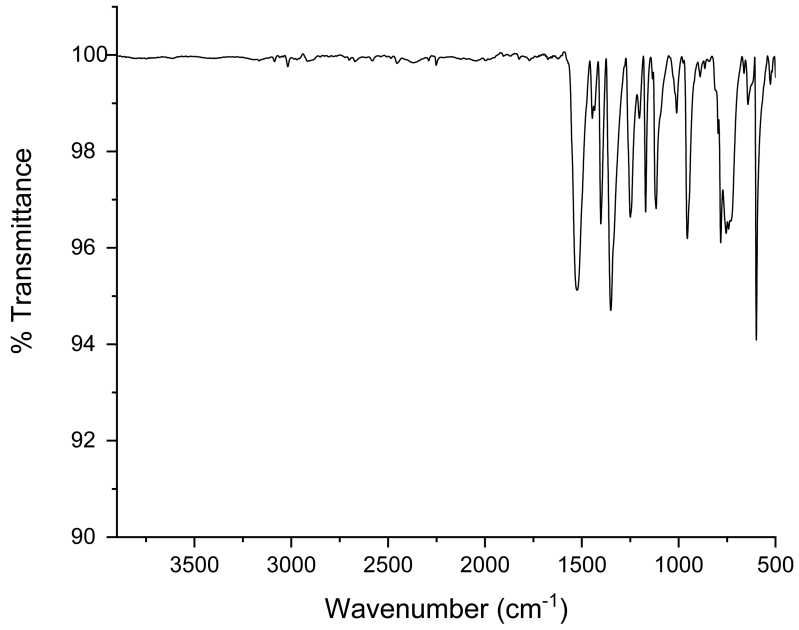

Figure A2.3 IR spectrum (KBr) of MoO(qdt)(Me_2Dt^0)

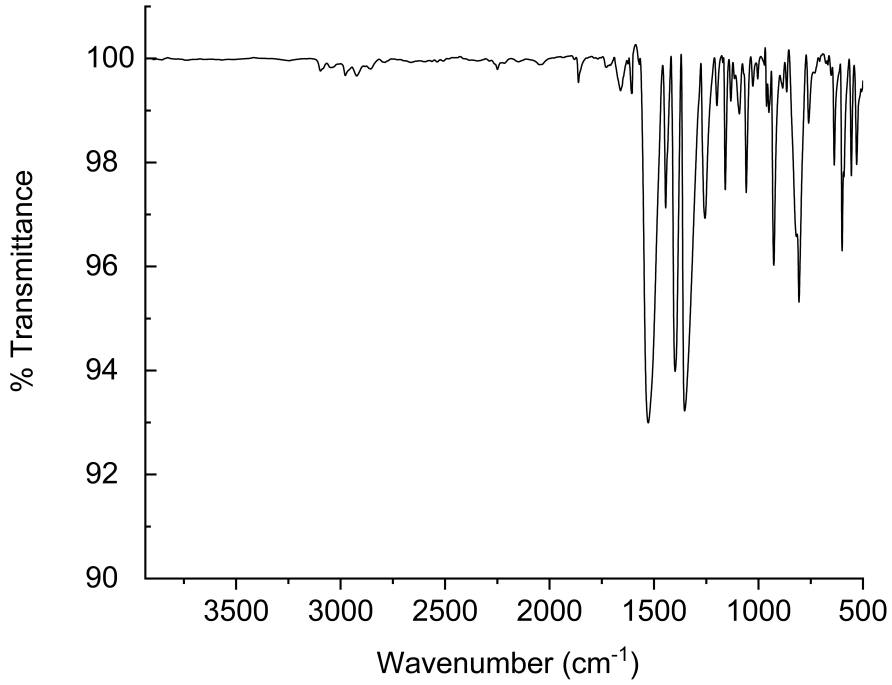

Figure A2.4 IR spectrum (KBr) of MoO($bdtCl_2$)(Me_2Dt^0)

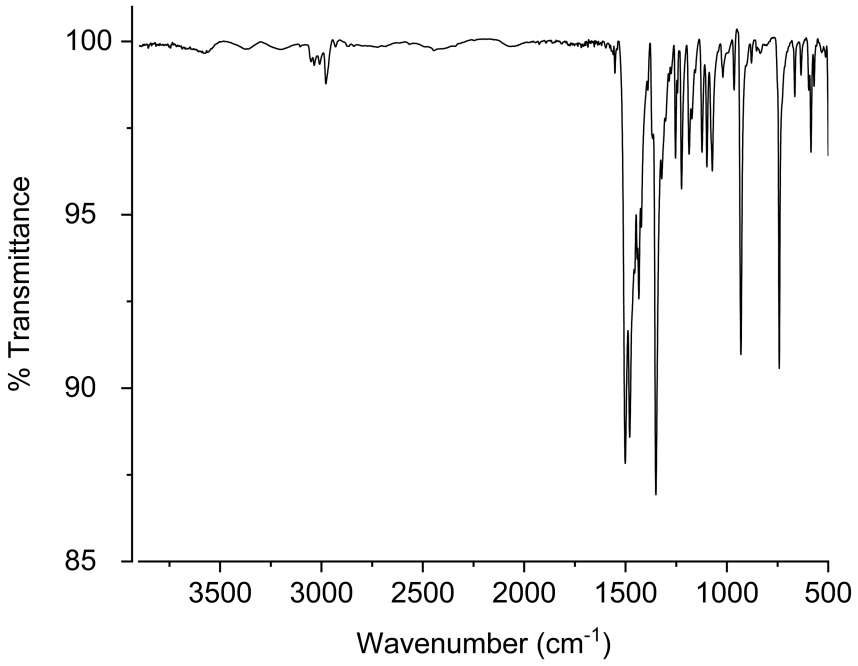

Figure A2.5 IR spectrum (KBr) of MoO(bdt)($^{i}Pr_2Dt^0$)

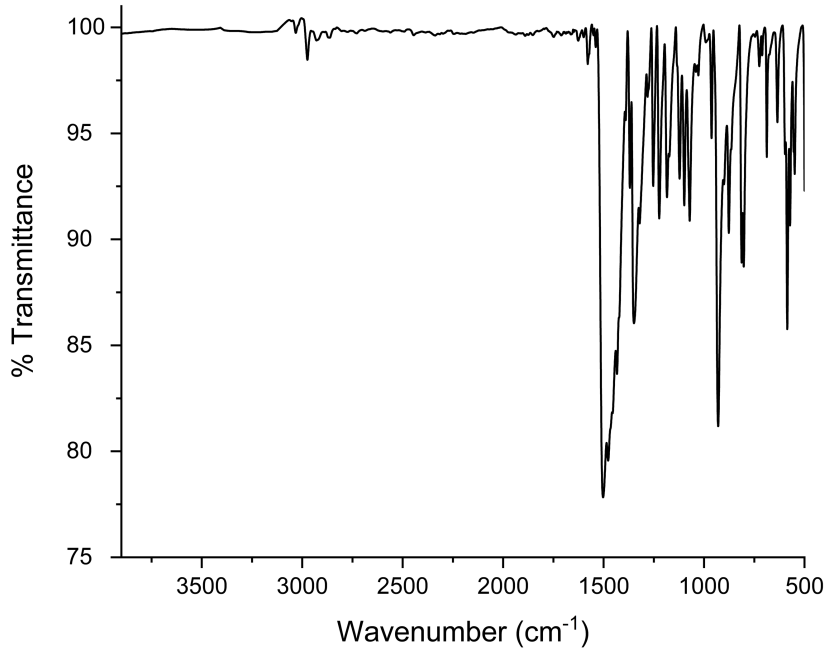

Figure A2.6 IR spectrum (KBr) of MoO(tdt)($^{i}Pr_2Dt^0$)

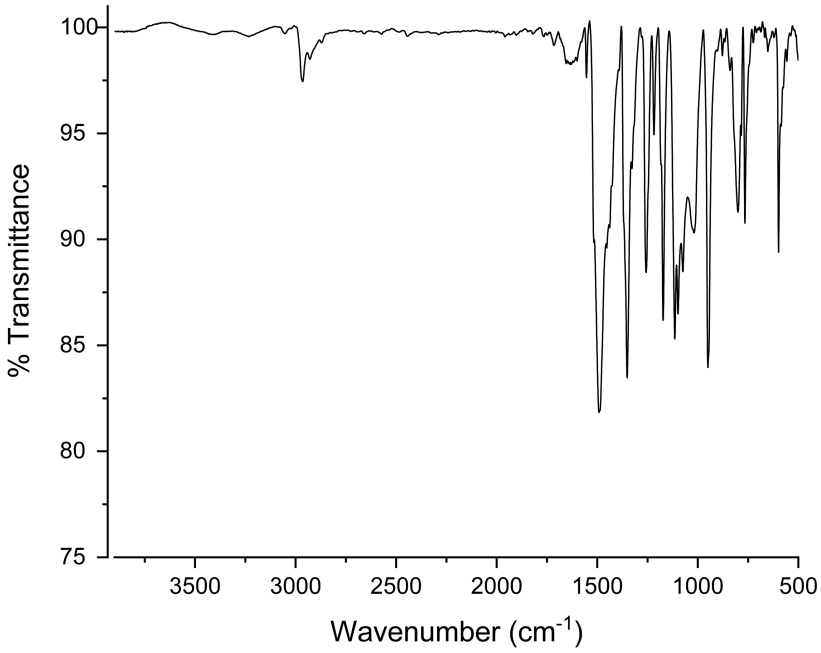

Figure A2.7 IR spectrum (KBr) of MoO(qdt)($^{i}Pr_2Dt^0$)

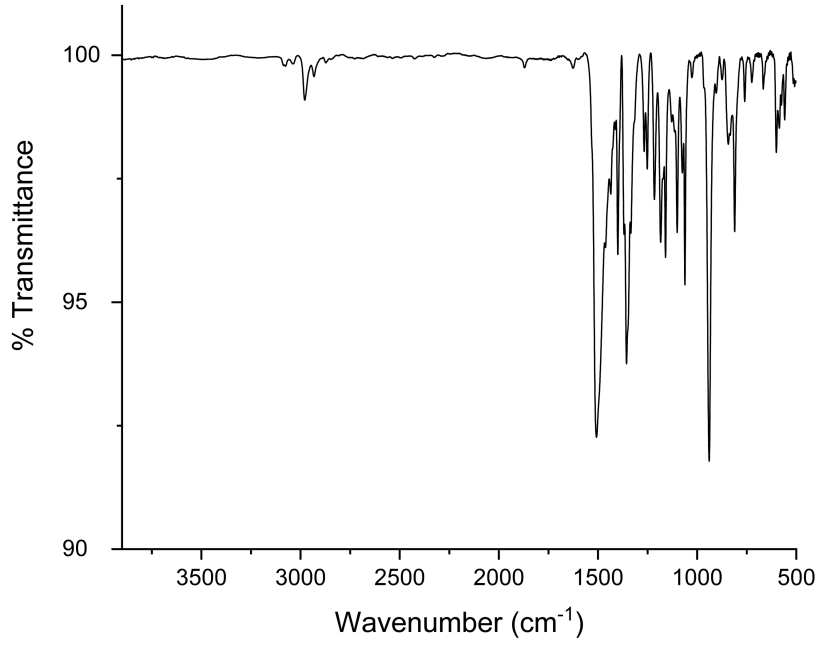

Figure A2.8 IR spectrum (KBr) of MoO($bdtCl_2$)($^{i}Pr_2Dt^0$)

A3. Electrochemistry

Cyclic voltammetry was recorded on a Metorhm PGSTAT204 galvanostat/potentiostat. A Pt disk working electrode, Ag^{+}/Ag reference electrode and Pt wire auxillary electrode and tetrabutylammonium hexafluorophosphate supporting electrolyte were used.

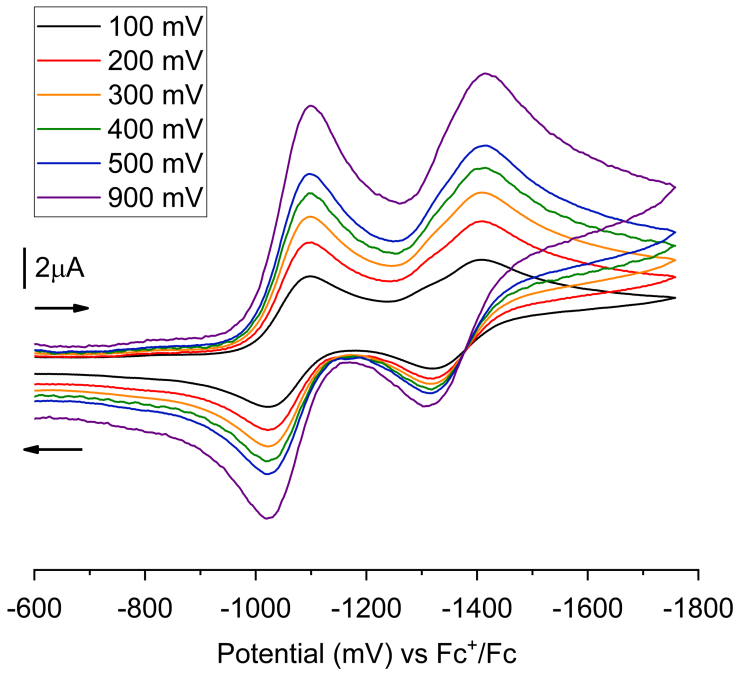

Figure A3.1 Cyclic voltammogram of MoO(bdt)(Me_2Dt^0). Scan rate, 100 mV s^{-1}; solvent, acetonitrile; temperature, 25oC; Pt-disk working electrode, Ag/Ag^{+} reference electrode, and a Pt-wire auxiliary electrode; supporting electrolyte, Bu_4NPF_6. Potentials referenced internally to Fc^{+}/Fc couple.

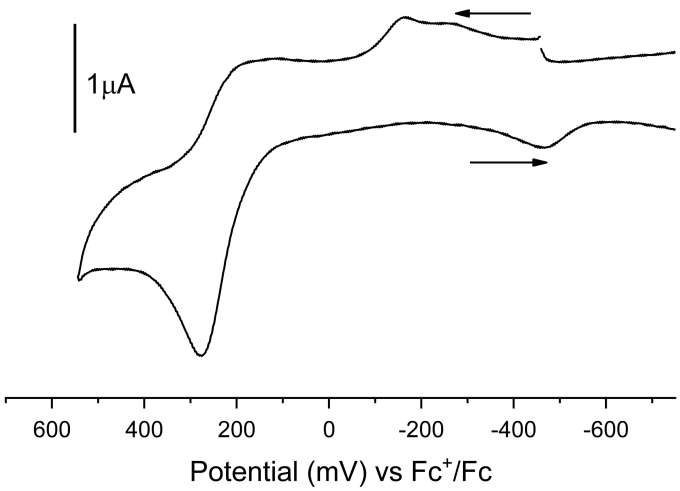

Figure A3.2 Cyclic voltammogram of MoO(bdt)(Me_2Dt^0). Scan rate, 100 mV s^{-1}; solvent, acetonitrile; temperature, 25 °C; Pt-disk working electrode, Ag/Ag+ reference electrode, and a Pt-wire auxiliary electrode; supporting electrolyte, Bu_4NPF_6. Potentials referenced internally to Fc+/Fc couple.

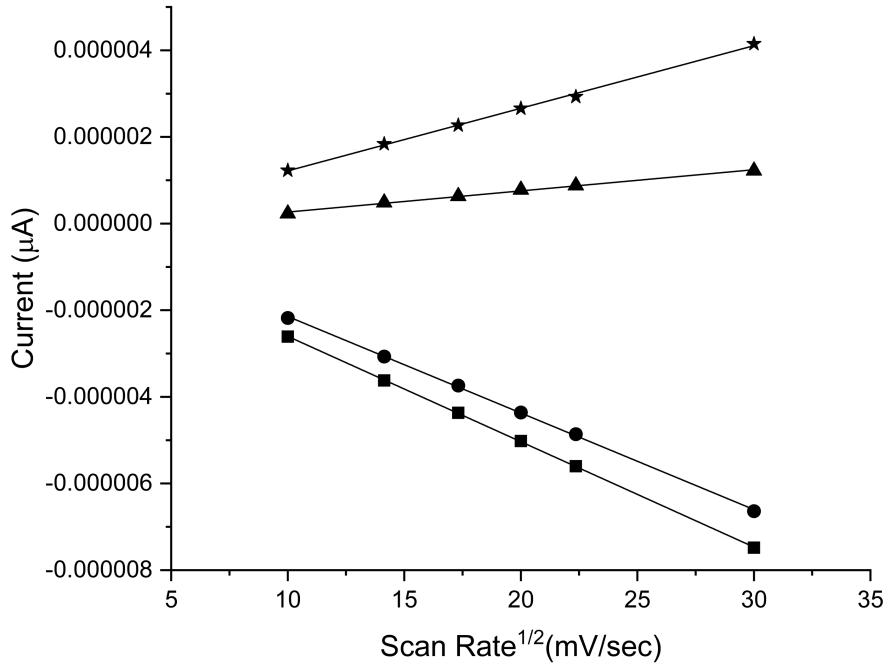

Figure A3.3 A plot showing the linearity of the peak current (i_p) versus the square root of the scan rate(v) for MoO(bdt)(Me_2Dt^0) suggesting diffusion-controlled processes. Fit of the equations are given below.

Oxidation

★ i_p= 1.45E-9(+/-2.88E-9)$n^{3/2}AD^{1/2}C^b$ -2.28E-7(+/-5.76E-8); r^2=0.99

▲ i_p= 4.88E-8 (+/-1.64E-9) $n^{3/2}AD^{1/2}C^b$ -2.22E-8 (+/- 1.57E-6); r^2=0.99

Reduction

● i_p= -2.22E-7 (+/- 2.43 E-7) $n^{3/2}AD^{1/2}C^b$ + 8.65E-8 (+/- 4.87E-8); r^2= 0.99

■ i_p= -2.430E-6 (+/- 9.03E-10) $n^{3/2}AD^{1/2}C^b$ – 1.69E-7 (+/- 1.89E-8); r^2= 0.99

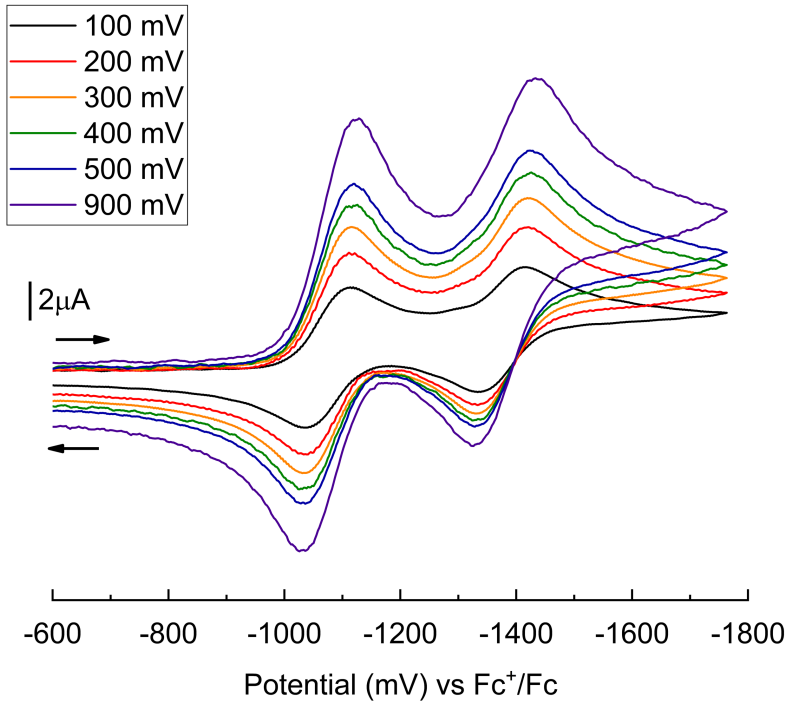

Figure A3.4 Cyclic voltammogram of MoO(tdt)(Me_2Dt^0). Scan rate, 100 mV $s^{-1;}$ solvent, acetonitrile; temperature, 25 ºC; Pt-disk working electrode, Ag/Ag^+ reference electrode, and a Pt-wire auxiliary electrode; supporting electrolyte, Bu_4NPF_6. Potentials referenced internally to Fc^+/Fc couple.

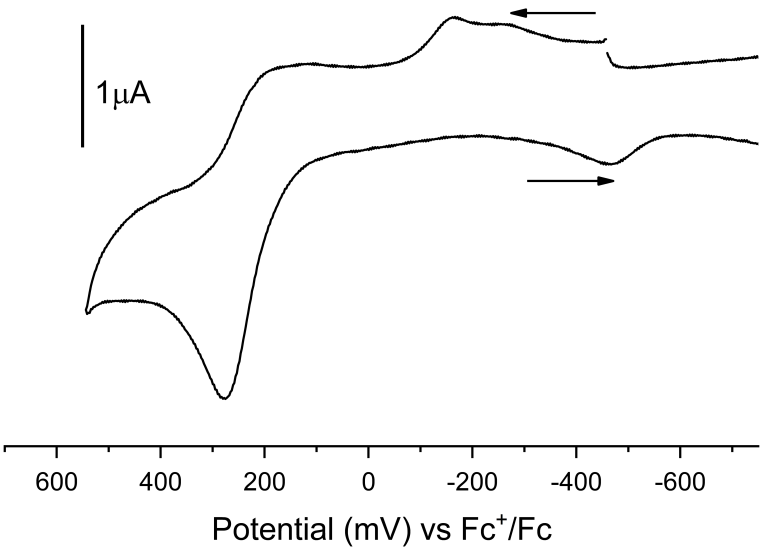

Figure A3.5 Cyclic voltammogram of MoO(tdt)(Me_2Dt^0). Scan rate, 100 mV s^{-1}; solvent, acetonitrile; temperature, 25 °C; Pt-disk working electrode, Ag/Ag^+ reference electrode, and a Pt-wire auxiliary electrode; supporting electrolyte, Bu_4NPF_6. Potentials referenced internally to Fc^+/Fc couple.

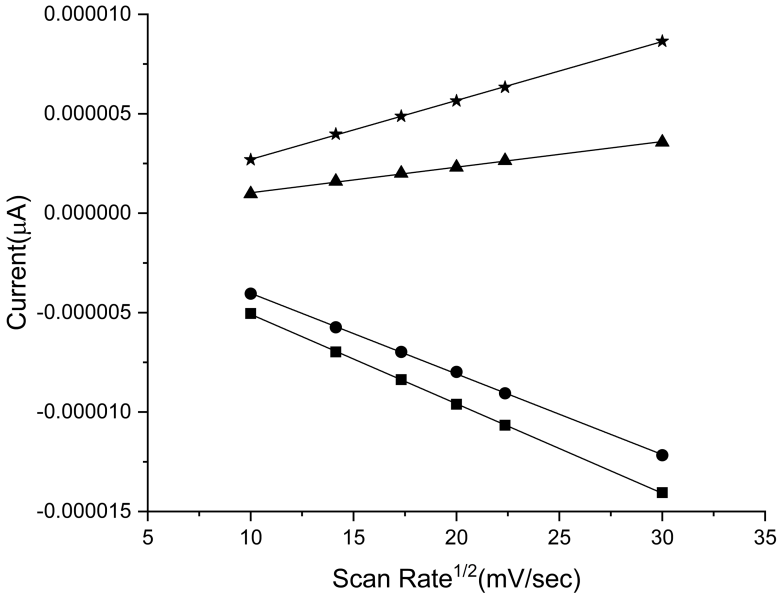

Figure A3.6 A plot showing the linearity of the peak current (i_p) versus the square root of the scan rate(v) for MoO(tdt)(Me_2Dt^0) suggesting diffusion-controlled processes. Fit of the equations are given below.

Oxidation

★ i_p= 2.96E-7(+/-1.97E-9)$n^{3/2}AD^{1/2}C^b$ -2.57E-7(+/-3.94E-8); r^2=0.99

▲ i_p= 1.28E-7 (+/-2.92E-9) $n^{3/2}AD^{1/2}C^b$ -2.58E-7 (+/- 5.85E-8); r^2=0.99

Reduction

● i_p= -4.06E-7 (+/- 3.70 E-9) $n^{3/2}AD^{1/2}C^b$ + 3.25E-8 (+/- 7.40E-8); r^2= 0.99

■ i_p= -4.50E-7 (+/- 1.98E-9) $n^{3/2}AD^{1/2}C^b$ – 5.82E-7 (+/- 3.95E-8); r^2= 0.99

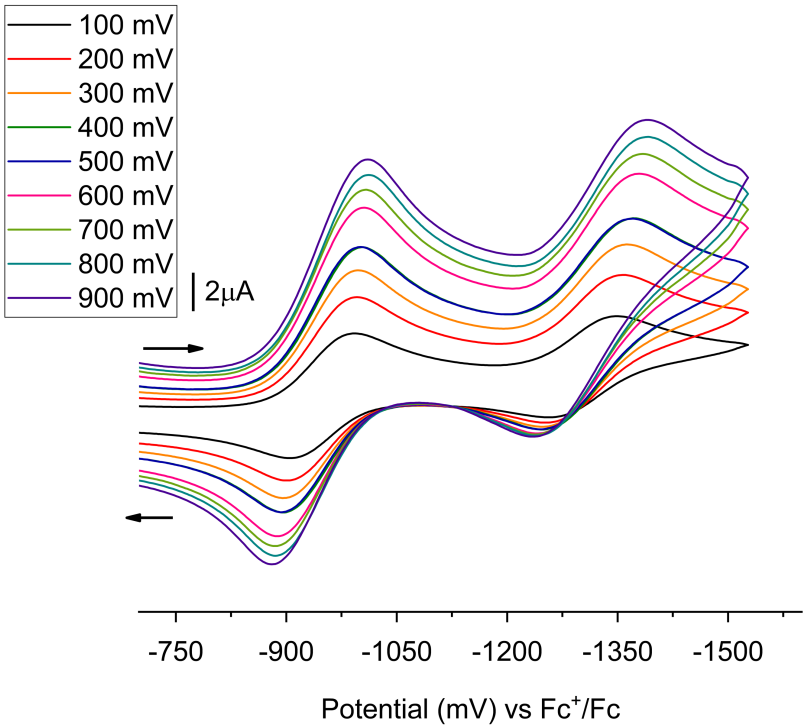

Figure A3.7 Cyclic voltammogram of MoO(qdt)(Me_2Dt^0). Scan rate, 100 mV s^{-1}; solvent, acetonitrile; temperature, 25 °C; Pt-disk working electrode, Ag/Ag^+ reference electrode, and a Pt-wire auxiliary electrode; supporting electrolyte, Bu_4NPF_6. Potentials referenced internally to Fc^+/Fc couple.

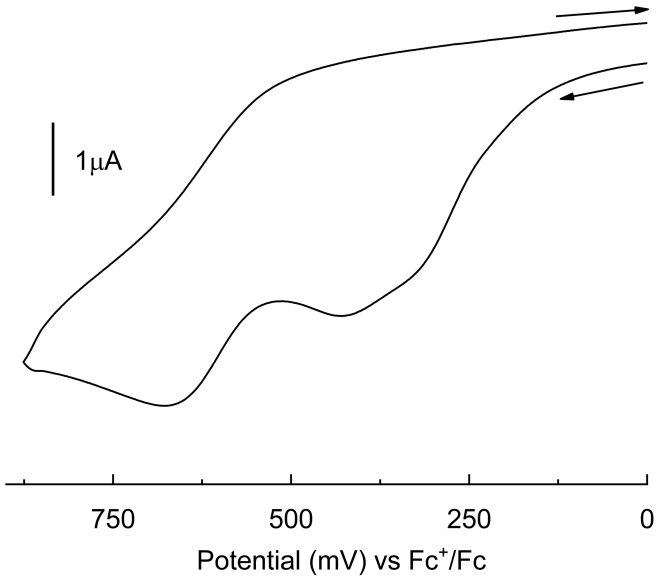

Figure A3.8 Cyclic voltammogram of MoO(qdt)(Me_2Dt^0). Scan rate, 100 mV s^{-1}; solvent, acetonitrile; temperature, 25 °C; Pt-disk working electrode, Ag/Ag^+ reference electrode, and a Pt-wire auxiliary electrode; supporting electrolyte, Bu_4NPF_6. Potentials referenced internally to Fc^+/Fc couple.

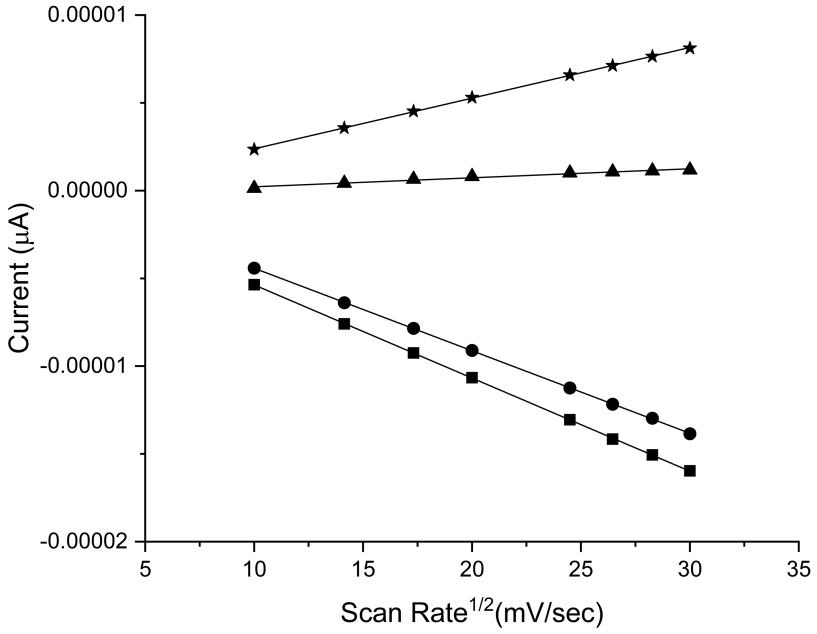

Figure A3.9 A plot showing the linearity of the peak current (i_p) versus the square root of the scan rate(v) for MoO(qdt)(Me_2Dt^0) suggesting diffusion-controlled processes. Fit of the equations are given below.
Oxidation

★ i_p= 2.88E-7(+/-1.59E-9)$n^{3/2}AD^{1/2}C^b$ -5.05E-7(+/-3.56E-8); r^2=0.99

▲ i_p= 5.13E-8 (+/-3.19E-9) $n^{3/2}AD^{1/2}C^b$ -2.98E-7 (+/- 7.15E-8); r^2=0.99

Reduction

● i_p= -4.70E-7 (+/- 1.44 E-9) $n^{3/2}AD^{1/2}C^b$ + 2.81E-7 (+/- 3.22E-8); r^2= 0.99

■ i_p= -5.30E-7 (+/- 1.53E-9) $n^{3/2}AD^{1/2}C^b$ – 6.48E-8 (+/- 3.42E-8); r^2= 0.99

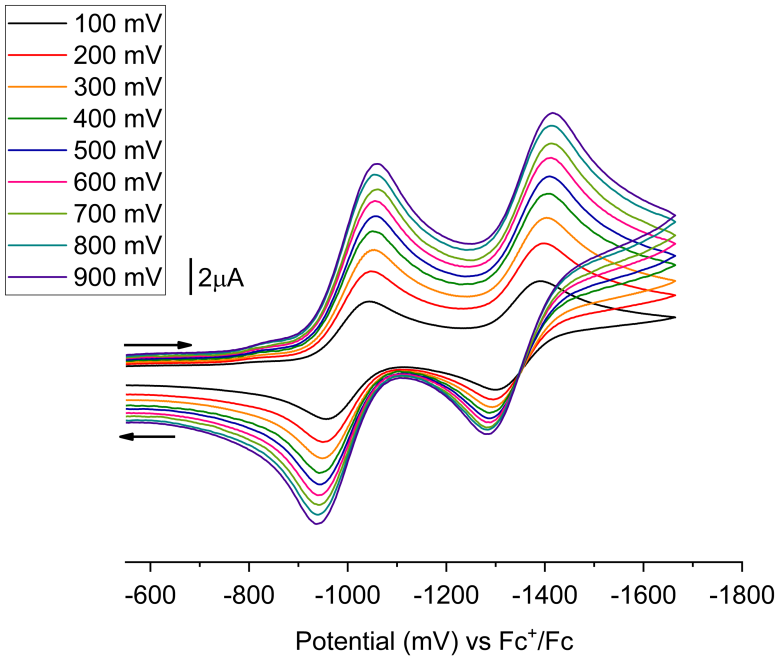

Figure A3.10 Cyclic voltammogram of $MoO(bdtCl_2)(Me_2Dt^0)$. Scan rate, 100 mV s^{-1}; solvent, acetonitrile; temperature, 25 °C; Pt-disk working electrode, Ag/Ag^+ reference electrode, and a Pt-wire auxiliary electrode; supporting electrolyte, Bu_4NPF_6. Potentials referenced internally to Fc^+/Fc couple.

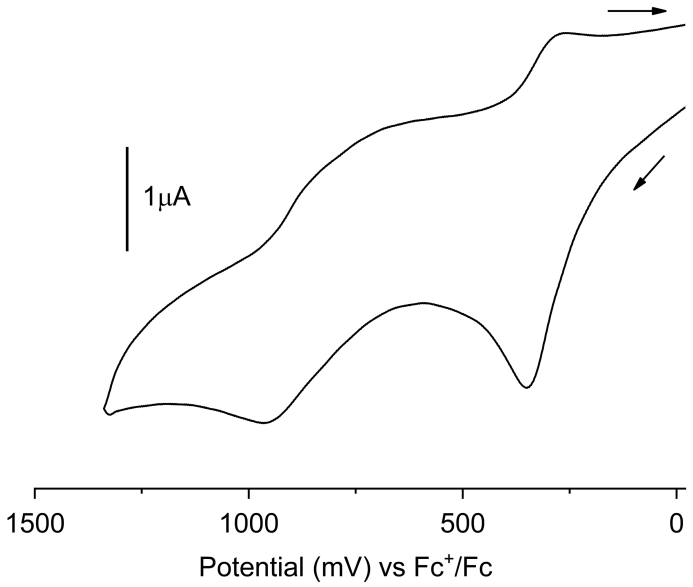

Figure A3.11 Cyclic voltammogram of $MoO(bdtCl_2)(Me_2Dt^0)$. Scan rate, 100 mV s^{-1}; solvent, acetonitrile; temperature, 25 °C; Pt-disk working electrode, Ag/Ag^+ reference electrode, and a Pt-wire auxiliary electrode; supporting electrolyte, Bu_4NPF_6. Potentials referenced internally to Fc^+/Fc couple.

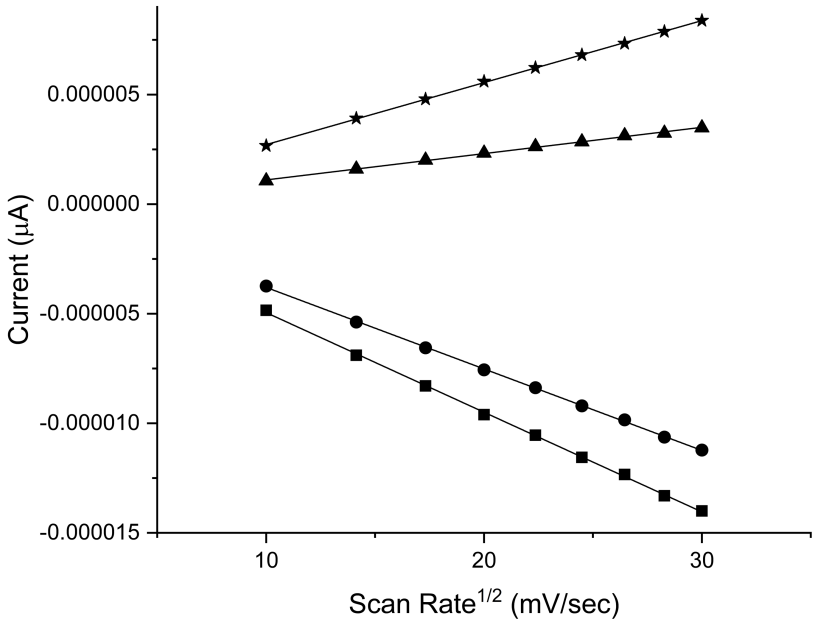

Figure A3.12 A plot showing the linearity of the peak current (i_p) versus the square root of the scan rate(v) for MoO($bdtCl_2$)(Me_2Dt^0) suggesting diffusion-controlled processes. Fit of the equations are given below.
Oxidation

★ i_p= 2.83E-7(+/-1.76E-9)$n^{3/2}AD^{1/2}C^b$ -1.12E-7(+/-3.95E-8); r^2=0.99

▲ i_p= 1.20E-7 (+/-2.04E-9) $n^{3/2}AD^{1/2}C^b$ -9.32E-8 (+/- 4.55E-8); r^2=0.99

Reduction

● i_p= -3.72E-7 (+/- 2.49E-9) $n^{3/2}AD^{1/2}C^b$ – 7.81E-8 (+/- 5.58E-8); r^2= 0.99

■ i_p= -4.54E-7 (+/- 4.01E-9) $n^{3/2}AD^{1/2}C^b$ – 3.99E-7(+/- 8.97E-8); r^2= 0.99

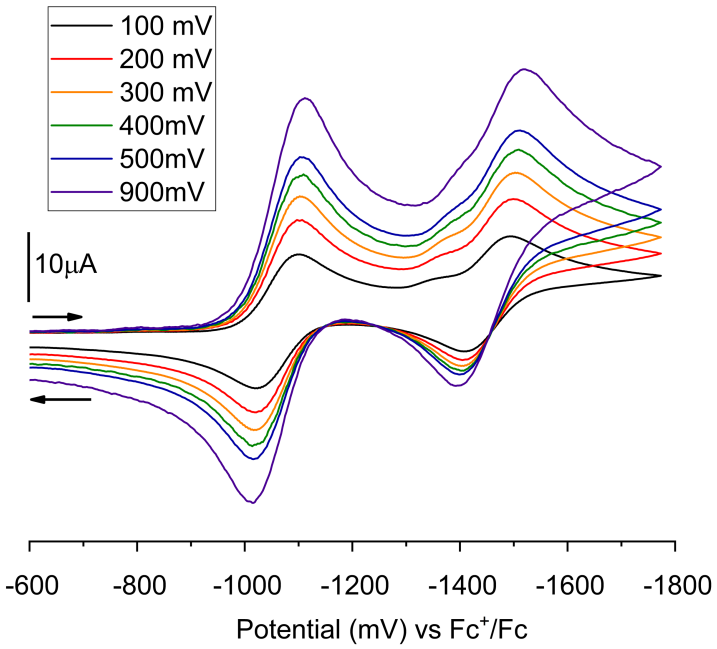

Figure A3.13 Cyclic voltammogram of MoO(bdt)($^{i}Pr_2Dt^0$). Scan rate, 100 mV s^{-1}; solvent, acetonitrile; temperature, 25 °C; Pt-disk working electrode, Ag/Ag^+ reference electrode, and a Pt-wire auxiliary electrode; supporting electrolyte, Bu_4NPF_6. Potentials referenced internally to Fc^+/Fc couple.

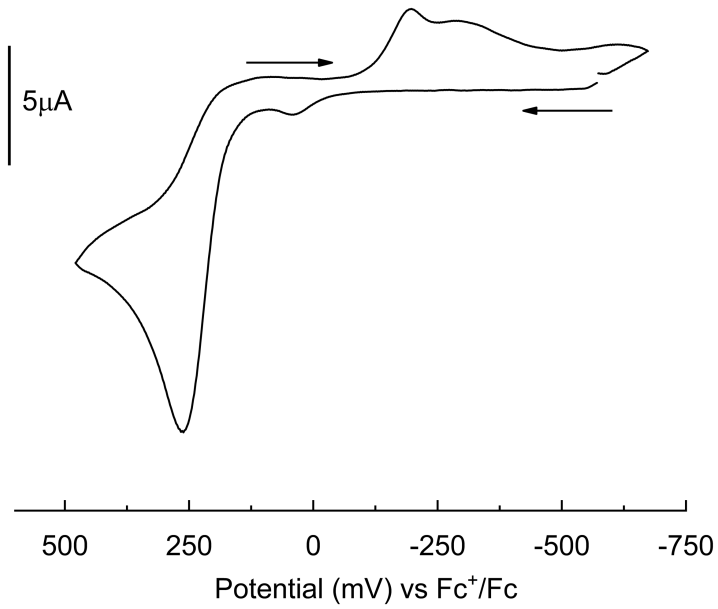

Figure A3.14 Cyclic voltammogram of MoO(bdt)($^{i}Pr_2Dt^0$). Scan rate, 100 mV s^{-1}; solvent, acetonitrile; temperature, 25 °C; Pt-disk working electrode, Ag/Ag^+ reference electrode, and a Pt-wire auxiliary electrode; supporting electrolyte, Bu_4NPF_6. Potentials referenced internally to Fc^+/Fc couple.

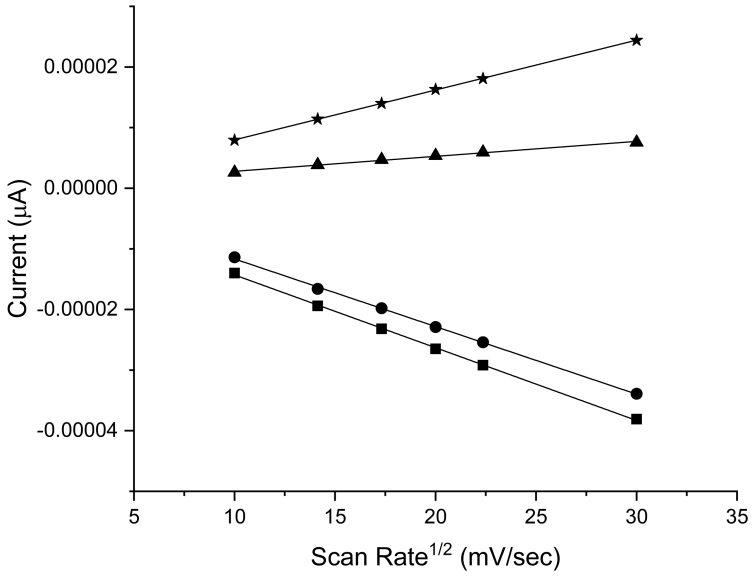

Figure A3.15 A plot showing the linearity of the peak current (i_p) versus the square root of the scan rate(v) for MoO(bdt)($^{i}Pr_2Dt^0$) suggesting diffusion-controlled processes. Fit of the equations are given below.

Oxidation

★ i_p= 8.22E-7(+/-3.90E-9)$n^{3/2}AD^{1/2}C^b$ -2.48E-7(+/-7.81E-8); r^2=0.99

▲ i_p= 2.47E-7 (+/-9.85-9) $n^{3/2}AD^{1/2}C^b$ +3.21E-7 (+/- 1.97E-7); r^2=0.99

Reduction

● i_p= -1.11E-6 (+/- 1.38 E-8) $n^{3/2}AD^{1/2}C^b$ – 5.06E-7 (+/- 2.77E-7); r^2= 0.99

■ i_p= -1.20E-6 (+/- 3.78E-8) $n^{3/2}AD^{1/2}C^b$ – 2.29E-6 (+/- 2.91E-7); r^2= 0.99

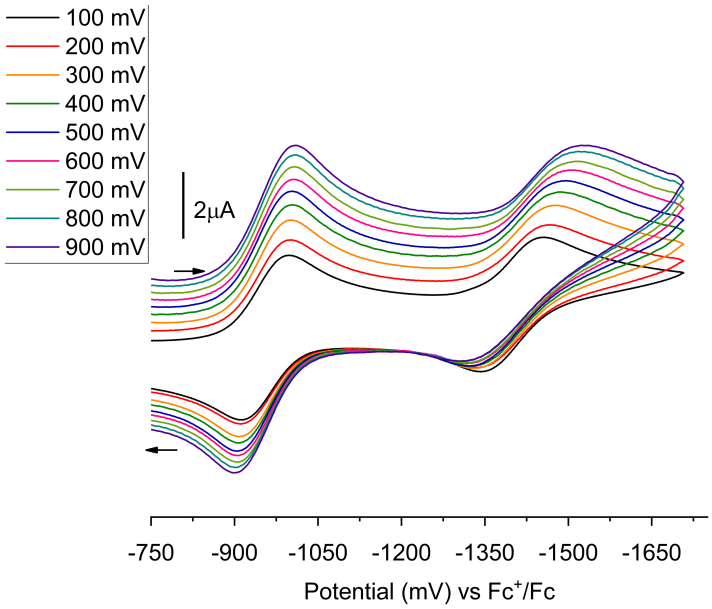

Figure A3.16 Cyclic voltammogram of MoO(qdt)(^{i}Pr$_2$Dt^0). Scan rate, 100 mV s^{-1}; solvent, acetonitrile; temperature, 25 ^{o}C; Pt disk working electrode, Ag/Ag$^+$ reference electrode, and a Pt-wire auxiliary electrode; supporting electrolyte, Bu$_4$NPF$_6$. Potentials referenced internally to Fc$^+$/Fc couple.

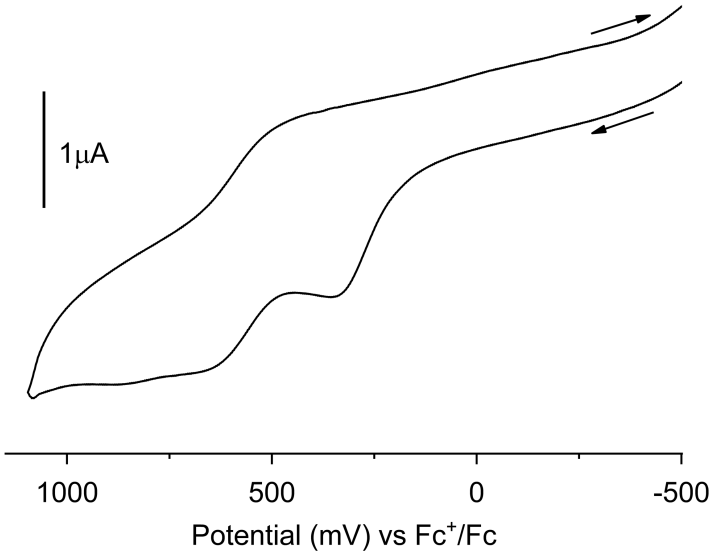

Figure A3.17 Cyclic voltammogram of MoO(qdt)($^{i}Pr_2Dt^0$). Scan rate, 100 mV s^{-1}; solvent, acetonitrile; temperature, 25 ºC; Pt-disk working electrode, Ag/Ag^+ reference electrode, and a Pt-wire auxiliary electrode; supporting electrolyte, Bu_4NPF_6. Potentials referenced internally to Fc^+/Fc couple.

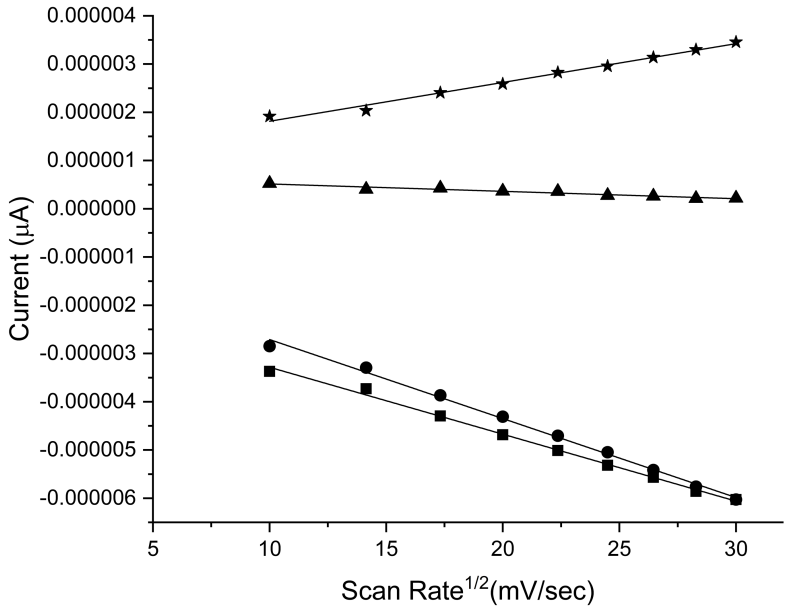

Figure A3.18 A plot showing the linearity of the peak current (i_p) versus the square root of the scan rate(v) for MoO(qdt)($^{i}Pr_2Dt^0$) suggesting diffusion-controlled processes. Fit of the equations are given below.

Oxidation

★ i_p= 8.04E-8(+/-3.20E-9)$n^{3/2}AD^{1/2}C^b$ +1.01E-6(+/-7.15E-8); r^2=0.99

▲ i_p= -1.52E-8 (+/-1.39E-9) $n^{3/2}AD^{1/2}C^b$ +6.67E-7 (+/- 3.12E-8); r^2=0.94

Reduction

● i_p= -1.63E-7 (+/- 3.89 E-9) $n^{3/2}AD^{1/2}C^b$ – 1.07E-6 (+/- 8.72E-8); r^2= 0.99

■ i_p= -1.38E-7 (+/- 3.32E-9) $n^{3/2}AD^{1/2}C^b$ – 1.89E-6 (+/- 7.42E-8); r^2= 0.99

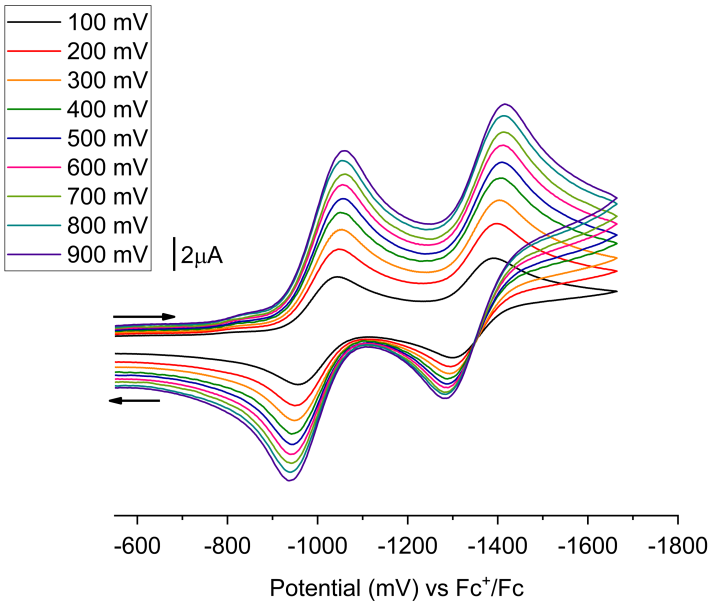

Figure A3.19 Cyclic voltammogram of $MoO(bdtCl_2)(^{i}Pr_2Dt^0)$. Scan rate, 100 mV s^{-1}; solvent, acetonitrile; temperature, 25 °C; Pt-disk working electrode, Ag/Ag^+ reference electrode, and a Pt-wire auxiliary electrode; supporting electrolyte, Bu_4NPF_6. Potentials referenced internally to Fc^+/Fc couple.

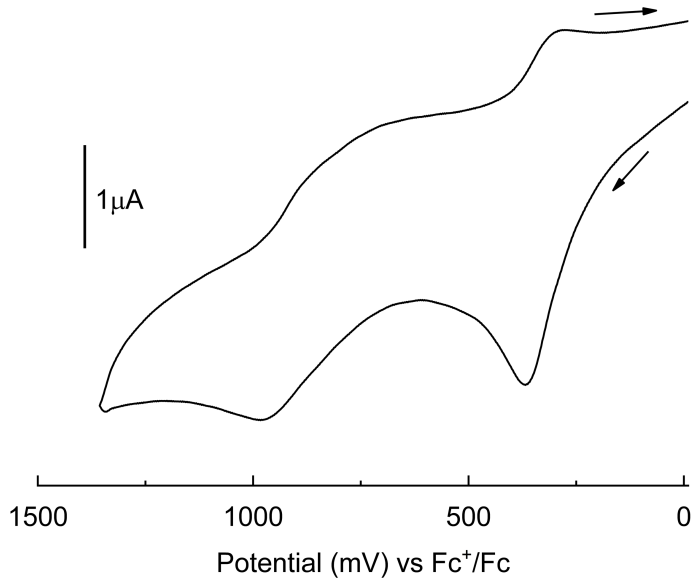

Figure A3.20 Cyclic voltammogram of $MoO(bdtCl_2)(^{i}Pr_2Dt^{0})$. Scan rate, 100 mV s^{-1}; solvent, acetonitrile; temperature, 25 °C; Pt-disk working electrode, Ag/Ag^{+} reference electrode, and a Pt-wire auxiliary electrode; supporting electrolyte, Bu_4NPF_6. Potentials referenced internally to Fc^{+}/Fc couple.

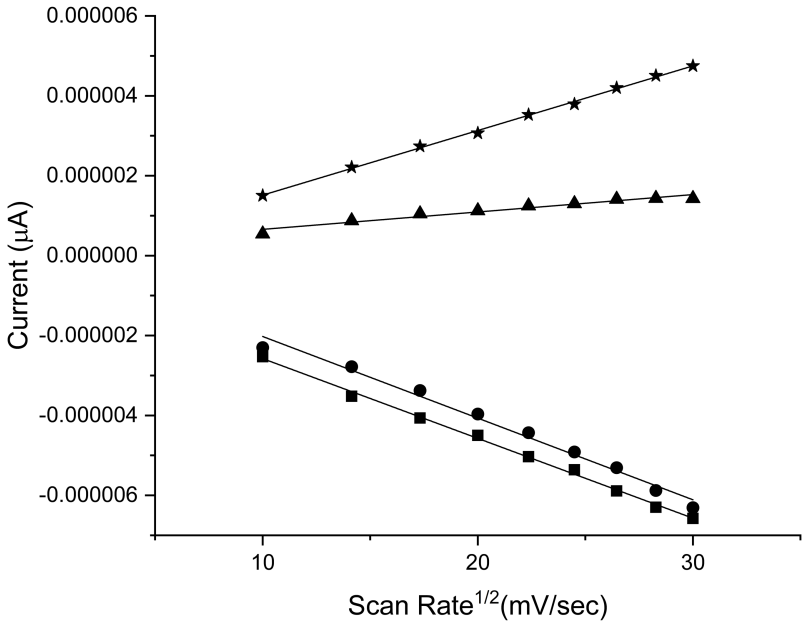

Figure A3.21 A plot showing the linearity of the peak current (i_p) versus the square root of the scan rate(v) for MoO(bdtCl$_2$)(^{i}Pr$_2$Dt^0) suggesting diffusion-controlled processes. Fit of the equations are given below.

Oxidation

★ i_p= 1.61E-7 (+/-2.25E-9)$n^{3/2}AD^{1/2}C^b$ -1.03E-7(+/-5.03E-8); r^2=0.99

▲ i_p= 4.53E-8 (+/-3.79E-9) $n^{3/2}AD^{1/2}C^b$ +2.22E-7 (+/- 8.27E-8); r^2=0.97

Reduction

● i_p= -2.04E-7 (+/- 8.83 E-9) $n^{3/2}AD^{1/2}C^b$ + 2.13E-8 (+/- 1.97E-7); r^2= 0.98

■ i_p= -1.99E-7 (+/- 4.03E-9) $n^{3/2}AD^{1/2}C^b$ – 5.78E-7 (+/-9.01E-8); r^2= 0.99

A4. Electronic Structure/Calculations

All computational work was performed using *Gaussian 09* software package running on UNIX OS and visualized utilizing *GaussView 5.0.9*. Calculations were done using the Lee-Yang-Parr nonlocal correlation functional[136] (B3LYP) and a combination of the LANL2DZ[137] effective core potential basis set for molybdenum and the 6-31G** basis set for all other atoms. Atomic composition for molecular orbitals was determined using C-squared population analysis from single-point calculations with the program *QM-Forge*. The lowest 60 transition energies were generated using non-equilibrium TDDFT calculations with the polarizable continuum model (PCM) algorithm. PCM-TDDFT calculations were performed using acetonitrile as the solvent to match experimental conditions. Electron density difference maps (EDDMs) were generated using the *cubman* package in *Gaussian09*.

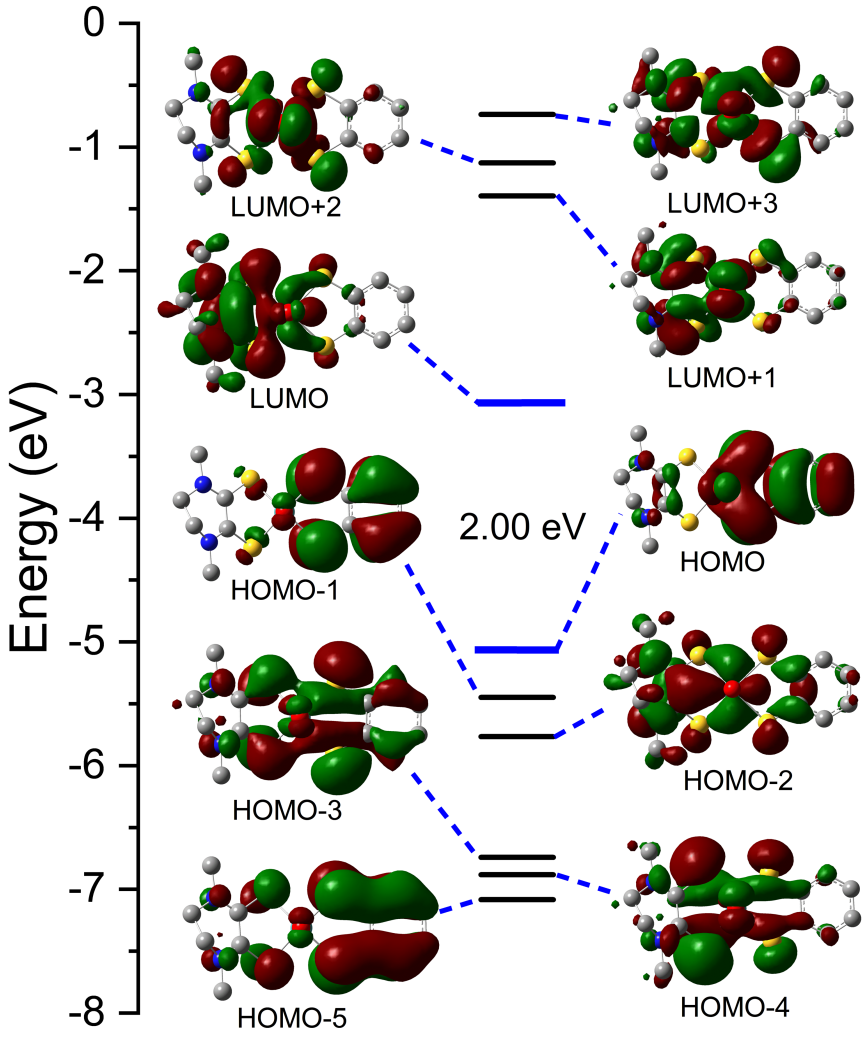

Figure A4.1 Molecular orbital diagrams for **1**. The energy gap between frontier orbitals (blue) is listed for each complex. Energies presented are relative.

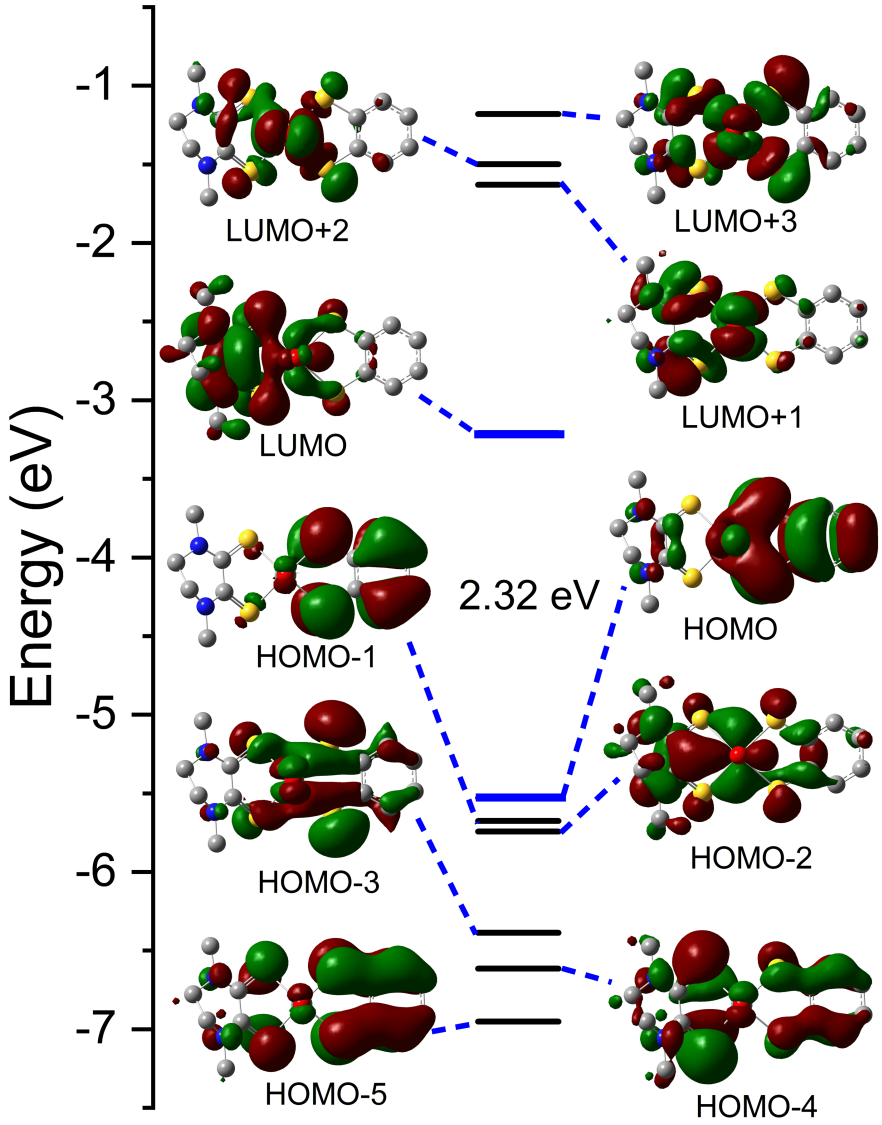

Figure A4.2 Molecular orbital diagrams for **3**. The energy gap between frontier orbitals (blue) is listed for each complex. Energies presented are relative.

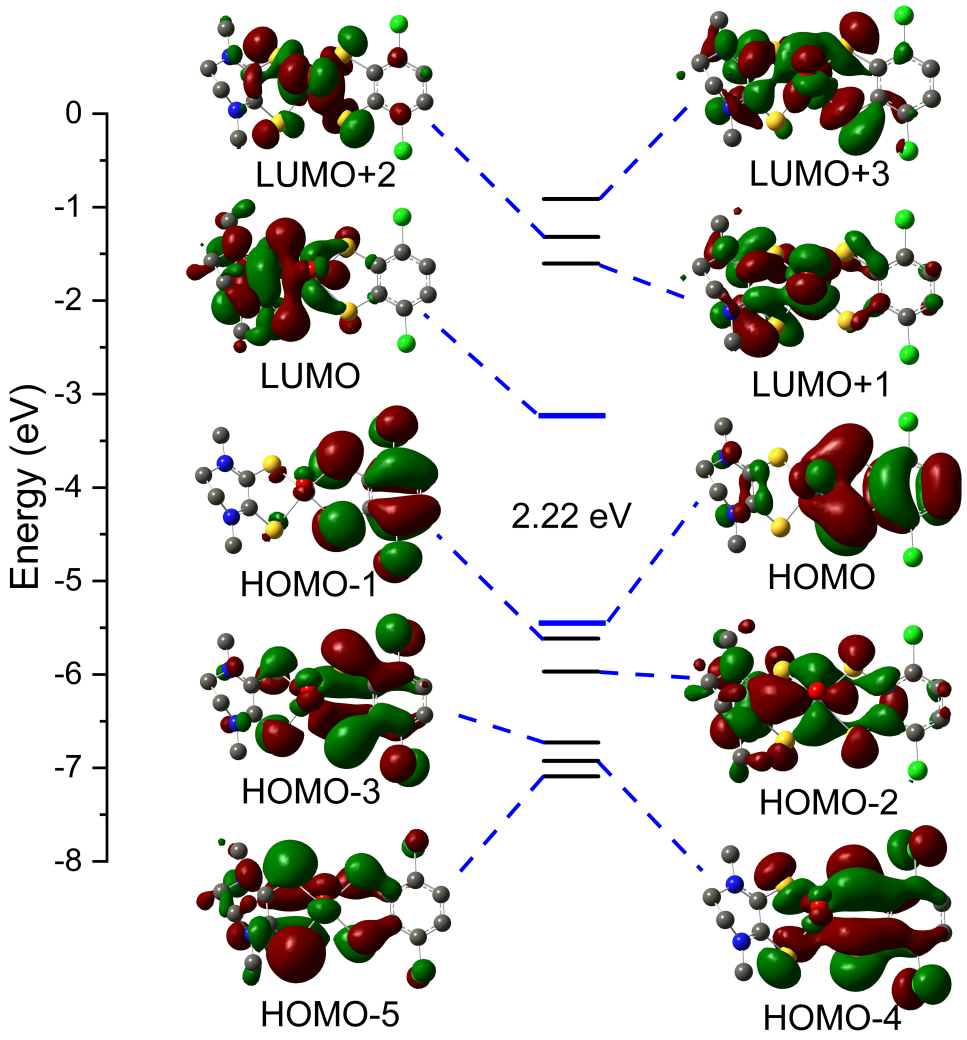

Figure A4.3 Molecular orbital diagrams for **4**. The energy gap between frontier orbitals (blue) is listed for each complex. Energies presented are relative.

Table A4.1 Population analysis for **1** and **5.**

MoO(bdt)(Me_2Dt^0) (**1**)							MoO(bdt)($^iPr_2Dt^0$) (**5**)						
Orbital	eV	Mo	Mo (d)	O	bdt	Me_2Dt^0	Orbital	eV	Mo	Mo (d)	O	bdt	$^iPr_2Dt^0$
-5	-7.084	0.77	0.31	2.01	79.47	17.75	-5	-7.02	1.64	0.91	0.42	83.41	14.53
-4	-6.881	4.71	2.02	6.97	16.73	71.59	-4	-6.766	9.7	5.24	9.02	40.52	40.76
-3	-6.74	9.76	7.28	1.62	62.41	26.21	-3	-6.613	4.08	3.43	0.03	31.08	64.82
-2	-5.764	47.89	45.15	0.05	14.94	37.13	-2	-5.666	47.09	44.12	0.09	13.68	39.14
-1	-5.449	1.29	0.89	1.9	87.44	9.37	-1	-5.385	1.18	0.89	2	87.84	8.98
HOMO	**-5.062**	**7.4**	**4.32**	**6.32**	**79.71**	**6.57**	**HOMO**	**-5.013**	**7.67**	**4.28**	**5.95**	**81.59**	**4.78**
LUMO	**-3.061**	**26.22**	**25.82**	**0.9**	**4.66**	**68.22**	**LUMO**	**-2.83**	**25.75**	**25.3**	**1.74**	**3.02**	**69.49**
1	-1.395	45.75	37.26	9.84	7.24	37.17	1	-1.436	42.64	35.53	9.78	9.32	38.25
2	-1.128	49.03	39.88	10.54	18.57	21.85	2	-1.081	48.54	39.84	10.21	17.76	23.49
3	-0.736	35.88	32.25	3.94	32.34	27.84	3	-0.718	39.62	31.79	6.62	27.33	26.43

Table A4.2 Population analysis for **3** and **7**.

MoO(qdt)(Me_2Dt^0) (**3**)							MoO(qdt)($^iPr_2Dt^0$) (**7**)						
Orbital	eV	Mo	Mo(d)	O	qdt	Me_2Dt^0	Orbital	eV	Mo	Mo(d)	O	qdt	$^iPr_2Dt^0$
-5	-6.952	13.16	8.98	1.69	69.41	15.75	-5	-6.873	2.44	2.13	1.72	22.17	73.67
-4	-6.615	2.49	1.64	1.76	85.26	10.49	-4	-6.533	2.91	2.03	1.51	81.08	14.51
-3	-6.386	22.15	20.97	0.06	58.28	19.51	-3	-6.288	19.03	17.78	0.04	61.15	19.78
-2	-5.743	27.64	24.99	0.1	51.03	21.23	-2	-5.644	29.83	27.04	0.19	46.85	23.14
-1	-5.675	1.29	0.9	1.55	89.74	7.43	-1	-5.616	2.87	2.4	1.5	87.36	8.27
HOMO	**-5.528**	**7.16**	**5**	**5.24**	**80.6**	**7**	**HOMO**	**-5.477**	**6.87**	**4.62**	**5.07**	**82.46**	**5.6**
LUMO	**-3.208**	**26.6**	**26.29**	**1.34**	**3.64**	**68.43**	**LUMO**	**-2.997**	**25.3**	**24.91**	**1.79**	**2.78**	**70.13**
1	-1.629	45.95	37.9	10.29	7.92	35.85	1	-1.628	42.6	35.81	9.89	9.6	37.91
2	-1.499	40.35	30.84	8.24	32.18	19.23	2	-1.431	39.11	29.39	7.74	33.67	19.47
3	-1.179	32.5	27.8	9.11	43.08	15.3	3	-1.144	34.81	30.02	9.99	36.14	19.06

Table A4.3 Population analysis for **4** and **8**

MoO(bdtCl$_2$)(Me$_2$Dt^0) (**4**)							MoO(bdtCl$_2$)(^{i}Pr$_2$Dt^0) (**8**)						
Orbital	eV	Mo	Mo (d)	O	bdtCl$_2$	Me$_2$Dt^0	Orbital	eV	Mo	Mo (d)	O	bdtCl$_2$	^{i}Pr$_2$Dt^0
-5	-7.09	1.74	0.55	6.05	12.77	79.44	-5	-6.889	1.17	0.69	3.5	42.08	53.24
-4	-6.924	5.64	3.64	1.13	73.03	20.19	-4	-6.845	6.83	4.09	3.74	49.53	39.9
-3	-6.727	7.33	5.39	2.63	77.3	12.74	-3	-6.586	6.48	4.83	1.65	69.49	22.38
-2	-5.969	48.04	45.12	0.05	16.46	35.45	-2	-5.829	46.8	43.71	0.1	14.98	38.12
-1	-5.616	0.81	0.51	1.27	92.24	5.69	-1	-5.584	0.8	0.52	1.37	92.13	5.71
HOMO	**-5.446**	**7.4**	**4.51**	**6.35**	**79.45**	**6.8**	**HOMO**	**-5.391**	**7.4**	**4.47**	**6.12**	**80.8**	**5.69**
LUMO	**-3.231**	**25.29**	**24.87**	**1.07**	**4.23**	**69.41**	**LUMO**	**-2.977**	**24.84**	**24.33**	**1.91**	**3**	**70.25**
1	-1.604	45.45	37.04	9.85	7.45	37.24	1	-1.612	41.26	34.17	9.51	8.97	40.26
2	-1.318	48.76	39.71	10.48	18.8	21.95	2	-1.244	48.32	39.58	10.18	18.39	23.11
3	-0.913	36.44	32.14	4.6	32.46	26.49	3	-0.9	38.82	29.89	7.72	24.74	28.71

Table A4. 4 Difference in orbital population between **1** and **5**.

Orbital	eV	Mo	Mo(d)	O	Dt^{2-}	Dt^{0}
-5	0.064	0.87	0.6	-1.59	3.94	-3.22
-4	0.115	4.99	3.22	2.05	23.79	-30.83
-3	0.127	-5.68	-3.85	-1.59	-31.33	38.61
-2	0.098	-0.8	-1.03	0.04	-1.26	2.01
-1	0.064	-0.11	0	0.1	0.4	-0.39
HOMO	**0.049**	**0.27**	**-0.04**	**-0.37**	**1.88**	**-1.79**
LUMO	**0.231**	**-0.47**	**-0.52**	**0.84**	**-1.64**	**1.27**
1	-0.041	-3.11	-1.73	-0.06	2.08	1.08
2	0.047	-0.49	-0.04	-0.33	-0.81	1.64
3	0.018	3.74	-0.46	2.68	-5.01	-1.41

Table A4. 5 Difference in orbital population between **2** and **6**.

Orbital	eV	Mo	Mo(d)	O	Dt^{2-}	Dt^{0}
-5	0.063	0.52	0.56	-2.42	7.62	-5.71
-4	0.108	4.66	2.97	2.57	19.47	-26.7
-3	0.125	-5.55	-3.73	-1.75	-29.3	36.6
-2	0.086	-0.85	-1.08	0.04	-1.26	2.07
-1	0.059	-0.09	0	0.14	0.38	-0.44
HOMO	**0.051**	**0.29**	**-0.02**	**-0.39**	**1.94**	**-1.83**
LUMO	**0.229**	**-0.33**	**-0.36**	**0.88**	**-1.85**	**1.3**
1	-0.053	-3.17	-1.8	-0.09	2.05	1.22
2	0.043	-0.55	-0.09	-0.36	-0.7	1.61
3	0.019	3.96	-0.26	2.67	-4.84	-1.79

Table A4. 6 Difference in orbital population between **3** and **7**.

Orbital	eV	Mo	Mo(d)	O	Dt^{2-}	Dt^{0}
-5	0.079	-10.72	-6.85	0.03	-47.24	57.92
-4	0.082	0.42	0.39	-0.25	-4.18	4.02
-3	0.098	-3.12	-3.19	-0.02	2.87	0.27
-2	0.099	2.19	2.05	0.09	-4.18	1.91
-1	0.059	1.58	1.5	-0.05	-2.38	0.84
HOMO	**0.051**	**-0.29**	**-0.38**	**-0.17**	**1.86**	**-1.4**
LUMO	**0.211**	**-1.3**	**-1.38**	**0.45**	**-0.86**	**1.7**
1	0.001	-3.35	-2.09	-0.4	1.68	2.06
2	0.068	-1.24	-1.45	-0.5	1.49	0.24
3	0.035	2.31	2.22	0.88	-6.94	3.76

Table A4. 7 Difference in orbital population between **4** and **8**.

Orbital	eV	Mo	Mo(d)	O	Dt^{2-}	Dt^{0}
-5	0.201	-0.57	0.14	-2.55	29.31	-26.2
-4	0.079	1.19	0.45	2.61	-23.5	19.71
-3	0.141	-0.85	-0.56	-0.98	-7.81	9.64
-2	0.14	-1.24	-1.41	0.05	-1.48	2.67
-1	0.032	-0.01	0.01	0.1	-0.11	0.02
HOMO	**0.055**	**0**	**-0.04**	**-0.23**	**1.35**	**-1.11**
LUMO	**0.254**	**-0.45**	**-0.54**	**0.84**	**-1.23**	**0.84**
1	-0.008	-4.19	-2.87	-0.34	1.52	3.02
2	0.074	-0.44	-0.13	-0.3	-0.41	1.16
3	0.013	2.38	-2.25	3.12	-7.72	2.22

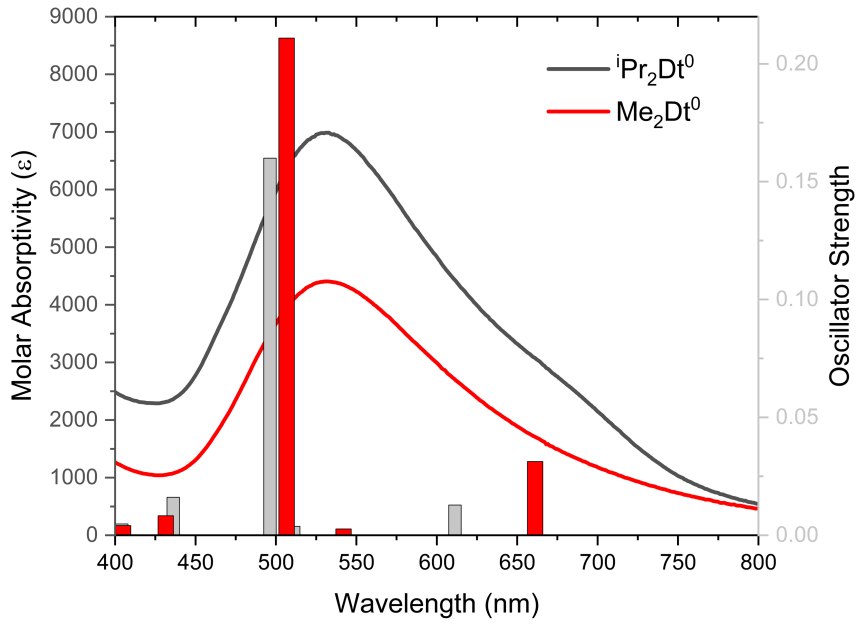

Figure A4.4 Electronic spectra (lines) with calculated excited state transitions superimposed (bars) for **1** (red line and bar) and **5** (black line/gray bar).

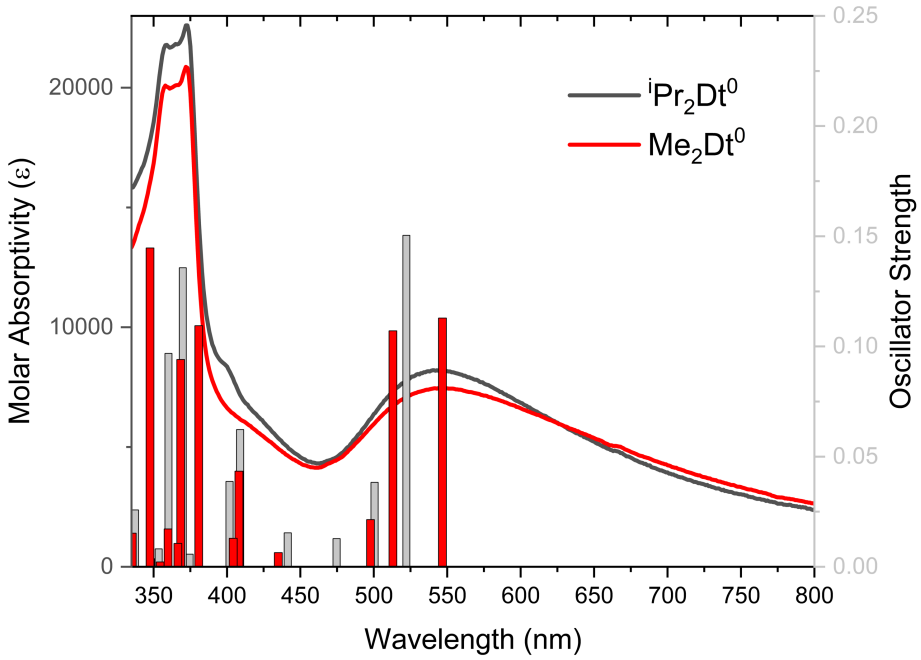

Figure A4.5 Electronic spectra (lines) with calculated excited state transitions superimposed (bars) for **3** (red line and bar) and **7** (black line/gray bar).

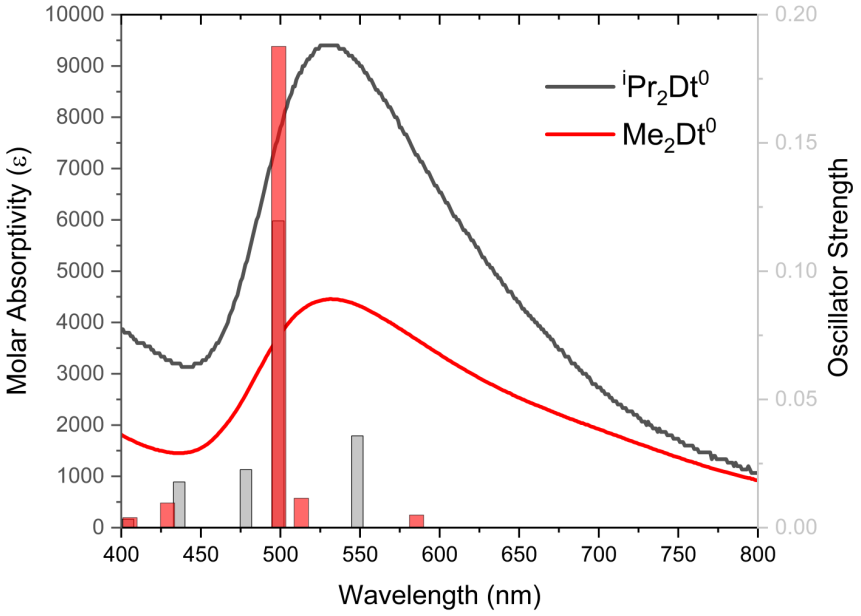

Figure A4.6. Electronic spectra (lines) with calculated excited state transitions superimposed (bars) for **4** (red line and bar) and **8** (black line/gray bar).

A5. Solvatochromic Effect

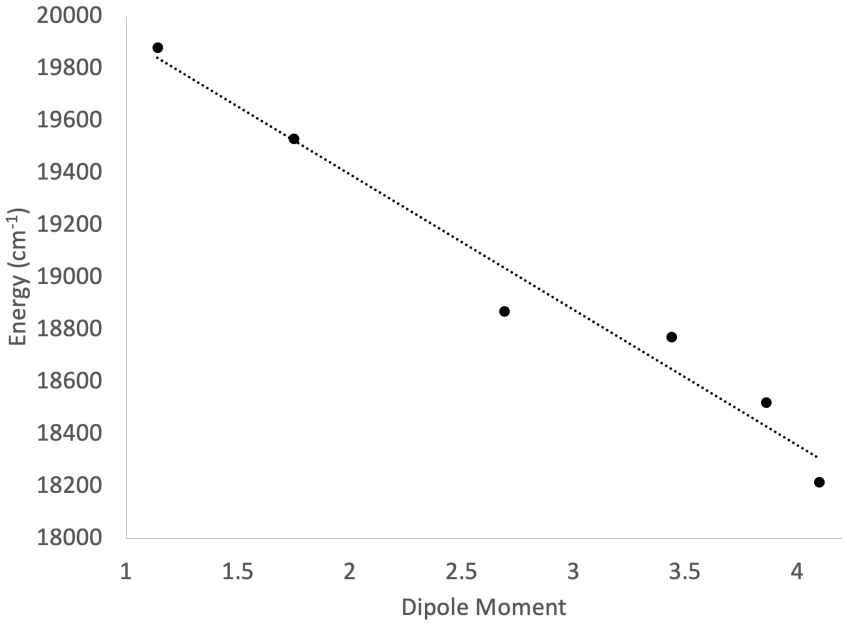

Figure A5.1 Linear correlation between dipole moment (μ) and the energy of the LL'CT of MoO(bdt)(Me_2Dt^0). Equation of fit: E = -518.86μ + 20432

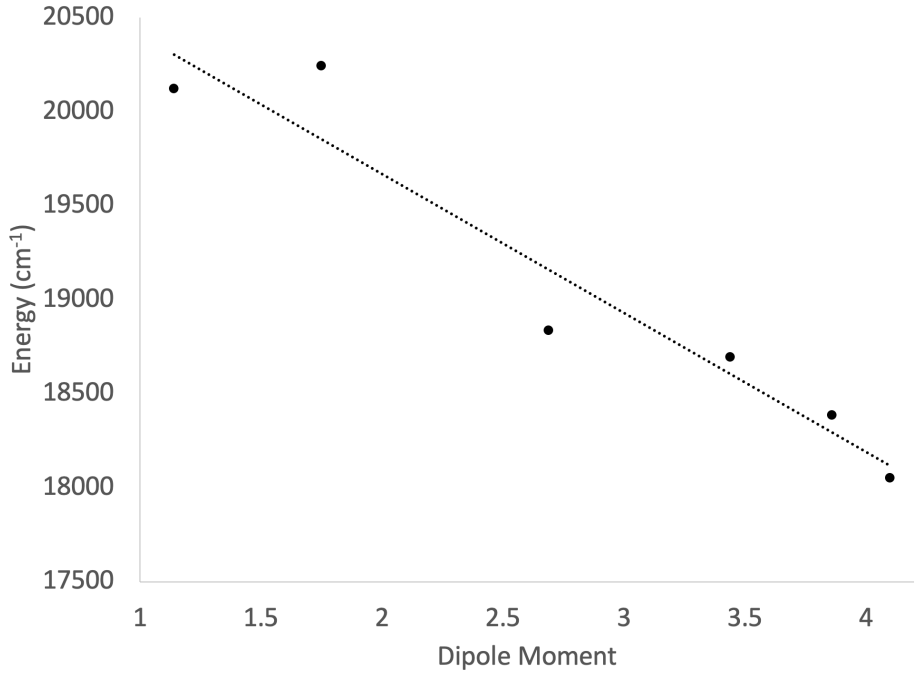

Figure A5.2 Linear correlation between dipole moment (μ) and the energy of the LL'CT of MoO(tdt)(Me_2Dt^0). Equation of fit: E = -739.58 μ + 21146

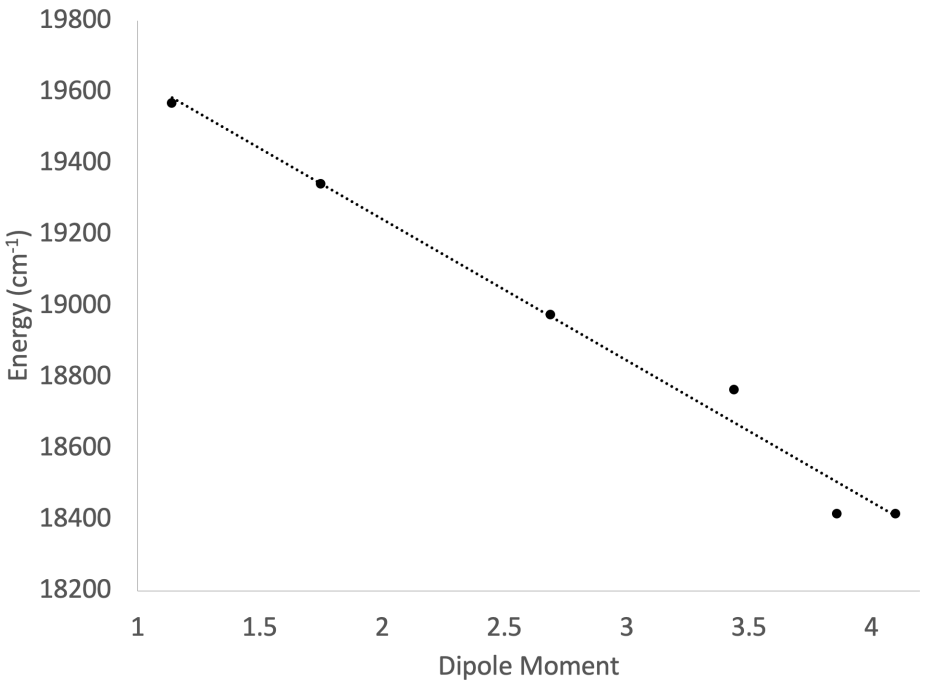

Figure A5.3 Linear correlation between dipole moment (μ) and the energy of the LL'CT of $MoO(bdtCl_2)(Me_2Dt^0)$. Equation of fit: E = -397.27 μ + 20038

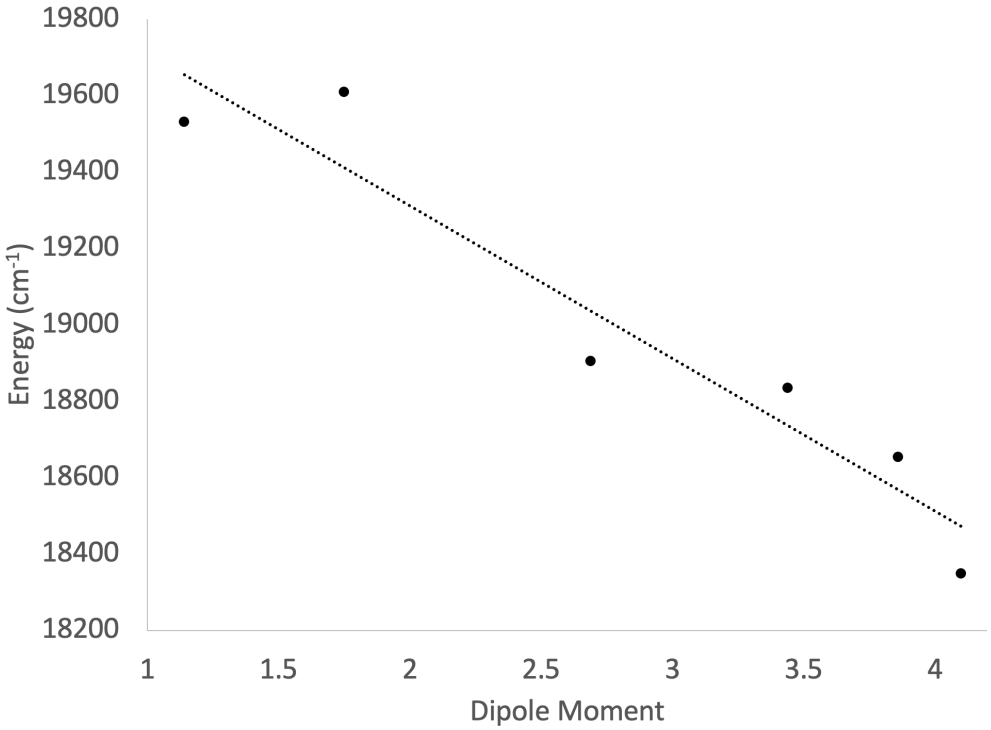

Figure A5.4 Linear correlation between dipole moment (μ) and the energy of the LL'CT of MoO(bdt)($^{i}Pr_2Dt^0$). Equation of fit: E = -399.03 μ + 20108

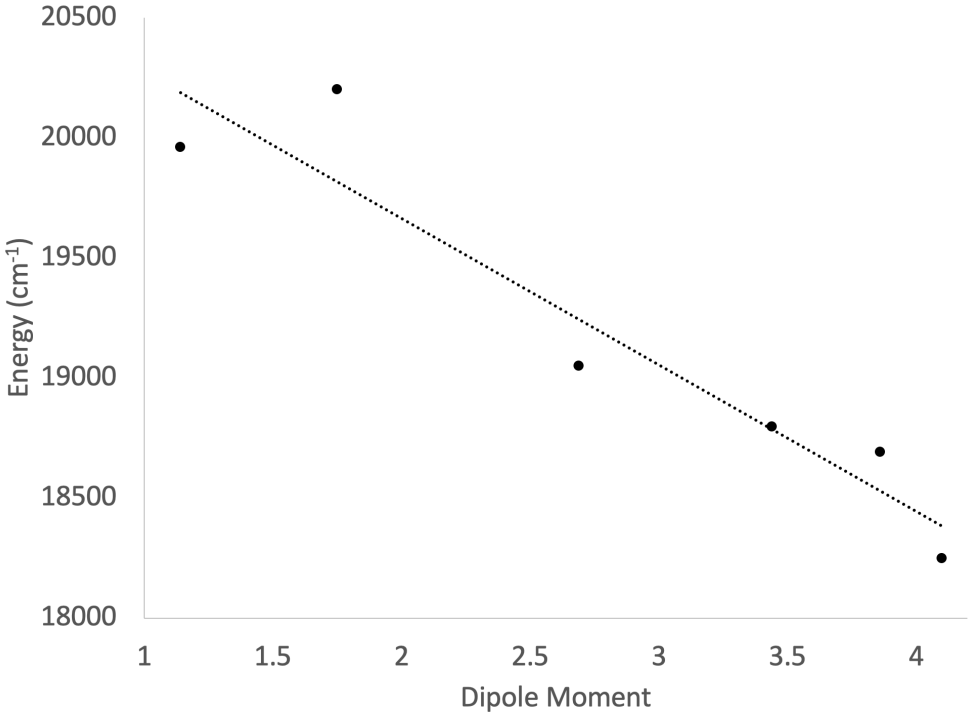

Figure A5.5 Linear correlation between dipole moment (μ) and the energy of the LL'CT of MoO(tdt)($^{i}Pr_2Dt^0$). Equation of fit: E = -610.17 μ + 20884

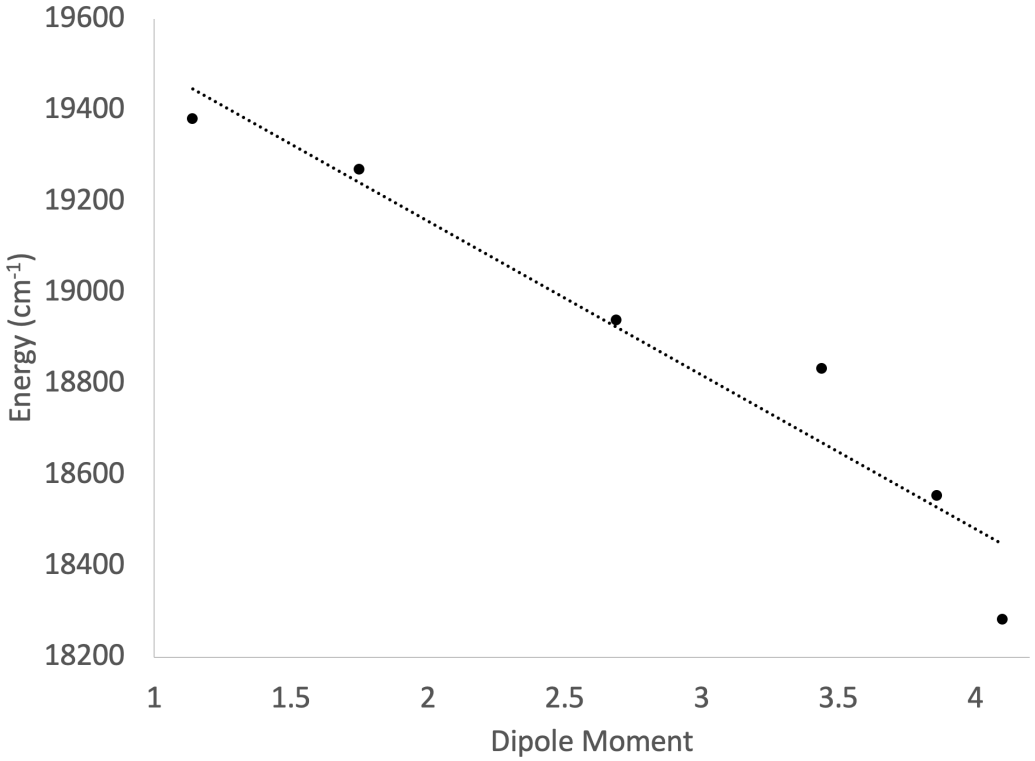

Figure A5.6 Linear correlation between dipole moment (μ) and the energy of the LL'CT of $MoO(bdtCl_2)(^iPr_2Dt^0)$. Equation of fit: E = -338.3 μ + 19833

Table A5.1 Equation of the fit for the multivariate regression using the Kamlet-Taft model.

Complex	Equation of Fit
$MoO(bdt)(Me_2Dt^0)$ (**1**)	23726+1514 π^*– 1675 α - 9347 β
$MoO(tdt)(Me_2Dt^0)$ (**2**)	26752+1785 π^*– 27025 α - 1406 β
$MoO(bdtCl_2)(Me_2Dt^0)$(**4**)	20777+3031 π^*– 425.9 α - 606 β
$MoO(bdt)(^iPr_2Dt^0)$ (**5**)	23041+366 π^*– 12720 α - 6794 β
$MoO(tdt)(^iPr_2Dt^0)$ (**6**)	25891+1336 π^*– 23442 α - 11962 β
$MoO(bdtCl_2)(^iPr_2Dt^0)$ (**8**)	21829+104 π^*– 7887 α - 4563 β

A6. Reduced Species [MoO(bdt)(Me_2Dt^{1-})]$^+$

Electron paramagnetic resonance signals were obtained in DCM at 298 K on a Bruker EMX X-band EPR spectrometer. Electronic absorbance spectra were collected on a Shimadzu UV-3600 Plus in a quartz cuvette.

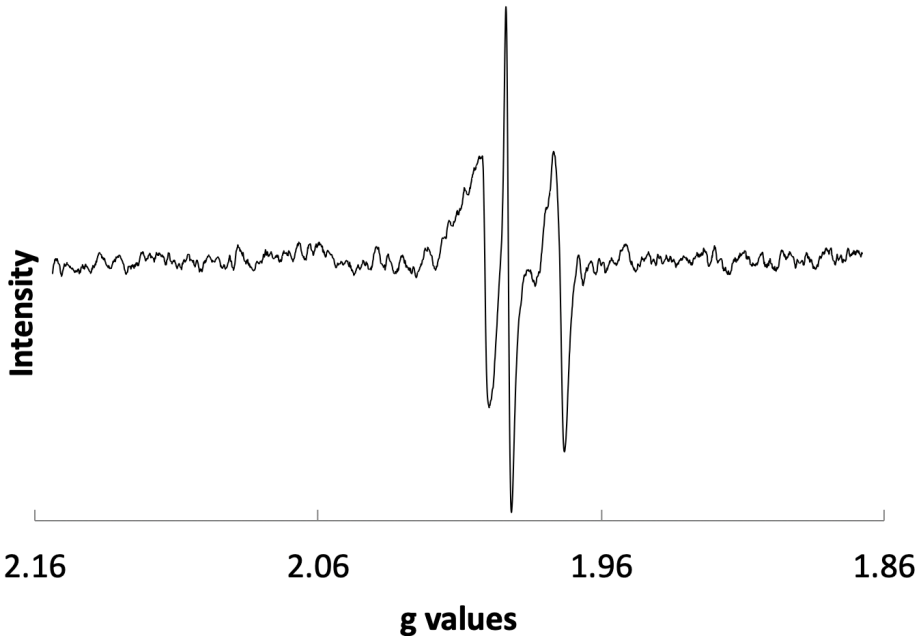

Figure A6.1 EPR of electrochemically generated [MoO(bdt)(Me_2Dt^{1-})]$^+$recorded in CH_2Cl_2 at 298K.

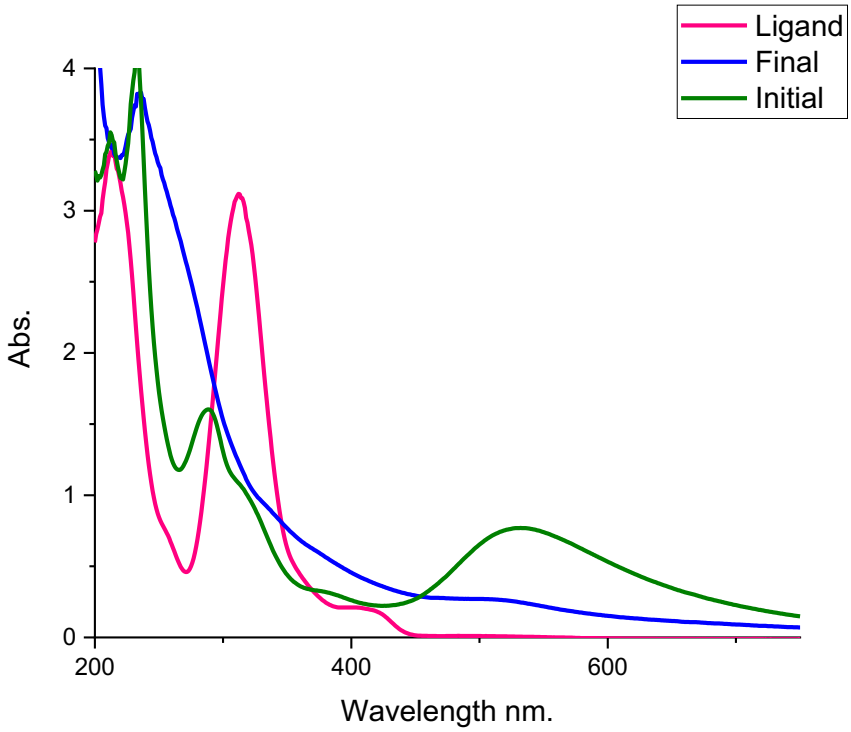

Figure A6.2Absorbance spectra collected during the spectroelectrochemistry of MoO(tdt)(^{i}Pr$_2$Dt^0) (green), compared to the absorbance spectrum of ^{i}Pr$_2$Dt^0 (blue).

A7. Oxygen Atom Transfer (OAT) Reactivity

^{1}H and ^{31}P NMR spectral data were collected using a Bruker 400 MHz spectrometer. Mass spectra were collected using either an Agilent Technologies 6520 Accurate Mass-QTOF LC/MS or an Agilent Technologies 6130 Quadrupole LC/MS.

$MoO(SPh)_2(Dt^0)$ Complexes

^{1}H NMR and ^{31}P NMR spectroscopy

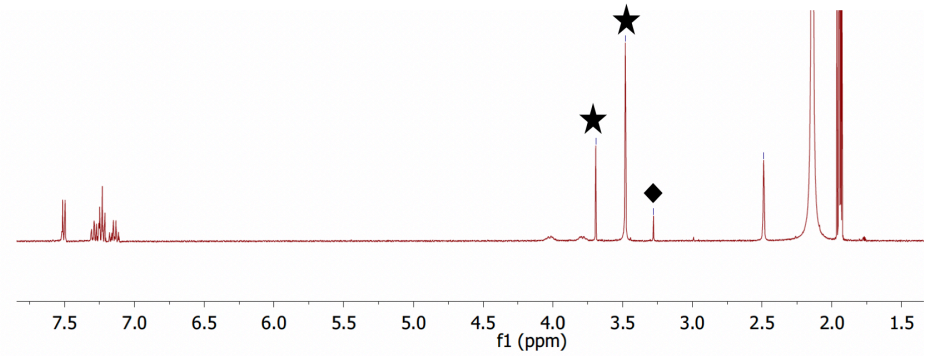

Figure A7.1. ^{1}H NMR spectrum (CD_3CN) of the reaction between **9** and TMAO. Uncoordinated dithione ligand is marked with ★ indicating degradation of the complex and unreacted TMAO is marked with ◆.

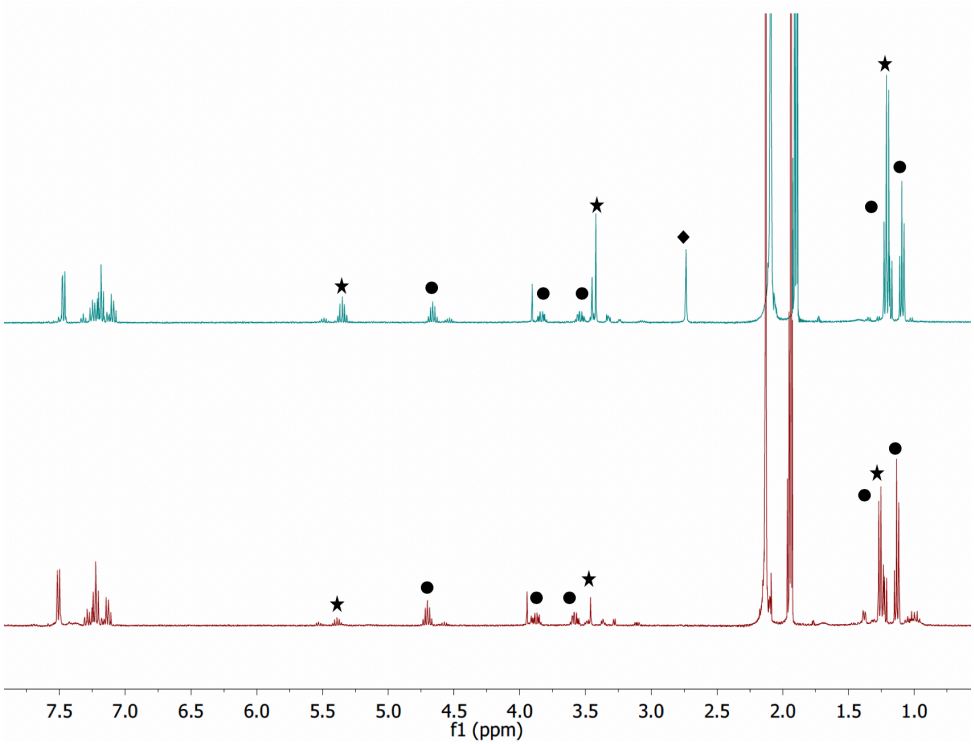

Figure A7.2 ^{1}H NMR (CD_3CN) spectra of the reaction between TMAO, PEt_2Ph and **10** in acetonitrile at room temperature. Bottom spectrum is the reaction between PEt_2Ph and **10**. The top spectrum is the reaction between TMAO and **10** Unreacted **10** is marked with ●, uncoordinated dithione ligand is marked with ★ and TMA is marked with ◆.

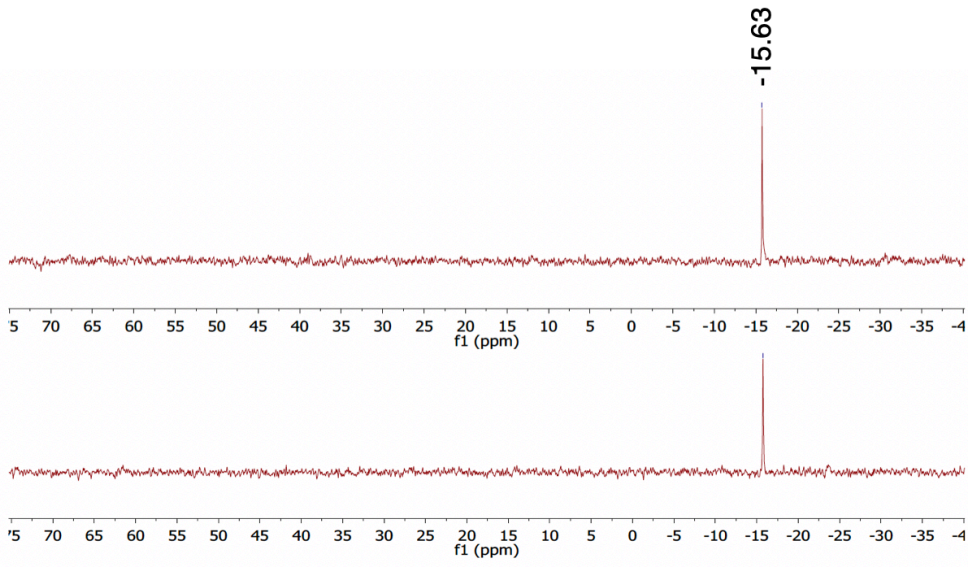

Figure A7.3. ^{31}P NMR (CD_3CN) spectral studies on the reaction between TMAO, PEt_2Ph and $MoO(SPh)_2(Me_2Dt^0)$ in acetonitrile at room temperature. Top spectrum is the reaction between **9**, TMAO, and PEt_2Ph. Bottom spectrum is the reaction between **9** and PEt_2Ph.

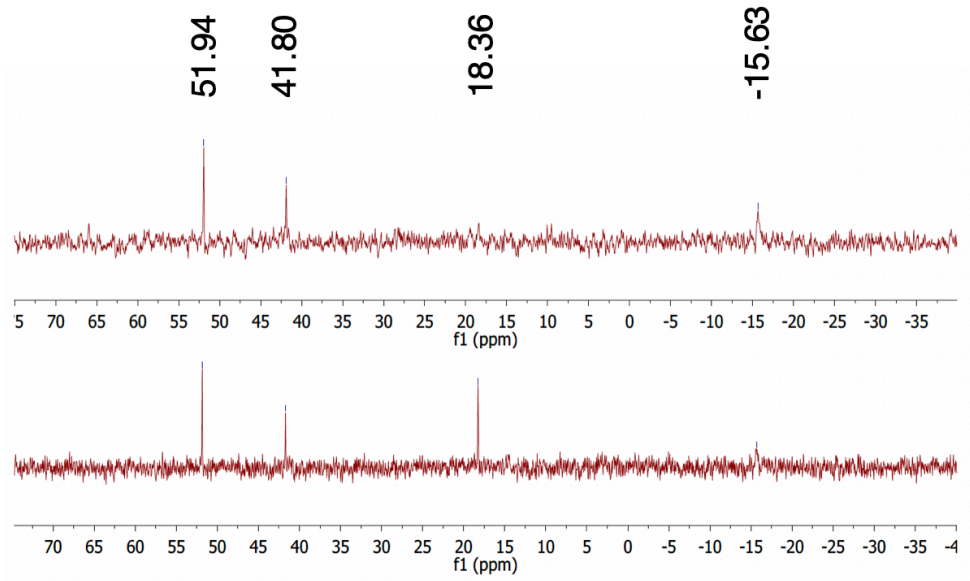

Figure A7.4. ^{31}P NMR (CD_3CN) spectral studies on the reaction between TMAO, PEt_2Ph, and $MoO(SPh)2(^{i}Pr_2Dt^{0})$ in acetonitrile at room temperature. Top spectrum is the reaction between **10**, TMAO, and PEt_2Ph. Bottom spectrum is the reaction between **10** and PEt_2Ph.

Mass Spectrometry

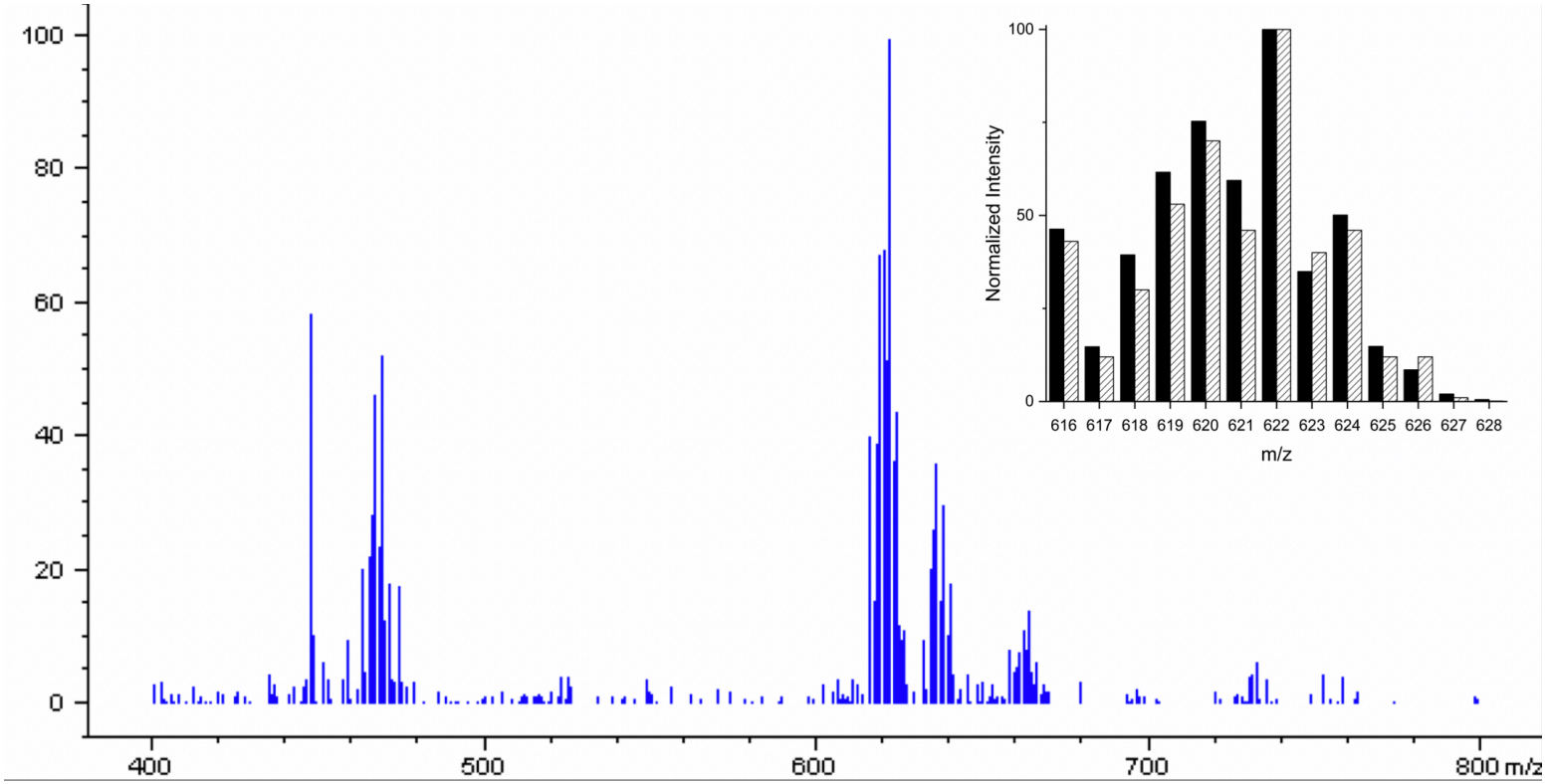

Figure A7.5 ESI-MS of $[Mo(SPh)_2(TMAO)(^iPr_2Dt^0)]^+$ formed during the reaction between **10** and TMAO. Inset: plotted are the experimental (hatched) and calculated (solid) spectra for $C_{25}H_{37}MoN_3OS_4^+$

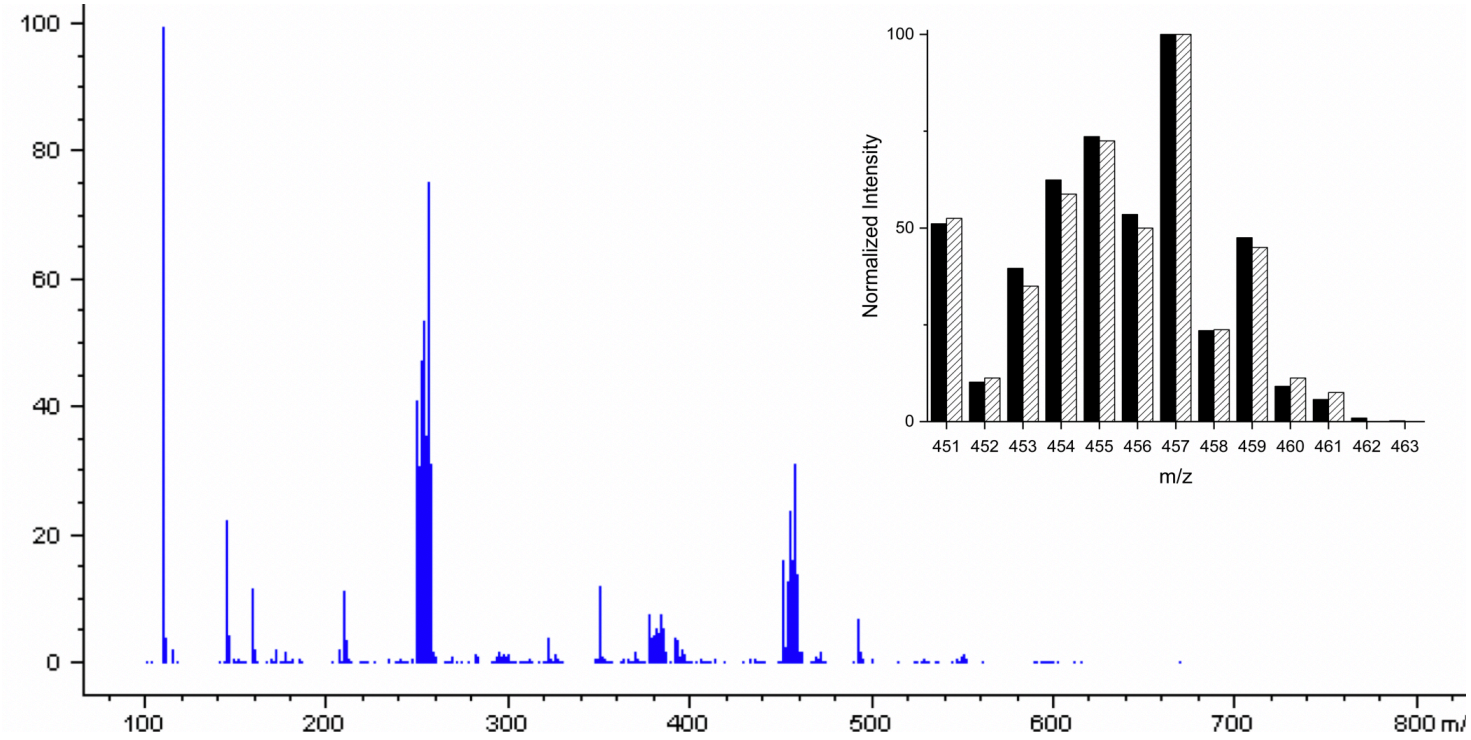

Figure A7.6. ESI-MS of $[Mo(SPh)(TMAO)(Me_2Dt^0)]^+$formed during the reaction between **9**, PEt_2Ph, and TMAO. Inset: plotted are the experimental (hatched) and calculated (solid) spectra for $C_{15}H_{24}MoN_3OPS_3^-$.

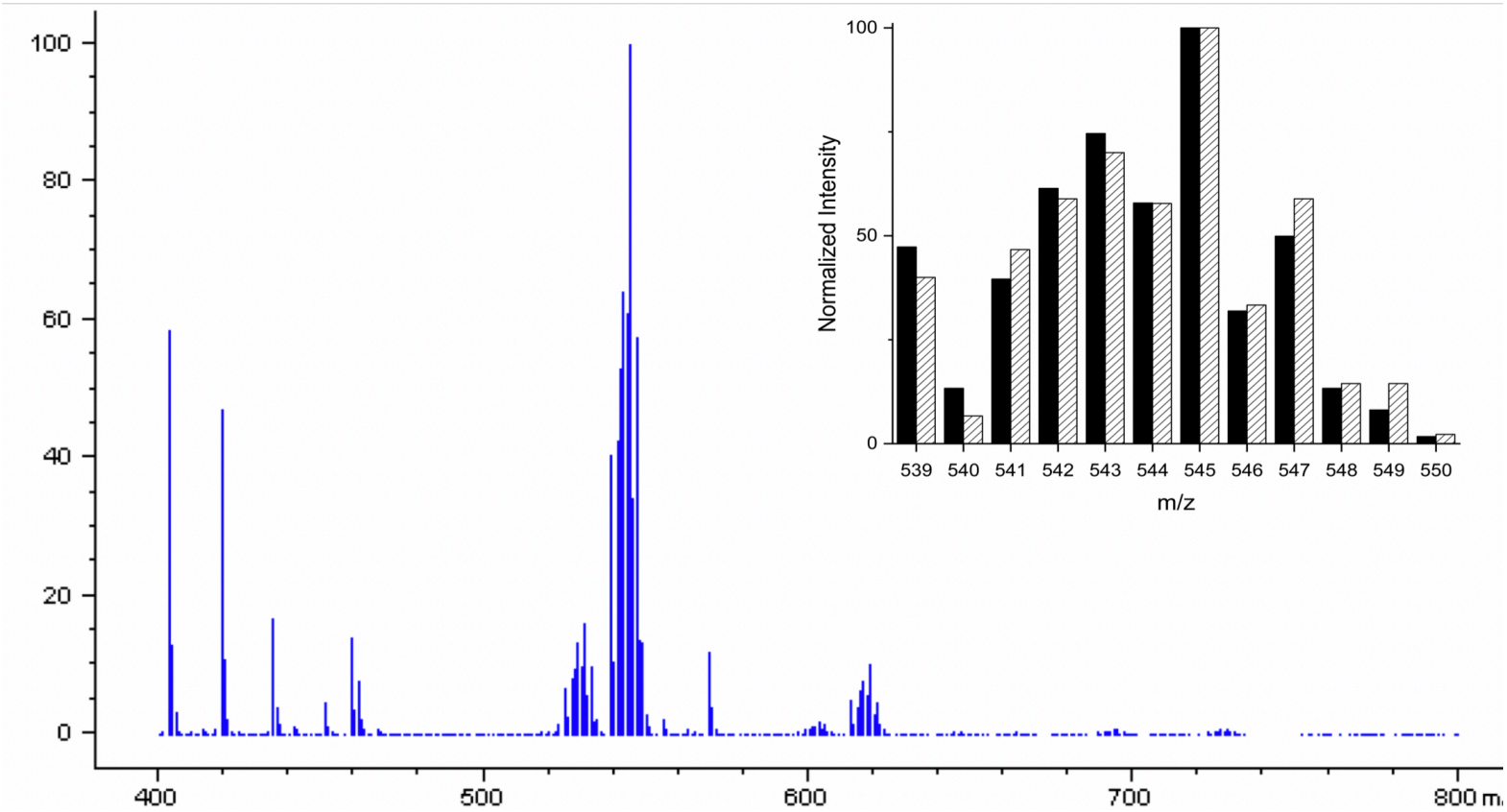

Figure A7.7 ESI-MS of $[Mo(SPh)_2(^iPr_2Dt^0)]^+$formed during the reaction between **10** and PEt_2Ph. Inset: plotted are the experimental (hatched) and calculated (solid) spectra for $C_{22}H_{28}MoN_2OS_3^+$

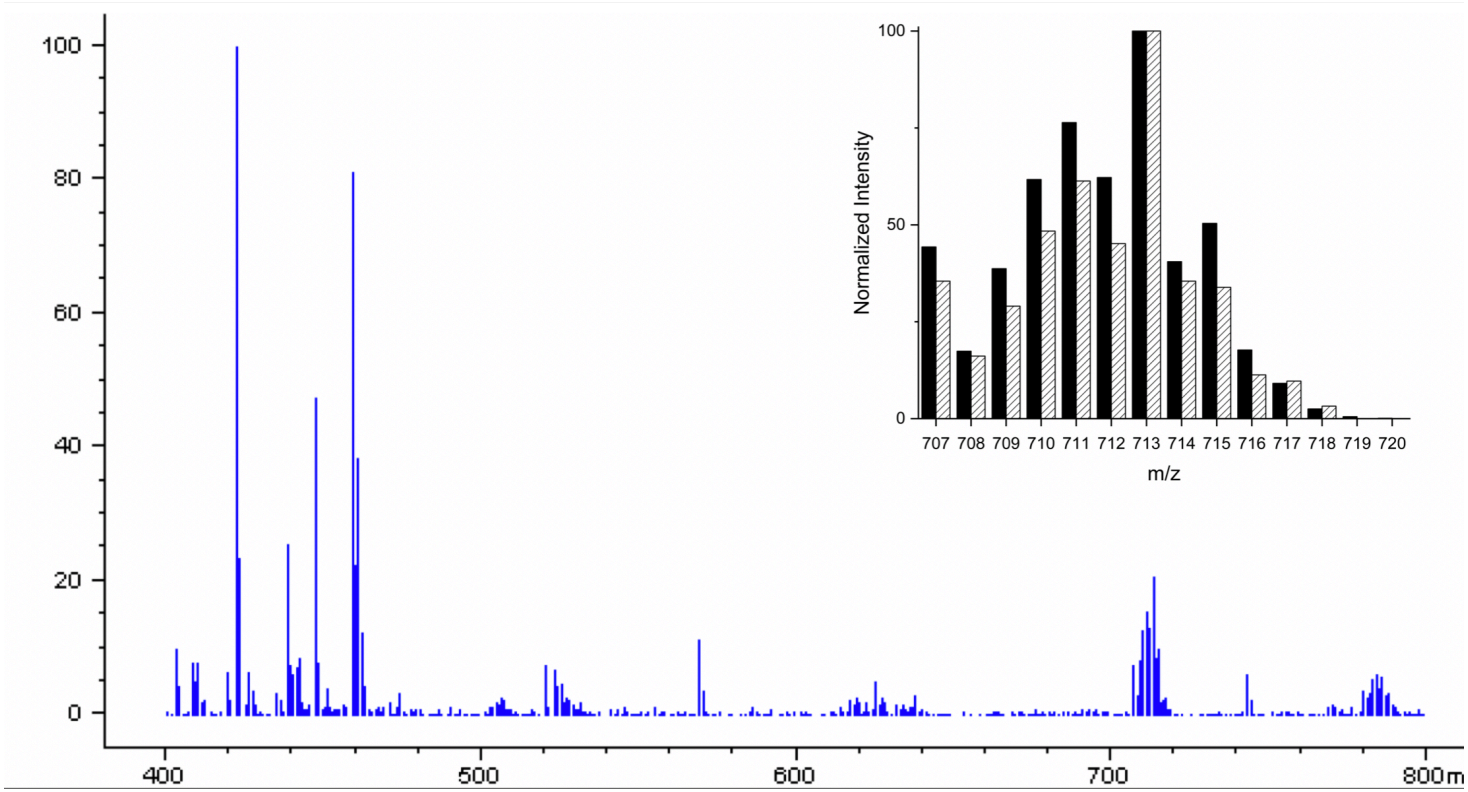

Figure A7.8. ESI-MS of $[Mo(SPh)_2(PEt_2Ph)(^iPr_2Dt^0)]^+$ formed during the reaction between **10**, PEt_2Ph, and TMAO. Inset: plotted are the experimental (hatched) and calculated (solid) spectra for $C_{15}H_{24}MoN_3OPS_3^+$.

[MoOCl(Dt^0)$_2$][PF$_6$] Complexes

^{1}H NMR and ^{31}P NMR spectroscopy

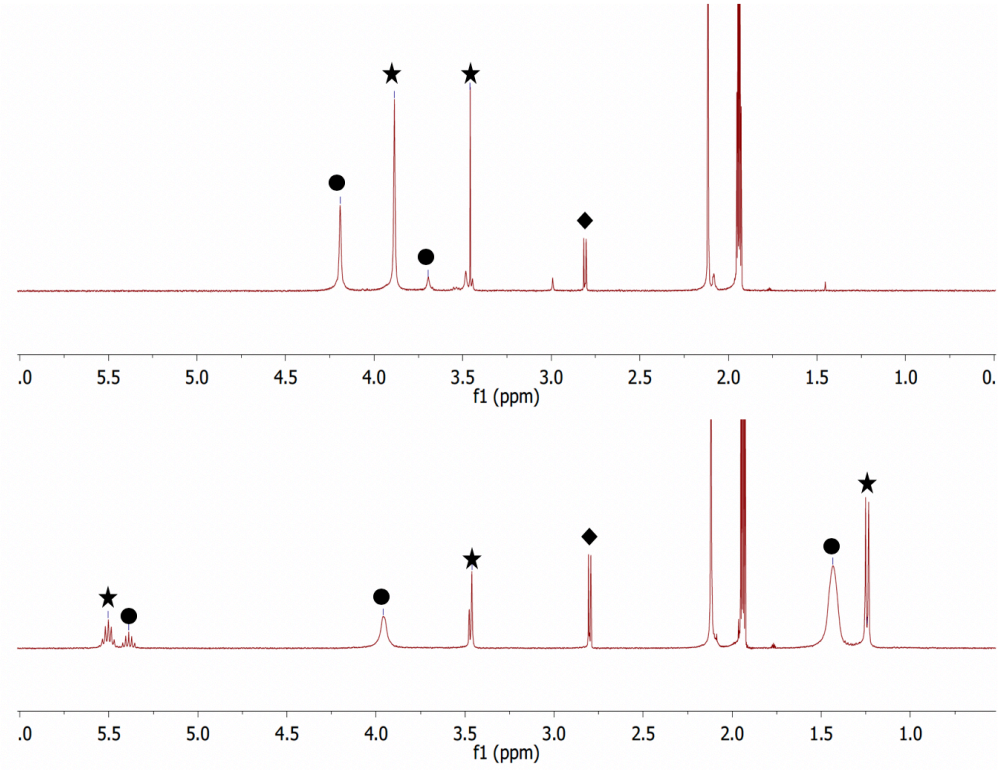

Figure A7.9. ^{1}H NMR (CD_3CN) spectra of the reaction between TMAO, and **11** (Top) and **12** and TMAO (Bottom) in acetonitrile at room temperature. Unreacted starting material is marked with ●, uncoordinated dithione ligand is marked with ★ and TMA is marked with ◆.

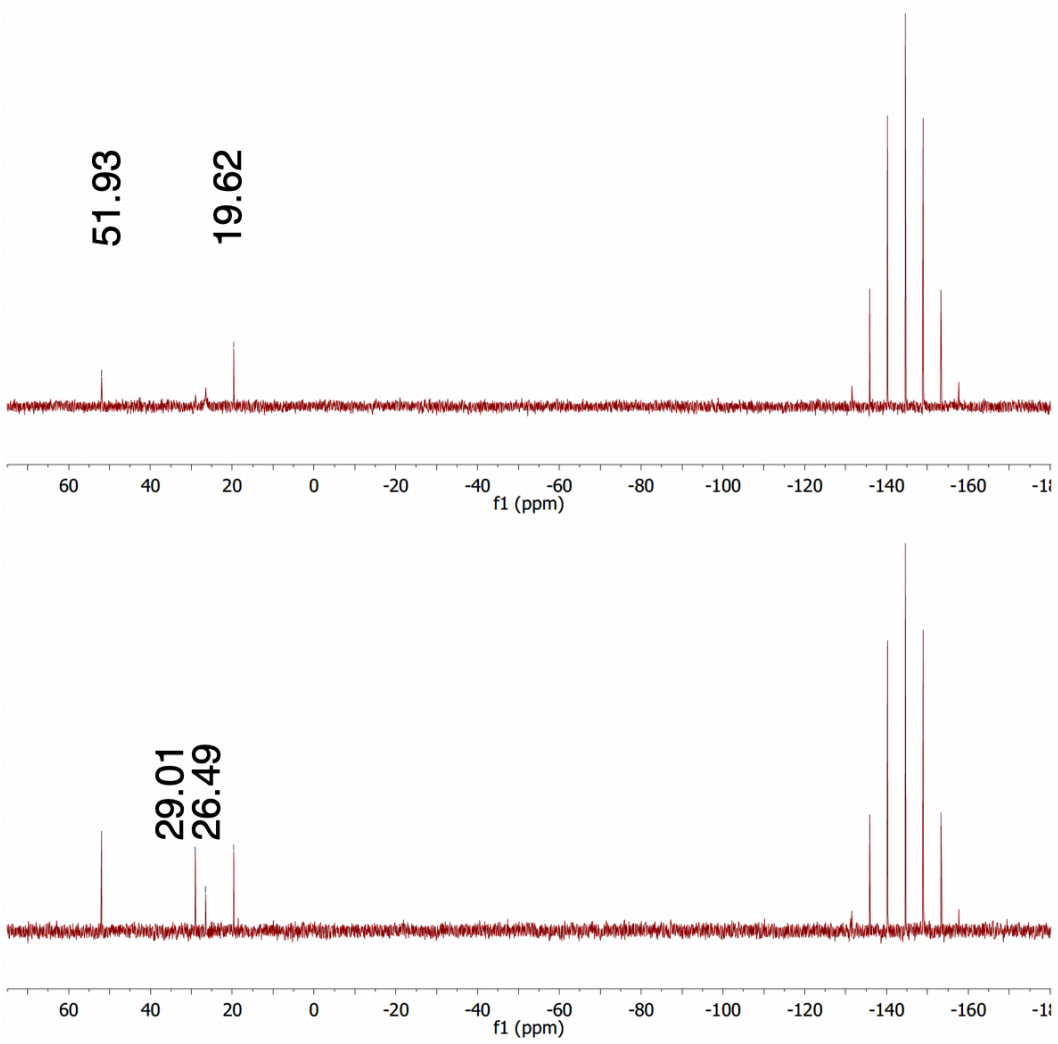

Figure A7.10. ^{31}P NMR (CD_3CN) spectral studies on the reaction between TMAO, PEt_2Ph and **11** in acetonitrile at room temperature. Top spectrum is the reaction between **11**, PEt_2Ph. Bottom spectrum is the reaction between **11**, TMAO and PEt_2Ph.

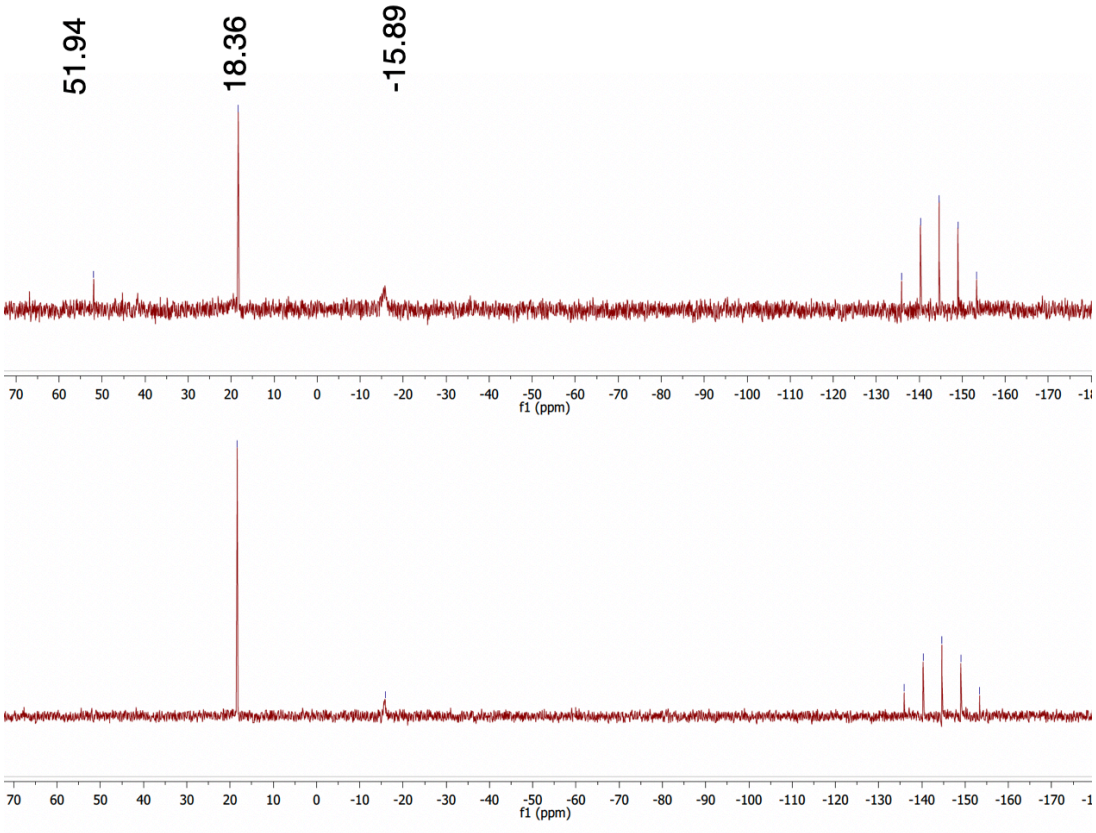

Figure A7.11. ^{31}P NMR (CD_3CN) spectral studies on the reaction between TMAO, PEt_2Ph and **12** in acetonitrile at room temperature. Top spectrum is the reaction between **12**, TMAO, and PEt_2Ph. Bottom spectrum is the reaction between **12** and PEt_2Ph.

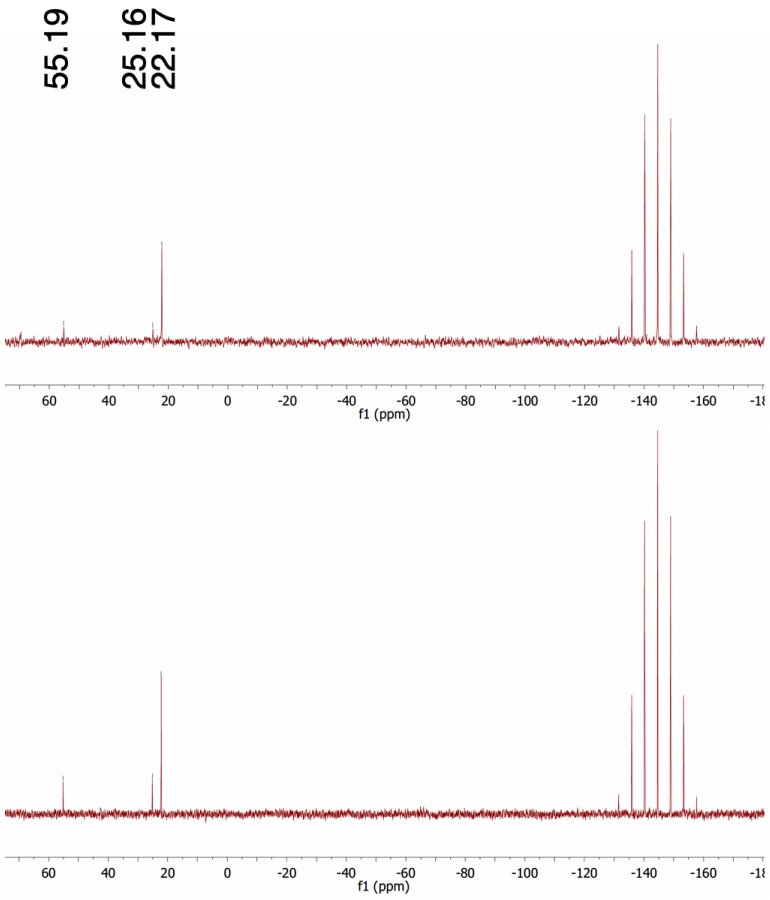

Figure A7.12. ^{31}P NMR (CD_3CN) spectral studies on the reaction between TMAO, PEt_3 and **11** in acetonitrile at room temperature. Top spectrum is the reaction between **11**, TMAO, and PEt_3. Bottom spectrum is the reaction between **11** and PEt_3.

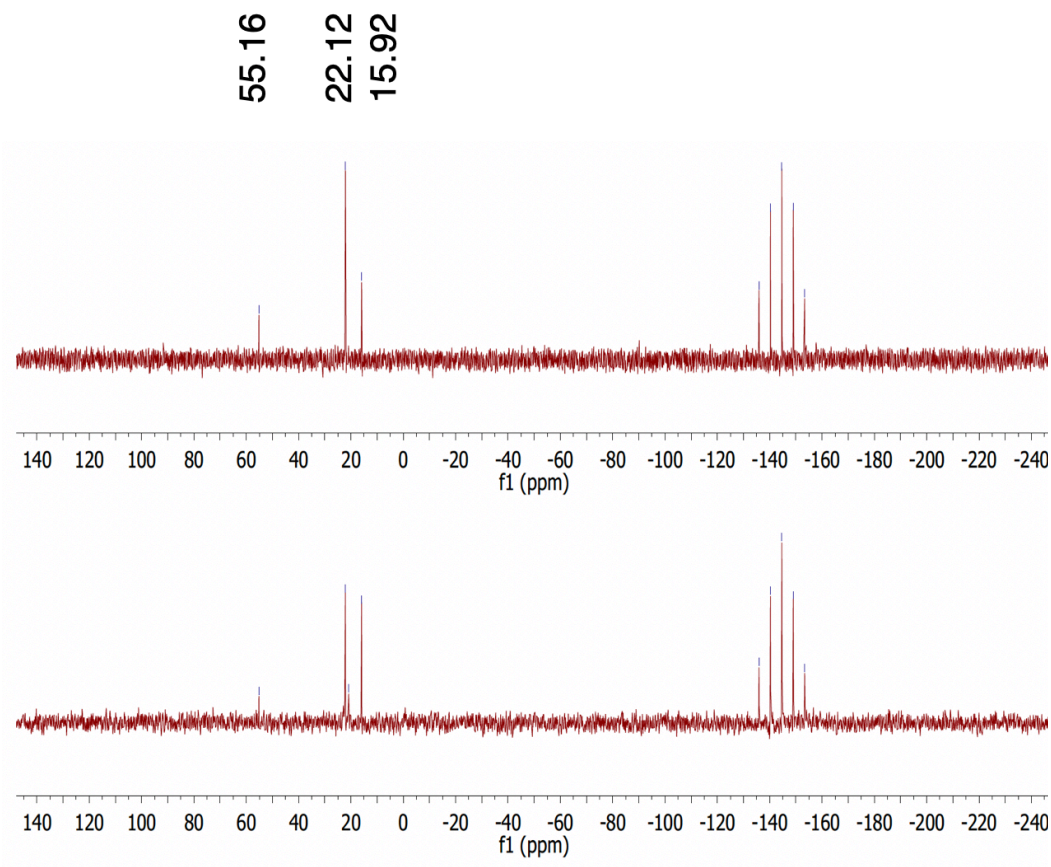

Figure A7.13. ^{31}P NMR (CD_3CN) spectral studies on the reaction between TMAO, PEt_3 and **12** in acetonitrile at room temperature. Top spectrum is the reaction between **12**, TMAO, and PEt_3. Bottom spectrum is the reaction between **12** and PEt_3.

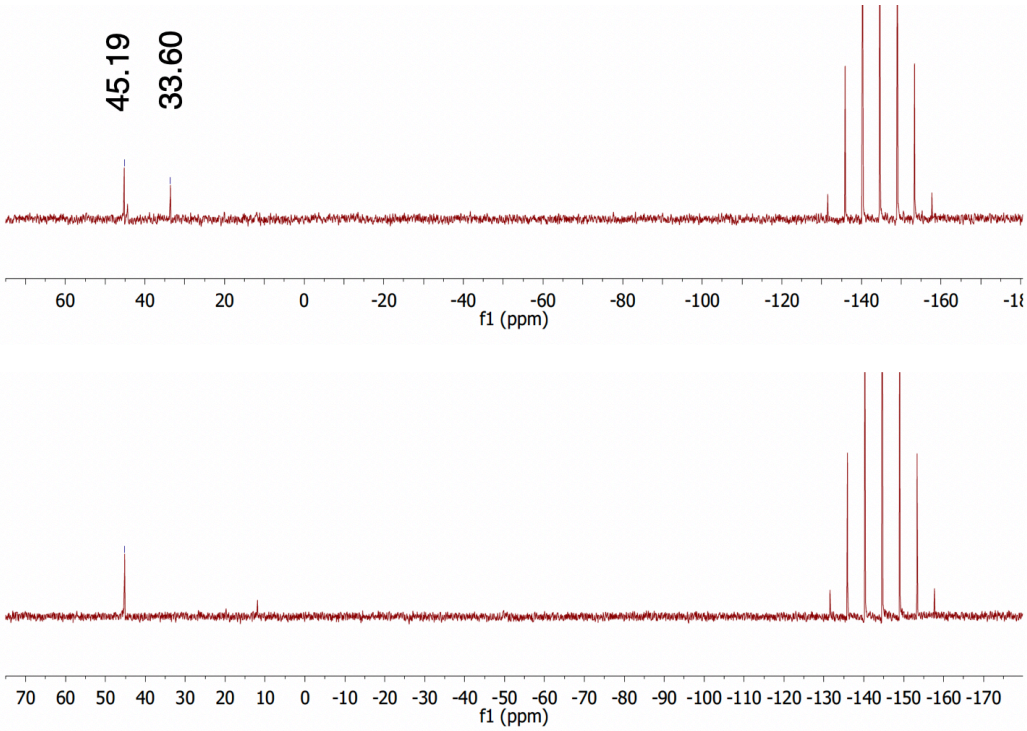

Figure A7.14. ^{31}P NMR (CD_3CN) spectral studies on the reaction between TMAO, PPh_2Et, and **11** in acetonitrile at room temperature. Top spectrum is the reaction between **11**, TMAO, and PPh_2Et. Bottom spectrum is the reaction between **11** and PPh_2Et.

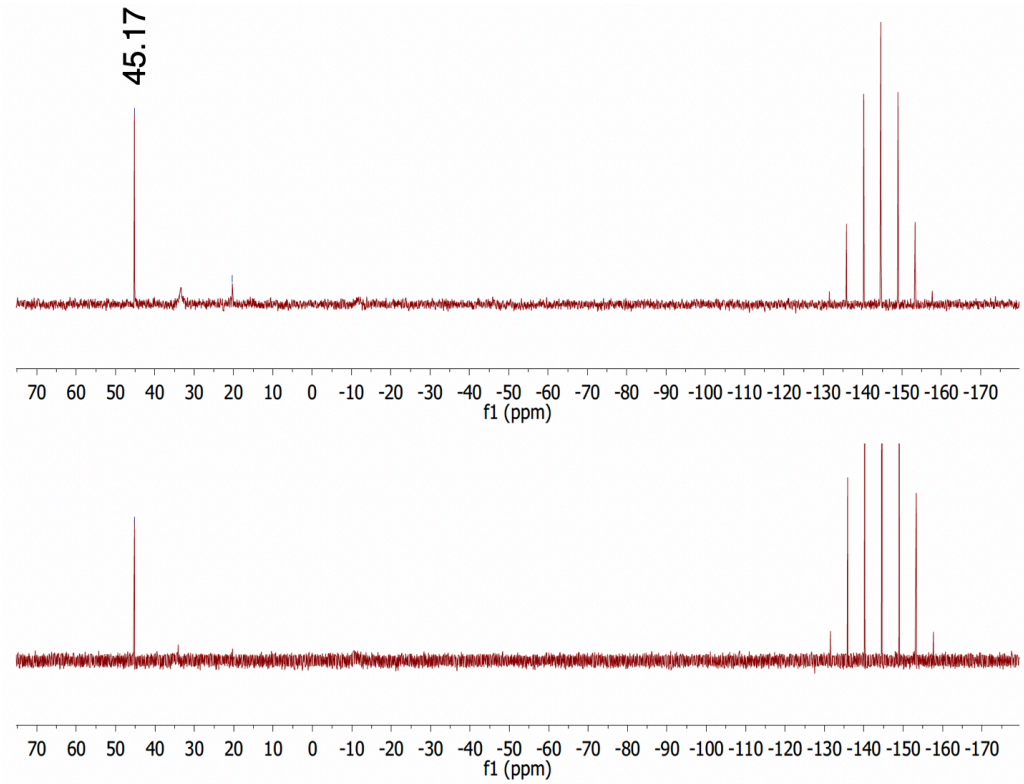

Figure A7.15. ^{31}P NMR (CD_3CN) spectral studies on the reaction between TMAO, PPh_2Et, and **12** in acetonitrile at room temperature. Top spectrum is the reaction between **12**, TMAO, and PPh_2Et. Bottom spectrum is the reaction between **12** and PPh_2Et..

$[MoOCl(Dt^0)_2][PF_6]$ Complexes

Mass Spectrometry

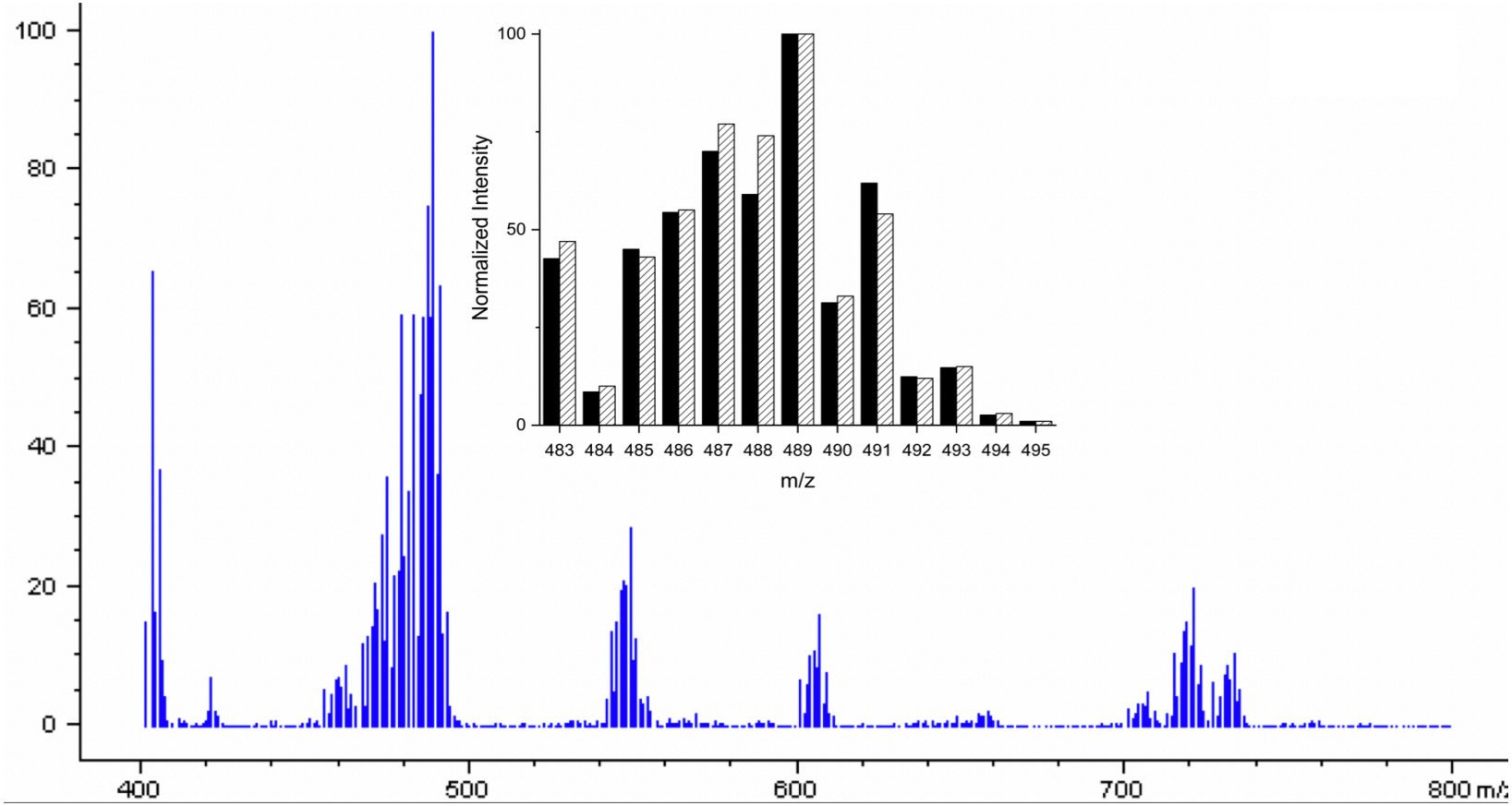

Figure A7.16. ESI-MS of $[MoOCl(PEt_2Ph)(Me_2Dt^0)]^+$ formed during the reaction between **11** and PEt_2Ph. Inset: plotted are the experimental (hatched) and calculated (solid) spectra for $C_{16}H_{25}MoClN_2OPS_2^+$.

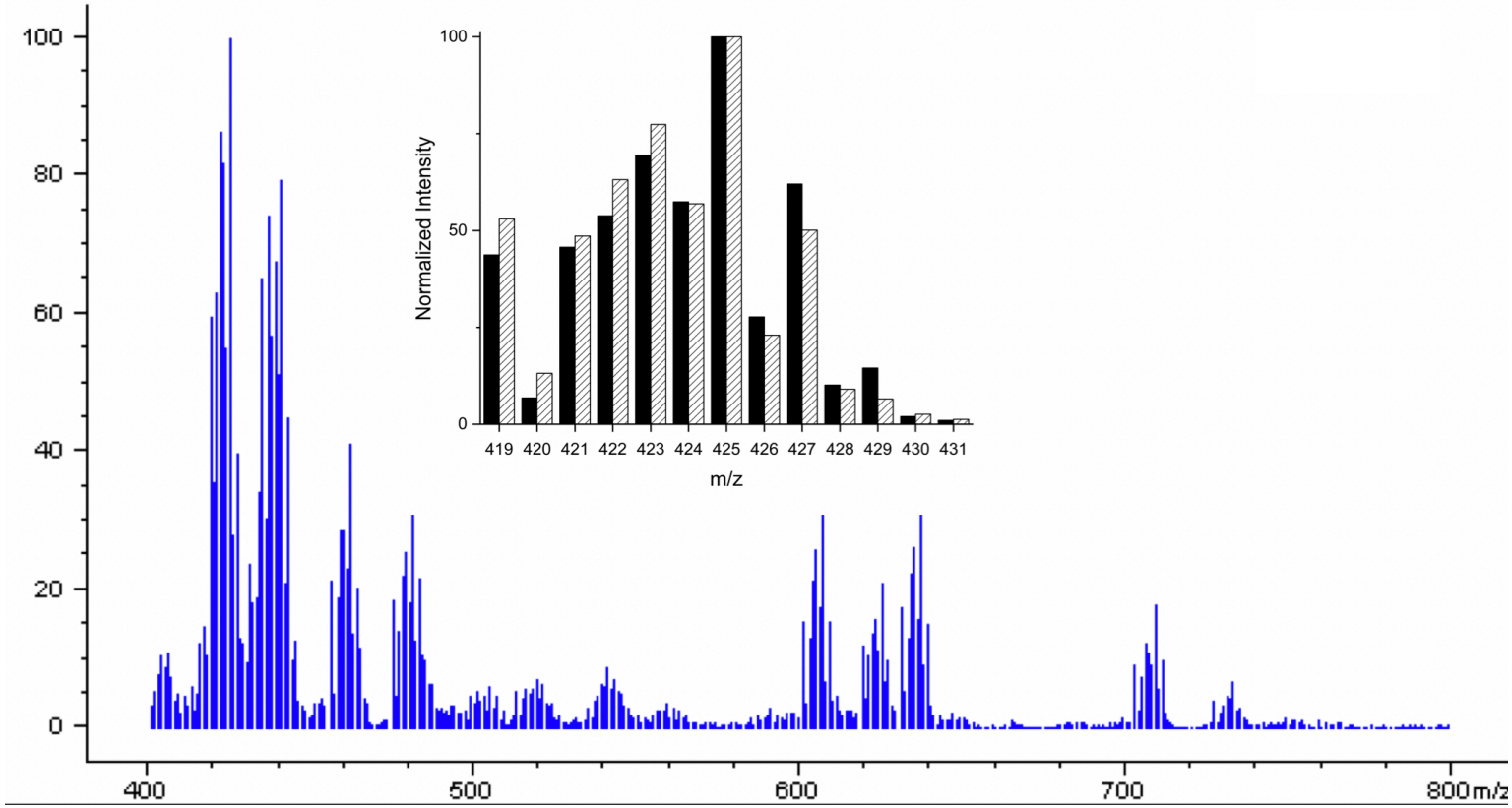

Figure A7.17. ESI-MS of $[MoCl(PEt_3)(Me_2Dt^0)]^+$ formed during the reaction between **11** and PEt_3. Inset: plotted are the experimental (hatched) and calculated (solid) spectra for $C_{12}H_{25}MoClN_2OPS_2^+$.

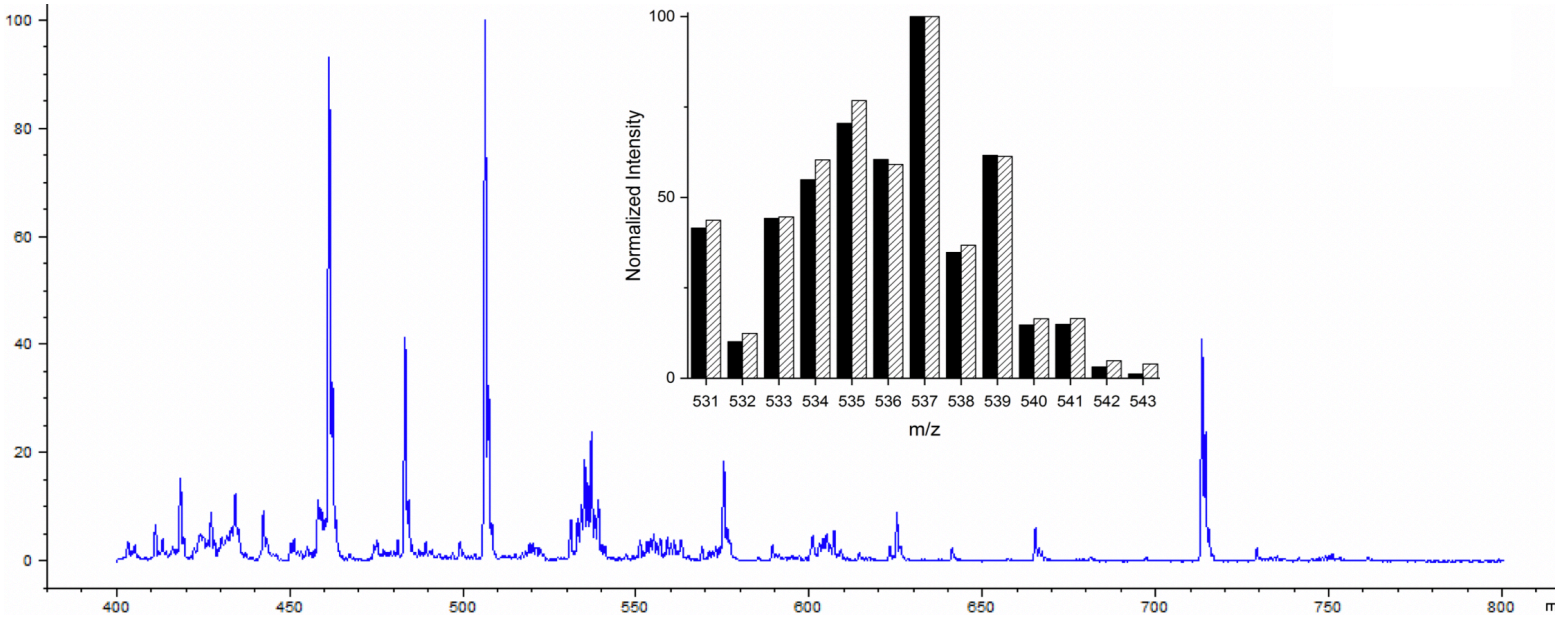

Figure A7.18. ESI-MS of[$MoOCl(PPh_2Et)(Me_2Dt^0)]^+$ formed during the reaction between **11** and PPh_2Et. Inset: plotted are the experimental (hatched) and calculated (solid) spectra for $C_{20}H_{25}MoClN_2OPS_2^+$.

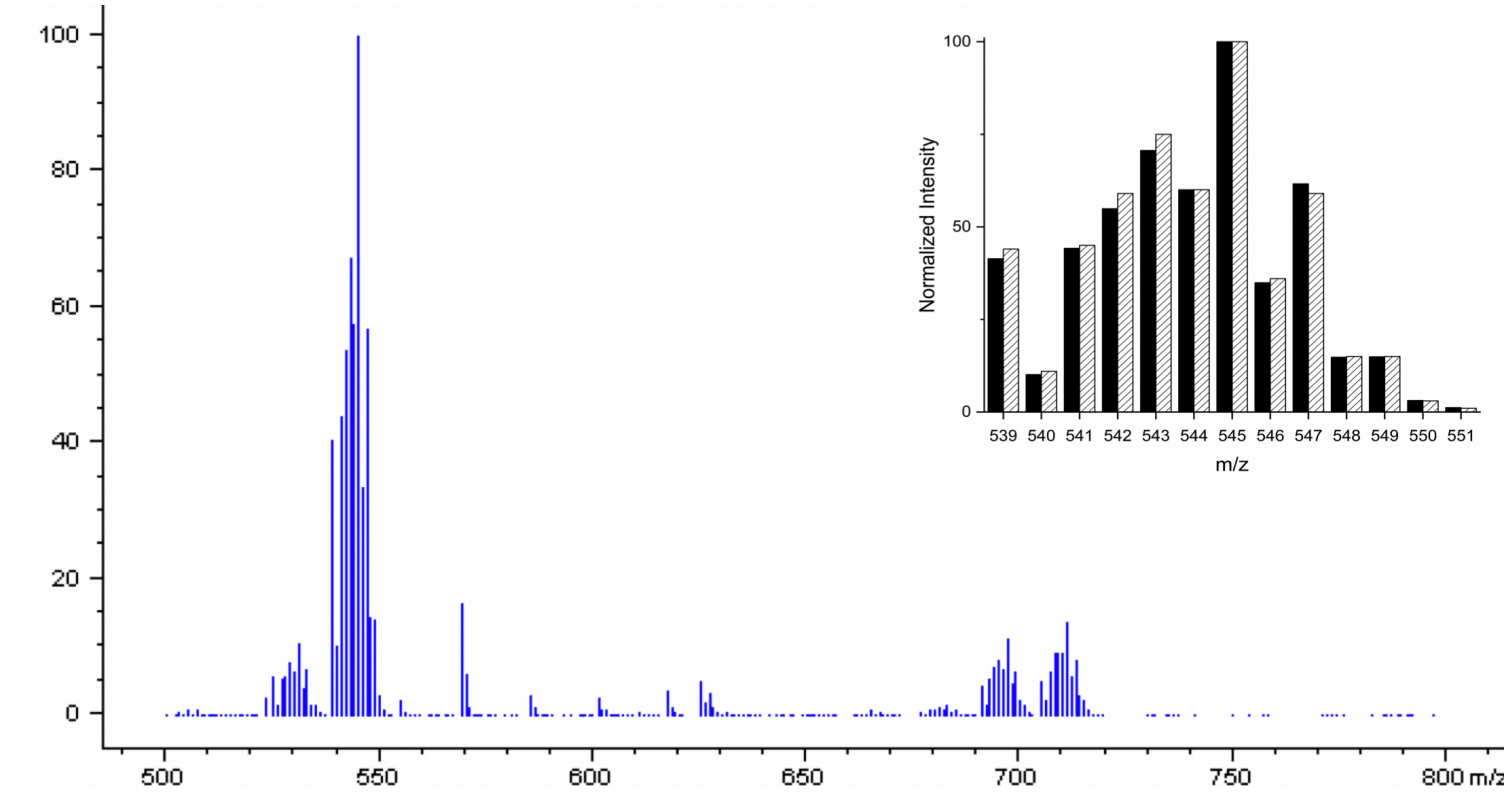

Figure A7.19. ESI-MS of $[MoOCl(PEt_2Ph)(iPr_2Dt^0)]^+$ formed during the reaction between **12** and PEt_2Ph. Inset: plotted are the experimental (hatched) and calculated (solid) spectra for $C_{20}H_{33}MoClN_2OPS_2^+$.

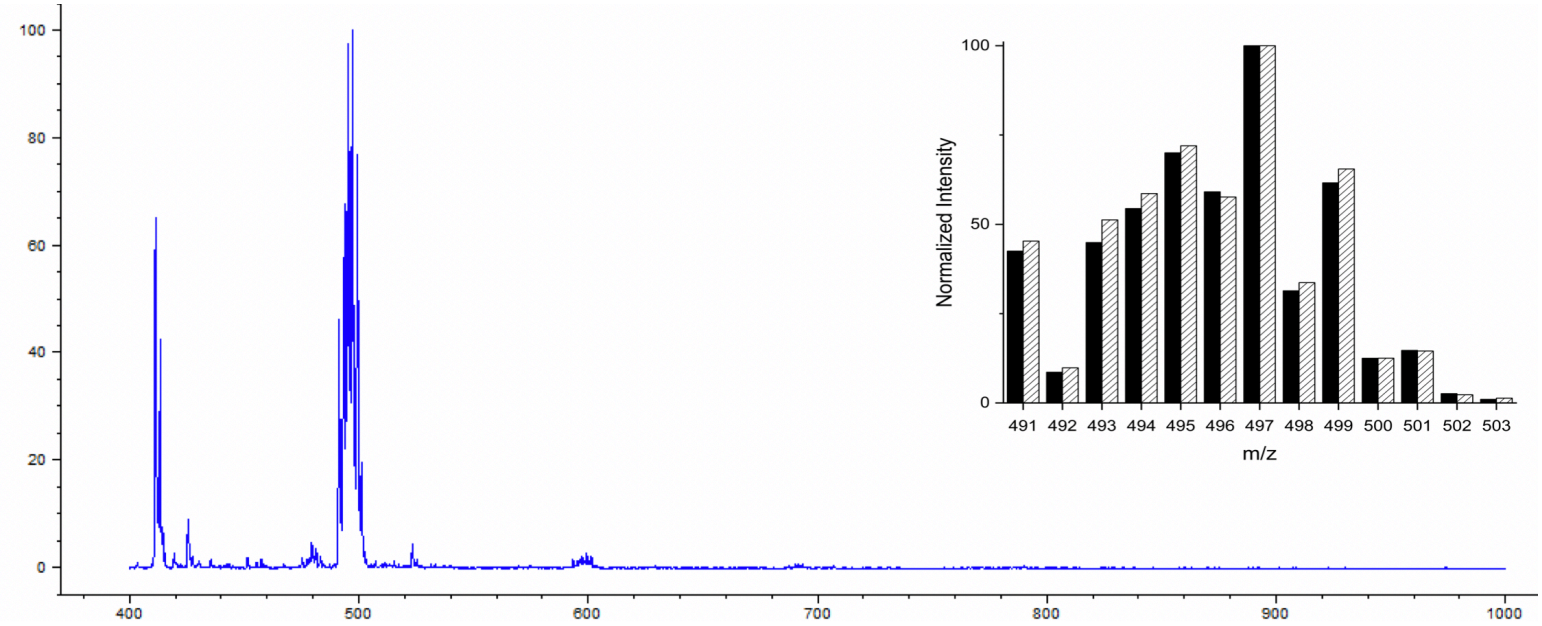

Figure A7.20. ESI-MS of $[MoOCl(PEt_3)(^iPr_2Dt^0)]^+$ formed during the reaction between **12** and PEt_3. Inset: plotted are the experimental (hatched) and calculated (solid) spectra for $C_{16}H_{33}MoClN_2OPS_2^+$.

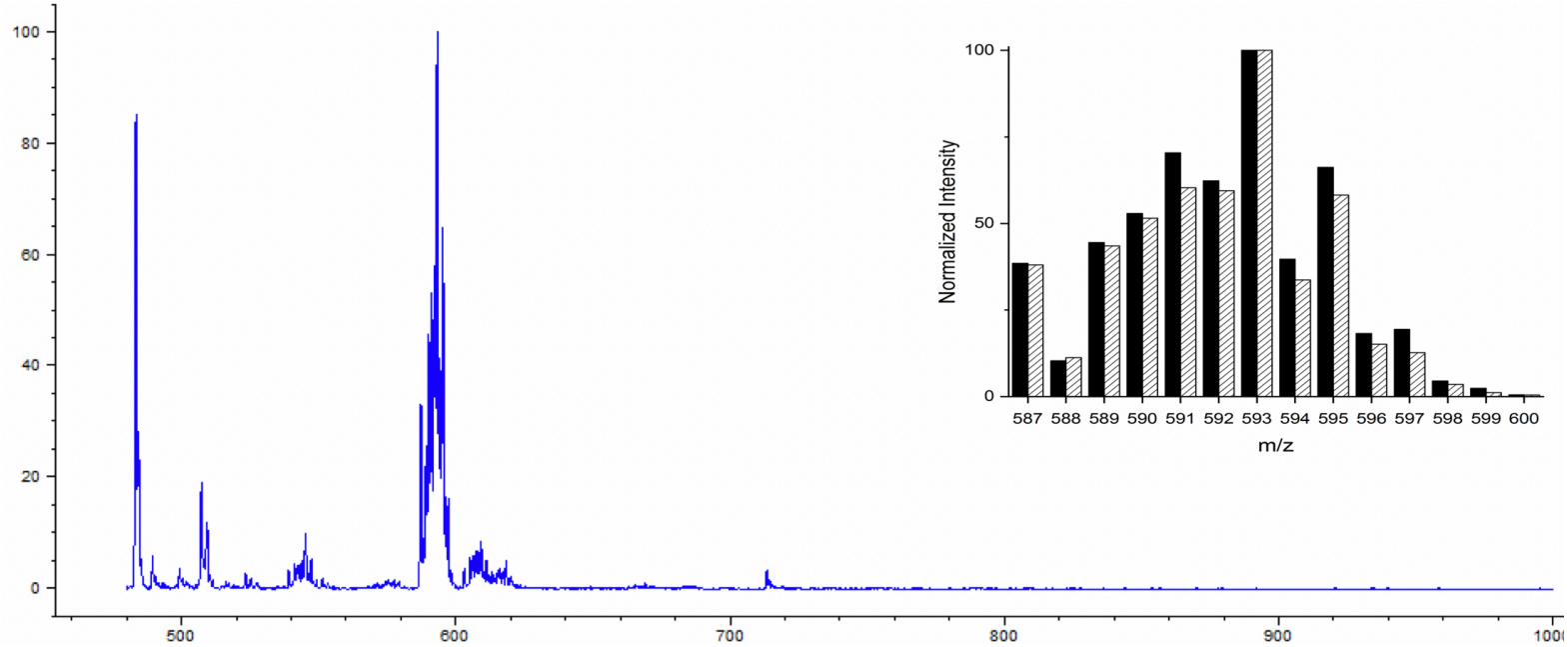

Figure A7.21. ESI-MS of $[MoCl(^{i}Pr_2Dt^{0})_2]^+$ formed during the reaction between **12** and PPh_2Et. Inset: plotted are the experimental (hatched) and calculated (solid) spectra for $C_{20}H_{36}MoClN_4OS_4^+$.